Cooperative Ligand Design for Late Transition Metal Coordination Compounds

by

Truman C. Wambach

B.A., The University of Minnesota 2008

A THESIS SUBMITTED IN PARTIAL FULFILLMENT OF

THE REQUIREMENTS FOR THE DEGREE OF

Doctor of Philosophy

in

THE FACULTY OF GRADUATE AND POSTDOCTORAL STUDIES

(Chemistry)

THE UNIVERSITY OF BRITISH COLUMBIA

(Vancouver)

January 2015

Abstract

This thesis describes several cyclopentyl linked enamide phosphine ligands. Reactivity and mechanistic studies using coordination compounds featuring these ligands enable exploration of ligand cooperativity.

Despite complex behavior in solution due to tautomerization, coordination of $(NPN)^{DMP/DIPP}H_2$ to Rh generates $RhCl\{(NPN)^{DMP/DIPP}H_2\}(COE)$. Synthesis of $RhCl\{(NPN)^{DMP/DIPP}H_2\}(CO)$ and $RhHCl_2\{(NPN)^{DMP/DIPP}H_2\}$ is possible. NMR spectroscopy and in certain cases X-ray analysis establishes the diimine tautomer of the ligand coordinates to Rh in each case.

Enamide phosphine complexes, $Ir\{(NP)^{DIPP}\}(COD)$ and $Ir\{(NP)^{DMP}\}(COD)$ are synthesized from simple imine phosphine ligands. $Ir\{(NP)^{DIPP}\}(COD)$ reacts with H_2 or Pr^iOH to form $[IrH_3\{(NP)^{DIPP}H\}]_2$. The imine tautomer of the ligand coordinates to Ir. Treating $[IrH_3\{(NP)^{DIPP}H\}]_2$ with CO generates $Ir\{(NP)^{DIPP}\}(CO)_2$. A proton from the imine ligand of $[IrH_3\{(NP)^{DIPP}H\}]_2$ combines with an Ir hydride to release H_2. Observation of three intermediates, involved in conversion of $[IrH_3\{(NP)^{DIPP}H\}]_2$ to $Ir\{(NP)^{DIPP}\}(CO)_2$, suggests that tautomerization of the dissociated arm is involved in cooperative H_2 loss.

Four imine phosphine ligands ($^R(NP)^{R'}H$), where the *N*-aryl groups (R) and the groups attached to P(R') are varied, are synthesized. Combining each ligand with $RuHCl(PPr^i_3)_2(CO)$ and $KOBu^t$ generates four enamide phosphine complexes: $RuH\{^R(NP)^{R'}\}(PPr^i_3)(CO)$. Reacting $RuH\{^R(NP)^{R'}\}(PPr^i_3)(CO)$ with H_2 generates $RuH_2\{^R(NP)^{R'}H\}(PPr^i_3)(CO)$. The imine tautomeric form of the ligand coordinates to Ru in all four cases. The R' groups influence the rate of reaction and percent conversion to $RuH_2\{^R(NP)^{R'}H\}(PPr^i_3)(CO)$. The mechanism for H_2 activation is explored using $RuH\{^{Pri}(NP)^{Pri}\}(PPr^i_3)(CO)$. An intermediate is identified as

$RuH_2(H_2)\{^{Pri}(NP)^{Pri}H\}(PPr^i_3)(CO)$. The $T_{1,min}$ value of a ^1H NMR resonance at δ -7.2 is 22 ms at 238 K (measured to 400 MHz), consistent with a Ru dihydrogen dihydride complex. The N donor of the enamine tautomeric form of the ligand is protonated by H_2 or D_2 and has dissociated from Ru. Tautomerization of the dissociated arm is involved in formation of the final product.

Certain factors inhibit alcohol dehydrogenation catalysis for $Ir\{(NP)^{DIPP}\}(COD)$ and $RuH\{^{Pri}(NP)^{Pri}\}(PPr^i_3)(CO)$. Two tridentate enamide phosphine ligands are developed in an effort to generate a catalyst. These ligands enable synthesis of $RuH\{(PNN)^{But}\}(CO)$ and $RuH\{(PNN)^{Pri}\}(CO)$. Exposing $RuH\{(PNN)^{But}\}(CO)$ to 1000 equivalents of benzyl alcohol yields a TON of 13 and TOF of 0.6 h^{-1} after 22 hours. Nearly identical results are obtained for $RuH\{(PNN)^{Pri}\}(CO)$.

Preface

The author of this work identified and designed the research program under the supervision of Dr. Michael D. Fryzuk. The author carried out all of the synthesis and collected all of the characterization data with the exception of X-ray crystallographic data. Dr. Nathan R. Halcovitch, Mr. Frasier F. Pick, Dr. Brian O. Patrick or Ms. Alyssa Yeo collected the X-ray data, which was analyzed by the author.

Portions of Chapter 2, including parts of the introduction as well as the solution and solid state characterization of the ligands, are reported in a publication; Zhu, T.; [Wambach, T.C.]; Fryzuk, M. D. *Inorg. Chem.* 2011, *50*, 11212. Chapter 3 is also based on a publication; [Wambach, T.C.]; Ahn, J. M.; Patrick. B. O.; Fryzuk, M. D. *Organometallics* 2013, *32*, 4431. Ahn, J. M. contributed by performing the initial synthesis of **3.7b**; additionally, he isolated crystals suitable for X-ray analysis of the structure of **3.7b**. Patrick, B. O. aided in the analysis of the X-ray crystallographic data collected for **3.9a**. All writing in this work was a collaborative effort between Dr. Michael D. Fryzuk and the author, where initial drafts of the manuscript were generated by the author, and refined based on the feedback of Dr. Michael D. Fryzuk.

Table of Contents

List of Tables

List of Figures

List of Symbols

θ	-	Tolman cone angle
°C	-	Degrees Celsius
‡	-	A transition state
C_s	-	A point group containing a mirror plane of reflection and the identity operators
C_1	-	A point group containing the identity operator
C_i	-	A point group containing an inversion center and the identity operators
α-CH	-	The position on the linker of the ligand connected directly to phosphorus where the carbon is protonated
α-C	-	The position on the linker of the ligand connected directly to phosphorus where the carbon is not protonated
β-CH_2	-	The position on the linker of the ligand adjacent to the α position
γ-CH_2	-	The position on the linker of the ligand adjacent to the β position
δ-CH_2	-	The position on the linker of the ligand adjacent to the γ position
${}^{n}J_{xy}$	-	A notation for scalar coupling where n is the number of bonds between the two nuclei x and y.
η	-	Denotes the number of atoms of the same element of a ligand, which coordinate to an ion
ν	-	Wavenumbers (cm^{-1})
$P2_1/c$	-	A monoclinic space group containing a c-glide plane and a screw axis
$T_{1,min}$	-	The shortest decay constant (in the z-direction) in NMR spectroscopy measured as a function of temperature

Δ - Heat

$>$ - Greater than

$<$ - Less than

μ - Micro, a prefix in the metric system denoting a factor of 10^{-6}

° - Degrees, a unit of angle

Å - Angstroms, a unit of measure of distance corresponding to 10^{-10} meters

T_{max} - The maximum transmission factor for a crystal studied by X-ray crystallography

T_{min} - The minimum transmission factor for a crystal studied by X-ray crystallography

Θ_{max} - The highest angle at which data was collected on a crystal studied by X-ray crystallography

Σ - Summation

F_o - Observed data collected by X-ray diffraction

F_c - Calculated data pertaining to X-ray diffraction

R_1 - A measure of agreement between a crystallographic model and the data collected given by: $R_1 = \Sigma \, ||F_o|-|F_c|| / \Sigma |F_o|$

wR2 - A measure of agreement between a crystallographic model and the data collected given by: $wR2 = [\Sigma \, (w(F_o^2-F_c^2)/\Sigma(F_o^2)^2]^{1/2}$

Z - The number of asymmetric units in the unit cell of space group

α - The angle between edges b and c of a unit cell

β - The angle between edges c and a of a unit cell

γ - The angle between edges a and b of a unit cell

V - Volume

K - Degrees Kelvin

M - Moles/ liter

List of Abbreviations

Me	-	A methyl (CH_3) group
Pr^i	-	An isopropyl ($CH(CH_3)_2$) group
Et	-	An ethyl (CH_2CH_3) group
Bu^t	-	A *tert*-butyl ($C(CH_3)_3$) group
Cp	-	A cyclopentyl $CH(-CH_2-)_4$ group
Ph	-	A phenyl (C_6H_5) group
Ar	-	An aromatic ring group
C_6F_5	-	A 2,3,4,5,-pentaflourophenyl group
BINAP	-	2,2'-bis(diphenylphosphino)-1,1'-binapthyl)
(*R*,*R*)-DIPAMP	-	(*R*,*R*)-1,2-Bis[(2-methoxyphenyl)(phenylphosphino)]ethane
N-CH_3	-	Methyl substituents at the 2,6-positions of an aromatic ring connected to N
N-Pr^iCH_3	-	Methyl substituent of the isopropyl groups at the 2,6-positions of an aromatic ring connected to N
N-Pr^iCH	-	Methine CH of the isopropyl groups at the 2,6-positions of an aromatic ring connected to N
P-Pr^iCH_3	-	Methyl substituent of the isopropyl groups connected to P
P-Pr^iCH	-	Methine CH of the isopropyl groups connected to P
P-Bu^tCH_3	-	Methyl substituent of the *tert*-butyl groups attached to P
P-Bu^tC		Carbon of the *tert*-butyl groups attached to P
N-C_{imine}	-	The carbon attached to nitrogen by a double bond in the neutral form of the

ligand

N-$C_{enamide}$ - The linker sp^2 carbon attached to N by a single bond which connects the N and P donors of the ligand

N-ArCMe - The 2 and/ or 6 carbon of an aromatic ring decorated with methyl groups connected to N

N-ArCPr^i - The 2 and/ or 6 carbon of an aromatic ring decorated with isopropyl groups connected to N

COE-CH - Olefin CH groups of COE

COD - 1,5-cyclooctadiene

COE - *cis*-cyclooctene

Pr^iOH - isopropanol

Bu^tOH - *tert*-butanol

$KOBu^t$ - Potassium *tert*-butoxide

KHMDS - Potassium bis(trimethylsilyl)amide

cat. - catalyst

atm - A unit of measurement of pressure

Torr - A unit of measure of pressure

mmHg - A unit of measure of pressure

AD - Acceptorless dehydrogenation

NP - A representation of a bidentate ligand with N and P donor atoms

NPN - A representation of a tridentate ligand with two N donor atoms and one P donor atom

PNP	-	A representation of a tridentate ligand with two P donor atoms and one N donor atom
P_2N_2	-	A representation of a tetradentate, macrocyclic ligand where the two P donor atoms are *trans* to one another and the two N donor atoms are *trans* to one another
PNNP	-	A representation of a tetradentate ligand with two P donor atoms and two N donor atoms
LDA	-	Lithium diisopropyl amide
DMP	-	2,6-Dimethyl phenyl substituents on an aromatic ring
DIPP	-	2,6-Diisopropyl phenyl substituents on an aromatic ring
APT	-	Attached Proton Test
HSQC	-	Heteronuclear single quantum coherence
COSY	-	Correlation spectroscopy
HMBC	-	Heteronuclear multiple bond correlation
NMR	-	Nuclear magnetic resonance
ATR	-	Attenuated total reflectance
FTIR	-	Fourier transform infrared spectroscopy
EA	-	Elemental analysis
GC	-	Gas chromatography
MS	-	Mass spectrometry
FID	-	Flame ionization detection
THF	-	Tetrahydrofuran

C_6D_6	-	Deuterated benzene
d_n	-	Deuteration at *n* positions
Et_2O	-	Diethyl ether
equiv.	-	Equivalent based on stoichiometry
Vac.	-	Vacuum
Hz	-	Hertz, (s^{-1})
ppm	-	Parts per million
ORTEP	-	Oak Ridge Thermal Ellipsoid Plot
DFT	-	Density functional theory
dens.	-	Density
o	-	ortho
m	-	meta
p	-	para
sept	-	A septet splitting pattern
m	-	A multiplet splitting pattern
d	-	A doublet splitting pattern
ddd	-	A doublet of doublet of doublet splitting pattern
td	-	A triplet of doublet splitting pattern
br.	-	A broad resonance observed by NMR spectroscopy
HRMS-EI	-	High Resolution Mass Spectrometry - Electron Ionization
(m/z)	-	Mass to charge ratio
Anal.	-	Analysis

Calcd. - Calculated

Acknowledgements

The years at UBC in pursuit of my doctoral thesis have been a transformative experience for me. The numerous individuals I interacted with during my stay have enriched my graduate career with a diversity of ideas, opinions, and cultures.

I would sincerely like to thank Dr. Michael D. Fryzuk for his patient supervision and continuous support as I faced demanding problems in the lab and elsewhere during my graduate degree.

I would like to thank the faculty members at UBC - especially my committee members, Derek Gates, Chris Orvig and Lawrence McIntosh - for generously sharing their insights and advice. In addition, I would like to acknowledge Mark Maclachlan for always being ready with a greeting, joke or smile.

The Chemistry Department staff has been invaluable in both the maintenance of day to day operations in the chemistry department and in addressing my own research questions. In particular, Ken Love has been helpful on a number of occasions regarding glove box and vacuum pump repairs; he is always good for a story or discussion. Maria Ezhova aided in addressing any NMR question and suggested techniques that inspired insights into systems explored in this thesis. Brian Ditchburn can assemble flame sealable NMR tubes faster than anyone I know. He was instrumental in the assembly of a high vacuum line, which I utilized regularly during my time in the Fryzuk lab. I will always admire Milan Choschizza for his ability to fix anything electronic.

My lab mates and fellow D-wing members have greatly enriched my day to day experiences. Brimming with knowledge, ideas, and a passion for teaching chemistry, Joachim Ballmann was influential in my early development as a graduate student. His perseverance and

methodical problem solving skills impressed me as valuable assets for a synthetic chemist. He also went out of his way to be a friend and mentor. Rui Munhá's love of the Fryzuk lab, enthusiasm for silliness, and expert goal-tending skills on the soccer pitch added greatly to my early days the in Fryzuk lab. Conversations with Nathan Halcovitch were always enjoyable and informative. Bryan Shaw's sense of humor enlivened my time in the lab and beyond; his tutorials regarding powder stashes on the ski hill will continue to serve me well. Howard Jong always brought a bit of class to the lab. I appreciated Lee Wence's enthusiasm for a trip to the ski hill or a camping spot. He is a wizard on the Frisbee golf course. The many camping, skiing and surfing trips taken in "the Van" were highlights of my time at UBC and would not have been possible without Fraser Pick and Sonia Brodie; their companionship always made me feel at home. Takahiko Ogawa was a calm presence in the lab. I feel lucky to have gotten to know him during his stay. Tatsuya Suzuki's love of fun and jokes were a welcome addition to my days in the Fryzuk group. Sharing dinner at The Pit before IDG with Nick Hein, Alyssa Yeo and Amanda Zimmerman brightened the week. In addition, I thank Thomas Ostapowicz, Kyle Parker, Vincent Annibale, Lee Wence, Nathan Halcovitch, and Dr. Michael D. Fryzuk for offering much needed help during the writing process.

Outside the lab, many people supported my efforts to pursue a graduate degree. My parents Annie Choate, and Joseph Wambach, as well as my brother Mike and sister Leia have always made me feel loved and supported. My Aunt and Uncle, Susan and Alan Wolf, and Cousin Julian Wolf welcomed me into their home after I completed my undergraduate degree, which allowed me to start my life on the west coast. Elisa, for all of the fun, love, and support you have given me, and all of the wonderful memories we have created together, thank you very much.

Dedication

For Elisa, may there be many adventures to come

Chapter 1: Cooperative Ligand Design for Late Transition Metal Coordination Compounds

1.1 General Introduction

A ligand is a molecule with one or more Lewis basic sites (donors) that can bind to a central atom or ion to form a coordination complex.[1] In general, ligands can affect the reactivity and structure of coordination compounds either by steric effects or the ability to donate or accept electron density from the metal (i.e. electronic effects).[1] Until recently, ligands were designed to be ancillary in nature, in other words, to remain innocent by providing the appropriate steric and electronic environment at the metal center to allow a reaction to occur without getting involved in the actual process.[2]

In the last decade, new types of ligands[3-8] have been discovered that share the steric and electronic flexibility of ancillary or innocent ligands, however they can get involved in the reaction of interest. Such donor sets are referred to as *cooperative ligands* as they can participate in a chemical transformation, for example, a proton can transfer between the ligand and metal, or between the ligand and a substrate.[3,4,7,9-16]

Ligand design in the Fryzuk lab has focused on amide ($^{-}NR_2$)[17] and phosphine (PR_3) donor types separated by a variety of linkers[18-20] into chelating or macrocyclic[21] arrays (Scheme 1.1). Both early and late metal (d^6 or greater valence electron count) coordination complexes have been studied, the original designs were developed to be innocent.[22] However, investigating the reactivity of iridium amide phosphine complexes with dihydrogen (H_2) uncovered an unanticipated reaction in which the ligand is involved in the H_2 activation process.[23,24] Since this discovery, ligands that cooperate with a metal center to activate H_2 have remained an active area

of research in the fields of coordination chemistry and catalysis.[3-8,17,25-28] Of particular interest in this work is an emerging class of cooperative ligand, enamide phosphine ligands (Scheme 1.1). For these scaffolds, the C-C double bond of the linker and/ or the amide donor can potentially react in concert with a metal center during processes such as H_2 activation and/ or catalysis.[3,6] This thesis focuses on synthesis and reactivity of enamide phosphine ligands coordinated to late transition metals and compares their reactivity patterns to other systems highlighted in Sections 1.5-1.7.

Scheme 1.1:

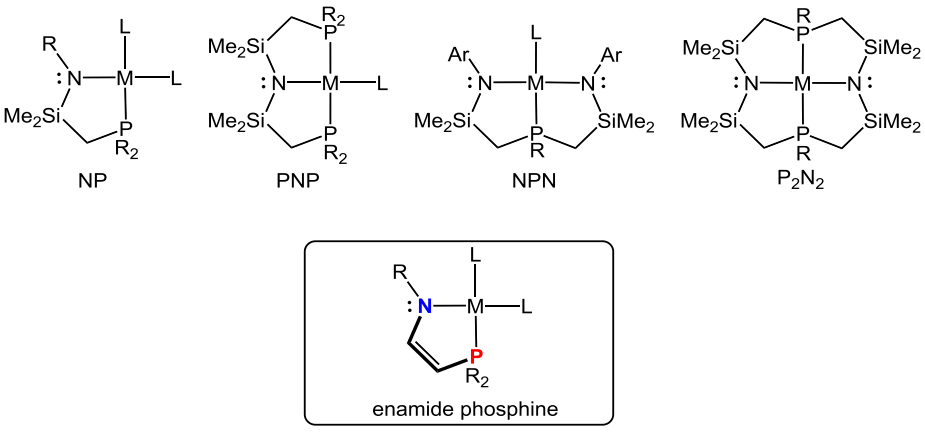

In this introduction, a description of the bonding and reactivity of amide ($^{-}NR_2$) and phosphine (PR_3) ligands coordinated to late transition metals will be described. In addition, examples of ancillary or innocent ligands will be presented to show the difference between these kinds of donor sets and *cooperative ligands*. A perspective on homogeneous hydrogenation catalysis highlights one important application of coordination compounds where both ancillary and cooperative ligands have been used to great effect. Comparing the different reactivity of hydrogenation catalysts generated using these different donor types highlights the degree to which ligand design can dictate coordination compound reactivity. The remainder of the

introduction reviews recent work concerning the stoichiometric and catalytic reactivity of enamide phosphine coordination compounds directly relevant to the research chapters.

1.2 Ancillary Ligands

Phosphines (PR_3) are good examples of ancillary ligands. They act as two electron donors that bind to a metal through σ-donor and π-acceptor interactions (Scheme 1.2), which can be tuned by varying the R groups attached to phosphorus.[1,29] For example, the trialkyl phosphine, PBu^t_3 is a stronger σ-donor than the triaryl phosphine PPh_3.[1] As the σ-donating capacity of a phosphine ligand decreases, the π-accepting ability generally increases; for example, PF_3 is a very weak σ-donor, but an excellent π-acceptor.[1] The interplay of these two bonding interactions makes exchanging the R groups attached to phosphorus a powerful strategy for altering the electronic environment at the metal center. The size or steric demand of phosphine ligands can also be readily modified. Scheme 1.2 presents a graphical depiction of σ-donation, π-back bonding and cone angle (θ), a measure of steric bulk.[1,30]

Scheme 1.2:

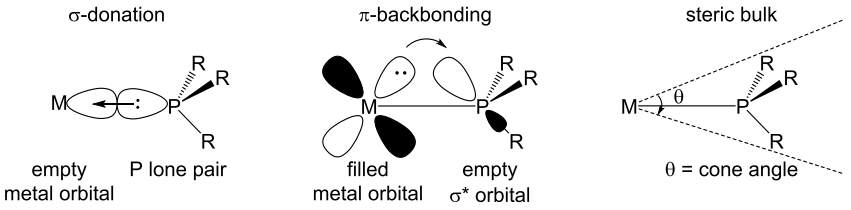

The structure and reactivity late transition metal coordination compounds with neutral phosphine ligands are consistent with the above bonding picture. One example of a common reactivity pattern for certain late transition metal phosphine complexes is oxidative addition.[1] Scheme 1.3 illustrates the oxidative addition of H_2 to a Rh(I) center supported by PPh_3 ligands. Overall, **1.1** converts to **1.4** under dihydrogen; this process occurs by addition of H_2 to the Rh

center, forming two new H^- (hydride) ligands; thus, the formal oxidation state changes from Rh(I) to Rh(III).[31-34] During this reaction, the phosphine ligands can dissociate from the metal, or change orientation with respect to one another; however, only the metal center is directly involved in reactivity with H_2.[31,32,35]

Scheme 1.3:

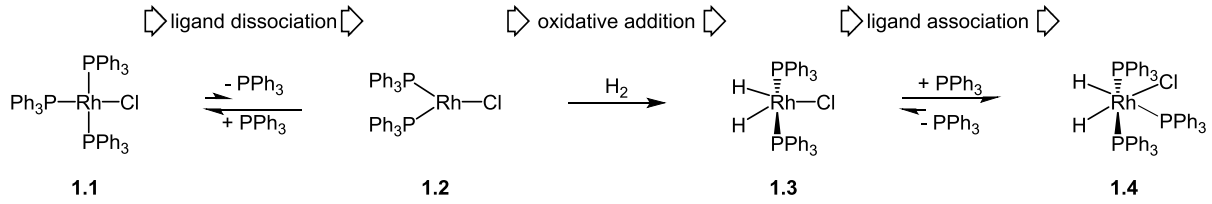

Cooperative ligands react in concert with a metal center to activate chemical bonds such as the σ-bond of H_2.[7] A common feature of many cooperative ligands is the presence of an amide ($^-NR_2$) in the ligand design.[8,17] Amides are anionic nitrogen donors that can supply two or four electrons to a metal.[17] The overall bonding picture of an amide with a transition metal can be described by donation of one lone pair through a coordinate σ-bond, as well as donation of the remaining lone pair from an unhybridized p-orbital of the amide nitrogen into a metal d-orbital of appropriate symmetry (Scheme 1.4).[17,36] For the late metals, because the appropriate d-orbitals are often filled, this latter π interaction is destabilizing.[17,36] The reactivity of simple monodentate amide ligands ($^-NR_2$) coordinated to rhodium is generally consistent with the bonding picture in Scheme 1.4. Some common reactivity patterns include β-hydride elimination/ insertion reactions,[37,38] acid-base reactivity,[39,40] and reactions with electrophiles (S_N2 and E2 reactivity).[41]

Scheme 1.4:

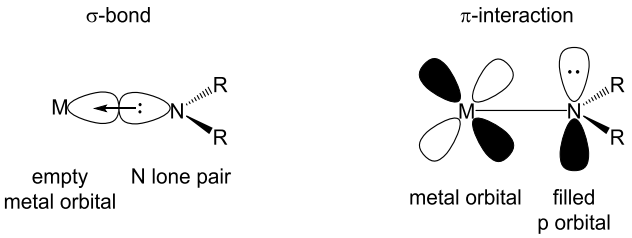

Early synthetic efforts at generating late transition metal amide complexes were initially difficult due to β-hydride elimination reactivity, thus resulting in thermally unstable species.[37,38] An example of a failed attempt to synthesize a late transition metal amide (Scheme 1.5) demonstrates β-hydride elimination, where one of the β-protons from the dimethylamide unit is shuttled to rhodium (**1.6** to **1.7**). In this case, elimination of an imine from the coordination sphere of rhodium occurs along with formation of the rhodium hydride complex $HRh(PPh_3)_3$ (**1.7**).

Scheme 1.5:

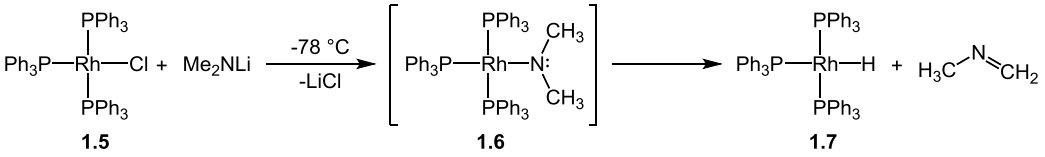

Exchanging the methyl groups for trimethylsilyl groups ($SiMe_3$) eliminates the possibility for β-hydride elimination and allowed for the isolation and full characterization of the first example of a late transition metal amide, **1.9** in Scheme 1.6.[37]

Scheme 1.6:

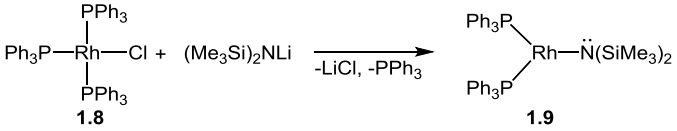

Building on previous synthetic efforts shown in Schemes 1.5 and 1.6, the PNP ligand design in Scheme 1.7 eliminates β-hydride elimination as a possible reaction; furthermore, the phosphine donors tether the amide ligand to late metals such as rhodium and iridium.[42,43] This ligand system allowed for the first systematic investigation of the heterolytic cleavage of H_2, an important example of ligand cooperativity.[23,24,43,44] Before exposure to H_2, the iridium (I) center of **1.10** is coordinated to the anionic PNP ligand and cyclooctene. Upon addition of H_2 and subsequent exposure to vacuum, **1.10** converts into intermediate **1.12** via oxidative addition of dihydrogen.[23,45] During conversion of intermediate **1.12** to the product **1.11**, the amide donor accepts a proton (H^+), and the iridium center binds a hydride (H^-). Both the amide moiety and metal are functionalized during addition of the second equivalent of H_2,[23] which is an example of ligand cooperativity.

In this work, cooperative ligand reactivity is categorized based on the site of the ligand that reacts. Scheme 1.7 illustrates an example of *donor reactivity* as the amide donor participates in the H_2 activation process. *Linker reactivity* is the alternative to donor reactivity and is discussed in Section 1.5. These concepts are important, as they are relevant to the cooperative reactivity of enamide phosphine ligands explored in the research chapters.

Scheme 1.7:

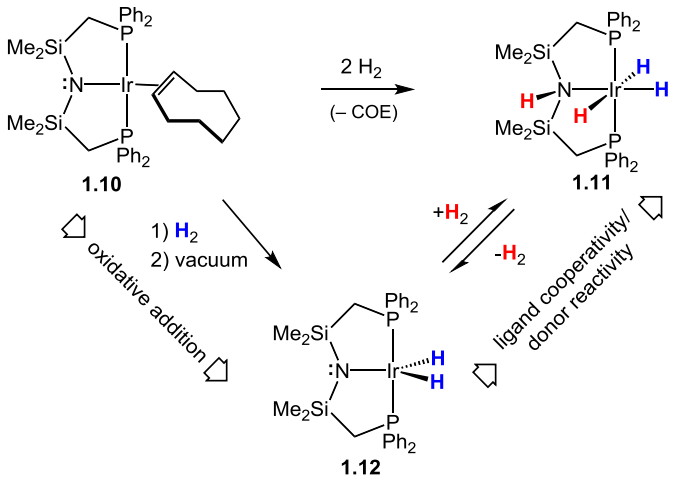

1.3 Ancillary and Cooperative Ligands in Homogeneous Hydrogenation Catalysis

One major achievement in synthetic chemistry is the development of industrial homogeneous hydrogenation processes for olefins and ketones.[10,46] These two catalytic processes can involve very different types of ligand-metal combinations.[47,48] For example, ancillary phosphine ligands are an important feature of the catalyst precursors for olefin hydrogenation.[48] Metal-based processes such as oxidative addition of H_2 generate the catalytically active species.[31-34] Ruthenium compounds with chelating diamine ligands form active catalysts for ketone hydrogenation,[10,49,50] heterolytic cleavage of H_2 and donor reactivity are important features of these systems.[51,52] Discussion of olefin and ketone hydrogenation below highlights the importance ancillary phosphine and cooperative diamine ligands to industrially relevent catalystic reactions.

One example of olefin hydrogenation is the industrial production of L-DOPA, an amino acid used for treatment of Parkinson's disease.[46] The design of chiral diphosphine ligands led to an industrial scale process for this important pharmaceutical.[31,46,53-57] As shown in Figure 1.1, DIPAMP is a chiral bidentate phosphine ligand that upon combination with a suitable Rh starting

material forms an efficient, enantioselective catalyst system for the homogeneous asymmetric hydrogenation of enamides.[56]

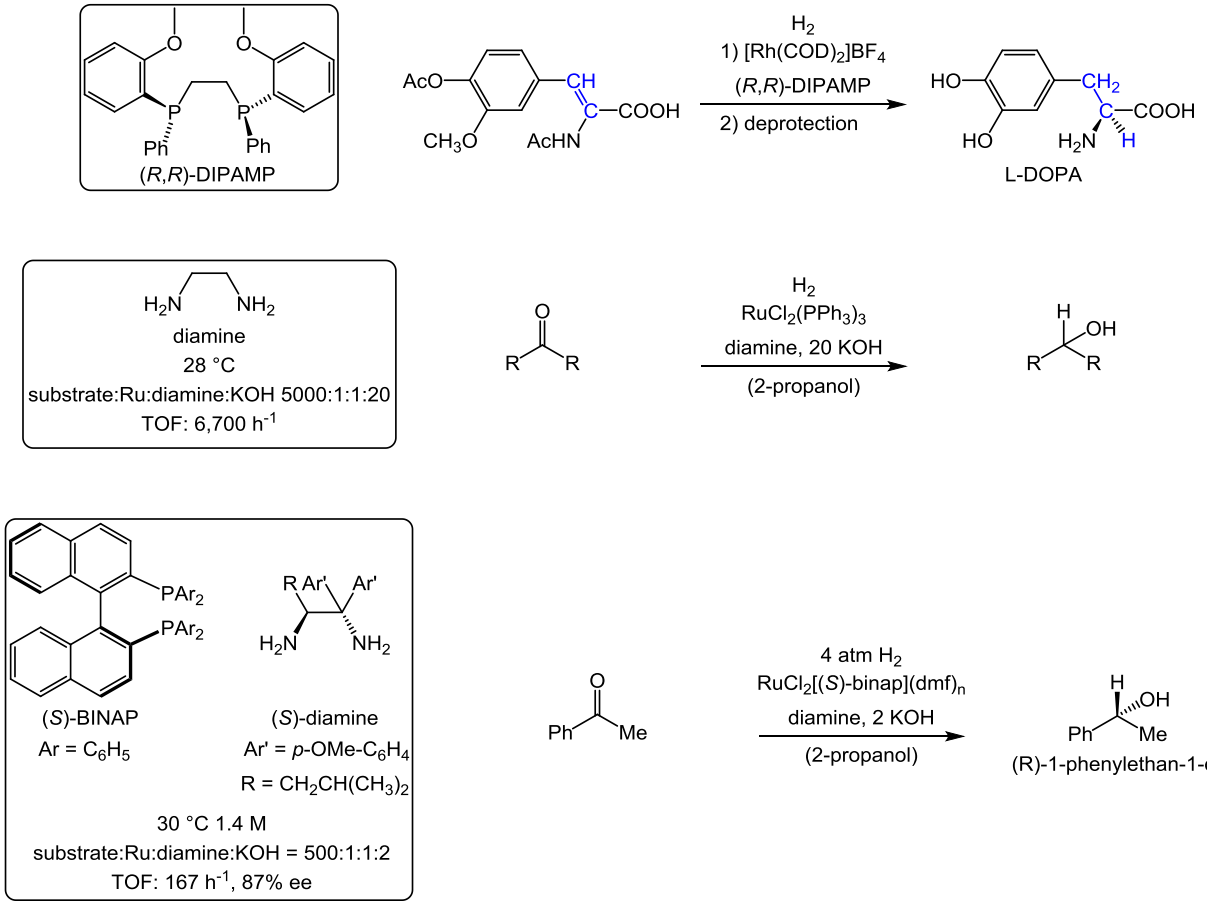

Figure 1.1: A graphical illustration of changes in ligand design as a function of synthetic goal. The upper left highlights a chiral diphosphine ligand for the enantioselective hydrogenation of olefins. In the middle, a neutral diamine ligand forms an active ketone hydrogenation catalyst *in situ*. At the bottom, an enantioselective catalyst for ketone hydrogenation combines a bidentate chiral phosphine with a chiral diamine.

An entirely different type of ligand is beneficial for Ru-based catalytic hydrogenation of ketones. Initial attempts to make a catalyst for this reaction focused on neutral phosphine ligand designs coordinated to rhodium and iridium, a logical choice given their widespread use in systems for homogeneous hydrogenation of olefins.[48] Chiral diphosphine ligands similar to DIPAMP gave modest success;[58-62] however, addition of diamine ligands to otherwise sluggish

Ru phosphine catalysts provided the real breakthrough (Figure 1.1).[10,49,50] An additional aspect of these systems is use of an (*S*)-diamine paired with the axially chiral neutral phosphine, (*S*)-BINAP, forms a ruthenium catalyst capable of high activity and excellent enantioselectivity.[49] These features make Ru ketone hydrogenation catalysts useful for synthesis of a variety of important chemicals on an industrial scale.[10]

At the time of discovery these highly active Ru catalysts were ill-defined, however, the active catalyst was later identified,[50] and mechanistic investigations revealed a new type of reactivity that explains the beneficial influence that diamine ligands have on ketone hydrogenation.[51,52] Deprotonation of one of the diamine donors generates a ruthenium amide bond *in situ* (**1.13**).[51,52] **1.13** activates hydrogen for addition to a substrate by heterolytic cleavage of the H-H σ-bond to generate **1.14**.[51,52] A proton from H_2 transfers to an N donor of the ligand (*donor reactivity*) the hydride from H_2 coordinates to ruthenium.[51,52] After H_2 activation, **1.14** transfers an equivalent of H_2 to a polar substrate in the outer coordination sphere of the metal (Scheme 1.8).[51,52] Donor reactivity is a key feature of the reaction with dihydrogen (**1.13** to **1.14**) and the reaction with substrate (**1.14** to **1.13**), which highlights the importance of ligand cooperativity for homogeneous hydrogenation of ketones using **1.13**.

Scheme 1.8:

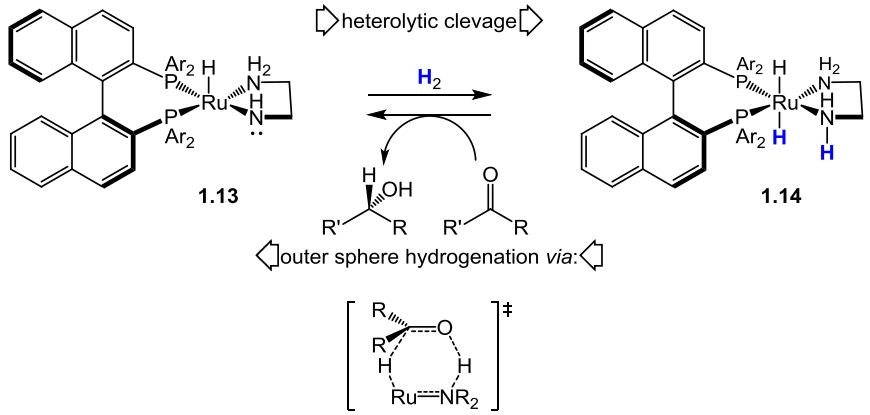

1.4 Linker Reactivity

As mentioned above, another kind of cooperative ligand is one that displays linker reactivity,[3,5] which is defined as a system where a remote site of the ligand becomes involved in a reaction. A PNP ligand design that utilizes -CH_2- linkers (Scheme 1.9) participates in a variety of cooperative ligand reactions. Both the donor and linker of the ligand are reactive. Prior to discussion of an example of linker reactivity using this -CH_2- linked PNP design, it is worth highlighting three differences between the donor reactive -$SiMe_2$- design and the -CH_2- linked design of interest in this section. The first is that the -$SiMe_2$- groups are sterically more demanding than -CH_2- groups; secondly, the $(CH_2)_2N$ unit is more electron rich than the $(SiMe_2)_2N$ unit is.[63,64] The final difference is that the -CH_2- groups that flank the amide unit are susceptible to β-hydride elimination, which is a key factor in the linker reactivity of these systems.[65] These differences have a profound impact on the electronic structure and reactivity of the late transition metal complexes that feature these ligands.

Scheme 1.9:

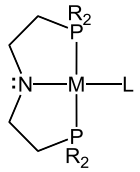

PNP

The synthesis of low coordinate Ru(II) chloride complexes with both ligand types highlights some of the differences between the -$SiMe_2$- linked and -CH_2- linked scaffolds. The anionic ligand with a -$SiMe_2$- linker reacts with $[(cymene)RuCl_2]_2$ to form **1.15**, which is stable at room temperature and paramagnetic (Scheme 1.10).[66]

Scheme 1.10:

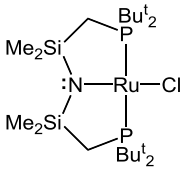

1.15

For the aliphatic analog, interestingly, deprotonation of the neutral ligand of complex **1.16** at -78 °C forms a diamagnetic complex (**1.17**). The difference in spin state from **1.15** to **1.17** is attributed to the different donor properties of the amide unit in each ligand design.[63] At room temperature in solution, **1.17** is prone to β-hydride elimination, this process transforms the ligand from being an anionic amide donor to a neutral imine donor (**1.17** to **1.18**).[63] In the context of ligand cooperativity, β-hydride elimination, in this example, demonstrates one form of linker reactivity.

Scheme 1.11:

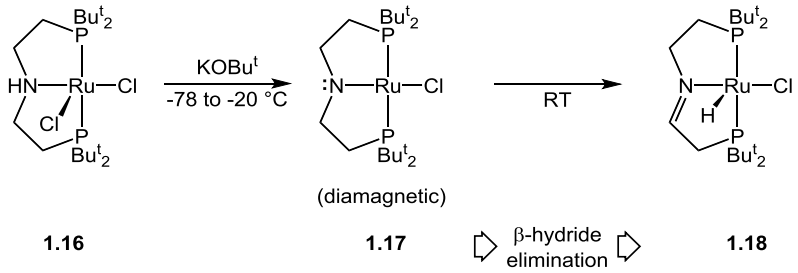

1.16 **1.17** **1.18**

There are additional linker reactivity patterns beyond β-hydride elimination where the -CH_2- protons of the ligand become involved. The conversion of **1.19** to **1.20** after addition of excess KOBu^t is one example. During this transformation, two equivalents of HCl are lost and a new hydride that presumably originates from the backbone of the ligand is coordinated to ruthenium (Scheme 1.12).

Scheme 1.12:

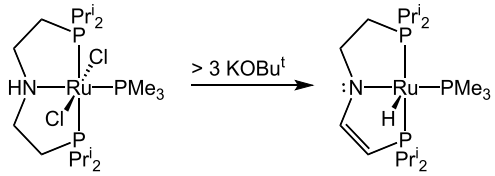

In a related transformation, complex **1.20** reacts with dihydrogen by a complex series of transformations (Scheme 1.13). Two equivalents of H_2 are added to **1.20** to form **1.23**, the first equivalent is used to hydrogenate the C=C double bond present in the linker of the ligand (**1.20** to **1.22**), the other adds across the ruthenium amide bond (**1.22** to **1.23**).[65,67] Computational evidence, supported by deuterium labeling studies, suggests that direct proton transfer from dihydrogen coordinated to ruthenium to the linker of the ligand forms **1.21**. This initial step in dihydrogen addition to the enamide phosphine double bond is the highest energy process of the overall reaction (26.7 kcal/mol relative to **1.20**).[65] While related to the heterolytic addition of H_2 across a late transition metal-amide bond, protonation of a remote site on the ligand is a different and important example of linker reactivity.[65]

Scheme 1.13:

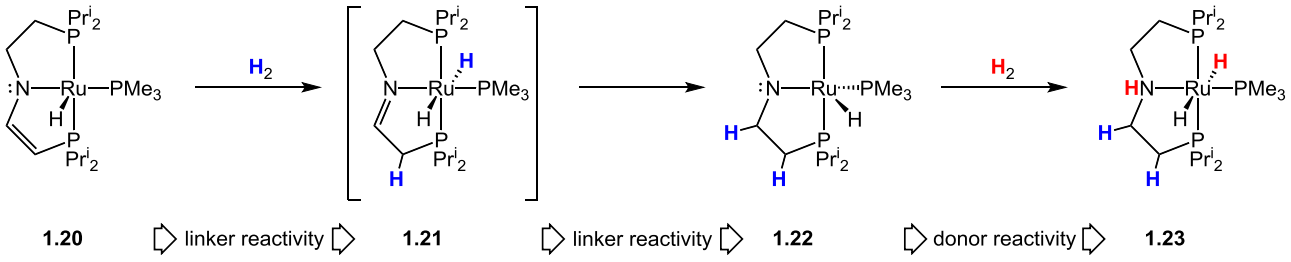

Numerous complexes that pair Os,[68-70] Ir,[71,72] Fe[73] or Ru[70,74,75] with multidentate PNP or PNN ligands utilize aliphatic linkers and are catalysts for hydrogenation and dehydrogenation of polar functional groups. The conditions used to generate an active catalyst for these processes

are similar to the stoichiometric reactions above; an excess of a base such as $KOBu^t$ generates the active species. In light of the stoichiometric cooperative ligand reactivity for both enamide phosphine and amide-phosphine ligands, which can interconvert in the presence of base and hydrogen, the catalytically active species involved in these reactions is unclear at this point. However, the mechanism likely involves some form of cooperativity.

Reactive, low spin, Fe(II) complexes, coordinated by aliphatic tridentate[73] and tetra dentate ligands are of interest as they are successful examples of recent efforts to carry out catalytic transformations using cheap abundant metals.[73,76-84] Catalytic transfer hydrogenation uses an alcohol, usually isopropanol, as the dihydrogen source. It is an excellent way of generating chiral alcohols (equation 1.1).[11,85,86] Ongoing efforts to optimize transfer hydrogenation using Fe catalysts have identified some intriguing cooperative ligand reactivity patterns for a PNNP system (**1.24**).

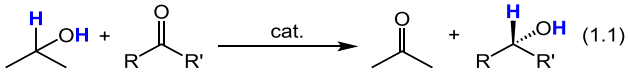

(1.1)

The iron coordination complex **1.24** is an extremely active, enantioselective catalyst for the transfer hydrogenation of ketones (Scheme 1.14).[84] In initial reports, cationic Fe precatalysts treated with base generated the active catalyst *in situ*; these conditions showed promising results for transfer hydrogenation catalysis.[77,79] Kinetics,[83] computations,[82] reactivity studies with isopropanol, and quenching catalytic reactions with strong acid (HCl)[81] aided in identifying **1.24** as the likely catalytically active species. **1.24** was then synthesized and successfully applied to catalysis.[84]

Scheme 1.14

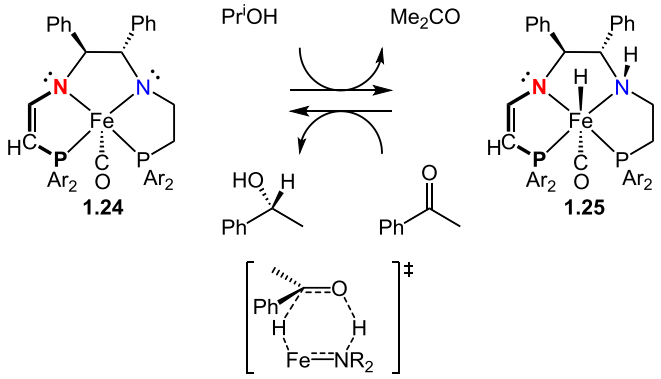

Interestingly, **1.24** has three potentially cooperative sites capable of accepting a proton from isopropanol. The enamide phosphine unit could participate in donor reactivity at either the enamide nitrogen (red), or the linker methine attached to phosphorus (black CH). Another possible reactive site is the amide donor (blue). Multinuclear NMR studies[84] and computational evidence[82] suggest a proton is transferred to the amide nitrogen to form **1.25**. Treating **1.25** with 1-phenyl ethanol, (a common transfer hydrogenation substrate) reforms **1.24**, which strongly suggests that **1.24** and **1.25** are the catalytically active species.[84] The proposed transition state is shown in Scheme 1.14 to highlight the importance of donor reactivity. It is remarkable that three potentially cooperative sites exist in the same molecule, all are necessary for optimum catalytic performance; however, only donor reactivity involving the amide nitrogen is directly involved in catalysis. Under more acidic conditions, such as the addition of excess HCl, both the amide and methine sites of the ligand are protonated (Scheme 1.15).[84]

Scheme 1.15:

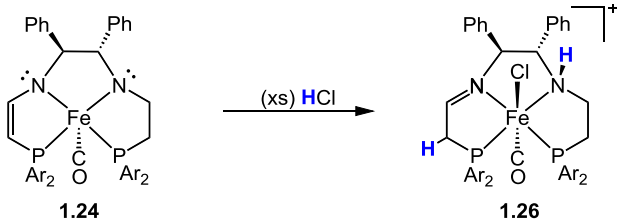

1.5 Dearomatized Ligands

A different cooperative ligand incorporates a pyridine ring into a pincer ligand scaffold. In contrast to the PNP pincer ligands where sp^3 hybridized -$SiMe_2$- and -CH_2- groups flank the amide donor; in this design sp^2 hybridized carbons of a pyridine ring occupy the position adjacent to the central nitrogen donor. While the convention used in this work is to exclude the formal charge of atoms in a ligand, two resonance forms illustrated in Scheme 1.16 break this convention to show the delocalized nature of the negative formal charge. Early discussion of the bonding of this ligand to palladium and platinum suggests that the dearomatized structure (**1.27**) or a delocalized, sp^2 hybridized carbanion (**1.28**) are most consistent with bond lengths and angles observed in the solid state.[87] Subsequent studies favor the dearomatized resonance form (**1.27**) that is used for the remainder of this work.[3,88]

Scheme 1.16:

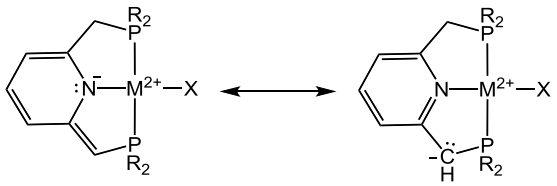

1.27 M = Pd, Pt **1.28**

One remarkable feature of these pyridine-based ligands is that linker reactivity is a prominent feature of a diverse library of coordination compounds generated using the above or similar scaffolds. For example, PNN,[89,90] CNN,[90,91] and PNS[92] designs exchange a phosphine donor present in **1.27** for another donor (nitrogen, carbon or sulfur). In every case, the linker of the ligand becomes involved in the reactivity. Likewise, coordination of this ligand architecture to a variety of late transition metals, for example cobalt,[93,94] rhodium,[95,96] iridium,[97-99] nickel,[100] palladium,[87] platinum,[87,101] iron,[102,103] and ruthenium[89,104-107] generates coordination compounds that participate in linker reactivity.

Scheme 1.17 depicts two coordination compounds. Notably, a PNN ligand design is bound to ruthenium in each case. The reaction occurring when **1.29** reacts to form **1.30**, overall, results in the heterolytic cleavage of dihydrogen. Analogous to the initial example used to introduce linker reactivity in Scheme 1.13, a proton shuttles to the linker of the ligand and the hydride binds to Ru.[89,104] Computational evidence supports that this reaction occurs in a single step.[108-111] Related studies show electrophiles such as CO_2, formaldehyde, and ketones react with the linker of the ligand.[107,112-114]

Scheme 1.17:

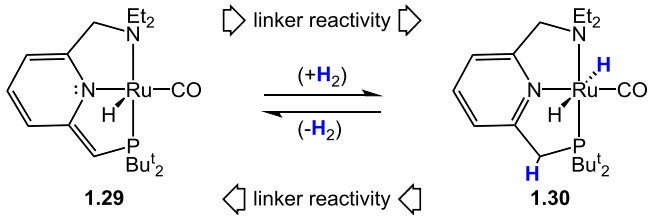

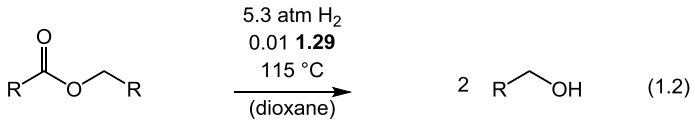

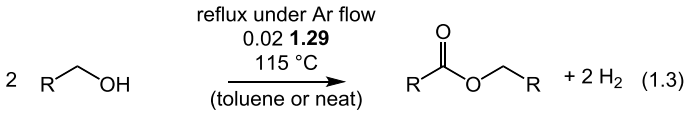

Ruthenium-based systems similar to **1.29** catalyze a variety of transformations. The ability of these compounds to reversibly add and lose H_2 as a function of reaction conditions allows them to act as both hydrogenation and dehydrogenation catalysts. For example, **1.29** is a catalyst for addition of dihydrogen to substrates such as esters (equation 1.2),[104] as well as the reverse reaction, acceptorless dehydrogenation (AD) of primary alcohols to form esters (equation 1.3).[89] From a synthetic perspective, equations 1.2 and 1.3 are attractive alternatives to traditional methodologies that generate stoichiometric amounts of waste along with the product.[6]

From an application-based perspective, coupling hydrogenation and AD reactivity into a single catalyst could lead to new methods for storing hydrogen.[6] For example, recently, efforts directed at chemically storing H_2 have identified ammonia borane as a desirable medium.[67,115-119] Unfortunately, while ammonia borane is an attractive compound for storing hydrogen from certain perspectives, the AD reaction for ammonia borane is not reversible.[119] Thus, exploring different substrate-catalyst systems, which allow for reversible H_2 release, is one way to improve on the state of the art.

Of particular interest in this work is the acceptorless dehydrogenation (AD) of primary alcohols. Once an active catalyst for primary alcohol AD is available, varieties of different reactivity patterns become accessible.[6] Figure 1.2 highlights the importance of primary alcohol oxidation via H_2 release for a selection of reactions. Changes to the sterics and electronics of the pyridine ligand scaffold influence the product formed during catalysis. For example, **1.29** is a catalyst for formation of amides from primary alcohols and amines,[120] **1.31** forms imines under similar conditions.[121]

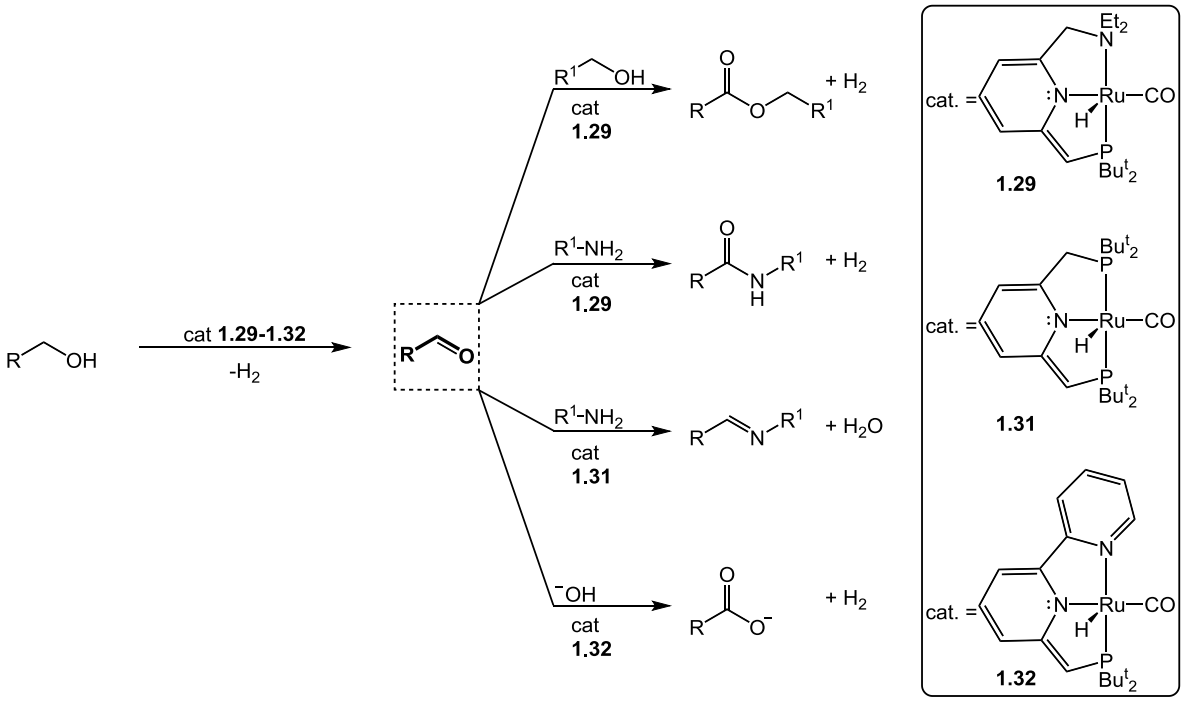

Figure 1.2: A selection of AD reactions catalyzed by ruthenium pincer complexes.

1.6 Scope of Thesis

In the above introduction, coordination compounds that participate in linker reactivity all employ ligands that incorporate the enamide phosphine motif, which is an anionic nitrogen donor (blue) linked to a phosphine donor (red) by a carbon-carbon double bond, highlighted in bold in Scheme 1.18.

Scheme 1.18:

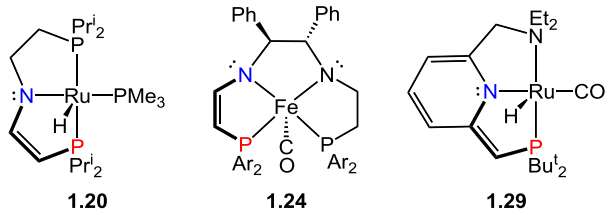

For the pyridine based systems an enamide phosphine forms when the -CH_2- linker loses a proton and the pyridine ring dearomatizes; this unit can reversibly accept and release protons from dihydrogen as shown in Scheme 1.19 (equation 1.4). To simplify this system, just the

enamide phosphine unit is included in the ligand designs explored in this work. The route used to generate the enamide phosphine group is synthesis of imine phosphine scaffolds that can tautomerize to enamine phosphine systems (equation 1.5). Deprotonation of the mixture of imine or enamine tautomers of these neutral ligands, and coordination to a late transition metal allows investigation of the cooperative reactivity of these systems. Once a late transition metal enamide phosphine coordination complex is made, it is probed with stoichiometric and catalytic reactions for behavior that is consistent with ligand cooperativity. For example, the enamide phosphine scaffold can reversibly add dihydrogen to generate an imine phosphine metal hydride (*linker reactivity*) or the enamine phosphine metal hydride (*donor reactivity*) (equation 1.6).

Scheme 1.19:

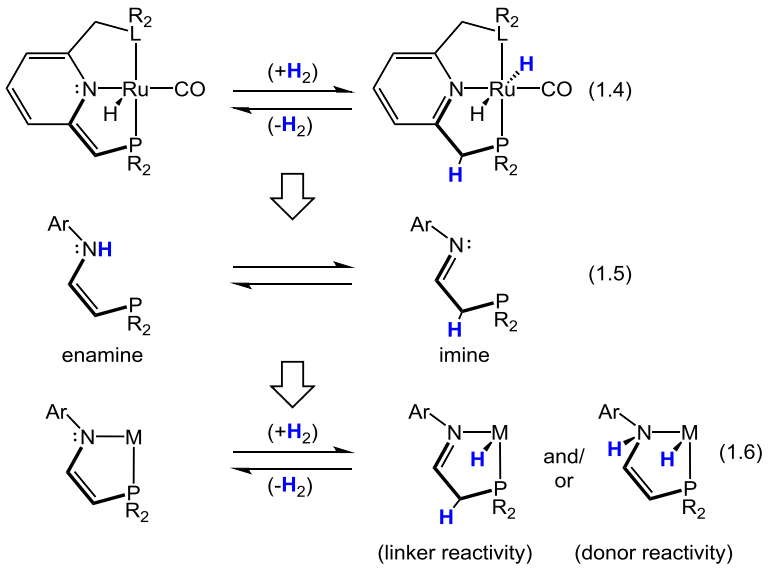

In Chapter 2, a tridentate NPN diimine phosphine ligand design is explored that displays complex solution behavior due to tautomerization when not coordinated to a metal. Coordination of this ligand to Rh(I) forms a single compound that undergoes reactivity with hydrogen, carbon monoxide and dichloromethane. Solid state molecular structures of a variety of Rh(I) and Rh(III) coordination compounds establish the neutral NPN ligand scaffold prefers

the diimine tautomeric form upon coordination to Rh(I) or Rh(III). Bidentate coordination is preferred for Rh(I) and tridentate coordination is preferred for Rh(III). Treating these complexes with base generates ill-defined mixtures of products.

In Chapter 3, a bidentate enamide phosphine ligand is coordinated to Ir(I). This complex is a starting point for exploring cooperative ligand chemistry. Reactivity with $Pr^{i}OH$ and H_2 show the enamide phosphine unit participates in linker reactivity. Further reactivity with primary alcohols and CO demonstrate protonation of the linker position of the ligand is a reversible process and is a function of the electronic environment at Ir. Close examination of the mechanism of linker reactivity with multinuclear NMR studies combined with ^{13}C labeling experiments identify intermediates involved in H_2 addition and loss. Based on these studies oxidative addition/ reductive elimination, N donor dissociation and tautomerization are proposed as key features of the mechanism.

Chapter 4 extends the work done with bidentate enamide phosphine ligands from Ir to Ru(II). These Ru complexes are able to reversibly add and release hydrogen by storing a proton from H_2 or $Pr^{i}OH$ at the linker position of the ligand. Multinuclear NMR and deuterium labeling studies suggest tautomerization is involved in shuttling a proton from dihydrogen between the donor and linker of the ligand. In addition to stoichiometric reactions with hydrogen, some limited catalytic AD reactions are explored. In the final research chapter, Chapter 5, a new enamide phosphine PNN ligand design coordinated to Ru(II) generates catalyst systems for AD of benzyl alcohol to form benzyl benzoate. Chapter 6 presents a brief summary of this thesis and suggests potential directions for future research efforts.

Chapter 2: Characterization and Coordination Chemistry of Diimine Phosphine Ligands with Rhodium

2.1 Introduction

As discussed briefly in Section 1.1 of Chapter 1, amidophosphine hybrid ligands are multidentate scaffolds that incorporate hard amido ($^{-}NR_2$) and soft phosphine donors (PR_3) in various permutations.[19,122-129] A variety of combinations with -CH_2SiMe_2- linking units, as shown in Scheme 2.1 have been previously explored by the Fryzuk lab.

Scheme 2.1:

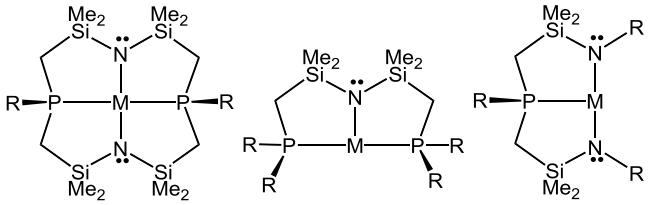

Depending on the charge of the ligand donor set a variety of oxidation states and coordination geometries can be accessed. Of recent interest in the Fryzuk lab are the diamidophosphine arrays (NPN), which have shown rich chemistry in small molecule activation.[122,130-138] Previously explored NPN derivatives with different linker units ranging from the original -CH_2SiMe_2- to *o*-phenylene[18,125] and 2,3-thiophene[19] are shown in Scheme 2.2 along with the cyclopentylidene linked scaffold explored in this chapter.

Scheme 2.2:

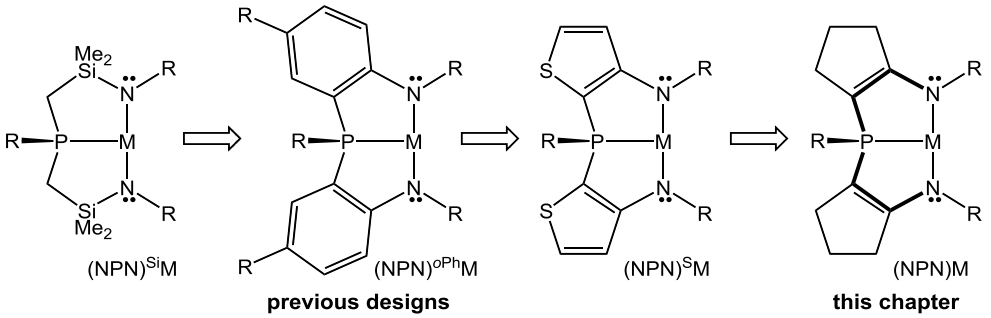

The scaffolds in Scheme 2.2 avoid the kinetically labile Si-N bond[137] found in $(NPN)^{Si}$ and opt for a robust linker composed of sp^2 carbons.[18,125] The previously mentioned *o*-phenylene linked system $(NPN)^{oPh}$, and $(NPN)^{S}$ use Hartwig-Buchwald aryl amination procedures to generate the C-N bond present in each ligand design.[19,125] The use of condensation chemistry to generate the C-N bond of **2.1a,b**, simplifies the ligand synthesis in comparison to $(NPN)^{oPh}$ and $(NPN)^{S}$. Incorporating a cyclopentylidene ring into the linker of the ligand ensures the imine and phosphine donors remain *syn* to one another.

Despite the straight forward synthetic protocol, which yields pure material consistent with cyclopentyl linked (NPN) diimine phosphine ligands (*vide infra*); characterization of these scaffolds was complicated by observation of a variety of isomers corresponding to **2.1a,b**. Treating these mixtures with $Zr(NMe_2)_4$ results in conversion to a single product corresponding to the *bis*-enamide phosphine form of the ligand coordinated to zirconium (**2.2a,b**, Scheme 2.3).[20] Isolation and full characterization **2.2a,b** occurred prior to the work reported in this chapter and is important as it shows cyclopentyl linked imine phosphine ligands (**2.1a,b**) are precursors to the enamide phosphine scaffold of interst in this work.

Scheme 2.3:

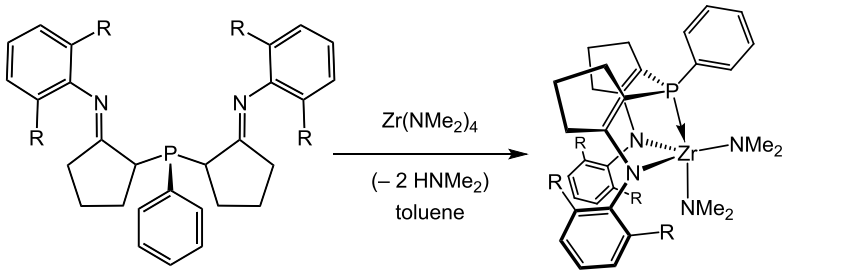

2.1a R = Me, $(NPN)^{DMP}H_2$
2.1b R = Pr^i, $(NPN)^{DIPP}H_2$
mixture of tautomers

2.2a R = Me, $Zr\{(NPN)^{DMP}\}(NMe_2)_2$
2.2b R = Pr^i, $Zr\{(NPN)^{DIPP}\}(NMe_2)_2$

In this chapter, multinuclear NMR studies allow for identification of a variety of tautomers and stereoisomers involved in the complex solution behavior of **2.1a**. The coordination chemistry of **2.1a** and **2.1b** with rhodium is explored. These studies reveal that despite the presence of numerous isomers of **2.1a,b** in the absence of a metal, upon coordination to rhodium, a single isomer of the ligand is favored. The observations recorded in this chapter inspired the exploration of cyclopentyl linked enamide phosphine ligands reported in subsequent chapters for ligand cooperativity.

2.2 Characterization of Diimine Phosphine Ligands in the Solid State and Solution

The tridentate ligands **2.1a,b** are assembled by a straightforward synthetic protocol in moderate yield (Scheme 2.4).[139,140] Reacting either cyclopentylidene-2,6-dimethylaniline or cyclopentylidene-2,6-diisopropylaniline with lithium diisopropylamide (LDA) at low temperature followed by quenching with 0.5 equivalents of dichlorophenylphosphine generates the tridentate diimine phosphine derivatives. The original literature preparation[139] describes the synthesis of bidentate (NP) ligands, and reports the use of n-butyl lithium as the preferred method of generating the enamide via deprotonation of an α-methylene proton of the cyclopentylidene ring. However, it was found that this method was not reliable for the synthesis

of **2.1a** and **2.1b**; therefore, the LDA deprotonation protocol was used instead. The abbreviation NPN represents the three Lewis basic donors of the tridentate ligand scaffold, superscripted DMP or DIPP outside of the brackets denote the R groups at the 2 and 6 positions of the *N*-aryl moiety; for example, DMP corresponds to 2,6-dimethyl and DIPP corresponds to 2,6 diisopropyl groups.

Scheme 2.4:

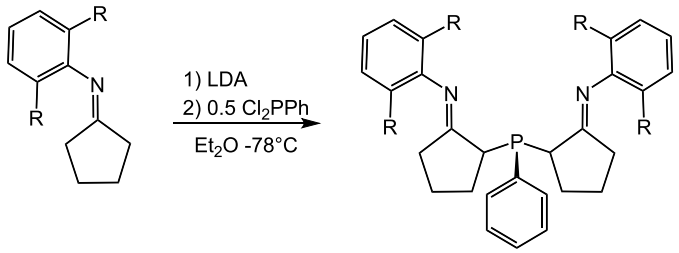

2.1a R = Me, $(NPN)^{DMP}H_2$
2.1b R = Pr^i, $(NPN)^{DIPP}H_2$

From the ligand synthesis, one could isolate oily yellow materials that were mixtures of products. For both **2.1a** and **2.1b**, five singlets were initially observed in the $^{31}P\{^1H\}$ NMR spectrum corresponding to five different species in variable amounts. Purification of these oily mixtures by precipitation from a pentane solution generates pure solids. In the case of **2.1a**, depending on the workup, the solid could be either a mixture of five species in similar amounts to the crude oily mixture or just one pure compound. For **2.1b**, a single compound assigned to a $^{31}P\{^1H\}$ NMR signal at δ -8.8 was isolated as a powder in moderate yield and identified as the diiminophosphine ligand by ^1H NMR spectroscopy, mass spectrometry, and elemental analysis. Inspection of the multinuclear NMR spectra of this material suggests it corresponds to the diimine tautomer of **2.1b**. For example, a ^1H-^{13}C HSQC NMR spectrum shows cross correlations between every ^1H NMR signal and a ^{13}C resonance. Definitive assignment of the solution structure of **2.1b** as the *meso*-diimine stereoisomer was possible, as the two α-CH

protons of the ligand appear as a single resonance in the ^{1}H NMR spectrum, consistent with relation of these two nuclei by an internal mirror plane of symmetry (*vide infra*). X-ray analysis confirms this result.

The solid state structural data for **2.1a** and **2.1b** represent one of the many species formed during the ligand synthesis. There is a short contact, perhaps due to hydrogen bonding between the α-CH bond and the distal imine nitrogen (H7 ⋯ N1, 2.55(3) Å) in the solid state molecular structure of **2.1a**. This feature is not present in **2.1b**, possibly due to the increased steric bulk of the 2,6-diisopropyl groups on the *N*-arylimine arms, which precludes a conformation that orients the imine nitrogen atoms toward those particular α protons. All of the relevant bond lengths and angles for both **2.1a** and **2.1b** are consistent with the diimine tautomeric form of the ligand.

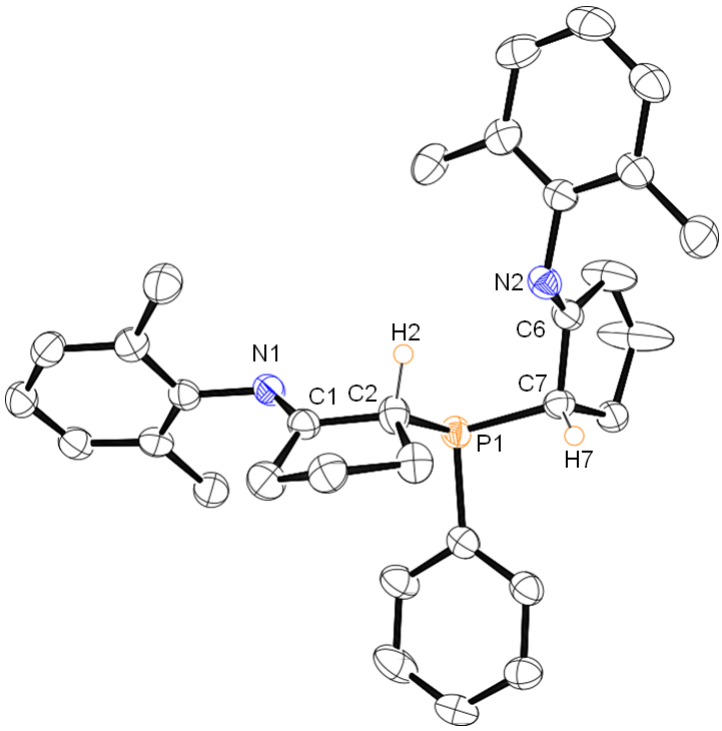

Figure 2.1: ORTEP drawing of the solid state molecular structure of the (SrR)-*meso*-diimine form of **2.1a** with probability ellipsoids at 50%. The hydrogen atoms are omitted for clarity except for H2 and H7, the positions of these hydrogen atoms were determined from the difference map. Selected bond lengths (Å) and bond angles (°):

N1-C1 1.2767(4), C1-C2 1.5074(3), C2-P1 1.8509(7), P1-C7 1.8535(5), C7-C6 1.4887(5), C6-N2 1.2731(4), N1-C1-C2 122.7(2), C2-P1-C7 102.52(13), P1-C7-C6 114.16(19), C7-C6-N2 122.9(3).

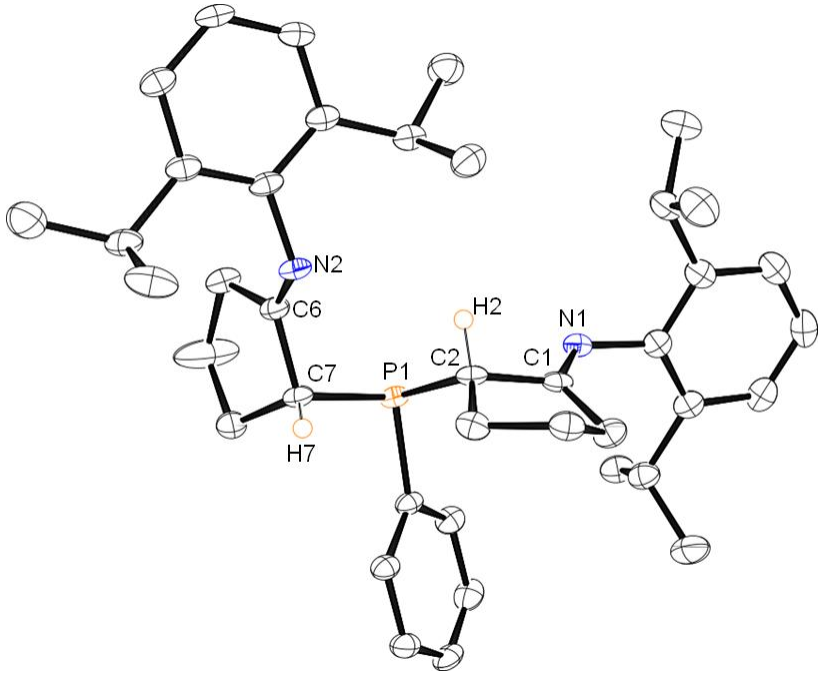

Figure 2.2: ORTEP drawing of the solid state molecular structure of the (SrR)-*meso*-diimine form of **2.1b** with probability ellipsoids at 50%. The hydrogen atoms are omitted for clarity except for H2 and H7, the positions of these hydrogen atoms were determined from the difference map. Selected bond lengths (Å) and bond angles (°): N1-C1 1.280(3), C1-C2 1.529(3), C2-P1 1.887(2), P1-C7 1.883(2), C7-C6 1.535(3), C6-N2 1.283(3), N1-C1-C2 122.5(2), C2-P1-C7 101.42(9), P1-C7-C6 113.3(1), C7-C6-N2 122.5(2).

The original ligand synthesis for the bidentate relative of this NPN ligand framework reports a tautomeric equilibrium between the two forms of the ligand.[139,140] In addition to multiple tautomeric forms, for the tridentate NPN analogue, there are several stereoisomers possible depending on the tautomeric form the ligand has adopted. In total, this ligand system can adopt six possible forms illustrated below in Figure 2.3. Dissolution of solid samples of **2.1a** isolated from pentane in C_6D_6 showed five resonances in the $^{31}P\{^1H\}$ NMR spectrum at δ -5.6 (28%), -6.0 (6%), -8.5 (47%), -32.1 (6%) and -36.7 (13%). The integration values of each

resonance vary slightly depending on conditions, however, the major resonance always occurs at δ -8.5. By use of a series of multinuclear NMR experiments, these resonances could be identified and assigned. Figure 2.4 depicts the ^{1}H-^{31}P HMBC NMR spectrum of the mixture and shows that the major singlet at δ -8.5 only correlates to a triplet at δ 3.9 in the ^{1}H NMR spectrum. The other two peaks in this region of the $^{31}P\{^{1}H\}$ NMR spectrum (i.e. at δ -5.6 and -6.0) also correlate to signals between δ 3.6 and 5.0 in the ^{1}H NMR spectrum. As will be shown below, these ^{1}H NMR peaks are due to the α protons next to the phosphine in the cyclopentyl substituent, and are assigned to the *rac* and two *meso* forms of the diimine tautomer. Another set of resonances in the $^{31}P\{^{1}H\}$ NMR spectrum are the upfield peaks at δ -32.1 and -36.7. Using ^{1}H-^{31}P HMBC NMR spectroscopy, these two resonances correlate with two small doublets between δ 6.2 and 6.6, as well as the α protons in the CH region of the ^{1}H NMR spectrum. The two small doublets (J_{NP} ~ 4-6 Hz) at δ 6.2 and 6.6 arise from NH protons of the enamine-imine tautomers of the ligand. This was confirmed using a ^{1}H-^{13}C HSQC NMR experiment that showed no correlation of these two doublets with any carbon resonances in the ^{13}C APT NMR spectrum. Thus, the two upfield singlets in the ^{31}P NMR spectrum (δ -32.1 and -36.7) are due to enamine-imine tautomers. Two diastereomers result from the stereogenic phosphorus and carbon centers in this tautomeric form.

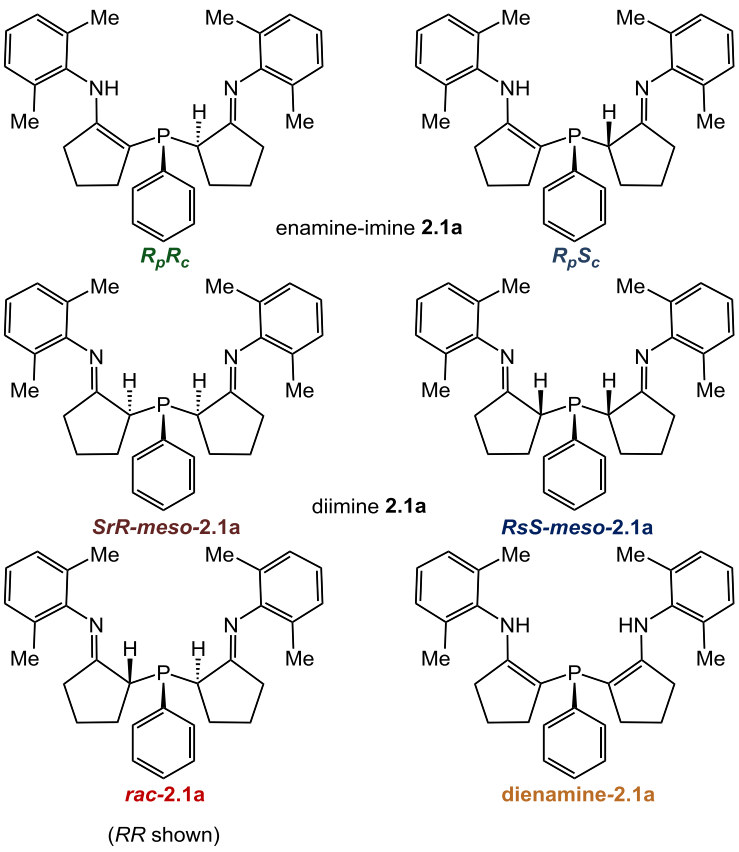

Figure 2.3: Stereoisomers and tautomers of **2.1a**.

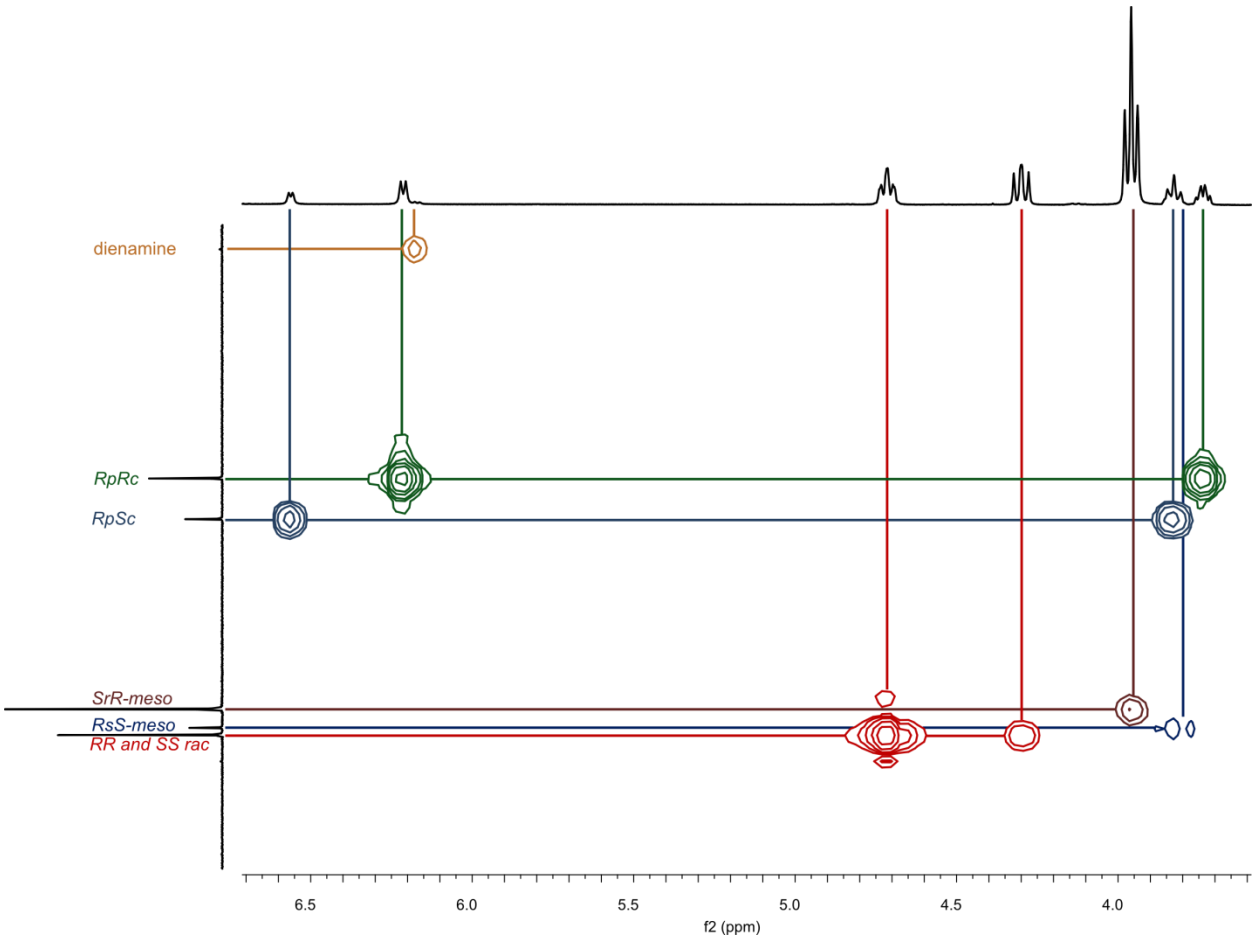

Figure 2.4: ^{31}P HMBC NMR of **2.1a** at 400 MHz taken in C_6D_6. Color coding corresponds to labels in Figure 2.3. The assignment of ***RpRc*** and ***RpSc*** assumes that the most sterically favorable conformation (***RpRc***) of the ligand is present in higher concentration.

Thus far, the five species identified consist only of diimine and enamine-imine forms of **2.1a**, with no peaks attributable to the dienamine tautomer. On the basis of the upfield shift of the enamine-imine form compared to the diimine, it was reasoned that the ^{31}P NMR resonance for the putative dienamine species would likely be located upfield of the enamine-imine form, perhaps in the range of δ -60 to -70. Upon close examination of this region, a very small resonance at δ -63 was identified, which correlated in the ^{31}P HMBC NMR experiment to a shoulder in the NH region of the ^{1}H NMR spectrum at δ 6.2.

As previously mentioned, the major resonance in the $^{31}P\{^{1}H\}$ NMR spectrum of **2.1a** occurs at δ -8.5 and correlates to a single CH resonance at δ 3.9; this identifies it as a *meso* diastereomer of the diimine tautomer of the ligand, which has been confirmed by X-ray crystallography. A second diastereomer of the diimine tautomer of the ligand is assigned to a ^{31}P resonance at δ -5.4. This signal correlates with two α-CH protons, supporting its assignment as the *rac* stereoisomer of the diimine tautomer of the ligand. As illustrated in Figure 2.3, the two α protons of the *rac* enantiomers (*RR* and *SS*) are not related by symmetry; therefore, two unique resonances are expected in the ^{1}H NMR spectrum. The protons of both *meso* diastereomers are related by a mirror plane and thus appear as a single resonance.

In the mixture of isomers of **2.1a**, the ^{31}P resonance at δ -6.0 (~6-7% of the mixture) is a second *meso* diastereomer, which is present due to the pseudochiral phosphorus center.[141] This signal is very close to the resonances of the *rac* and *meso* diimine diastereomers, which is consistent with a diimine framework because the chemical shift is consistent with sp^3 hybridization of both α-carbons of the cyclopentyl linker that flank the ^{31}P nucleus. The ^{1}H-^{31}P HMBC NMR spectrum shows a single cross peak in the region of interest; this ^{31}P resonance correlates with a ^{1}H signal at δ 3.8, which overlaps with the previously discussed resonances assigned as α-CH protons.

2.3 Coordination Chemistry of Neutral Ligands with $[RhCl(COE)_2]_2$

Given the ability of this ligand framework to shuttle protons between the linker and donor positions via tautomerization, probing how this process might change upon coordination to a metal was of interest. Rhodium is an attractive choice as ^{103}Rh is a 100% abundant S = 1/2 isotope, which can be beneficial for elucidating the structure of coordination compounds by multinuclear NMR spectroscopy.

Reacting either **2.1a** or **2.1b** with $[RhCl(COE)_2]_2$ results in formation of yellow solids corresponding to **2.3a** and **2.3b**, respectivly (Scheme 2.5). Elemental analysis suggests these solids are not entirely pure. ^{1}H NMR spectroscopy indicates traces of silicon grease are present for both samples. Despite some impurities, as discussed below, multinuclear NMR spectroscopy identifies the key structural features of **2.3a,b**. Both of the arms of the ligand have adopted the imine tautomeric form, and one of the imine nitrogen arms of the ligand is not coordinated to rhodium. Additionally, a cyclooctene ligand from the starting material is present in the structures of **2.3a** and **2.3b**.

Scheme 2.5:

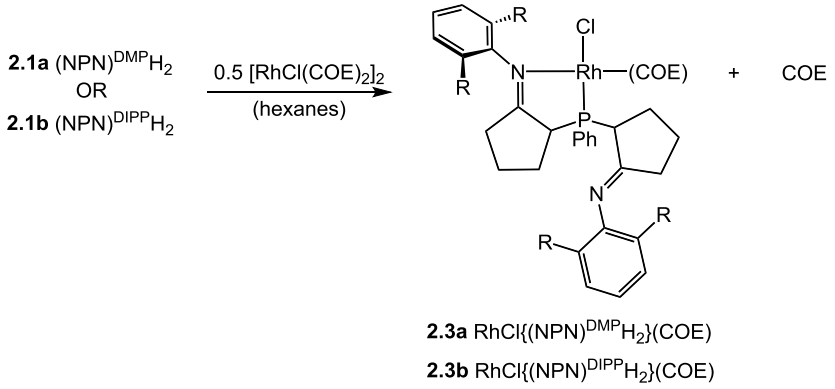

2.3a $RhCl\{(NPN)^{DMP}H_2\}(COE)$

2.3b $RhCl\{(NPN)^{DIPP}H_2\}(COE)$

^{1}H NMR spectra of **2.3a** and **2.3b** are complex; however, identification of distinct features that are consistent with the structures proposed in Scheme 2.5 is possible. Monitoring the reaction of the neutral ligand precursors with $[RhCl(COE)_2]_2$ by ^{1}H NMR spectroscopy shows the presence of free cyclooctene. The remaining COE ligand remains coordinated as evidenced by pairing a ^{13}C APT NMR experiment with ^{1}H-^{13}C HSQC data (Figure 2.5). Using these experiments two doublet resonances at δ 67.9 ($^2J_{RhC}$ = 13.2 Hz) and 65.6 ($^2J_{RhC}$ = 12.9 Hz) are correlated to CH resonances in the ^{1}H NMR spectrum consistent with the olefin-CH of a coordinated COE ligand. The remaining two doublet resonances at δ 40.4 ($^1J_{PC}$ = 18.8 Hz) and

56.8 ($^{1}J_{PC}$ = 21.8 Hz) correlate to signals in the ^{1}H NMR spectrum consistent with the α-CH protons of the ligand. The above observations are consistent with the diimine tautomeric form of the ligand coordinated to rhodium. Despite several attempts, crystals suitable for X-ray analysis were not obtained for **2.3a** or **2.3b**.

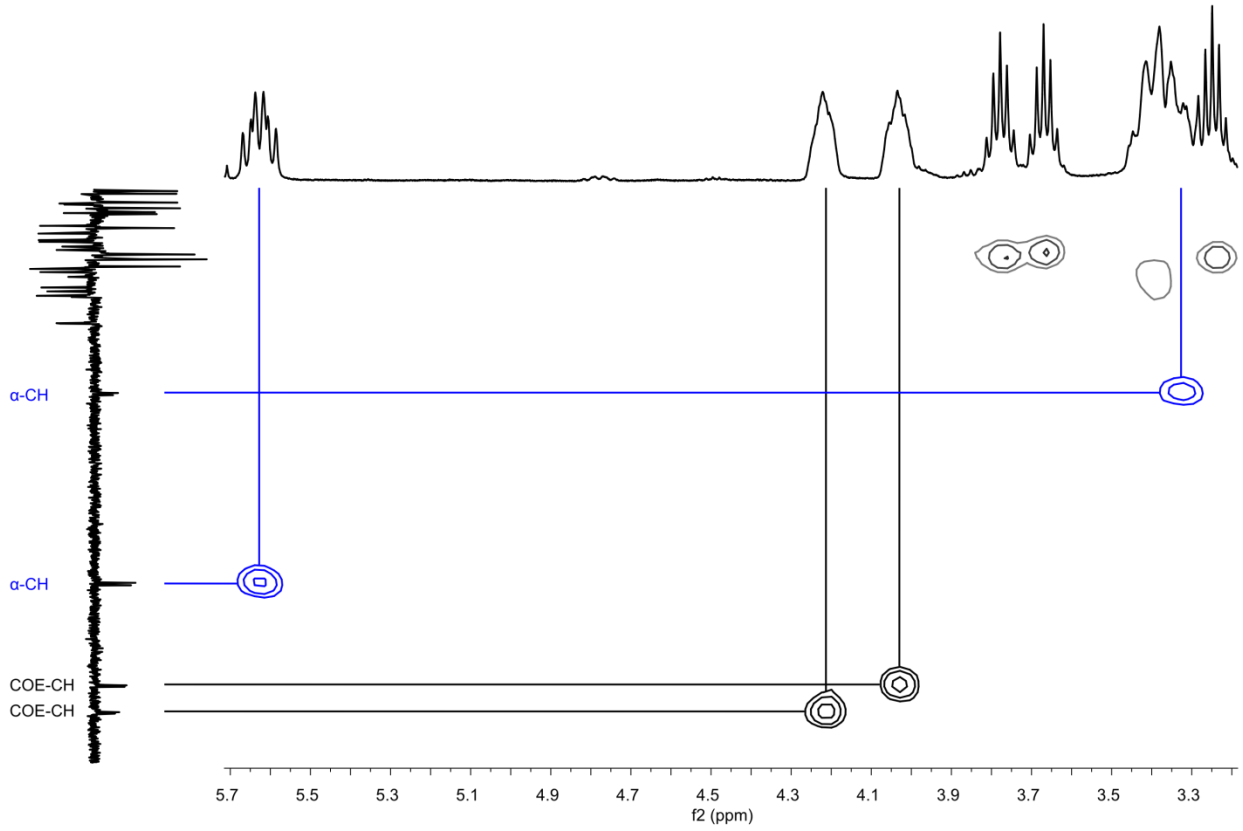

Figure 2.5: ^{1}H-^{13}C HSQC of **2.2b** in C_6D_6. The **blue** lines are assigned as α-CH protons of the ligand the **black** lines are CH-olefin resonances from a coordinated COE ligand.

Theoretically, treating **2.3a** or **2.3b** with an appropriate base could generate an enamide phosphine ligand coordinate to rhodium; however, experiments using potassium *tert*-butoxide gave complex mixtures of products as determined by ^{1}H and ^{31}P{^{1}H} NMR spectroscopy. Further purification was not attempted. Instead of attempting additional deprotonation studies using **2.3a,b** syntheses of new complexes without a COE ligand coordinated to Rh were

explored. Elimination of the potentially reactive C-C double bond of the COE ligand from the coordination sphere of Rh motivated this decision. Initial efforts focused on thermally inducing loss of COE and thereby encouraging coordination of the dangling imine arm to rhodium. Heating a mixture of **2.3a** dissolved in d_8-THF to 55 °C overnight and monitoring this reaction by ^{1}H and ^{31}P{^{1}H} NMR spectroscopy shows a solution of free COE along with an ill-defined mixture of rhodium complexes. In light of this result, other methods of removing the COE ligand were explored such as hydrogenation and displacement of COE with CO.

2.4 Reactivity of Rh(I) COE Compounds with CO

Exploring the reactivity of **2.3a** and **2.3b** with CO establishes the COE ligand of both compounds readily exchanges for CO. As will be discussed shortly, the major products of reaction between **2.3a** or **2.3b** and CO are consistent with **2.4a** or **2.4b**, respectively (Scheme 2.6). One factor complicating the synthesis and purification of **2.4a** and **2.4b** is the presence of an unidentified minor product that forms when mixtures of **2.3a** or **2.3b**, dissolved in dichloromethane, react with CO. For example, a ^{31}P{^{1}H} NMR spectrum of the reaction mixture resulting from treatment of **2.3a** with CO features a major resonance at δ 64.3 (d, $^{1}J_{RhP}$ = 170.4 Hz), assigned to **2.4a**, and a minor resonance at δ 23.6 (d, $^{1}J_{RhP}$ = 149.9 Hz). The major and minor resonances integrate 17:1 relative to one another. Similar results occur when **2.3b** is reacted with CO. After workup, solid samples of both **2.4a** and **2.4b** contain traces of this unidentified minor product. In both cases, the structure of this contaminant remains unknown. Importantly, despite the presence of a minor contaminant, both **2.4a** and **2.4b** display spectral features that are consistent with the Rh(I) monocarbonyl complexes shown in Scheme 2.6.

Scheme 2.6:

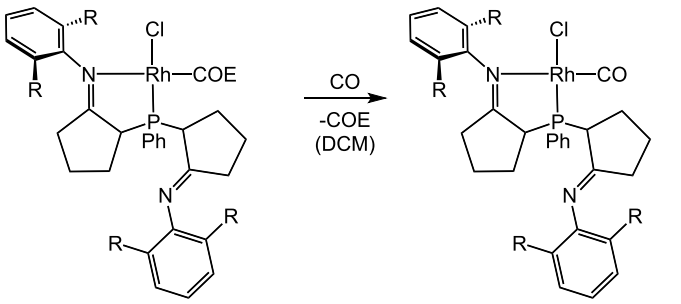

2.3a RhCl{(NPN)^{DMP}H$_2$}(COE) **2.4a** RhCl{(NPN)^{DMP}H$_2$}(CO)

2.3b RhCl{(NPN)^{DIPP}H$_2$}(COE) **2.4b** RhCl{(NPN)^{DIPP}H$_2$}(CO)

The important features of the ^{1}H NMR spectra of **2.4a,b** can be identified with the aid of ^{1}H-^{13}C HSQC experiments. These data confirm the ligand has retained the diimine tautomeric form during the reaction with CO. The complex nature of both the ^{1}H and ^{13}C NMR spectra indicate low symmetry complexes are formed, similar to what is observed for the COE complexes **2.3a,b**. For example, the ^{1}H NMR spectrum of **2.4a** has two well resolved resonances at δ 3.8 and 5.6 corresponding to the α-CH protons of the ligand. The signals assigned as α-CH protons of **2.4a** correlate to multiplet resonances in the ^{13}C APT NMR spectrum at δ 41.5 (dd, $^{2}J_{RhC}$ = 2.8 Hz, $^{1}J_{PC}$ = 31.0 Hz) and 56.1 (d, $^{1}J_{PC}$ = 22.5 Hz), which is consistent with carbon atoms connected directly to phosphorus. These observations strongly suggest the ligand has retained the diimine tautomeric form in solution and binds to rhodium with one of two imine arms. Similar features are present in the multinuclear NMR spectra of **2.4b**. Elemental analysis for both **2.4a** and **2.4b** suggest the solids isolated from the synthesis are not entirely pure. In addition to the presence of an unidentified product in samples of **2.4a** and **2.4b** (discussed previously), traces of silicon grease appear as small resonances in the ^{1}H NMR spectra of both compounds.

The solid state molecular structure of **2.4a** shown in Figure 2.6 is consistent with previously discussed solution data. The dissociated nitrogen donor, N2, is 3.879(6) Å from Rh1, suggesting there is no interaction with rhodium in the solid state. Instead, N2 is directed at an α-CH proton (H2). The N1-H2 distance is 2.58(7) Å. The dissociated imine arm C-N double bond length is very similar to the C-N bond of the coordinated imine arm. All of the other bond lengths and angles are consistent with the neutral, diimine tautomeric form of the ligand. An additional common feature between the solid state structure of the neutral ligand in the absence of a metal (Figure 2.1) and **2.4a** (Figure 2.6) is the ligand protons H2 and H7 are *anti* disposed to the phenyl group attached to phosphorus.

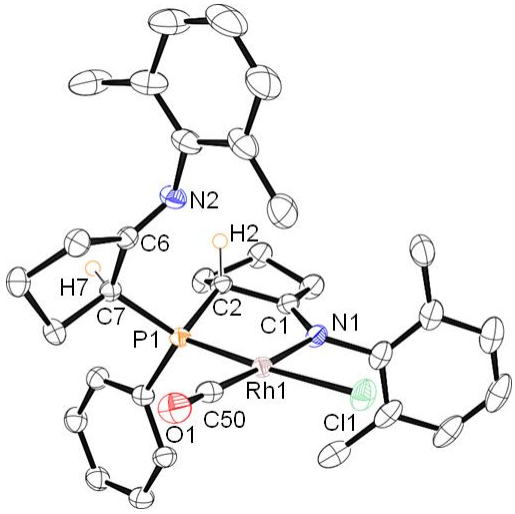

Figure 2.6: ORTEP drawing of the solid state molecular structure of **2.4a** with probability ellipsoids at 50%. The (SsR)-*meso*-diimine form of the ligand is coordinated to rhodium. The hydrogen atoms are omitted for clarity except for H2 and H7. The positions of these hydrogen atoms were determined from the difference map. Although only one molecule is shown there is another molecule present in the asymmetric unit, which is also the (SsR)-diimine enantiomer of **2.4a.** The c-glide plane of the space group (P21/c) generates the other enantiomer. Selected bond lengths (Å) and bond angles (°): Rh1-N1 2.131(3), Rh1 ... N2 2 3.878(2), Rh1-P1 2.2253(7), Rh1-Cl1 2.3797(7), N1-C1 1.289(3), N2-C6 1.263(4), C1-C2 1.502(4), C6-C7 1.524(4), C2-P1 1.850(3), C7-P1 1.835(3), N2

... H7 2.587, N1-C1-C2 122.0(3), N2-C6-C7 121.5(2), C1-C2-P1 108.5(2), C6-C7-P1 104.7(1), P1-Rh1-Cl1 173.72(3), Cl1-Rh1-N1 90.63(7) N1-Rh1-P1 83.21(7)

Attempts to deprotonate **2.4a,b** with base failed to generate a well-defined enamide phosphine complex. For example, treating **2.4b** with one equivalent of potassium *tert*-butoxide in THF gave an initially promising cloudy red-orange solution; however, upon workup by removing the solvent under vacuum, multinuclear NMR analysis of the reaction mixture in C_6D_6 gave no $^{31}P\{^1H\}$ NMR signal and broad resonances in the ^1H NMR spectrum. Similar results were observed for **2.4a**. Attempts to deprotonate **2.4b** with potassium hexamethyldisilylamide (KHMDS) gave no reaction, likely due to steric factors.

2.5 Reactivity of Rh(I) COE Compounds with H_2

Monitoring the reaction of **2.3a** with H_2 by $^{31}P\{^1H\}$ NMR spectroscopy shows a mixture of products initially forms. Overnight, this mixture converts to a single resonance at δ 110.2 ($^1J_{RhP}$ = 130. 3 Hz) corresponding to **2.5a** (Scheme 2.7). Although the reaction is much slower, similar reactivity occurs to form **2.5b**. Repeating these reactions on a larger scale allows for isolation and characterization of new Rh(III) complexes; however, impurities remain after workup, as indicated by several signals from δ 1.6-2.3 of the ^1H NMR spectra of **2.5a,b**. Despite the presence of some unidentified impurities, key features of the ^1H NMR spectra of **2.5a,b** can be interpreted. For **2.5a**, a single hydride resonance at δ -15.7 ($^2J_{PH}$ = 4.7 Hz, $^1J_{RhH}$ = 19.3 Hz) and a resonance at δ 6.0 (td, $^3J_{HH}$ = 8.2 Hz, $^3J_{PH}$ = 12.8 Hz) integrate 1:2 relative to one another, suggesting the two α-CH protons of the diimine ligand are related by symmetry. Supporting this assignment, ^1H-^{13}C HSQC NMR spectroscopy correlates the resonance at δ 6.0 in the ^1H NMR spectrum to a ^{13}C resonance at δ 54.5 (d, $^1J_{PC}$ = 26.5 Hz). Similar features are present in the multinuclear NMR spectra collected for **2.5b**. Overall, these data are consistent with the

assignment of **2.5a,b** as C_s symmetric rhodium monohydride complexes coordinated by the *meso*-diimine form of the ligand.

Scheme 2.7:

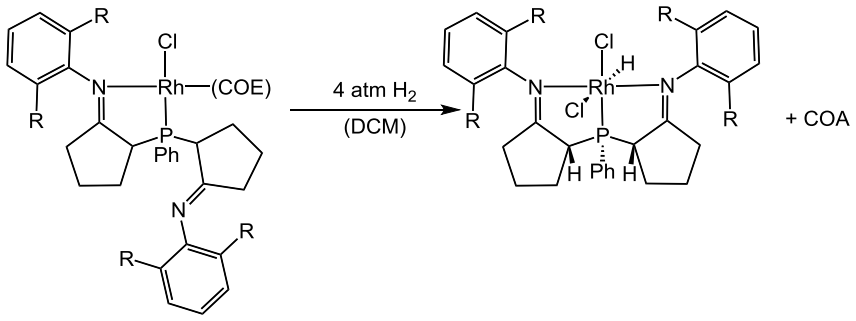

2.3a $RhCl\{(NPN)^{DMP}H_2\}(COE)$ **2.5a** $RhCl_2H\{(NPN)^{DMP}H_2\}$

2.3b $RhCl\{(NPN)^{DIPP}H_2\}(COE)$ **2.5b** $RhCl_2H\{(NPN)^{DIPP}H_2\}$

The structures of **2.5a,b** were further elucidated by X-ray diffraction studies for both compounds. The solid state structures for **2.5a,b** match the multinuclear NMR data and importantly confirm that an additional chloride ligand, presumably resulting from reaction with dichloromethane, is coordinated to rhodium. Abstraction of a chloride from DCM is a well established reactivity pattern for a variety of Rh complexes.[142-144] In both structures (Figure 2.7 for **2.5a** and Figure 2.8 for **2.5b**) the bond lengths and angles are consistent with the neutral diimine tautomeric form of the ligand coordinated to Rh(III) in a meridional geometry. The two ligand protons (H2 and H7) are *syn* disposed to one another, as well as the apical chloride ligand (Cl2) coordinated to rhodium. A mirror plane relates the imine arms of the ligand, therefore the phosphorus donors of both **2.5a** and **2.5b** are pseudochiral centers.[141] The *P*-phenyl group of the ligand is *anti* disposed to the two ligand protons H2 and H7.

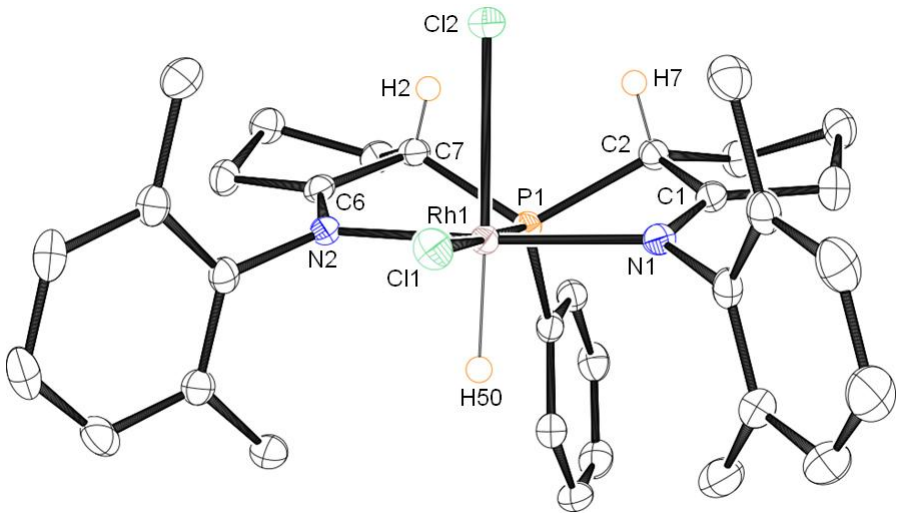

Figure 2.7: ORTEP drawing of the solid state molecular structure of **2.5a** where the (SR)-*meso*-diimine form of the ligand is coordinated to rhodium shown with probability ellipsoids at 50%. The hydrogen atoms are omitted for clarity except for H2, H7 and H50, the positions of these hydrogen atoms were determined from the difference map. Selected bond lengths (Å) and angles (°): Rh1-N1 2.074(2), Rh1-N2 2.065(2), Rh1-P1 2.174(1), Rh1-Cl1 2.396(1), Rh1-Cl2 2.581(1), Rh1-H50 1.47(2), N1-C1 1.287(3), N2-C6 1.284(2), C1-C2 1.525(2), C6-C7 1.520(4), C2-P1 1.843(2), C7-P1 1.840(2), N1-C1-C2 122.7(2), N2-C6-C7 122.7(2), C1-C2-P1 104.4(1), C6-C7-P1 104.7(1), N1-Rh1-N2 167.49(7), P1-Rh1-Cl1 177.06(2), Cl1-Rh1-N1 96.82(5), Cl1-Rh1-N2 95.57(5) N1-Rh1-P1 83.76(7), N2-Rh1-P1 83.53(7).

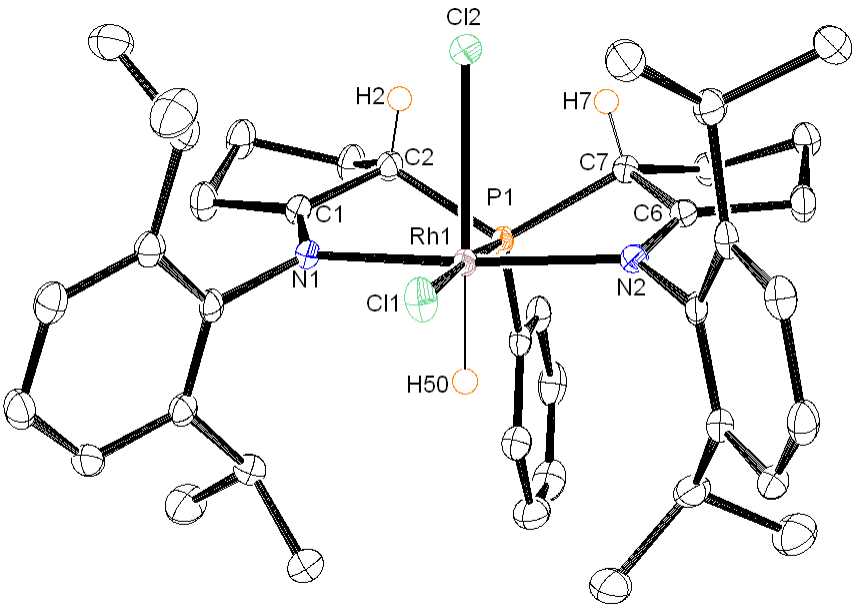

Figure 2.8: ORTEP drawing of the solid state molecular structure of **2.5b** where the (SR)-*meso*-diimine form of the ligand is coordinated to rhodium shown with probability ellipsoids at 50%. The hydrogen atoms are omitted for clarity except for H2, H7 and H50; the positions of these hydrogen atoms were determined from the difference map. Selected bond lengths (Å) and angles (°): Rh1-N1 2.074(2), Rh1-N2 2.065(2), Rh1-P1 2.174(1), Rh1-Cl1 2.396(1), Rh1-Cl2 2.581(1), Rh1-H50 1.47(2), N1-C1 1.287(3), N2-C6 1.284(2), C1-C2 1.525(2), C6-C7 1.520(4), C2-P1 1.843(2), C7-P1 1.840(2), N1-C1-C2 122.7(2), N2-C6-C7 122.7(2), C1-C2-P1 104.4(1), C6-C7-P1 104.7(1), N1-Rh1-N2 167.49(7), P1-Rh1-Cl1 177.06(2), Cl1-Rh1-N1 96.82(5), Cl1-Rh1-N2 95.57(5), Cl1-Rh1-N1 90.5(1), N1-Rh1-P1 82.91(5), N2-Rh1-P1 83.80(5).

2.6 Conclusions

In this chapter, the characterization of two NPN ligand scaffolds in solution and in the solid state aided ongoing efforts directed at exploration of amido phosphine hybrid ligands designed for early transition metals. The complex behavior of these ligands in solution is due to tautomerization. Upon coordination to rhodium, the diimine tautomeric form of the ligand is favored. Deprotonation studies failed to generate a well defined Rh enamide phosphine complex.

Chapter 3: A Linker Reactive Enamide Phosphine Ligand for Iridium

3.1 Introduction

As discussed in Chapter 1, Sections 1.1-2 ancillary or innocent ligands coordinated to a metal provide the required steric and electronic environment for the metal to react. One example of relevance to the work in this chapter is Vaska's complex (**3.1**, Scheme 3.1), where all of the donors attached to the square planar iridium (I) centre are considered ancillary ligands. Oxidative addition of H_2 to Vaska's compound (**3.1** to **3.2**) generates two new *cis* disposed hydride ligands attached to the iridium center.[145,146] The stereochemistry of the hydride ligands is rationalized by the generally accepted mechanism for oxidative addition, where concerted cleavage of the H-H bond via donation of electron density from a d orbital on Ir to a σ* orbital of H_2 breaks the σ-bond of hydrogen.[147] In this case, it is clear that the activation of H_2 occurs only at the iridium center without any direct participation of the ligands.

Scheme 3.1:

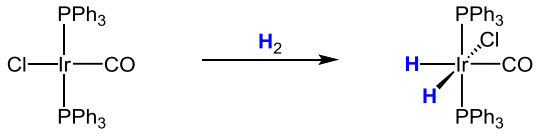

3.1 **3.2**

A different strategy for bond activation involves cooperative ligands, which provide a unique steric and electronic environment to a metal and can participate in a chemical transformation of interest (see Section 1.3). One class of cooperative ligands highlighted in Section 1.6 of the introduction incorporates a pyridine ring into the ligand design. The anionic form of these ligands contains an enamide phosphine unit and a dearomatized pyridine ring.[3,87,88] The enamide phosphine portion of the ligand is involved in shuttling protons between the ligand and metal, or between the ligand and a substrate.[3,6] Scheme 3.2 illustrates one example of

relevance to this chapter. Complex **3.3** reacts with dihydrogen to give **3.5** with two new *trans* disposed hydride ligands.[97] While a change in oxidation state at Ir occurs along with coordination of two new hydrides to iridium, deuterium labeling studies indicate the reaction that is occurring is not oxidative addition of H_2.[97] For example, exchanging H_2 gas for D_2 gas also forms **3.5**, however, deuterium scrambles into the linker position of the ligand scaffold and the Ir(III) center bonds to one hydride and one deuterated ligand (**3.5**).[97] These observations are rationalized by identification of **3.4** as an intermediate in the reaction. **3.4** forms by proton transfer from the linker of the ligand to iridium. Synthesis and reactivity of **3.4** under different conditions, and computational evidence strongly support that it is an intermediate in the conversion of **3.3** to **3.5**.[97,98] In this example, proton migration from the linker of the ligand accompanied by a change in formal oxidation state of iridium generates the enamide phosphine unit, which can accept a proton from H_2.

Scheme 3.2:

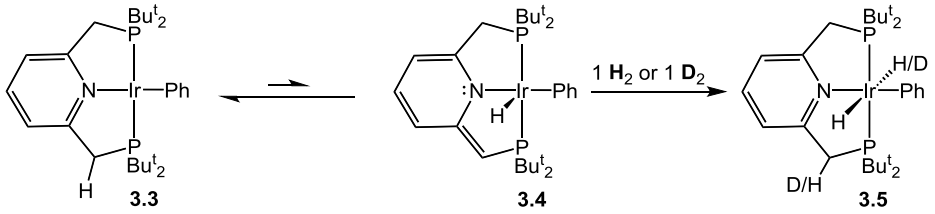

In this chapter, bidentate imine phosphine scaffolds that exist in the imine and enamine tautomeric forms in solution are used as precursors to generate iridium (I) enamide phosphine coordination compounds. Reactivity of one of the iridium complexes with H_2 or Pr^iOH establishes that the bidentate enamide phosphine unit is able to participate in linker reactivity by accepting a proton. Under different conditions, this proton can be lost as H_2 by combining with a hydride attached to Ir. Multinuclear NMR studies and ^{13}C labeling experiments show an entirely

different mechanism for linker reactivity is occurring with this system from what is illustrated in Scheme 3.2.

3.2 Synthesis of Potassium Salts of Enamide Phosphine Ligands

The known arylimine phosphine ligand systems **3.6a**,**b** were prepared through modifications of literature procedures,[139,140] as shown in Scheme 3.3. The short form descriptors used here are $(NP)^{DIPP}H$ (**3.6a**) and $(NP)^{DMP}H$ (**3.6b**), where DIPP and DMP are 2,6-diisopropylphenyl and 2,6-dimethylphenyl respectively, and correspond to the imine *N*-aryl substituents. In solution both **3.6a,b** exist predominantly in the imine form, with the enamine tautomer evident by a small upfield singlet in the $^{31}P\{^{1}H\}$ NMR spectrum.

Scheme 3.3:

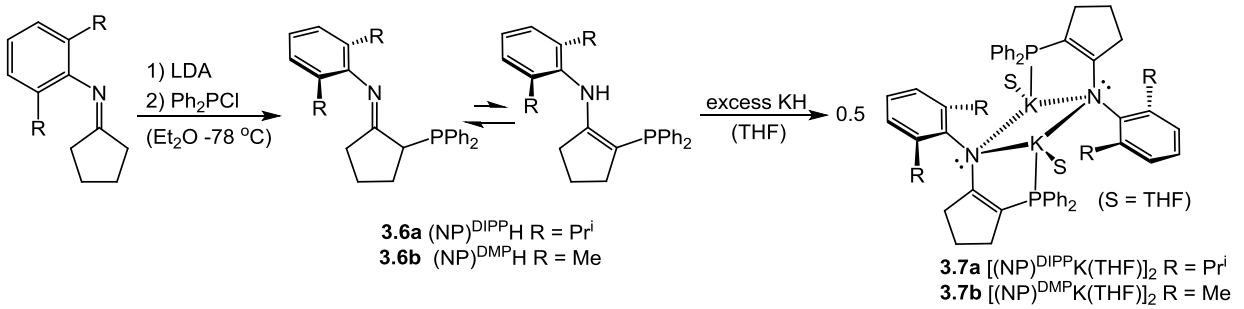

Addition of excess KH to solutions of **3.6a,b** in THF results in the formation of the corresponding potassium salts, **3.7a,b**, which can be isolated as solids in 68-78% yield. In solution, these species display singlets in their $^{31}P\{^{1}H\}$ NMR spectra at δ -22.7 and -19.1 for **3.7a,b**, respectively. The ^{1}H NMR spectra of both compounds are quite simple and feature resonances indicating that both the alkyl substituents in the *ortho* positions of the *N*-aryl moiety, and the phenyl groups attached to the phosphine are equivalent. For **3.7a** the ^{1}H-^{31}C HSQC experiment shows a carbon signal at δ 69.2 coupled to phosphorus ($^{1}J_{PC}$ = 14.8 Hz), that does not correlate to any resonance in the ^{1}H NMR spectrum. This resonance is assigned to the α-carbon

next to the PPh_2 unit in the deprotonated enamide structure. Similar features are evident for **3.7b**. In the ^{1}H NMR spectrum of **3.7a** the resonances for the β-CH_2 protons of coordinated THF are partially obscured by a doublet assigned to the methyl protons of the isopropyl groups of the *N*-aryl moiety at δ 1.4. Close inspection of the ^{13}C HSQC and ^{13}C APT NMR spectra show a correlation with a ^{13}C CH_2 resonance at 24.7 ppm. Resonances attributed to the α-CH_2 protons of coordinated THF are clearly visible at δ 3.4 ppm in the ^{1}H NMR spectrum of **3.7a**.

X-ray quality crystals of **3.7b** were obtained from THF by addition of hexanes; the solid state molecular structure is shown in Figure 3.1 along with selected bond lengths and bond angles. Overall, the structure of **3.7b** is dimeric, with the amide nitrogen atoms of the enamide units bridging the two potassium ions, and one coordinated THF bound per potassium. One of the *P*-phenyl rings of each unit participates in a η^3 interaction with the K^+; therefore, the two *P*-phenyl rings are structurally inequivalent, overall the structure is C_i symmetric in the solid state. As mentioned above, in solution, **3.7b** adopts a C_s symmetric structure; therefore, the inequivalent *P*-phenyl groups observed in the solid state are not maintained in solution.

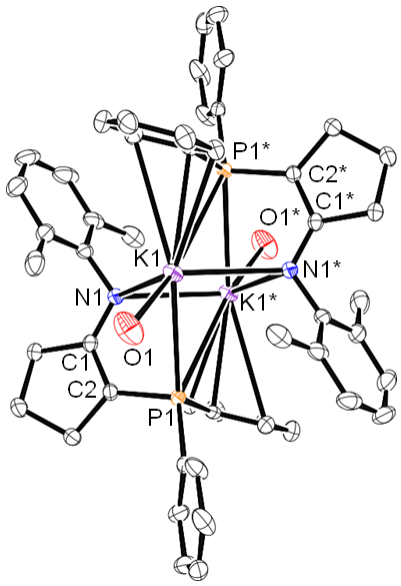

Figure 3.1: ORTEP drawing of the solid state molecular structure of **3.7b**, with probability ellipsoids at 50%. The carbon atoms of both molecules of THF as well as all of the hydrogen atoms are omitted for clarity. Selected bond lengths (Å) and angles (°): K1-O1 2.7050(8), K1-N1 2.9829(7), K1-N1* 2.8222(7), K1-C12 3.066(2), K1-C17 3.216(2), K1-C24 3.280(3), K1-P1 3.4141(10), K1-K1* 3.5045(3), N1-C1 1.347(2), C1-C2 1.347(2), N1-C1-C2 127.26(2), C1-C2-P1 120.46(1) N1-K1-P1 57.98(3).

3.3 Synthesis of Iridium Enamide Phosphine Complexes

The reaction of the potassium derivatives **3.7a,b** with $[(COD)IrCl]_2$ in toluene at room temperature results in an immediate color change to produce a bright red solution along with the formation of potassium chloride (Scheme 3.4). Monitoring the reaction of **3.7a,b** with $[(COD)IrCl]_2$ by $^{31}P\{^1H\}$ NMR spectroscopy shows that the formation of both **3.8a,b** is quantitative and virtually instantaneous at the time of mixing. After workup, the pure iridium enamide phosphine complexes **3.8a,b** could be obtained in good yields. Diagnostic of these complexes are upfield shifted singlets in the $^{31}P\{^1H\}$ NMR spectra as compared to the precursor potassium salts; for example, **3.8a**, gives rise to a resonance at δ 12.1, whereas the signal for **3.7a**

is found at δ -21.7. The ^{1}H and ^{13}C APT NMR spectroscopic data are consistent with the square planar enamide complexes shown in Scheme 3.4.

Scheme 3.4:

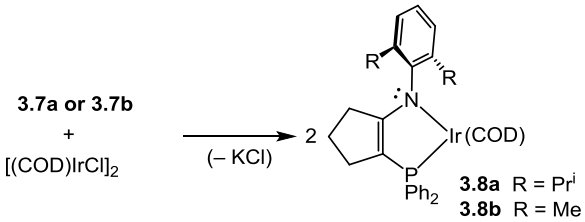

X-ray quality crystals of **3.8a** were obtained by allowing a hexanes solution of the complex to evaporate, or by cooling a concentrated hexanes solution to -35 °C. The solid state molecular structure of **3.8a** is shown in Figure 3.2, along with selected bond lengths and bond angles. The geometry around iridium is square planar, with the N1-C1-C2-P1 plane relatively flat and coplanar with the P1-Ir1-N1 plane. The Ir1-N1 bond length of 2.061(2) Å is similar to other iridium amide derivatives, and the Ir1-P1 distance of 2.3047(7) Å is typical.[97,148]

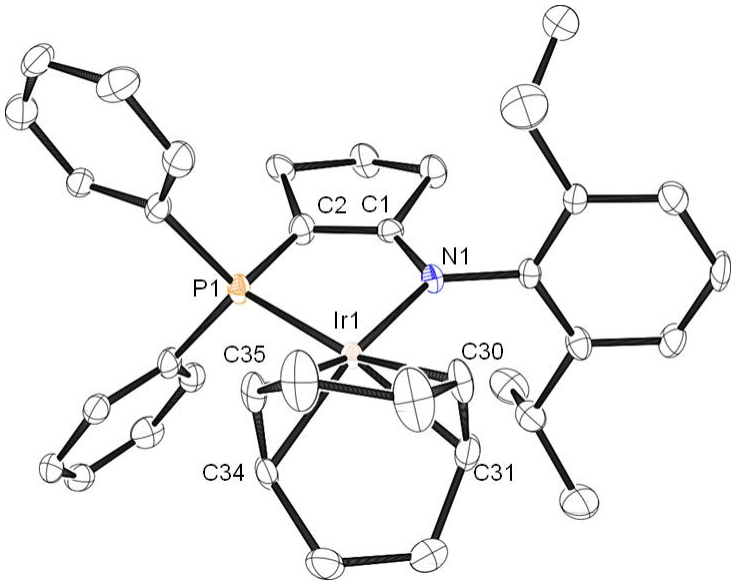

Figure 3.2: ORTEP drawing of the solid state molecular structure of **3.8a** with probability ellipsoids at 50%. All of the hydrogen atoms are omitted for clarity. Selected bond lengths (Å) and angles (°): Ir1-N1 2.061(2), Ir1-P1 2.3047(7), Ir1-C30 2.201(3), Ir1-C31 2.200(3), Ir1-C34 2.117(3), Ir1-C35 2.131(3), N1-C1 1.365(3), C1-C2

1.360(4), C2-P1 1.747(3), C30-C31 1.384(4), C34-C35 1.414(4), N1-C1-C2 124.6(3), C1-C2-P1 113.5(2), N1-Ir1-P1 81.12(6), C34-Ir1-P1 93.00(7), C35-Ir1-P1 96.55(8), N1-Ir1-C30 94.93(10), N1-Ir1-C31 97.86(10) N1-Ir1-P1 81.98(9).

3.4 Reactivity of Ir Enamide Phosphine Complexes

The complexes **3.8a,b** were reacted with hydrogen in an attempt to explore cooperative ligand reactivity. Exposing **3.8a** to 4 atm of H_2 in pentane causes the solution to darken to a deep red-orange, the color change is accompanied by the formation of a light yellow precipitate, identified as the hexahydride dimer **3.9a** (Scheme 3.5). A similar result occurs if the reaction of H_2 with **3.8a** is repeated in a J. Young NMR tube in C_6D_6. Monitoring this transformation by multinuclear NMR spectroscopy using a J. Young NMR tube charged with H_2 reveals that the reaction pathway is complex, involving a number of unidentified intermediates. Ultimately, after 12 hours, $^{31}P\{^1H\}$ NMR spectroscopy reveals a singlet attributed to **3.9a** at δ 32.7 as well as two unidentified signals at δ 11.3, and -7.4. ^1H NMR spectroscopy reveals the 1,5-cyclooctadiene ligand is completely hydrogenated to cyclooctane during this period. Attempts to extend these results with **3.8b** resulted in intractable mixtures of products.

Scheme 3.5:

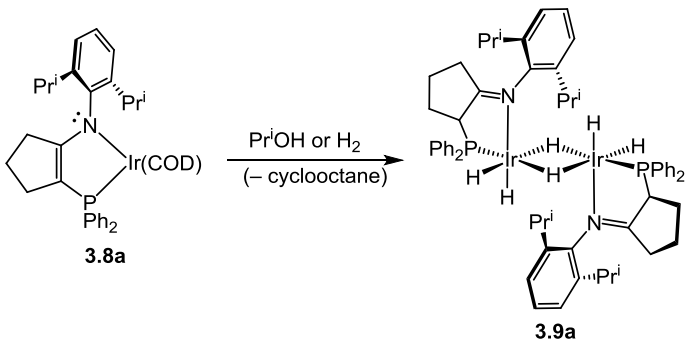

3.8a **3.9a**

The reaction using H_2 to generate **3.9a** proceeds by a complex series of steps and ultimately gives a mixture of products; a more efficient route to **3.9a** is the use of isopropanol in

place of hydrogen. Treating a benzene solution of **3.8a** with excess isopropanol and heating to 100 °C overnight in sealed reaction vessel forms **3.9a**. Repeating the reaction on a smaller scale in a J. Young tube generates X-ray quality crystals of **3.9a**. The solid state molecular structure is shown in Figure 3.3 along with selected bond lengths and angles. The metrical parameters of the ligand are unremarkable and confirm protonation of the ligand at carbon. The iridium-iridium distance is 2.7089(4) Å, which is shorter than the sum of the Van der Waals radii of the two atoms;[149] a similar compound with a tridentate ligand and a hemi-labile arm has an iridium-iridium distance of 2.7325(7) Å and has been assigned as an iridium-iridium double bond.[72] Cationic iridium polyhydride clusters have been previously investigated and their formation usually indicates catalyst deactivation during hydrogenation type processes.[150-154]

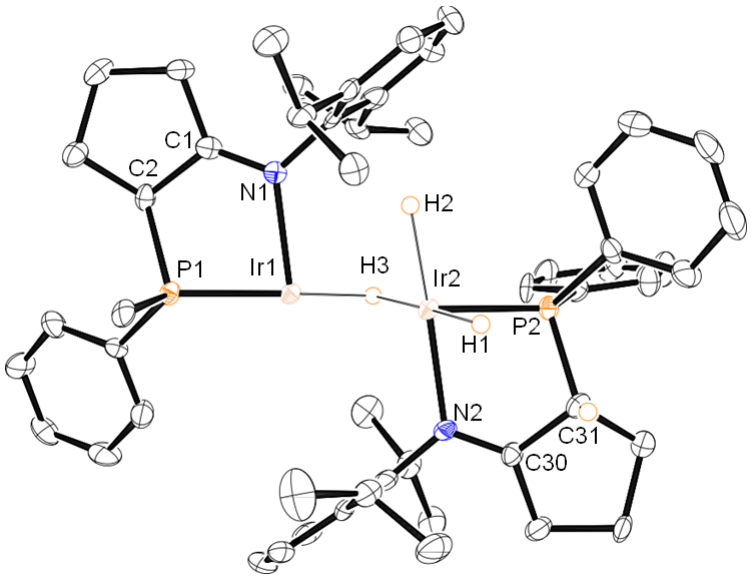

Figure 3.3: ORTEP drawing of the solid state molecular structure of **3.9a** with probability ellipsoids at the 50%. All of the hydrogen atoms except the α-CH protons and hydrides are omitted for clarity. One P1-phenyl ring has been removed for clarity. Three hydrides, H1, H2, and H3 were located from the difference map; their isotropic thermal parameters (U_{eq}) were coupled to Ir2, and their coordinates were freely refined. The X-ray data did not allow the remaining three hydrides to be located with any certainty. Selected bond lengths (Å) and angles (°): Ir1-N1 2.238(9), Ir1-P1 2.210(3), Ir2-N2 2.236(8), Ir2-P2 2.196(3), Ir1-Ir2 2.7089(4), N1-C1 1.288(2), C1-C2 1.522(3),

N2-C30 1.286(12), C30-C31 1.509(3), N1-C1-C2 120.9(9), P1-C2-C1 108.1(6), N1-Ir1-P1 81.3(2), N2-Ir2-P2 81.2(2).

Obtaining multinuclear NMR spectra of **3.9a** was difficult due to low solubility in benzene, toluene, THF, and other organic solvents. However, spectra could be obtained in CD_2Cl_2 even though the complex slowly decomposes in this solvent. Assignment of a ^{1}H NMR signal to the α-CH proton on the ligand was of particular importance to confirm the solid state structure. The ^{1}H NMR spectrum taken at 600 MHz in CD_2Cl_2 shows a resonance at δ 3.7, which the ^{13}C APT NMR and HSQC experiments correlate to a CH carbon signal at δ 62.8 strongly coupled to phosphorus ($^1J_{PC}$ = 33.1 Hz), confirming that protonation at the linker carbon has occurred. In the ^{1}H NMR spectrum, all of the signals assigned to the various CH_2 groups of the cyclopentylidene linker are well resolved diastereotopic multiplets, each integrating to one proton per iridium center. Additional information about the structure of **3.9a** was gleaned from the three unique signals in the hydride region of the spectrum, one of which is a triplet at δ -20.0, this splitting arises from coupling to two equivalent phosphorus-31 nuclei, and denotes that a dimeric structure exists in solution. When the ^{31}P nucleus is decoupled, the signal collapses into a broad singlet. No H-H coupling is observed between any of the three hydride signals. In solution, the overall symmetry of the dimer is C_i symmetric, which is identical to the symmetry observed in the solid state.

A possible mechanism for the formation of this hexahydride dimer (**3.9a**) by reaction of **3.8a** with isopropanol, is shown in Scheme 3.6. The first step is protonation of the enamide ligand to generate an imine phosphine derivative with a coordinated isopropoxide unit; subsequent β-elimination results in the formation of acetone and an Ir(I) hydride intermediate.

Further reactions with more isopropanol in a multistep process results in hydrogenation of 1,5-cyclooctadiene and the formation of the imine-phosphine iridium (III) trihydride (**3.9a**).

Scheme 3.6:

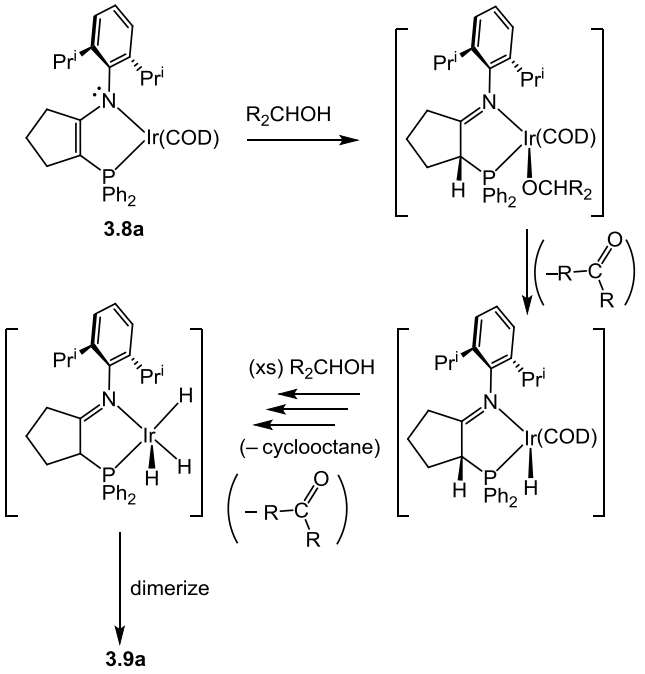

When primary alcohols such as ethanol or benzyl alcohol are used in place of isopropanol, entirely different reactivity is observed (Scheme 3.7). Refluxing a toluene solution of **3.8a** and a primary alcohol in an open (under argon) system results in a light red solution. Monitoring this reaction by $^{31}P\{^{1}H\}$ NMR spectroscopy shows clean conversion of the singlet at δ 12.1 (**3.8a**) to a new signal at δ 21.3 that is assigned as the dicarbonyl complex **3.10a**. Removing the volatiles under vacuum gives a red oil that can be dissolved into C_6D_6 for characterization by multinuclear NMR spectroscopy.

The ^{1}H NMR spectrum of **3.10a** shows that the COD ligand has been lost; furthermore, no resonance indicative of protonation of the ligand can be found. The ^{13}C APT NMR and HSQC spectra definitively establish that the ligand is in the enamide form, as the resonance

assigned to the carbon atom of the linker directly attached to phosphorus gives rise to a doublet at δ 83.5 (d, $^1J_{PC}$ = 64.4 Hz) that does not correlate with any signal in the ^{1}H NMR spectrum. Furthermore, no resonance attributable to an N-H proton occurs in the ^{1}H NMR spectrum of **3.10a**. The CH_2 protons of the linker appear as three signals with the expected splitting patterns, each integrating to two protons. Overall, these data point to a molecule with C_s symmetry in solution. The presence of two different carbonyl ligands was confirmed by ATR FTIR spectroscopy of a crystalline sample of the complex: two distinct CO stretches occur at 1966 cm^{-1} and 2041 cm^{-1}.

Scheme 3.7:

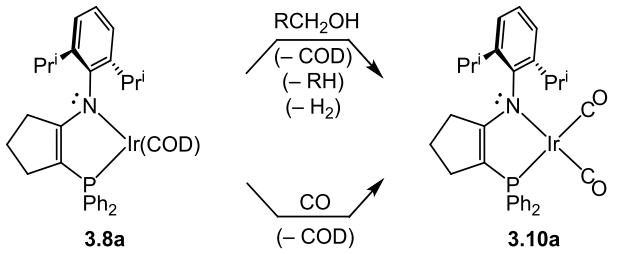

Further evidence for the proposed structure of **3.10a** was obtained by treating the COD complex **3.8a** with 1 atm of CO. Monitoring this reaction by $^{31}P\{^1H\}$ NMR spectroscopy reveals the rapid formation of **3.10a**, as evidenced by the expected singlet at δ 21.3. In addition, ^{1}H NMR spectroscopy confirms loss of the COD ligand. The reaction mixture was taken to dryness and subsequently dissolved in a minimal amount of hexanes. X-ray quality crystals were obtained by slow evaporation of hexanes from a loosely sealed vial in a glove box or by cooling a concentrated hexanes solution to -35 °C.

The solid state molecular structure of **3.10a** is shown in Figure 3.4, along with selected bond lengths and bond angles. As expected, the geometry of the metal center in complex **3.10a**

is square planar and matches the COD starting complex **3.8a** in terms of bond lengths and angles. The solution NMR spectroscopic data is consistent with this solid state molecular structure.

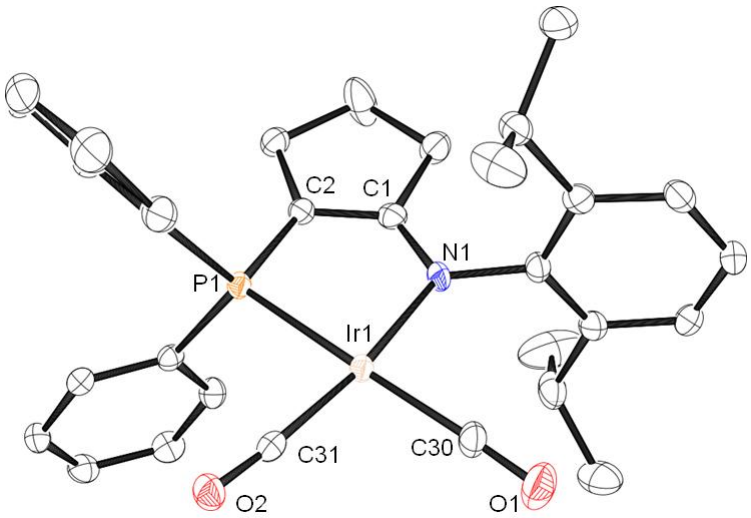

Figure 3.4: ORTEP drawing of the solid state molecular structure of **3.10a** with probability ellipsoids at 50%. All of the hydrogen atoms are omitted for clarity. Selected bond lengths (Å) and angles (°): Ir1-N1 2.047(2), Ir1-P1 2.3373(2), Ir1-C31 1.859(3), Ir1-C30 1.905(3), N1-C1 1.367(4), C1-C2 1.358(4), C2-P1 1.752(3), N1-C1-C2 125.0(2), C1-C2-P1 113.8(2), N1-Ir1-P1 82.26(7), C30-Ir1-N1 90.06(10), C31-Ir1-P1 90.05(8).

The oxidation of primary alcohols followed by decarbonylation of the resulting aldehydes has been documented for several late transition metal coordination compounds.[155-161] While the mechanism for this transformation has not been investigated further in this work, it may proceed in a similar fashion to the mechanism shown in Scheme 3.6. For formation of **3.10a** instead of **3.9a**, a key difference is the fact that upon β-elimination of a hydride from the primary alkoxy group, the aldehyde produced can be oxidatively added and decarbonylated.[156,159,161-163] At some stage, elimination of H_2 from an intermediate, perhaps cooperatively from the imine phosphine ligand and an iridium hydride, generates the enamide dicarbonyl derivative **3.10a**.

As shown by the reaction of alcohols with the iridium enamide derivative **3.9a** (Schemes 3.5 and 3.8), different outcomes are observed depending on whether a primary or a secondary

alcohol is used. As discussed above, the enamide and imine forms of the ligand were observed on various complexes, which clearly indicate that the ligand is acting in a cooperative manner. To probe this further, the Ir(III) hexahydride dimer **3.9a** was reacted with CO, which is another route to the enamide dicarbonyl complex **3.10a** (Scheme 3.8)

Scheme 3.8:

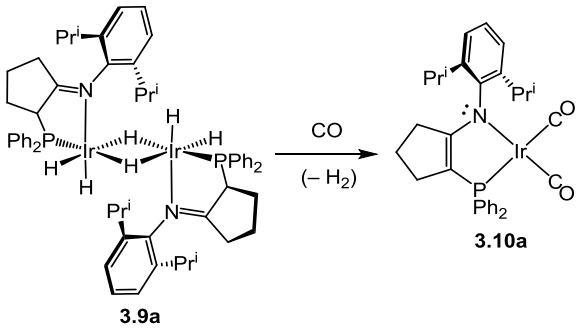

Conversion of **3.9a** to **3.10a** proceeds slowly over the course of several days under 1 atm CO at 25 °C. As a result, identification of three intermediates using multinuclear NMR spectroscopy and carbon-13 labeling experiments was possible. These intermediates are present, in varying amounts, on the way to **3.10a**. The same hydride complexes are identified when more forcing conditions are used, for example, 4 atm CO at 60 °C. Based on identification of these species, a mechanism shown in Scheme 3.9 is proposed that incorporates the observed species with other likely intermediates based on simple elementary reactions such oxidative addition and reductive elimination.

The first *observed* hydride intermediate, wherein the imine donor is dissociated from the Ir center, is identified as **3.12**. The NMR data are consistent with this species containing three inequivalent hydrides, two inequivalent CO ligands and one coordinated phosphine unit. With unlabeled CO, the hydrides are assigned to two overlapping doublets at δ -10.9 and -10.8 due to *cis* coupling to phosphorus-31, and a doublet at δ -11.2 with a larger, *trans* coupling to

phosphorus-31. Use of ^{13}CO results in a doublet of triplets for the hydride *trans* to phosphorus and complex multiplets for the inequivalent *cis* hydrides (Figure 3.5). As shown in Scheme 3.9, a reasonable pathway for the formation of **3.12** proceeds through the trihydride monocarbonyl species **3.11**, formed via the addition of 1 equivalent of CO to the hydride dimer **3.9a**. Complex **3.12** could then arise from the dissociation of the bulky imine donor from **3.13**, followed by coordination of another equivalent of CO.

Scheme 3.9:

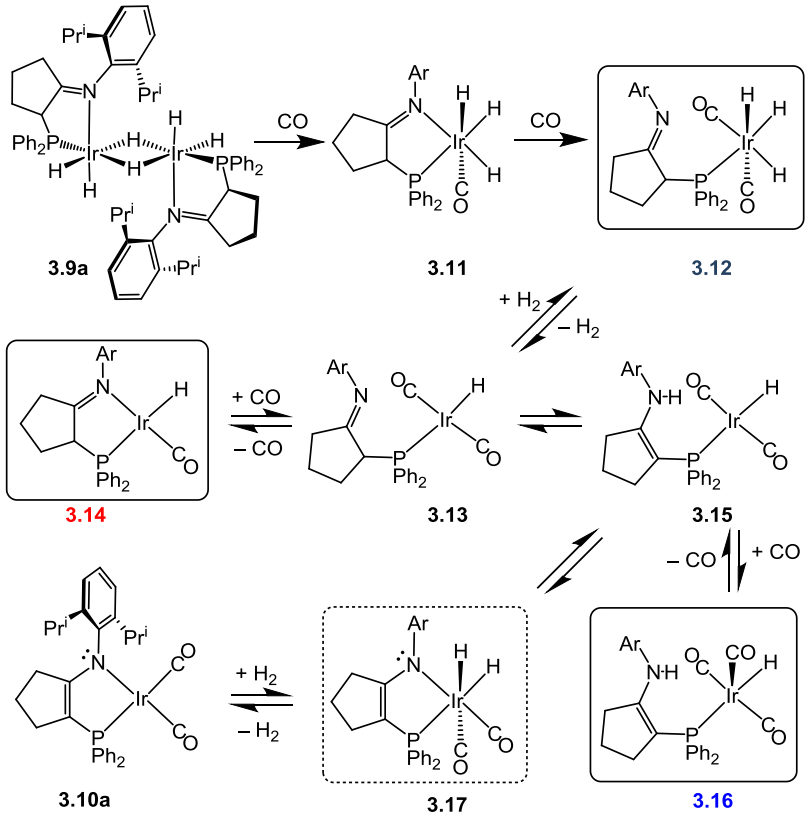

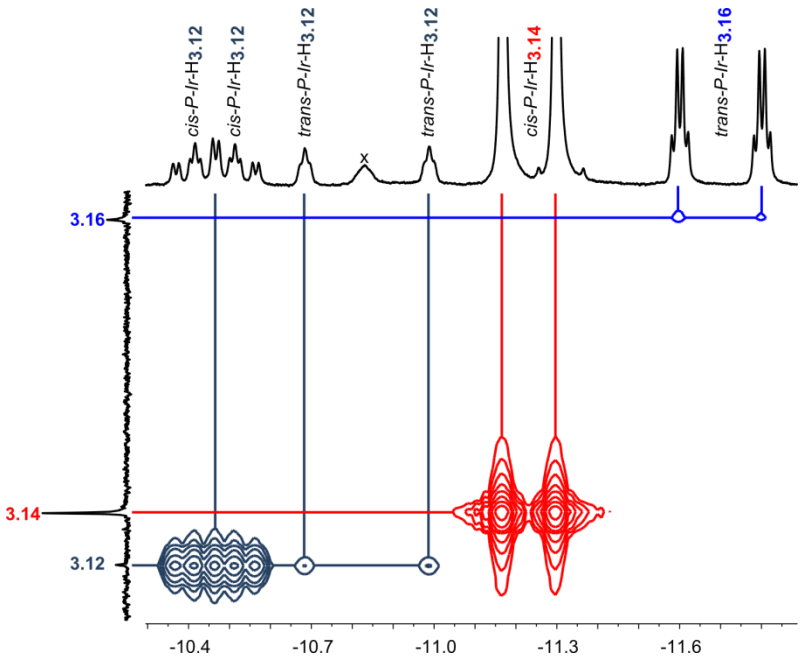

Figure 3.5: A ^{1}H-^{31}P HMBC NMR spectrum of the hydride region recorded during the conversion of **3.9a** to **3.10a** under an atmosphere of ^{13}CO.

The next observed intermediate is identified as **3.14**, a square planar, iridium (I) hydride complex with the imine unit coordinated and only one carbonyl ligand. The ^{31}P{^{1}H} NMR resonance (δ 1.6, s) for complex **3.14** was assigned based on correlations observed by ^{31}P HMBC (Figure 3.5) as well as ^{1}H and ^{1}H{^{31}P} NMR spectra. The hydride resonance for **3.14** in the ^{1}H NMR spectrum (δ -11.6, d, $^{2}J_{PH}$ = 52.2 Hz) as well as the α-CH of the linker (δ 4.2, v.dt, $^{2}J_{HH}$ = 7.7 Hz, $^{2}J_{PH}$ = 13.5 Hz) both correlate with the ^{31}P{^{1}H} signal at δ 1.6. Interestingly, no coupling of the hydride to the *cis* ^{13}CO could be resolved. However, correlation of a signal at δ 176.9 in the ^{13}C APT NMR spectrum to the Ir-H resonance by ^{13}C HMBC confirms the presence of a single CO ligand for **3.14**. The formation of **3.14** could result from reductive elimination of H_2 from **3.12** to form the dicarbonyl monohydride species **3.13** (not observed), which upon the overall associative binding of the imine and CO dissociation, results in the formation of **3.14**.

The third hydride intermediate detected is **3.16**, which corresponds to the $^{31}P\{^{1}H\}$ NMR singlet resonance at δ 30.6. The ^{31}P HMBC of the reaction conducted with ^{13}C-labeled CO correlates this ^{31}P resonance to an N-H resonance (δ 6.0, s) and a hydride signal (δ -12.1, dq, $^{2}J_{PH}$ = 80.3 Hz, $^{2}J_{CH}$ = 5.3 Hz); the quartet pattern for the hydride is a result of coupling to three equivalent ^{13}CO ligands, which are correlated to a resonance located in the ^{13}C APT NMR spectrum (δ 176.5, d, $^{2}J_{PC}$ = 8.5 Hz) by a ^{13}C HMBC NMR experiment. The most important structural feature of **3.16** is that the ligand is in the enamine form, bound only through the phosphine unit. One possible mechanism for formation of **3.16** is the unobserved dicarbonyl intermediate **3.13** undergoes imine-to-enamine tautomerism to form **3.15**, trapping **3.15** with CO forms **3.16**. This tautomerization (conversion of **3.13** to **3.15**) is potentially a key step by which these imine-phosphine ligands can replicate linker reactivity, as it provides a simple way for a proton to shuttle between the donor and linker of the ligand.

As shown in Scheme 3.8 and detailed in Scheme 3.9, the CO induced conversion of hexahydride **3.9a** to dicarbonyl **3.10a** requires loss of two equivalents of H_2 per iridium center, where three of the hydrogen atoms come from the iridium hydrides and one originates from the backbone of the ligand. Precisely how the hydrogen from the ligand combines with a metal hydride based on the results of the experiments reported above is not entirely clear, nevertheless, one can speculate on some of the possibilities.

The observation of **3.16** during the formation of **3.10a** suggests ligand tautomerization occurs. The equilibrium between **3.13** and **3.15** in Scheme 3.9 can account for this, but it should be emphasized that during the CO addition reaction to the hexahydride **3.9a** no other intermediates after **3.16** are observed. Changing the conditions by monitoring addition of H_2 to the dicarbonyl **3.10a** allows for identification of a new intermediate not present while H_2 is being

lost from **3.9a**. This new species is identified as the dihydride dicarbonyl **3.17** in Scheme 3.9. **3.17** is formed by oxidative addition of H_2 to **3.10a**. Particularly diagnostic of **3.17** are the two doublet hydride resonances, one of which shows a large *trans* coupling to phosphorus ($^2J_{PH}$ = 123.0 Hz) and the other shows a smaller coupling indicative of being *cis* to the phosphine ($^2J_{PH}$ = 12.0 Hz). Confirmation that **3.17** has two carbonyl ligands is obtained by addition of H_2 to the ^{13}CO-labeled isotopologue of **3.10a**, which results in more complex ^{1}H NMR resonances for the hydride ligands of **3.17**, consistent with one CO *trans* to one of the hydrides and one CO *cis* to both hydrides. After longer periods under excess H_2, **3.17** converts to **3.12**, the imine trihydride generated via the CO addition process discussed above. It is worth noting that the conversion of **3.17** to **3.12** results in transfer of a hydrogen atom from iridium to the ligand.

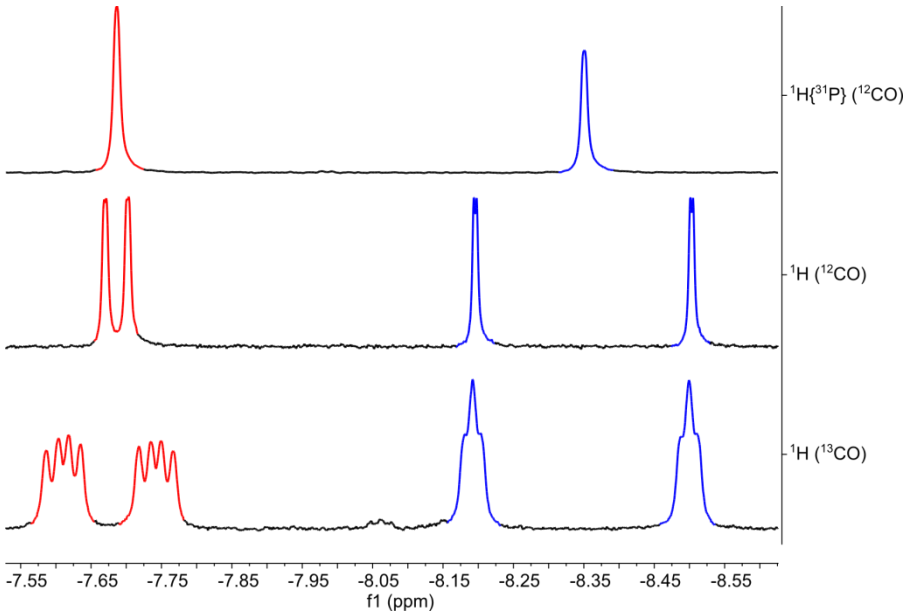

Figure 3.6: ^{1}H NMR spectra of hydride resonances assigned to **3.17** with and without ^{13}C labled CO coordinated to Ir. The resonances assigned as *trans* to P are highlighted in **blue**. The resonances assigned as *cis* to P are highlighted in **red**.

3.5 Conclusions

The identification of ligand-based processes that might combine with fundamental reactivity patterns namely oxidative addition and reductive elimination is the subject of this study, which involves a simple bidentate imine-phosphine ligand and its coordination chemistry and reactivity with iridium. Examination of some simple reactions provides evidence that a hydrogen atom from the ligand backbone can combine with an iridium hydride to generate dihydrogen, and conversely a hydride on iridium can be transferred to the ligand. Multinuclear NMR and ^{13}CO labeling studies suggest that this process results via oxidative addition of a dissociated enamine to generate an enamide hydride, shown in Scheme 3.9 as the equilibrium between **3.15** and **3.17**, which provides the key connection to relay the ligand proton to the iridium and ultimately form H_2. Additionally imine enamine tautomerism may relay the ligand proton between the donor nitrogen and the linker of the ligand (**3.13** to **3.15**). This reactivity is different from previous reports regarding how protons transfer to and from the linker of other multi-dentate enamide phosphine ligands, where the N donor of the ligand is tethered to Ir.[14,98,99]

Chapter 4: Linker Reactive Enamide Phosphine Ligands for Ruthenium

4.1 Introduction

As discussed in Sections 1.3-6 of Chapter 1, ligand systems that can participate in metal-catalyzed reactions are a topic of current interest. Of particular note are cooperative ligands that can act in concert with a metal to activate small molecules such dihydrogen (H_2). One such system is shown in Scheme 4.1 where the ruthenium complex **1.29** is coordinated by a linker-reactive pyridine-based ligand. This system acts as a catalyst for a variety of processes, for example, the acceptorless dehydrogenation (AD) of primary alcohols to give esters (equation 1.2).[3,6,89,104] As shown in the scheme below, one of the key processes is the addition and elimination of H_2, which occurs without a change in oxidation state at the ruthenium center and involves the overall heterolytic cleavage of H_2 with the linker of the ligand in **1.29** accepting a proton and the hydride binding to the ruthenium to generate **1.30**.

Scheme 4.1:

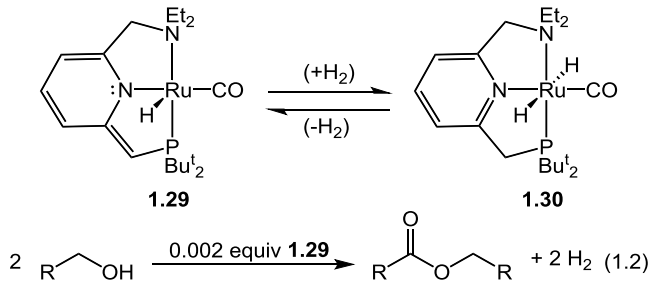

As discussed in Chapter 3, simplification of the cooperative ligand system in **1.29** by the use of a bidentate enamide phosphine ligand set coordinated to Ir(I), and examination of reactions involving H_2 and CO revealed ligand-assisted activation of dihydrogen occurs. While this Ir(I) system was able to add and release H_2 no AD catalysis was possible as a variety of stable iridium products formed upon reaction with primary and secondary alcohols. Changes in

oxidation state from Ir(I) to Ir(III), and the requirement for CO mediated loss of H_2 are associated with catalyst deactivation.

In this chapter, an expanded series of bidentate enamide-phosphine ligands similar to those reported in Chapter 3 are paired with an appropriate Ru(II) precursor to generate four different ruthenium enamide phosphine complexes. As highlighted in Section 1.6 of Chapter 1, varying the steric and electronic environment of the pyridine based ligand scaffold can cause changes in selectivity during catalysis;[3,6] however, little difference in reactivity with hydrogen has been reported.[3,6] The influence of ligand variation on reactivity with hydrogen is discussed here. Additionally, the catalytic AD reactivity of one of the four derivatives is explored.

4.2 Synthesis of Ruthenium Enamide Phosphine Complexes

The synthesis of cyclopentyl-linked imine phosphine ligands has been discussed previously in this work and elsewhere.[20,139,140,164] In this chapter, the *ortho* positions of the *N*-aryl group (R = Pr^i or Me), and the substituents on the phosphine donor (R' = Pr^i or Bu^t) are varied to explore the impact these modifications have on ligand cooperativity (Scheme 4.2). The short form descriptors of the ligands reported in this chapter are $^{R}(NP)^{R'}$. In solution, the imine-phosphine and enamine-phosphine tautomers each display unique singlets in their $^{31}P\{^{1}H\}$ NMR spectra, which allows easy determination of the amount of each tautomer. When R' is Pr^i the equilibrium between the two tautomers slightly favors the enamine form. When R' is Bu^t the equilibrium is shifted almost entirely toward the enamine form. The most sterically demanding ligand, **4.1c** exists exclusively in the enamine tautomeric form.

Scheme 4.2:

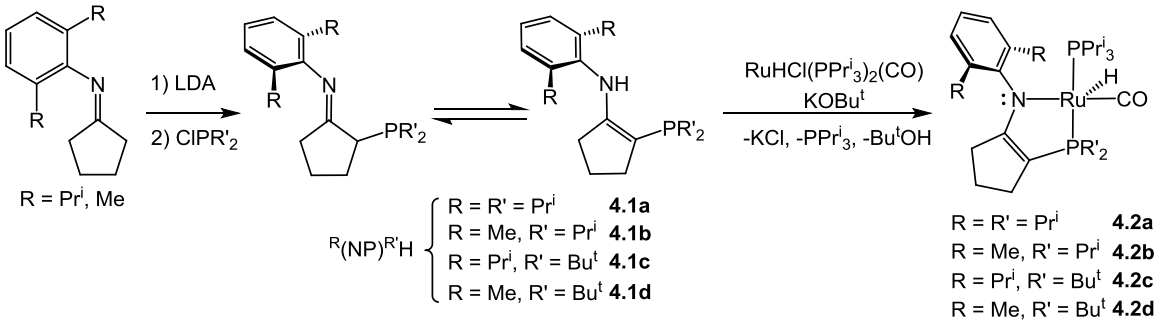

Reacting **4.1a-d** with $RuHCl(PPr^i_3)_2(CO)$ in the presence of one equivalent of potassium *tert*-butoxide forms a dark red solution in every case. $^{31}P\{^1H\}$ NMR spectroscopy shows two doublet resonances with large coupling constants indicative of *trans* disposed phosphines for **4.2a-d**. After the reaction is complete and following workup, analytically pure ruthenium enamide phosphine complexes are obtained in acceptable yields (~42 %). The multinuclear NMR spectra of **4.2a-d** are all consistent with C_1 symmetric, five-coordinate complexes.

When concentrated pentane solutions of **4.2a** or **4.2c** were cooled to -35 °C crystals of both compounds were obtained, and analyzed by X-ray diffraction. ORTEP representations of **4.2a** and **4.2c** are shown in Figure 4.1 and Figure 4.2, respectively. For both **4.2a** and **4.2c**, the hydride ligand could be located and freely refined. Both structures are distorted from an idealized geometry, but are approximately square pyramidal.[165] For the PPr^i derivative, **4.2a**, the N1-Ru1-C32 bond angle is 155.36(5)°, the corresponding angle in **4.2c** (N1-Ru1-C100) is more linear at 164.27(7)°, no doubt due to the large *tert*-butyl substituents on the latter. The H50-Ru1-C32 angle is 84.1(7)° for **4.2a**, the corresponding angle in **4.2c** is 85(1)°. The above angels are noteworthy as DFT calculations performed on a related Ru enamide phosphine complex, which could not be characterized by X-ray analysis, suggest upon switching from and amido phosphine[45] to an enamide phosphine donor a square-based pyramidal structure is favored over a

trigonal bipyramidal geometry.[65] The structures of **4.2a** and **4.2c** are consistent with this proposal.

The bond lengths and angles of the enamide phosphine unit are nearly identical for both **4.2a** and **4.2c**; however, some subtle differences occur in the bond lengths around the coordination sphere of the two ruthenium centers. The Ru1-N1 bond length is slightly longer for the PBu^t derivative; for example, for **4.2a** this length is 2.1287(2) Å, and lengthens to 2.143(2) Å for **4.2c**. The oxygen-carbon bond length of the carbonyl group attached to ruthenium is 1.1641(2) Å for **4.2a** and 1.171(3) Å for **4.2c**; therefore, changing from PPr^i_2 to PBu^t_2 groups corresponds to a slight lengthening in of the CO triple bond of the carbonyl ligand. The CO stretching frequencies of **4.2a-d** are very similar and range from 1893 to 1899 cm^{-1} (Table 4.1), which indicates that the difference in electronic influence of these ligands on Ru is minimal, as reflected by the CO ligand. Interestingly, the CO stretch for **1.29** is also 1899 cm^{-1}, which is virtually identical to the series of derivatives reported here. Given the differences in H_2 activation for complexes **4.2a-d** as compared to **1.29**, it is clear that electronic effects at the metal center are not that important for cooperative H_2 activation for these systems. CO stretching frequencies of 1.29 and 4.2a-d

Table 4.1: Carbonyl stretching values for **4.2a-d** and **1.29**

Complex	*N*-Aryl group	PR_2 group	ν (CO) (cm^{-1})
1.29	-	-	1899[a]
4.2a	Pr^i	Pr^i	1899
4.2b	Me	Pr^i	1895
4.2c	Pr^i	Bu^t	1893
4.2d	Me	Bu^t	1895

[a] recorded in KBr pellet[89]

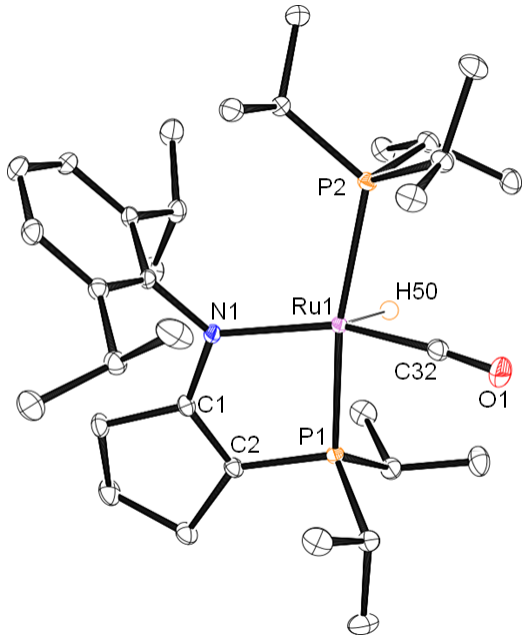

Figure 4.1: ORTEP drawing of the solid state molecular structure of **4.2a** with probability ellipsoids at 50%. Hydrogen atoms are omitted for clarity, with the exception of H50, which was found in the difference map. Selected bond lengths (Å) and angles (°): Ru1-N1 2.1287(2), Ru1-P1 2.3273(6), Ru1-P2 2.4080(6), Ru1-C32 1.8196(14), N1-C1 1.3795(2), C1-C2 1.3643(19), C2-P1 1.7629(2), C32-O1 1.1641(2), N1-C1-C2 125.43(2), C1-C2-P1 113.51(2), N1-Ru1-P1 81.47(4), C32-Ru1-P1 88.62(5), N1-Ru1-P2 106.42(4), P1-Ru1-P2 166.601(2), N1-Ru1-C32 155.36(5) C32-Ru1-H50 84.1(7).

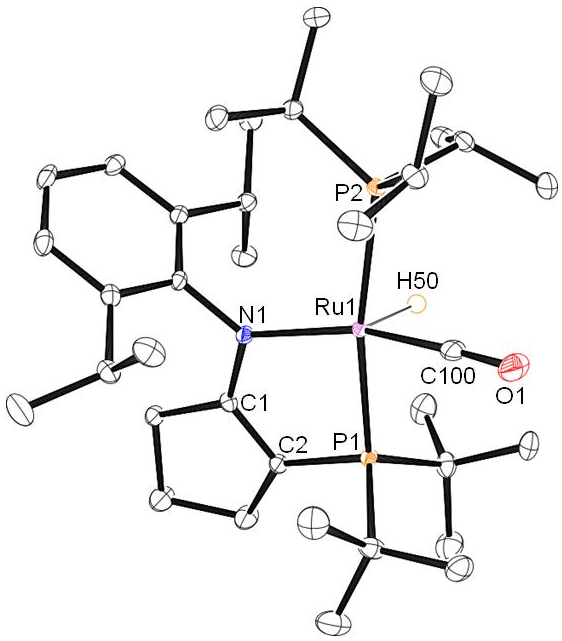

Figure 4.2: ORTEP drawing of the solid state molecular structure of **4.2c** with probability ellipsoids at 50%. Hydrogen atoms are omitted for clarity, with the exception of H50, which was found in the difference map. Selected bond lengths (Å) and angles (°): Ru-N1 2.143(2), Ru1-P1 2.3575(5), Ru1-P2 2.4217(5), Ru1-C100 1.822(2), N1-C1 1.377(2), C1-C2 1.373(2), C2-P1 1.770(2), C100-O1 1.171(3), N1-C1-C2 125.2(2), C1-C2-P1 113.9(1), N1-Ru1-P1 81.05(4), C100-Ru1-P1 90.21(6), N1-Ru1-P2 106.19(4), P1-Ru1-P2 169.06(2), N1-Ru1-C100 164.27(7) C100-Ru1-H50 85(1).

4.3 Reactivity of Ruthenium Enamide Phosphine Complexes with Dihydrogen

As monitored by ^{1}H , $^{1}H\{^{31}P\}$, and $^{31}P\{^{1}H\}$ NMR spectroscopy, exposing solutions of **4.2a-d** to one to four atmospheres of H_2 forms products consistent with **4.3a-d** (Scheme 4.3). Carefully controlling hydrogen pressure, solvent volume, and headspace volume allows addition of reproducible amounts of dihydrogen to a variety of samples. Therefore, the impact of changing the sterics and electronics of the ligand on reactivity with H_2 is possible. The least sterically demanding variant (**4.2b**) reacts to completion with H_2 to form two products in a 2.4:1 ratio. The two products potentially correspond to diastereomers due to the presence of the chiral center on the ligand and the chiral ruthenium center. The α-CH unit can be *syn* or *anti* to the apical Ru-H. The presence of these two diastereomers complicates the solution NMR data so much that assignment of the resonances for the minor diastereomer is not attempted here; however, multinuclear NMR studies are consistent with the two products being different isomeric forms of **4.3b**. Importantly, ^{1}H-^{13}C HSQC allows for assignment of ^{13}C resonances as α-CH protons for both the major and minor isomer, therefore, the imine tautomeric form of the ligand is bound to Ru in both cases.

When the alkyl groups decorating phosphorus (R') are changed from isopropyl to *tert*-butyl the rate of dihydrogen addition is much slower and the reactions never reach completion despite an observable (by ^{1}H NMR spectroscopy) excess of H_2 and extended reaction times. Identification of **4.3c,d** is based on ^{1}H NMR resonances consistent with the hydride ligands observed for complexes **4.3a,b**, the concentration of **4.3c,d** relative to the respective staring materials is such that obtaining ^{13}C NMR data was not attempted and no further characterization was possible.

Scheme 4.3:

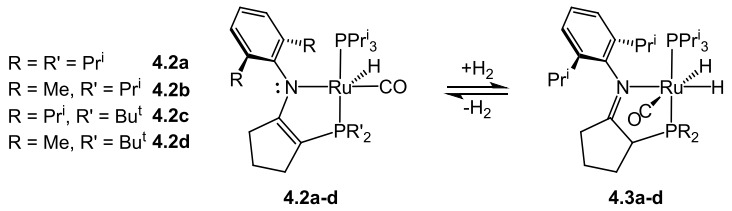

The conversion of **4.2a** to **4.3a** proceeds cleanly and to completion over the course of approximately 12 h at room temperature. Complex **4.3a** is isolated as a pale yellow, crystalline solid after workup. Several diagnostic features of the ^{1}H and ^{31}P{^{1}H} NMR spectra indicate formation of **4.3a**. In the ^{31}P{^{1}H} NMR spectrum, new resonances at δ 74.5 and 92.9 are observed. The P-P coupling constant ($^{2}J_{PP}$ = 252.3 Hz) is consistent with *trans* disposition of the two phosphine ligands. Two signals in the hydride region of the ^{1}H NMR spectrum at δ -18.4 and -5.5 and are observed. Additionally, a resonance assigned to the α-CH proton that results from the overall heterolytic cleavage of H_2 at δ 3.1 can be identified. Multinuclear NMR studies as well as deuterium labeling experiments confirm that the linker α-CH of **4.3a** originates from added H_2.

Dissolving **4.3a** in a minimal amount of pentane and cooling the mixture to -35 °C resulted in formation of X-ray quality crystals. Figure 4.3 shows an ORTEP representation of **4.3a**. The ruthenium center is bound to two hydride ligands that are *cis* disposed to one another. Two molecules corresponding to **4.3a** are present in the asymmetric unit of the crystal structure. In both cases, the geometry, bond lengths, and angles are consistent with the neutral imine tautomeric form of the ligand coordinated to ruthenium. The two molecules in the asymmetric unit of the space group $P2_1/c$ correspond to the (*S*) enantiomer. The (*R*) enantiomer is also present in the crystal lattice, and is generated by the c-glide plane of the space group. Overall,

the most notable feature of the solid state structure is the *cis* disposition of the two hydride ligands. The stereochemistry of the hydride ligands suggests a different mechanism than direct proton transfer to the linker of the ligand and hydride addition to the Ru center occurs, since the reaction of **1.29** and related compounds with dihydrogen all give products with *trans* disposed hydrides (Scheme 4.1).[65,67,89,104,166]

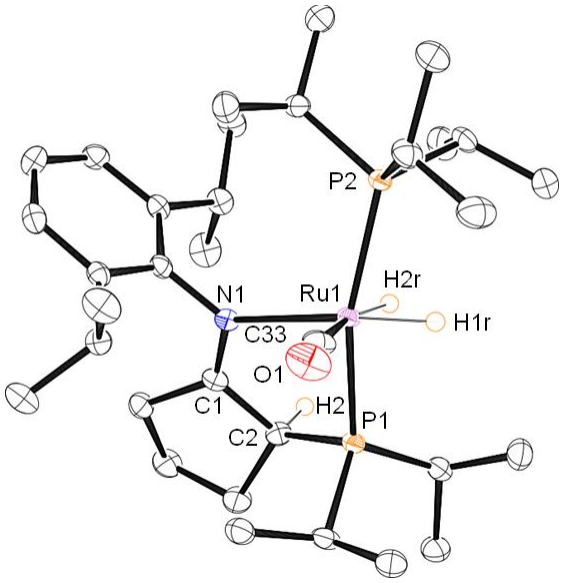

Figure 4.3: An ORTEP drawing of the solid state molecular structure of **4.3a** with probability ellipsoids at 50%. All of the hydrogen atoms except α-CH proton and hydrides are omitted for clarity. The α-CH proton and hydrides were located in the difference map. Selected bond lengths (Å) and angles (°): Ru1-N1 2.306(4), Ru1-P1 2.292(1), Ru1-P2 2.331(1), Ru1-C32 1.872(5), N1-C1 1.294(6), C1-C2 1.511(6), C2-P1 1.854(5), C32-O1 1.172(6), N1-C1-C2 122.2(4), C1-C2-P1 109.1(3), N1-Ru1-P1 80.8(1), C33-Ru1-P1 100.5(1), N1-Ru1-P2 107.8(1), P1-Ru1-P2 161.99(4), N1-Ru1-C33 101.3(2).

Monitoring the conversion of **4.2a** to **4.3a** under approximately 3.6 atm (6.5 equivalents) of dihydrogen by ^{1}H and $^{31}P\{^{1}H\}$ NMR spectroscopy reveals that an intermediate species, **4.4**, forms in less than 20 minutes and goes on to form **4.3a** (Scheme 4.4) over a period of 5.4 hours (95 % complete). While this intermediate was never isolated as a pure material, several

spectroscopic features are consistent with the dihydride dihydrogen complex (**4.4**) shown in Scheme 4.4.

Scheme 4.4:

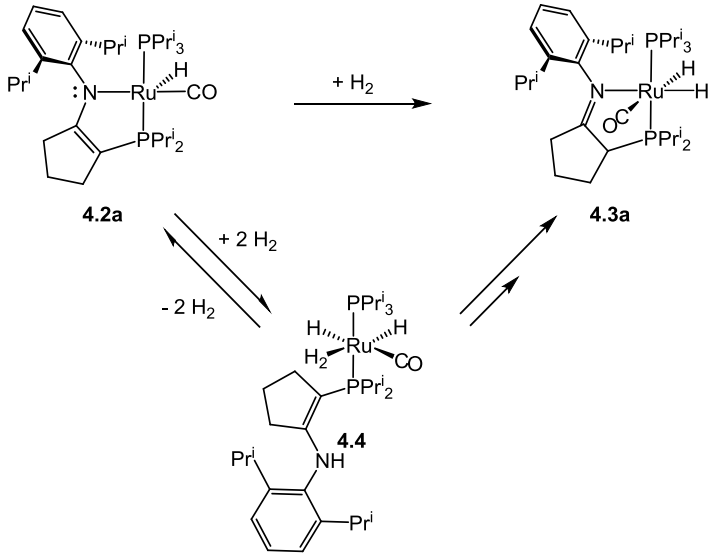

Doublet resonances at δ 80.1 and 41.2 assigned to **4.4** are observed by $^{31}P\{^{1}H\}$ NMR spectroscopy. The P-P coupling constant ($^{2}J_{PP}$ = 195.8 Hz) confirms that the phosphine ligands remain *trans* to one another. Certain resonances in the ^{1}H NMR spectrum are especially diagnostic. For example, a sharp singlet at δ 8.9 is assigned as the NH proton of **4.4**. A broad resonance at δ -7.2 that integrates to four protons relative to the signal at δ 8.9 is also observed. Measuring the relaxation time of this upfield resonance at 400 MHz in a solution of 5% CH_2Cl_2 in d_8-toluene as a function of temperature gives a $T_{1,min}$ value of 22 ms at 238 K (Figure 4.4). This relaxation time is comparable to $T_{1,min}$ values reported for two similar dihydrogen dihydride complexes: $RuH_2(H_2)(CO)(PPr^i_3)_2$ ($T_{1,min}$ = 15 ms at 200K, measured at 200 MHz)[167] and $RuH_2(H_2)(CO)(PCp_3)_2$ ($T_{1,min}$ = 42 ms at 233 K measured at 500 MHz).[168] The abbreviation PCp_3 in this case corresponds to tricyclopentylphosphine.

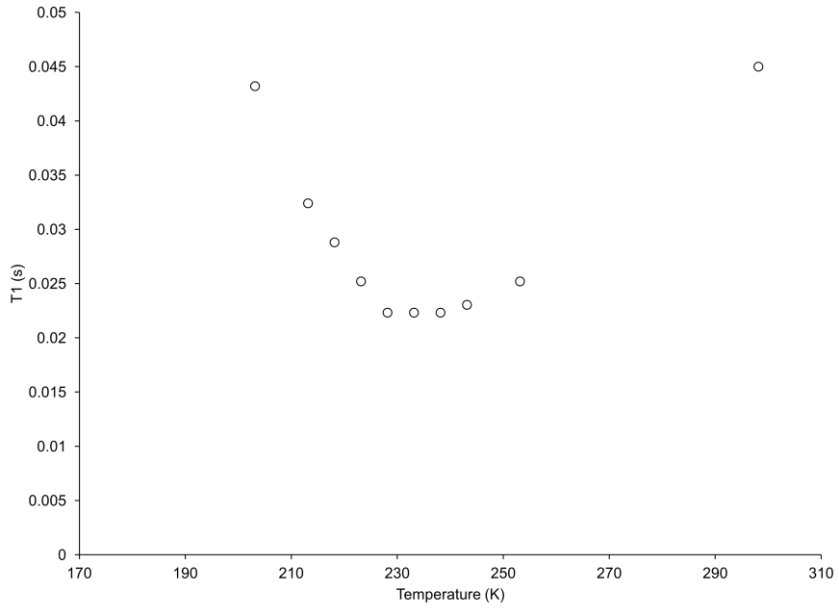

Figure 4.4: The plot of T_1 relaxation time (s) vs. Temperature (K) used to determine a $T_{1,min}$ value of 22 ms at 238 K measured at 400 MHz for the broad resonance at δ -7.2.

Despite several attempts, decoalescence of the hydride ligands from the dihydrogen ligand was never observed using the conditions employed. Complete disappearance of the dihydrogen-dihydride resonance occurred at temperatures below 213 K and the lowest temperature at which meaningful spectra could be recorded at was 173 K. Further cooling to 153 K did not give any return of signal intensity and very broad ^{1}H NMR resonances were observed, possibly due to freezing of the solvent.

Deuterium labeling studies support the assignment of **4.4** as a dihydrogen dihydride complex. Upon exposing **4.2a** to D_2 gas deuterium rapidly scrambles into the broad resonance at δ -7.2. This is consistent with a highly fluxional dihydrogen dihydride species.[167-169] A key feature of **4.4** is the protonated N donor that is de-coordinated from Ru. Presumably, the N-H

proton results from added H_2. Consistent with this proposal, the resonance at δ 8.9 is not observed when D_2 gas is used in place of H_2. An additional observation made during these experiments is the ^{1}H NMR resonance that corresponds to the hydride ligand of **4.2a** disappears much more quickly than the other diagnostic resonances of **4.2a**. Therefore, the hydride of **4.2a** exchanges for a deuteride under D_2.

The reverse reaction (Scheme 4.5), the loss of H_2 from **4.3a** to form **4.2a**, occurs slowly at room temperature under an atmosphere of nitrogen. Evacuating the headspace of a J. Young NMR tube containing a solution of **4.3a**, and heating this mixture to 60 °C gives full conversion of **4.3a** to **4.2a** overnight. Unfortunately, no intermediates were detected by $^{31}P\{^1H\}$ or ^{1}H NMR spectroscopy. Monitoring H_2 loss as a function of time shows only resonances for the dihydride starting material **4.3a** and the enamide-phosphine hydride product **4.2a**, although signals of the latter are broadened, presumably due to some reactivity with hydrogen that is released into the headspace of the NMR tube.

Scheme 4.5:

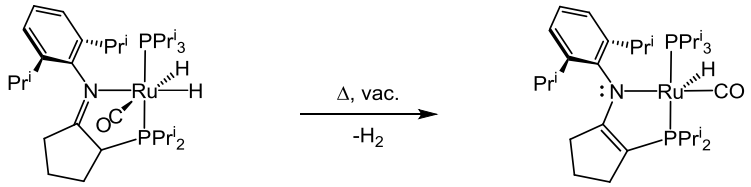

4.3a **4.2a**

4.4 Efforts Toward Catalytic Dehydrogenation of Alcohols

Having established the ability of these complexes to reversibly add and release H_2 attempts to apply this reactivity to the catalytic AD of isopropanol, cyclohexanol and/ or benzyl alcohol (Scheme 4.6) were made. These efforts show certain processes inhibit formation of an active catalyst. Initially, **4.2a** was found to be thermally unstable under catalytic conditions at

temperatures >110 °C, which are normally used for alcohol dehydrogenation reactivity (Table 4.2).[89] For example, heating **4.2a** in refluxing toluene with isopropanol, or cyclohexanol under Ar vented to a mercury bubbler gave no catalytic turnover. Analysis of the reaction mixture by $^{31}P\{^{1}H\}$ NMR spectroscopy showed free PPr^{i}_{3}, consistent with catalyst decomposition. Lowering the temperature to 60 °C allowed for catalytic dehydrogenation of isopropanol and cyclohexanol (Table 4.2, entries 2 and 4). Monitoring 0.9 turnovers of AD converting isopropanol to acetone in an evacuated J. Young tube by ^{1}H NMR spectroscopy shows hydride resonances that are consistent with **4.3a**. The relative concentrations of **4.2a** and **4.3a** vary somewhat during AD; however, full conversion to **4.3a** was not observed. The ratio of **4.2a**:**4.3a** is approximately 1:1.2 after 0.9 turnovers, suggesting **4.3a** can release H_2 under these conditions.

Scheme 4.6:

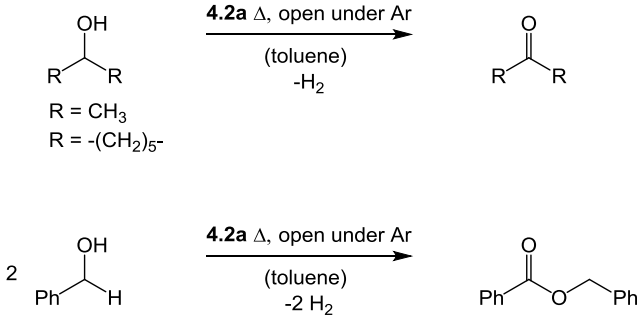

Attempts to dehydrogenate benzyl alcohol to benzyl benzoate at 60 °C under similar conditions to those used for secondary alcohol dehydrogenation were unsuccessful. Initial attempts gave ~ 1 % conversion to benzyl benzoate. $^{31}P\{^{1}H\}$ NMR spectra of recorded of the reaction mixture prior to heating show release of PPr^{i}_{3} and formation of a variety of products. Addition of one equivalent of pyridine relative to ruthenium had little effect on the catalytic performance (~ 2% conversion); likewise, addition of one equivalent of PMe_3 to **4.2a** had little effect (~ 3% conversion).

Table 4.2: Catalytic activity of **4.2a** toward AD of secondary alcohols and benzyl alcohol

Entry	Catalyst	Time (hr)	Temperature (°C)	Substrate	Product	TON[a]	TOF (h^{-1})
1	**4.2a**	12	115	2-propanol	-	-	-
2	**4.2a**	12	60	2-propanol	acetone	100	8.3
3	**4.2a**	12	115	cyclohexanol	-	0	
4	**4.2a**	12	60	cyclohexanol	cyclohexanone	50	4.3
5	**4.2a**	16	60	benzylalcohol	benzylbenzoate	~1	-
6	**4.2a**[b]	16	60	benzylalcohol	benzylbenzoate	~2	-
7	**4.2a**[c]	16	60	benzylalcohol	benzylbenzoate	~3	-

[a] calculated by dividing moles of desired product by moles of **4.2a**. [b] 1 equivalent of pyridine was added **4.2a** prior to addition of substrate and heating. [c] 1 equivalent of PMe_3 was added to **4.2a** prior to addition of substrate and heating.

4.5 Conclusion

The synthesis and reactivity of a series of bidentate enamide phosphine ligands coordinated to ruthenium extend the linker reactivity previously reported for **1.29** and related compounds[65,67,89,104] to new systems. Variation of the groups decorating the N and P donor atoms of the bidentate ligands explored here show that the sterics of the phosphorus donor have a profound impact on the reactivity of **4.2a-d** with H_2. Perhaps the most intriguing feature these studies is the reactivity of **4.2a** with H_2. Identification of **4.4** as an intermediate, which forms during conversion of **4.2a** to **4.3a**, demonstrates N-donor decoordination, and tautomerization of the dissociated arm of the ligand between enamine and imine forms is involved in linker reactivity for this system. The reactivity of **4.2a** with H_2 is reversible, a potentially important feature of an AD catalyst. Monitoring the reactivity of **4.2a** with primary and secondary alcohols

demonstrate it is a catalyst for secondary alcohol dehydrogenation. Attempts to use **4.2a** as an AD catalysts for benzyl alcohol dehydrogenation were unsuccessful.

Chapter 5: A Tridentate Enamide Phosphine Ligand Design

5.1 Introduction

In Chapter 4, it was shown that a series of ruthenium compounds coordinated by enamide phosphine ligands are capable of reversibly accepting and releasing protons from dihydrogen as well as secondary alcohols via a mechanism that involves ligand cooperativity. For one of the compounds, reversible H_2 addition allowed for acceptorless dehydrogenation (AD) of cyclohexanol and isopropanol; however, attempts to extend this reactivity to the formation of benzyl benzoate from benzyl alcohol resulted in catalyst decomposition and very low turnover numbers. In comparison, the pyridine-based ruthenium pincer complex shown in Scheme 5.1 (**1.29**) catalyzes the formation of 466 equivalents of benzylbenzoate from benzyl alcohol in 4 hours.[89] An obvious difference between the bidentate (NP) ligands from Chapter 4, and the tridentate (PNN) pincer ligand shown in Scheme 5.1 is the denticity of the scaffold, which leads to sterically and electronically different environments at each respective ruthenium center.

Scheme 5.1:

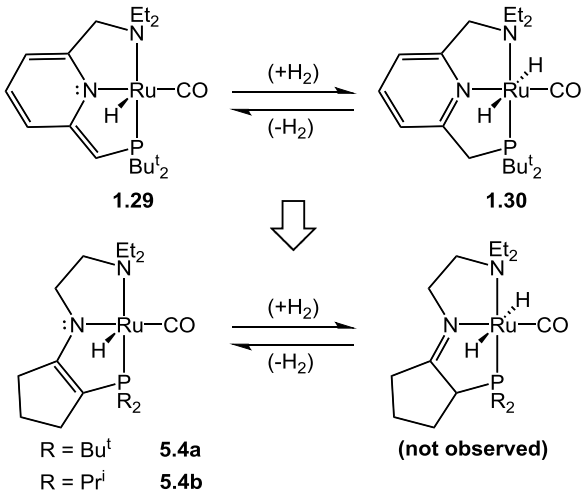

In an effort to generate a cyclopentylidene based ligand-metal system for AD catalysis more directly comparable to **1.29** than the designs used in Chapter 4, a new ligand scaffold was

developed. Features of this design include the cyclopentyl linked enamide phosphine unit as well as the NEt_2 and PBu^t_2 groups present in **1.29** (Scheme 5.1). Coordination of the neutral form of the ligand to ruthenium using an appropriate metal starting material and deprotonation of the resulting complexes with potassium *tert*-butoxide generates the enamide phosphine complexes **5.4a** and **5.4b**, which are catalyst precursors for AD of benzyl alcohol. In this chapter, the synthesis and coordination chemistry of this new ligand system is reported.

5.2 Ligand Synthesis

The tridentate PNN ligands reported in this chapter are prepared by a similar route to the ligands discussed in Chapters 2-4; however, the *N*,*N*-diethylene imine (**5.1**) is used in place of the aryl imine precursors used previously.[170] The synthesis of **5.1** is based on a preparation for related imines,[170] condensation of *N*,*N*-diethylethylenediamine and cyclopentanone generates **5.1** in modest yield after purification by distillation (>40 %, Scheme 5.2). Elemental analysis of samples of **5.1** after distillation shows they are not entirely pure; however, this material suffices for proceeding to the next step.

Deprotonation of **5.1** with LDA and treatment with a chlorophosphine generates the desired ligands in moderate yield after workup (55-80 %). It is worth noting that after distillation **5.2a,b** are of sufficient purity to proceed to the next step; however, analytically pure samples of have not been isolated to date. The short form descriptors of these ligands are $(PNN)^{But}$ (**5.2a**) and $(PNN)^{Pri}$ (**5.2b**), where Bu^t and Pr^i correspond to the different phosphine donors: either di-*tert*-butyl or diisopropyl. In solution, both **5.2a** and **5.2b** exist in exclusively the enamine tautomeric form as established by multinuclear NMR spectroscopy. Diagnostic of formation of the enamine tautomer are ^{1}H NMR resonances at δ 5.5 for **5.2a** and δ 5.3 for **5.2b**, assigned as the NH protons of the enamine form of these ligands.

Scheme 5.2:

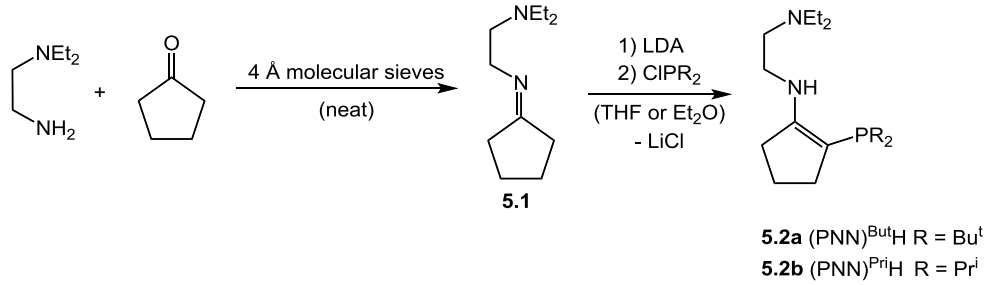

5.3 Coordination of the Neutral Ligands to Ruthenium

Reacting **5.2a** or **5.2b** with an equivalent amount of $RuHCl(PPr^i_3)_2(CO)$ results in coordination of the ligands to ruthenium and release of PPr^i_3 to form new ruthenium complexes (Scheme 5.3). New signals in the $^{31}P\{^1H\}$ NMR spectra at δ 109.6 (**5.3a**) and 94.2 (**5.3b**) indicate formation of the respective products.

Scheme 5.3:

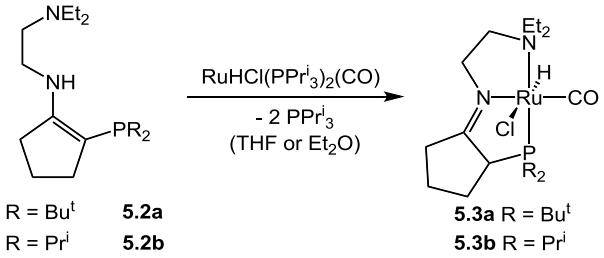

Both **5.3a** and **5.3b** are colorless solids, and can be obtained analytically pure in good yields (55-84 %) after workup. The solubilities of **5.3a** and **5.3b** are significantly different; **5.3a** is partially soluble in THF and insoluble in other non-polar solvents such as benzene, hexanes and pentane. **5.3b** is partially soluble in diethyl ether, and readily dissolves in benzene.

Multinuclear NMR spectroscopy indicates the formation of ruthenium hydride complexes coordinated by the imine form of the ligand for both **5.3a** and **5.3b**. For example, the ^1H NMR spectrum of **5.3a** recorded in CD_2Cl_2 shows a resonance at δ 4.0 that a ^1H-^{13}C HSQC NMR experiment correlates to a doublet ^{13}C resonance at δ 57.3 ($^1J_{PC}$ = 10.3 Hz), consistent with the

α-CH proton of the imine tautomer. The resonance at δ -16.3 ($^2J_{PC}$ = 23.5 Hz) is assigned to the hydride ligand attached to ruthenium. Similar NMR spectroscopic features are present for **5.3b**, and overall, the multinuclear NMR spectroscopic data for both compounds is consistent with the structure shown in Scheme 5.3. Elemental analysis confirms the composition and purity of both **5.3a** and **5.3b**.

5.4 Synthesis of Ruthenium Enamide Phosphine Complexes

Deprotonation of **5.3a** or **5.3b** dissolved in THF with potassium *tert*-butoxide proceeds slowly over the course of several hours to form new products consistent with **5.4a,b** (Scheme 5.4). The solution turns deep red as the reaction proceeds, and is accompanied by an upfield shift of the signals in the $^{31}P\{^1H\}$ NMR spectrum; for example, the resonance at δ 109.6 (**5.3a**) converts to a new resonance at δ 92.3 (**5.4a**). A similar upfield shift in the $^{31}P\{^1H\}$ NMR spectrum occurs upon deprotonation of **5.3b**.

Scheme 5.4:

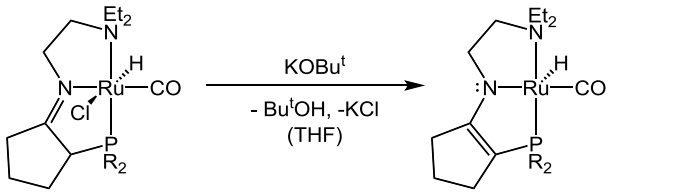

The solution NMR data for **5.4a,b** are consistent with the formation of the new Ru(II) hydride complexes shown in Scheme 5.4. The α-proton of the neutral ligand coordinated to ruthenium in **5.3a,b** has been deprotonated to generate an enamide phosphine scaffold. The resonance at δ 90.0 in the ^{13}C APT NMR spectrum of **5.3a**, which couples to ^{31}P ($^1J_{PC}$ = 41.3 Hz), is diagnostic of the α-C of the enamide phosphine unit. Supporting this assignment, no cross correlation in the ^1H-^{13}C HSQC NMR spectrum is observed for this ^{13}C signal. Other

features of the ^{1}H NMR spectrum of **5.4a** recorded in C_6D_6 include a hydride resonance at δ -25.2 (d, $^{2}J_{PH}$ = 25.5 Hz) and two sharp doublet resonances that couple to ^{31}P at δ 1.4 and 1.5; these resonances are assigned to the *tert*-butyl methyl groups on the phosphine. Overall, the diagnostic features of the ^{1}H NMR spectrum of **5.4a** indicate retention of the hydride ligand during the reaction with base and a C_1 symmetric structure in solution. Similar features are present for **5.4b**, and elemental analysis of both compounds confirms their composition and purity.

For comparison of **5.4a** and **5.4b** with the pyridine based system (**1.29**) shown in Scheme 5.1 some features of the ^{13}C APT NMR data and CO stretching frequencies recorded by FTIR spectroscopy are presented in Table 5.1. Perhaps unsurprisingly, there are considerable differences between **5.4a,b** and **1.29**. The ^{13}C NMR resonances of the linker for **1.29** are shielded in comparison to the relevant resonances of **5.4a,b**. The FTIR data for **5.4a,b** give values that are very similar to one another, but smaller than the value recorded for **1.29**. One plausible rationale for the spectroscopically observed variance between these two systems could rely on differences in electron density distribution in the linker unit of these ligands.

Table 5.1: ^{13}C NMR and ATR-FTIR spectroscopic features of Ru enamide phosphine complexes

Entry	Complex	Linker/ α-C δ (ppm)	$^{1}J_{PC}$ (Hz)	*N*-$C_{enamide}$ δ (ppm)	$^{2}J_{PC}$ (Hz)	ν (CO) (cm^{-1})
1[a]	**1.29**	65.3	50.3	169.1	15.1	1899
2	**5.4a**	90.0	41.3	180.2	26.0	1875
3	**5.4b**	88.7	44.1	180.6	18.4	1874

[a] all ^{13}C NMR data recorded in C_6D_6, CO stretching frequency for Entry 1 recorded a KBr pellet.

Storing a concentrated pentane solution of **5.4a** at -35 °C overnight results in formation of crystals, which were analyzed by X-ray diffraction. Figure 5.1 depicts an ORTEP representation of the solid state molecular structure of **5.4a**. Overall, it is similar to the enamide

phosphine ruthenium complexes discussed in Chapter 4. The N1-C2 bond length of 1.370(4) Å is similar to the values recorded for **4.2a** (1.380(2) Å) and **4.2c** (1.377(2) Å). The C1-C2 bond length of 1.358(3) Å is typical. One notable difference between the solid state structures of **5.4a** and **4.2a,c** is that the Ru1-N1 bond length is contracted for the tridentate system (2.042(3) Å) in comparison to the Ru1-N1 bond lengths for **4.2a** (2.1287(2) Å) and **4.2c** (2.143(2) Å). Unfortunately, a solid state structure of **1.29** has not been reported to date; therefore, a comparison is not possible.

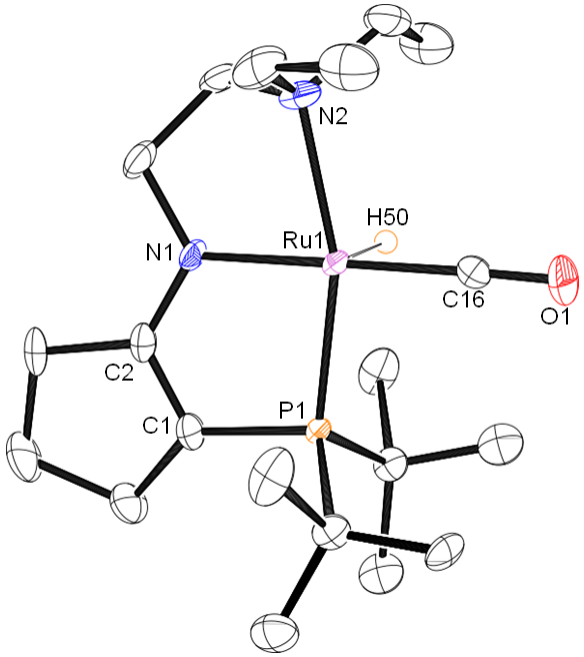

Figure 5.1: ORTEP drawing of the solid state molecular structure **5.4a** shown with 50% thermal ellipsoids. The hydrogen atoms have been omitted for clarity except for H50, which was located in the difference map. The structure of **5.4a** is severely disordered about a mirror plane; a simplified structure that does not illustrate the modeled disorder is illustrated here. Selected bond lengths (Å) and bond angles (°): Ru1-N1 2.042(3), Ru1-N2 2.235(2), Ru1-P1 2.2912(6), Ru1-C16 1.844(3), N1-C1 1.370(4), C1-C2 1.358(3), C2-P1 1.795(2), C16-O1 1.164(3), N1-C1-C2 122.1(2), C1-C2-P1 113.91(2), N1-Ru1-P1 82.58(8), C16-Ru1-P1 95.59(8), N1-Ru1-N2 79.28(9), P1-Ru1-N2 161.73(6), N1-Ru1-C16 174.0(2).

5.5 Reactivity of Ruthenium Enamide Phosphine Complexes

In Chapters 3 and 4, pairing bidentate enamide phosphine scaffolds with iridium and ruthenium revealed that these ligands are capable of shuttling protons from dihydrogen to and from the donor and linker positions of the ligand. In every case where a proton is shuttled from the metal to the linker of the ligand, evidence suggests that the N donor of the ligand is protonated and dissociates from the metal. Tautomerization of the dissociated arm transfers a proton between the N donor and the α-C of the linker.

For **5.4a,b**, the potentially reactive enamide nitrogen is tethered to the metal with N and P donors. Tethering the enamide N to ruthenium should disfavor dissociation and therefore potentially change the mechanism for linker reactivity in comparison to the bidentate systems discussed above. For the above reasons, exploring the potential of this ligand design to participate in cooperative reactivity was of interest. Both **5.4a** and **5.4b** were exposed to ~4 atm of H_2 in a flame sealed NMR tube. After several days under an observable (by ^{1}H NMR spectroscopy) excess of H_2, the resonances corresponding to **5.4a** did not change, and no new species were detected. Upon heating this mixture to 100 °C for 24 hours ~13 % conversion to a new resonance at δ 32.2 (s) in the $^{31}P\{^1H\}$ NMR spectrum occurs. The unidentified resonance does not match the anticipated chemical shift for a ruthenium dihydride complex; furthermore, no new hydride signals are observed by ^{1}H NMR spectroscopy.

The less sterically demanding derivative, with isopropyl groups decorating phosphorus (**5.4b**) slowly reacts with hydrogen, but not in the manner anticipated based on the experiments carried out in Chapter 4 (Scheme 5.5). Monitoring the reaction by $^{31}P\{^1H\}$ NMR spectroscopy (Figure 5.2) shows formation three new resonances in addition to a resonance at δ 76.4 corresponding to starting material (**5.4b**). The singlet resonance at δ 104.3 assigned as **5.5b** is

observed initially. As the reaction proceeds to completion, this resonance converts into two new doublet resonances corresponding to the final product (**5.6b**) at δ 78.7 and 90.1 ($^2J_{PP}$ = 6.9 Hz).

Scheme 5.5:

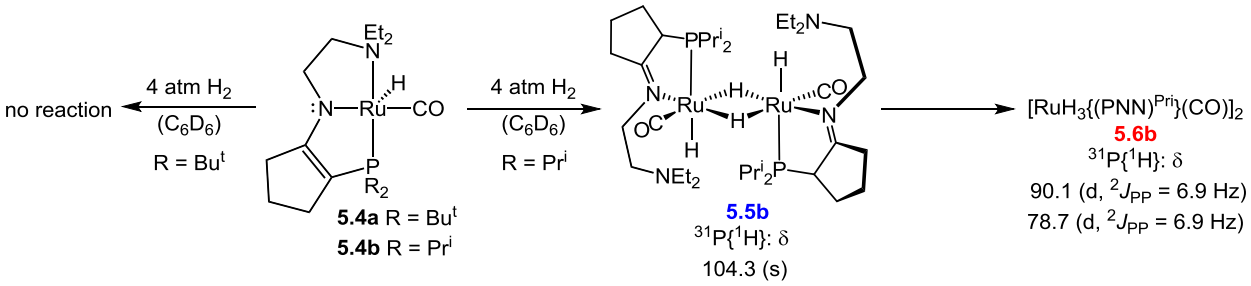

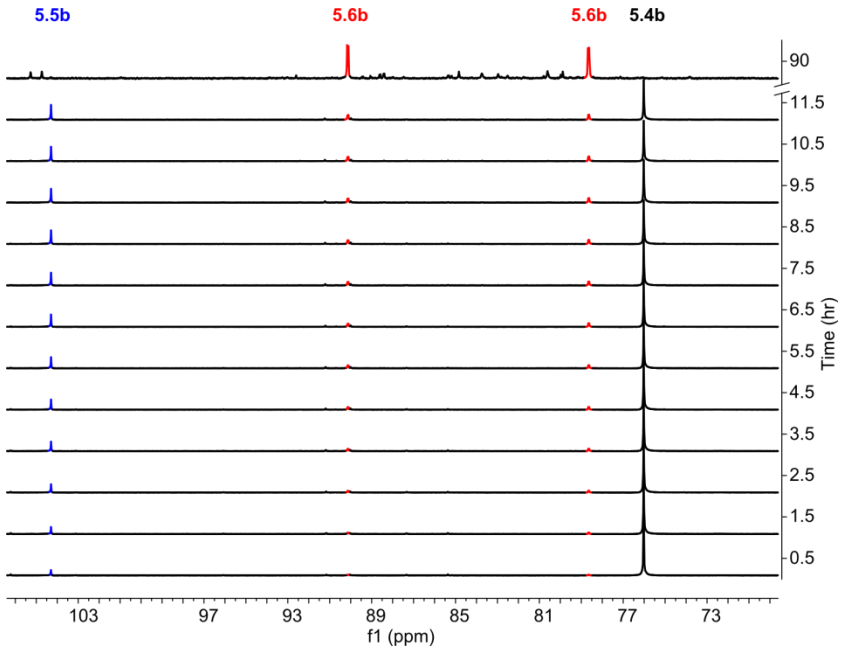

Figure 5.2: A series of $^{31}P\{^1H\}$ NMR spectra collected overtime monitoring the reaction of **5.4b** with H_2 to form **5.5b** and subsequently **5.6b.**

A ^1H NMR spectrum recorded while monitoring the conversion of **5.4b** to new products under hydrogen shows resonances in the hydride region from δ -7.6 to -11.6 (Figure 5.3). For **5.5b**, resonances at δ -7.6 and -11.6 are observed that integrate 1:1 relative to one another. The triplet splitting pattern of the resonance at δ -11.6 is due to coupling to two equivalent ^{31}P nuclei ($^2J_{PH}$ = 16.4 Hz). The large coupling constant observed for the signal at δ -7.6 is indicative of

trans disposition of the hydride ligand relative to ^{31}P ($^{2}J_{PC}$ = 61.0 Hz). Based on the above observations, a structure for **5.5b** is proposed in Scheme 5.5. Although, it should be noted, the complexity of the ^{1}H NMR spectra recorded for **5.5b** prohibited definitive identification of an α-CH proton. Therefore, it is uncertain if linker reactivity is involved in the formation of **5.5b** based on the above experiments.

Assigning a structure for **5.6b** is more challenging. The three hydride resonances corresponding to this species at δ -8.5, -10.5 and -10.6 integrate 1:1:1 relative to one another, suggesting one of the four hydride ligands corresponding to **5.5b** is lost during conversion to **5.6b**. The chemical shift of one of the $^{31}P\{^{1}H\}$ NMR resonances (δ 78.7) is similar to what is observed for **5.4b**, an enamide phosphine complex. However, the color of the reaction mixture (light yellow) suggests a ruthenium enamide phosphine complex (deep red) is not formed. An additional possibility for the structure of **5.6b** is hydrogenation of the imine C-N bond has occurred.[65] The complexity of the multinuclear NMR spectra recorded to date has thus far prohibited further insight into the structure of **5.6b**; therefore, a structure is not proposed in Scheme 5.5.

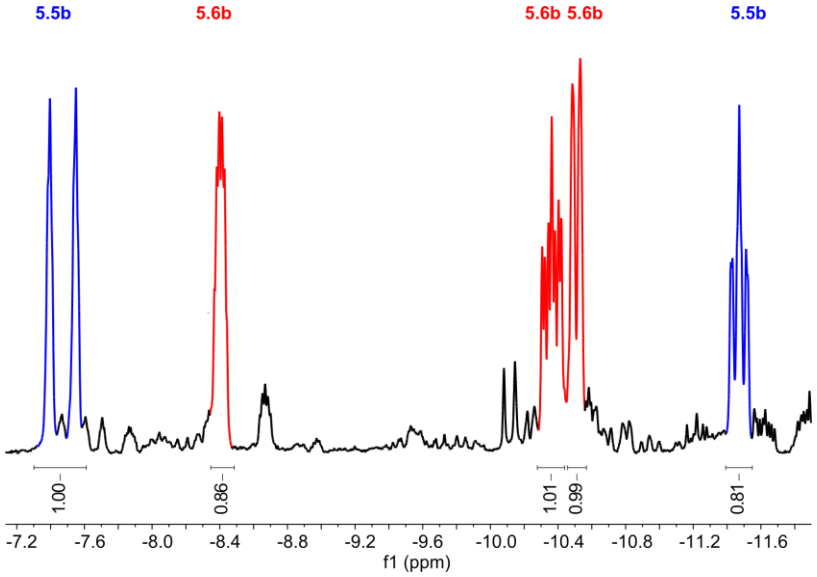

Figure 5.3: A plot of a ^{1}H spectrum (400 MHz, C_6D_6) recorded when the concentration of the intermediate (**5.5b**) is approximately equal to the final product (**5.6b**). Colors highlight the diagnostic resonances corresponding to **5.5b** (**blue**) and **5.6b** (**red**).

In relation to ruthenium complexes coordinated by pyridine based ligands (**1.29**), and the ruthenium complexes explored in Chapter 4, dimer formation is unexpected; however, a similar PNN ligand design paired with iridium forms a hydride bridged dimer upon exposure H_2.[72] Dissociation of the *N*,*N*-diethylamine donor accompanies formation of an equilibrium mixture of dimeric clusters for this iridium system (Scheme 5.6).[72] It is possible a similar process is occurring here.

Scheme 5.6:

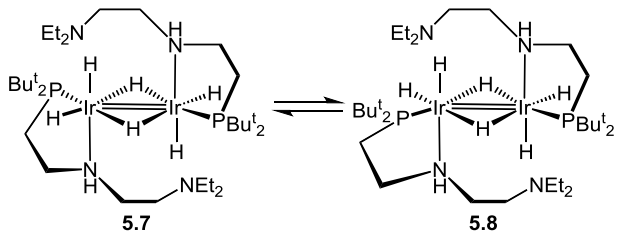

In an effort to explore the potential of **5.4a,b** to act as a catalyst precursors for AD reactivity **5.4a** was exposed to 100 and 1000 equivalents of benzyl alcohol in toluene. As

mentioned in the introduction of this chapter, **1.29** converts ~1000 equivalents of benzyl alcohol to benzylbenzoate in four hours (466 TON, 117 h^{-1} TOF).[89] In an initial experiment, treating **5.4a** with 100 equivalents of benzyl alcohol in a J. Young NMR tube connected to Ar manifold results in 80 % conversion to benzyl benzoate over several days, corresponding to a TON of 40 and a TOF of 0.2 h^{-1}. The conversion profile of this reaction is shown in Figure 5.4. It is consistent with normal catalytic behavior without inhibition. To compare the catalytic activity of **5.4a** directly with **1.29** the previously reported conditions for AD of benzyl alcohol to benzyl benzoate were used.[89] In two separate experiments,1000 equivalents of benzyl alcohol were added to a toluene solution of **5.4a**, the progress of the reaction was monitored by GC-FID. After 4 hours, approximately 0.7 % conversion to benzylbenzoate occurs, heating for 22 hours improved the conversion to 1.3 %. Nearly identical results are obtained for **5.4b** under closely matched conditions. A summary of the catalytic reactivity for **5.4a** and **5.4b** is presented in Table 5.2.

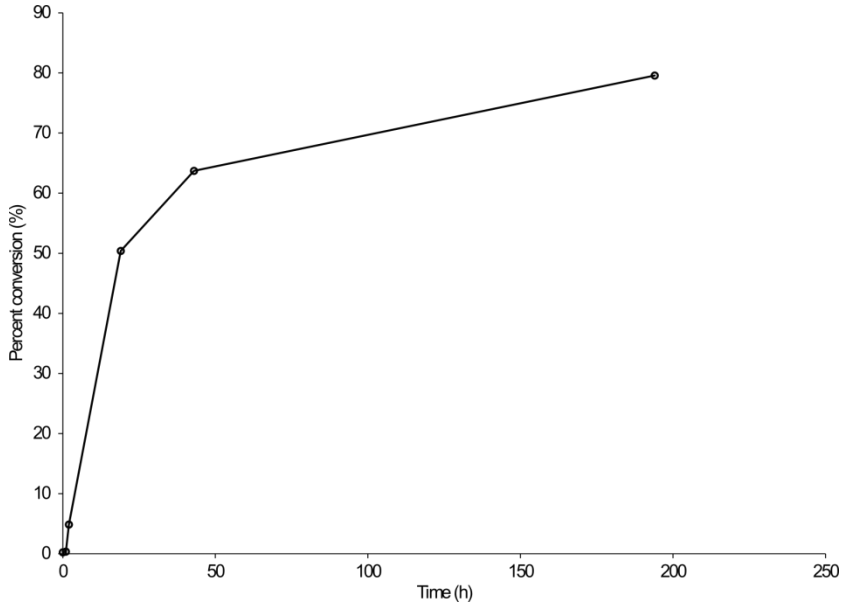

Figure 5.4: Catalytic AD of benzyl alcohol to benzyl benzoate in a J. Young NMR tube vented to an Ar manifold. Reaction progress monitored by ^{1}H NMR spectroscopy (0.041 mmol **5.4a** in 0.5 ml 1.0 M mesitylene in d_8-toluene, 4.1 mmol benzyl alcohol).

Table 5.2: AD of benzyl alcohol to benzyl benzoate using **5.4a** and **5.4b** as catalyst precursors, the substrate to precatalyst ratio is 1000:1.

Entry	Catalyst	Time (hr)	Temperature (°C)	TON	TOF (h^{-1})
1	**5.4a**	22	115	13	0.6
2	**5.4b**	22	115	13	0.6

5.6 Conclusions

In an attempt to probe the effect of incorporating, cyclopentyl linked enamide phosphine units into an overall scaffold similar to the pyridine based system (**1.29**) the synthesis and reactivity of two tridentate enamide phosphine ligands coordinated to ruthenium are reported here. Treating **5.4a,b** with H_2 gave no reaction with **5.4a** and a mixture of products consistent with ruthenium hydride bridged dimers for **5.4b**. Addition of **5.4a** or **5.4b** to toluene solutions of

benzyl alcohol facilitates limited AD catalysis to form benzyl benzoate. The rate if conversion is much slower than what is reported for **1.29**.[104]

Chapter 6: Overview and Future Work

6.1 Overview

This thesis presents the coordination chemistry of multidentate imine and enamide phosphine ligands with Rh, Ir and Ru. The initial goal was to explore whether cyclopentyl linked enamide phosphine scaffolds could participate in ligand cooperativity when coordinated to late transition metals. Identification of metal complexes that participate in cooperative reactivity patterns as well as some limited acceptorless dehydrogenation (AD) catalysis were outcomes of this work. Previous reports of enamide phosphine ligands coordinated to a variety of late transition metals show that the linker position of the enamide phosphine scaffold can become involved in reactivity. Coordination compounds featuring dearomatized pyridine based ligands paired with ruthenium are particularly notable as they form active catalysts for a variety of AD reactions (Section 1.6).[3,6,89] Linker reactivity is an important feature of these catalysts.[3,6]

The enamide phosphine ligands explored in this thesis are designed to operate without aromatization/ dearomatization processes; in certain cases, it could be demonstrated that they still act as cooperative ligands. Reagents such as H_2 or alcohols transfer a proton to the ligand scaffold and concurrently functionalize the metal (Ir or Ru) with a hydride ligand. Probing the mechanism of these transformations with multinuclear NMR and isotopic labeling experiments establishes what appears to be linker reactivity, is in fact a series of steps that shuttle a proton between the metal and the linker of the ligand (Chapters 3 and 4). These steps are; protonation of the enamide N donor coordinated directly to the metal (donor reactivity), dissociation of the N donor from the metal, tautomerization of the dissociated arm between enamine and imine forms, and coordination of the imine tautomeric form of the ligand to the metal. Scheme 6.1 illustrates

a simplified system undergoing each step and compares this reactivity to previous reports of linker reactivity.

Scheme 6.1:

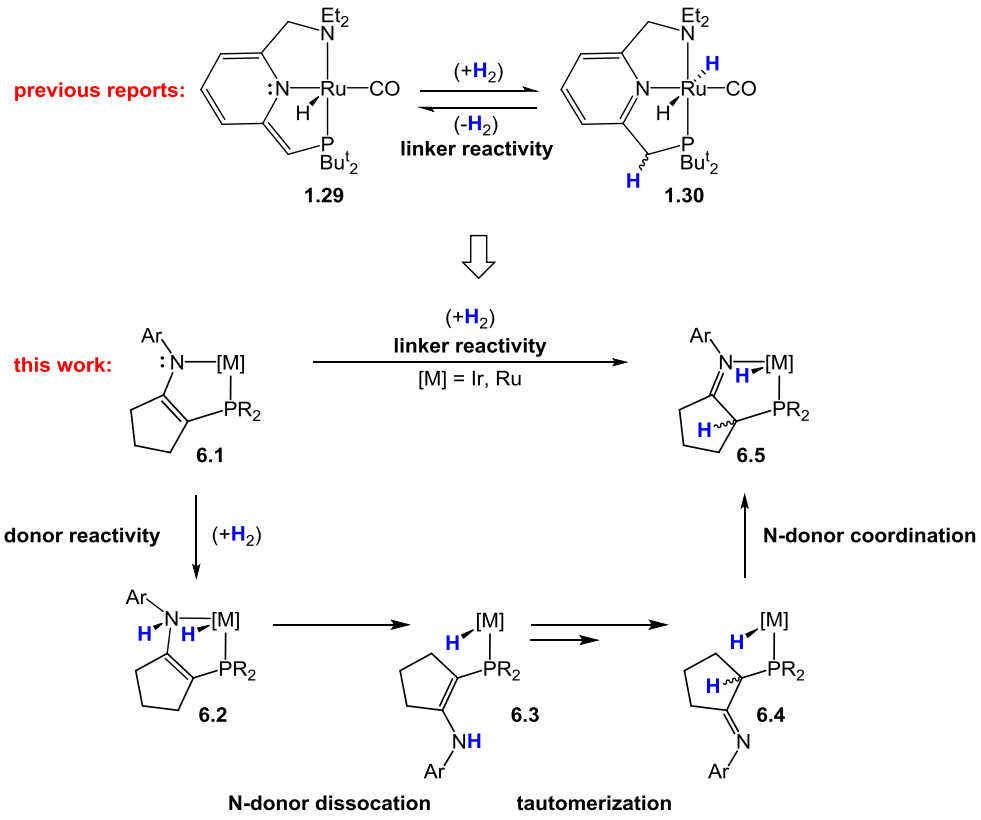

One question raised by the discovery of a stepwise mechanism for linker reactivity in this thesis (Scheme 6.1) is whether or not these processes are relevant to previously reported tridentate and tetradentate ligand designs outlined in the introduction of this work. Descriptions of stoichiometric reactivity with H_2 for **1.29** and related complexes with H_2 all propose direct proton transfer to the linker of the ligand as a single step.[3,89,97,104] Supporting these observations, numerous DFT studies carried out for linker reactive Ru and Ir systems also purpose linker reactivity occurs in a single step.[98,99,108-111] Thus, the mechanism for linker reactivity described in this thesis is a unique alternative to what is commonly reported.

6.2 Future Work

Continued efforts towards probing ligand cooperativity through the synthesis of enamide phosphine ligands may result in the development of new cooperative metal-ligand systems, which are potentially donor or linker reactive. The ligand synthesis reported in this thesis is highly flexible and allows for exploration of a variety of enamide phosphine ligands. Promising design alternatives to what is reported in the research chapters include; incorporating the enamide phosphine motif into different arrays of donors, and exploring different linker scaffolds beyond the cyclopentylidene ring used in this work (Scheme 6.2).

Previous attempts were made to synthesize and isolate **6.8**, a potential precursor to a PNP enamide phosphine ligand (**6.10**). Screening a variety of conditions for imine formation using cyclopentanone and 2-bromoaniline as a starting materials was unsuccessful. Approximately 50 % conversion to the desired product occurs; however, undesired condensation reactivity between the imine (**6.8**) and cyclopentanone forms side products, which inhibit purification of the desired product. Selection of a different ketone starting material, with less reactive α-CH protons may allow for synthesis of a structure similar to **6.8**. Recent studies regarding the preparation of a related ligand scaffold suggest lithium halogen exchange to form the P-C bond on the aromatic ring proceeds smoothly (step 1, Scheme 6.2).[171] Deprotonation of the α-CH proton on the imine scaffold and quenching with an appropriate chlorophosphine (Step 3 and 4, Scheme 6.2) generates **6.9**. One intriguing feature of **6.10** in comparison to the well known diaryl amide system **6.11** is **6.10** can potentially participate in donor or linker reactivity, whereas presumably **6.11** is limited to donor reactivity.[12,129,172]

Scheme 6.2:

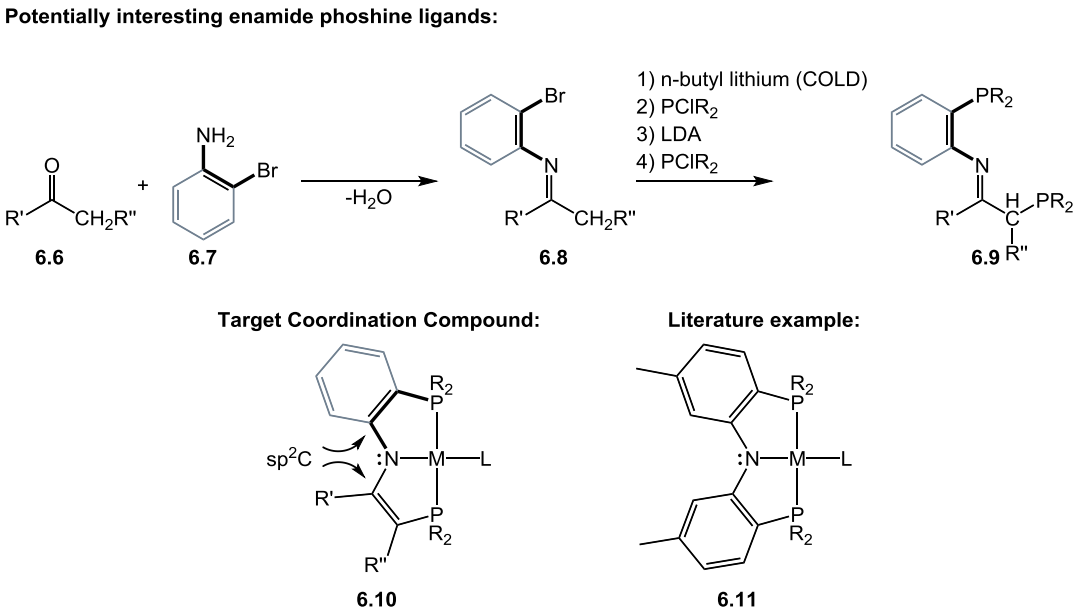

A question raised by the research performed in this thesis is whether an aliphatic enamide phosphine ligand, similar to what is explored here can be used to generate a metal-ligand system that is an active catalyst for AD reactivity. Related to this topic is an example of an active catalyst for transfer hydrogenation, discussed in Section 1.5 of this thesis (Scheme 6.3). The important feature of this system is the fact that both a donor reactive amide phosphine arm (blue) and a potentially donor or linker reactive enamide phosphine arm (black bold) are present in the same ligand design.

Scheme 6.3:

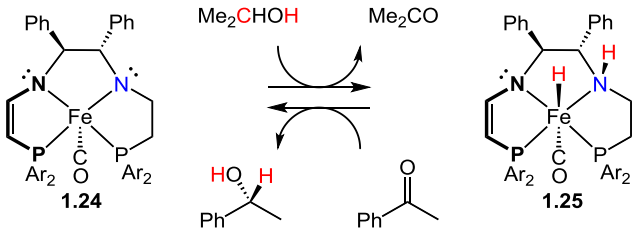

Multinuclear NMR studies suggest that the amide nitrogen undergoes cooperative reactivity during catalysis;[84] therefore, the enamide phosphine unit is not a reactive site on the complex, as

it does not directly participate in cooperative substrate activation. Whether or not this applies to AD catalysis in general remains an unexplored topic at this point.

The apparent preference for protonation of the amide phosphine N donor in lieu of the enamide phosphine unit under catalytic conditions (Scheme 6.3), suggests that synthesis of donor reactive amide phosphine ligands could be a complementary strategy to the synthesis of new enamide phosphine ligands. One route to amide phosphine scaffolds based on the structures explored in this work is reduction of the C-N double bond of imine phosphine ligands. Recent efforts using imine phosphine scaffolds coordinated to Fe have shown promising results using this strategy.[73] Typical procedures for reduction of imines have been employed for reduction of imine phosphines; select examples include: reaction with hydride reagents such as $NaBH_4$,[173-175] or $LiAlH_4$.[84] Another potential strategy is $B(C_6F_5)_3$ mediated hydrosilylation of the C-N double bond.[176] For the cyclopentyl linked ligands explored in this work, reduction of the imine C-N double bond generates a chiral center, exploring enantioselective protocols for imine reduction may allow for the synthesis of a chiral cooperative ligand-metal catalysts.[177] Given the versatility of the synthetic route established in this and previous works[20,139,140] for the assembly of a variety of imine phosphine ligands, developing a general protocol for reduction of these scaffolds to amine phosphine ligands would be a powerful tool for continued exploration of ligand cooperativity (Scheme 6.4).

Scheme 6.4:

Reduction of imine phosphine ligands:

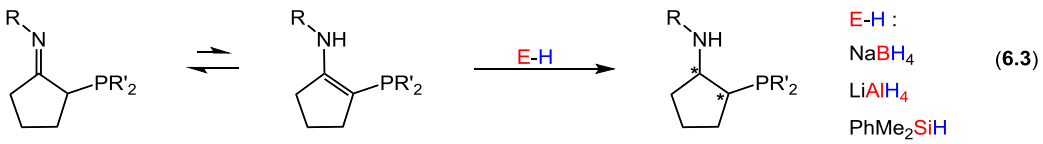

(**6.3**)

Bibliography

(1) Housecroft, C. E.; Sharpe, A. G. *Inorganic Chemistry*; Second ed.; Pearson Education Limited: Edinburgh Gate 2005.

(2) Fryzuk, M. D.; Haddad, T. S.; Berg, D. J.; Rettig, S. J. *Pure Appl. Chem.* **1991**, *63*, 845.

(3) Gunanathan, C.; Milstein, D. *Acc. Chem. Res.* **2011**, *44*, 588.

(4) Gelman, D.; Musa, S. *ACS Catal.* **2012**, *2*, 2456.

(5) Annibale, V. T.; Song, D. *RSC Adv.* **2013**, *3*, 11432.

(6) Gunanathan, C.; Milstein, D. *Science* **2013**, *341*.

(7) Grützmacher, H. *Angew. Chem., Int. Ed.* **2008**, *47*, 1814.

(8) Askevold, B.; Roesky, H. W.; Schneider, S. *ChemCatChem* **2012**, *4*, 307.

(9) Maire, P.; Büttner, T.; Breher, F.; Le Floch, P.; Grützmacher, H. *Angew. Chem., Int. Ed.* **2005**, *44*, 6318.

(10) Noyori, R. *Angew. Chem., Int. Ed.* **2002**, *41*, 2008.

(11) Clapham, S. E.; Hadzovic, A.; Morris, R. H. *Coord. Chem. Rev.* **2004**, *248*, 2201.

(12) Calimano, E.; Tilley, T. D. *Dalton Trans.* **2010**, *39*, 9250.

(13) Chang, Y.-H.; Nakajima, Y.; Tanaka, H.; Yoshizawa, K.; Ozawa, F. *J. Am. Chem. Soc.* **2013**, *135*, 11791.

(14) Chang, Y.-H.; Nakajima, Y.; Tanaka, H.; Yoshizawa, K.; Ozawa, F. *Organometallics* **2014**, *33*, 715.

(15) Tsvetkov, N. P.; Laird, M. F.; Fan, H.; Pink, M.; Caulton, K. G. *Chem. Commun.* **2009**, 4578.

(16) Dahlenburg, L.; Götz, R. *Eur. J. Inorg. Chem.* **2004**, *2004*, 888.

(17) Fryzuk, M. D.; Montgomery, C. D. *Coord. Chem. Rev.* **1989**, *95*, 1.

(18) MacLachlan, E. A.; Hess, F. M.; Patrick, B. O.; Fryzuk, M. D. *J. Am. Chem. Soc.* **2007**, *129*, 10895.

(19) Menard, G.; Jong, H.; Fryzuk, M. D. *Organometallics* **2009**, *28*, 5253.

(20) Zhu, T.; Wambach, T. C.; Fryzuk, M. D. *Inorg. Chem.* **2011**, *50*, 11212.

(21) Fryzuk, M. D.; Love, J. B.; Rettig, S. J. *Chem. Commun.* **1996**, 2783.

(22) Fryzuk, M. D. *Can. J. Chem.* **1992**, *70*, 2839.

(23) Fryzuk, M. D.; MacNeil, P. A. *Organometallics* **1983**, *2*, 682.

(24) Fryzuk, M. D.; MacNeil, P. a.; Rettig, S. J. *J. Am. Chem. Soc.* **1987**, *109*, 2803.

(25) Liang, L.-C. *Coord. Chem. Rev.* **2006**, *250*, 1152.

(26) Gunnoe, T. B. *Eur. J. Inorg. Chem.* **2007**, *2007*, 1185.

(27) Albrecht, M.; Lindner, M. M. *Dalton Trans.* **2011**, *40*, 8733.

(28) Zargarian, D.; Castonguay, A.; Spasyuk, D. In *Organometallic Pincer Chemistry*; van Koten, G., Milstein, D., Eds.; Springer Berlin Heidelberg: 2013; Vol. 40, p 131.

(29) Marynick, D. S. *J. Am. Chem. Soc.* **1984**, *106*, 4064.

(30) Tolman, C. A. *Chem. Rev.* **1977**, *77*, 313.

(31) Osborn, J. A.; Jardine, F. H.; Young, J. F.; Wilkinson, G. *J. Chem. Soc. A* **1966**, 1711.

(32) Halpern, J.; Wong, C. S. *J. Chem. Soc., Chem. Commun.* **1973**, 629.

(33) Halpern, J.; Okamoto, T.; Zakhariev, A. *J. Mol. Catal.* **1977**, *2*, 65.

(34) Halpern, J. *Inorg. Chim. Acta* **1981**, *50*, 11.

(35) Daniel, C.; Koga, N.; Han, J.; Fu, X. Y.; Morokuma, K. *J. Am. Chem. Soc.* **1988**, *110*, 3773.
(36) Caulton, K. G. *New J. Chem.* **1994**, *18*, 25.
(37) Cetinkaya, B.; Lappert, M. F.; Torroni, S. *J. Chem. Soc., Chem. Commun.* **1979**, 843.
(38) Diamond, S. E.; Mares, F. *J. Organomet. Chem.* **1977**, *142*, C55.
(39) Bryndza, H. E.; Fong, L. K.; Paciello, R. A.; Tam, W.; Bercaw, J. E. *J. Am. Chem. Soc.* **1987**, *109*, 1444.
(40) Holland, P. L.; Andersen, R. A.; Bergman, R. G.; Huang, J.; Nolan, S. P. *J. Am. Chem. Soc.* **1997**, *119*, 12800.
(41) Holland, A. W.; Bergman, R. G. *J. Am. Chem. Soc.* **2002**, *124*, 14684.
(42) Fryzuk, M. D.; MacNeil, P. A. *Organometallics* **1983**, *2*, 355.
(43) Fryzuk, M. D.; MacNeil, P. A.; Rettig, S. J. *Organometallics* **1986**, *5*, 2469.
(44) Fryzuk, M. D.; MacNeil, P. A.; Rettig, S. J. *Organometallics* **1985**, *4*, 1145.
(45) Riehl, J. F.; Jean, Y.; Eisenstein, O.; Pelissier, M. *Organometallics* **1992**, *11*, 729.
(46) Knowles, W. S. *Angew. Chem., Int. Ed.* **2002**, *41*, 1998.
(47) Fache, F.; Schulz, E.; Tommasino, M. L.; Lemaire, M. *Chem. Rev.* **2000**, *100*, 2159.
(48) Harmon, R. E.; Gupta, S. K.; Brown, D. J. *Chem. Rev.* **1973**, *73*, 21.
(49) Ohkuma, T.; Ooka, H.; Hashiguchi, S.; Ikariya, T.; Noyori, R. *J. Am. Chem. Soc.* **1995**, *117*, 2675.
(50) Doucet, H.; Ohkuma, T.; Murata, K.; Yokozawa, T.; Kozawa, M.; Katayama, E.; England, A. F.; Ikariya, T.; Noyori, R. *Angew. Chem., Int. Ed.* **1998**, *37*, 1703.
(51) Sandoval, C. A.; Ohkuma, T.; Muñiz, K.; Noyori, R. *J. Am. Chem. Soc.* **2003**, *125*, 13490.
(52) Abdur-Rashid, K.; Faatz, M.; Lough, A. J.; Morris, R. H. *J. Am. Chem. Soc.* **2001**, *123*, 7473.
(53) Knowles, W. S.; Sabacky, M. J. *Chem. Commun.* **1968**, 1445.
(54) Knowles, W. S.; Sabacky, M. J.; Vineyard, B. D. *J. Chem. Soc., Chem. Commun.* **1972**, 10.
(55) Fryzuk, M. D.; Bosnich, B. *J. Am. Chem. Soc.* **1977**, *99*, 6262.
(56) Vineyard, B. D.; Knowles, W. S.; Sabacky, M. J.; Bachman, G. L.; Weinkauff, D. J. *J. Am. Chem. Soc.* **1977**, *99*, 5946.
(57) Knowles, W. S. *J. Chem. Educ.* **1986**, *63*, 222.
(58) Nagel, U.; Roller, C. *Z. Naturforsch., B: Chem. Sci*, *53*, 267.
(59) Zhang, X.; Taketomi, T.; Yoshizumi, T.; Kumobayashi, H.; Akutagawa, S.; Mashima, K.; Takaya, H. *J. Am. Chem. Soc.* **1993**, *115*, 3318.
(60) Robin, F.; Mercier, F.; Ricard, L.; Mathey, F.; Spagnol, M. *Chem. Eur. J.* **1997**, *3*, 1365.
(61) Jiang, Q.; Jiang, Y.; Xiao, D.; Cao, P.; Zhang, X. *Angew. Chem., Int. Ed.* **1998**, *37*, 1100.
(62) Cao, P.; Zhang, X. *J. Org. Chem.* **1999**, *64*, 2127.
(63) Askevold, B.; Khusniyarov, M. M.; Herdtweck, E.; Meyer, K.; Schneider, S. *Angew. Chem., Int. Ed.* **2010**, *49*, 7566.

(64) Askevold, B.; Nieto, J. T.; Tussupbayev, S.; Diefenbach, M.; Herdtweck, E.; Holthausen, M. C.; Schneider, S. *Nat. Chem.* **2011**, *3*, 532.

(65) Friedrich, A.; Drees, M.; Kass, M.; Herdtweck, E.; Schneider, S. *Inorg. Chem.* **2010**, *49*, 5482.

(66) Watson, L. A.; Ozerov, O. V.; Pink, M.; Caulton, K. G. *J. Am. Chem. Soc.* **2003**, *125*, 8426.

(67) Käß, M.; Friedrich, A.; Drees, M.; Schneider, S. *Angew. Chem., Int. Ed.* **2009**, *48*, 905.

(68) Bertoli, M.; Choualeb, A.; Lough, A. J.; Moore, B.; Spasyuk, D.; Gusev, D. G. *Organometallics* **2011**, *30*, 3479.

(69) Bertoli, M.; Choualeb, A.; Gusev, D. G.; Lough, A. J.; Major, Q.; Moore, B. *Dalton Trans.* **2011**, *40*, 8941.

(70) Spasyuk, D.; Smith, S.; Gusev, D. G. *Angew. Chem., Int. Ed.* **2012**, *51*, 2772.

(71) Clarke, Z. E.; Maragh, P. T.; Dasgupta, T. P.; Gusev, D. G.; Lough, A. J.; Abdur-Rashid, K. *Organometallics* **2006**, *25*, 4113.

(72) Choualeb, A.; Lough, A. J.; Gusev, D. G. *Organometallics* **2007**, *26*, 5224.

(73) Lagaditis, P. O.; Sues, P. E.; Sonnenberg, J. F.; Wan, K. Y.; Lough, A. J.; Morris, R. H. *J. Am. Chem. Soc.* **2014**, *136*, 1367.

(74) Spasyuk, D.; Gusev, D. G. *Organometallics* **2012**, *31*, 5239.

(75) Nielsen, M.; Alberico, E.; Baumann, W.; Drexler, H.-J.; Junge, H.; Gladiali, S.; Beller, M. *Nature* **2013**, *495*, 85.

(76) Mikhailine, A. A.; Kim, E.; Dingels, C.; Lough, A. J.; Morris, R. H. *Inorg. Chem.* **2008**, *47*, 6587.

(77) Mikhailine, A. A.; Morris, R. H. *Inorg. Chem.* **2010**, *49*, 11039.

(78) Lagaditis, P. O.; Mikhailine, A. A.; Lough, A. J.; Morris, R. H. *Inorg. Chem.* **2010**, *49*, 1094.

(79) Lagaditis, P. O.; Lough, A. J.; Morris, R. H. *Inorg. Chem.* **2010**, *49*, 10057.

(80) Sues, P. E.; Lough, A. J.; Morris, R. H. *Organometallics* **2011**, *30*, 4418.

(81) Lagaditis, P. O.; Lough, A. J.; Morris, R. H. *J. Am. Chem. Soc.* **2011**, *133*, 9662.

(82) Prokopchuk, D. E.; Morris, R. H. *Organometallics* **2012**, *31*, 7375.

(83) Mikhailine, A. A.; Maishan, M. I.; Lough, A. J.; Morris, R. H. *J. Am. Chem. Soc.* **2012**, *134*, 12266.

(84) Zuo, W.; Lough, A. J.; Li, Y. F.; Morris, R. H. *Science* **2013**, *342*, 1080.

(85) Noyori, R.; Hashiguchi, S. *Acc. Chem. Res.* **1997**, *30*, 97.

(86) Ikariya, T.; Blacker, J. *Acc. Chem. Res.* **2007**, *40*, 1300.

(87) Sacco, A.; Vasapollo, G.; Nobile, C. F.; Piergiovanni, A.; Pellinghelli, M. A.; Lanfranchi, M. *J. Organomet. Chem.* **1988**, *356*, 397.

(88) Gunanathan, C.; Milstein, D. *Top. Organomet. Chem.* **2011**, *37*, 55.

(89) Zhang, J.; Leitus, G.; Ben-David, Y.; Milstein, D. *J. Am. Chem. Soc.* **2005**, *127*, 10840.

(90) Balaraman, E.; Fogler, E.; Milstein, D. *Chem. Commun.* **2012**, *48*, 1111.

(91) Sun, Y.; Koehler, C.; Tan, R.; Annibale, V. T.; Song, D. *Chem. Commun.* **2011**, *47*, 8349.

(92) Gargir, M.; Ben-David, Y.; Leitus, G.; Diskin-Posner, Y.; Shimon, L. J. W.; Milstein, D. *Organometallics* **2012**, *31*, 6207.

(93) Khaskin, E.; Diskin-Posner, Y.; Weiner, L.; Leitus, G.; Milstein, D. *Chem. Commun.* **2013**, *49*, 2771.
(94) Semproni, S. P.; Milsmann, C.; Chirik, P. J. *J. Am. Chem. Soc.* **2014**, *136*, 9211.
(95) Feller, M.; Diskin-Posner, Y.; Shimon, L. J. W.; Ben-Ari, E.; Milstein, D. *Organometallics* **2012**, *31*, 4083.
(96) Gloaguen, Y.; Rebreyend, C.; Lutz, M.; Kumar, P.; Huber, M.; van, d. V. J. I.; Schneider, S.; de, B. B. *Angew. Chem., Int. Ed.* **2014**.
(97) Ben-Ari, E.; Leitus, G.; Shimon, L. J. W.; Milstein, D. *J. Am. Chem. Soc.* **2006**, *128*, 15390.
(98) Iron, M. A.; Ben-Ari, E.; Cohen, R.; Milstein, D. *Dalton Trans.* **2009**, 9433.
(99) Schwartsburd, L.; Iron, M. a.; Konstantinovski, L.; Diskin-Posner, Y.; Leitus, G.; Shimon, L. J. W.; Milstein, D. *Organometallics* **2010**, *29*, 3817.
(100) Vogt, M.; Rivada-Wheelaghan, O.; Iron, M. A.; Leitus, G.; Diskin-Posner, Y.; Shimon, L. J. W.; Ben-David, Y.; Milstein, D. *Organometallics* **2013**, *32*, 300.
(101) Vuzman, D.; Poverenov, E.; Shimon, L. J. W.; Diskin-Posner, Y.; Milstein, D. *Organometallics* **2008**, *27*, 2627.
(102) Langer, R.; Iron, M. A.; Konstantinovski, L.; Diskin-Posner, Y.; Leitus, G.; Ben-David, Y.; Milstein, D. *Chem. Eur. J.* **2012**, *18*, 7196.
(103) Zell, T.; Langer, R.; Iron, M. A.; Konstantinovski, L.; Shimon, L. J. W.; Diskin-Posner, Y.; Leitus, G.; Balaraman, E.; Ben-David, Y.; Milstein, D. *Inorg. Chem.* **2013**, *52*, 9636.
(104) Zhang, J.; Leitus, G.; Ben-David, Y.; Milstein, D. *Angew. Chem., Int. Ed.* **2006**, *45*, 1113.
(105) Khaskin, E.; Iron, M. A.; Shimon, L. J. W.; Zhang, J.; Milstein, D. *J. Am. Chem. Soc.* **2010**, *132*, 8542.
(106) Kohl, S. W.; Weiner, L.; Schwartsburd, L.; Konstantinovski, L.; Shimon, L. J. W.; Ben-David, Y.; Iron, M. A.; Milstein, D. *Science* **2009**, *324*, 74.
(107) Vogt, M.; Gargir, M.; Iron, M. A.; Diskin-Posner, Y.; Ben-David, Y.; Milstein, D. *Chem. Eur. J.* **2012**, *18*, 9194.
(108) Li, H.; Wang, X.; Wen, M.; Wang, Z.-X. *Eur. J. Inorg. Chem.* **2012**, *2012*, 5011.
(109) Hasanayn, F.; Baroudi, A.; Bengali, A. A.; Goldman, A. S. *Organometallics* **2013**, *32*, 6969.
(110) Li, H.; Wen, M.; Wang, Z.-X. *Inorg. Chem.* **2012**, *51*, 5716.
(111) Zeng, G.; Li, S. *Inorg. Chem.* **2011**, *50*, 10572.
(112) Huff, C. A.; Kampf, J. W.; Sanford, M. S. *Organometallics* **2012**, *31*, 4643.
(113) Montag, M.; Zhang, J.; Milstein, D. *J. Am. Chem. Soc.* **2012**, *134*, 10325.
(114) Huff, C. A.; Kampf, J. W.; Sanford, M. S. *Chem. Commun.* **2013**, *49*, 7147.
(115) Denney, M. C.; Pons, V.; Hebden, T. J.; Heinekey, D. M.; Goldberg, K. I. *J. Am. Chem. Soc.* **2006**, *128*, 12048.
(116) Friedrich, A.; Drees, M.; Schneider, S. *Chem. Eur. J.* **2009**, *15*, 10339.
(117) Staubitz, A.; Sloan, M. E.; Robertson, A. P. M.; Friedrich, A.; Schneider, S.; Gates, P. J.; Günne, J. S. a. d.; Manners, I. *J. Am. Chem. Soc.* **2010**, *132*, 13332.
(118) Marziale, A. N.; Friedrich, A.; Klopsch, I.; Drees, M.; Celinski, V. R.; Schmedt auf der Guenne, J.; Schneider, S. *J. Am. Chem. Soc.* **2013**, *135*, 13342.
(119) Staubitz, A.; Robertson, A. P. M.; Manners, I. *Chem. Rev.* **2010**, *110*, 4079.
(120) Gunanathan, C.; Ben-David, Y.; Milstein, D. *Science* **2007**, *317*, 790.

(121) Gnanaprakasam, B.; Zhang, J.; Milstein, D. *Angew. Chem., Int. Ed.* **2010**, *49*, 1468.
(122) Fryzuk, M. D.; MacNeil, P. A. *J. Am. Chem. Soc.* **1981**, *103*, 3592.
(123) Schrock, R. R.; Seidel, S. W.; Schrodi, Y.; Davis, W. M. *Organometallics* **1998**, *18*, 428.
(124) Bailey, B. C.; Huffman, J. C.; Mindiola, D. J.; Weng, W.; Ozerov, O. V. *Organometallics* **2005**, *24*, 1390.
(125) MacLachlan, E. A.; Fryzuk, M. D. *Organometallics* **2005**, *24*, 1112.
(126) Lee, J.-H.; Pink, M.; Tomaszewski, J.; Fan, H.; Caulton, K. G. *J. Am. Chem. Soc.* **2007**, *129*, 8706.
(127) Whited, M. T.; Grubbs, R. H. *Acc. Chem. Res.* **2009**, *42*, 1607.
(128) Brookes, N. J.; Whited, M. T.; Ariafard, A.; Stranger, R.; Grubbs, R. H.; Yates, B. F. *Organometallics* **2010**, *29*, 4239.
(129) Gregor, L. C.; Chen, C.-H.; Fafard, C. M.; Fan, L.; Guo, C.; Foxman, B. M.; Gusev, D. G.; Ozerov, O. V. *Dalton Trans.* **2010**, *39*, 3195.
(130) Fryzuk, M. D.; MacNeil, P. A.; Rettig, S. J.; Secco, A. S.; Trotter, J. *Organometallics* **1982**, *1*, 918.
(131) Fryzuk, M. D.; Giesbrecht, G. R.; Rettig, S. J. *Inorg. Chem.* **1998**, *37*, 6928.
(132) Fryzuk, M. D.; Love, J. B.; Rettig, S. J. *Organometallics* **1998**, *17*, 846.
(133) Fryzuk, M. D.; Giesbrecht, G. R.; Rettig, S. J.; Yap, G. P. A. *J. Organomet. Chem.* **1999**, *591*, 63.
(134) Fryzuk, M. D.; Johnson, S. A.; Rettig, S. J. *Organometallics* **1999**, *18*, 4059.
(135) Fryzuk, M. D.; Jafarpour, L.; Kerton, F. M.; Love, J. B.; Patrick, B. O.; Rettig, S. J. *Organometallics* **2001**, *20*, 1387.
(136) Fryzuk, M. D.; Petrella, M. J.; Coffin, R. C.; Patrick, B. O. *C. R. Chim.* **2002**, *5*, 451.
(137) Fryzuk, M. D.; Shaver, M. P.; Patrick, B. O. *Inorg. Chim. Acta* **2003**, *350*, 293.
(138) Shaver, M. P.; Thomson, R. K.; Patrick, B. O.; Fryzuk, M. D. *Can. J. Chem.* **2003**, *81*, 1431.
(139) Keim, W.; Killat, S.; Nobile, C. F.; Paolo, G.; Englert, U.; Wang, R.; Mecking, S.; Schroder, D. L. *J. Organomet. Chem.* **2002**, *662*, 150.
(140) Guan, Z.; Marshall, W. J. *Organometallics* **2002**, *21*, 3580.
(141) Nourse, J. G. *J. Am. Chem. Soc.* **1975**, *97*, 4594.
(142) Zeng, J. Y.; Hsieh, M.-H.; Lee, H. M. *J. Organomet. Chem.* **2005**, *690*, 5662.
(143) Brunet, J.-J.; Couillens, X.; Daran, J.-C.; Diallo, O.; Lepetit, C.; Neibecker, D. *Eur. J. Inorg. Chem.* **1998**, *1998*, 349.
(144) Ball, G. E.; Cullen, W. R.; Fryzuk, M. D.; James, B. R.; Rettig, S. J. *Organometallics* **1991**, *10*, 3767.
(145) Vaska, L.; DiLuzio, J. W. *J. Am. Chem. Soc.* **1962**, *84*, 679.
(146) Vaska, L. *Acc. Chem. Res.* **1968**, *1*, 335.
(147) Johnson, C. E.; Eisenberg, R. *J. Am. Chem. Soc.* **1985**, *107*, 3148.
(148) Askevold, B.; Friedrich, A.; Buchner, M. R.; Lewall, B.; Filippou, A. C.; Herdtweck, E.; Schneider, S. *J. Organomet. Chem.* **2013**, *744*, 35.
(149) Batsanov, S. S. *Inorg. Mater.* **2001**, *37*, 871.

(150) Smidt, S. P.; Pfaltz, A.; Martínez-Viviente, E.; Pregosin, P. S.; Albinati, A. *Organometallics* **2003**, *22*, 1000.

(151) Wang, H. H.; Pignolet, L. H. *Inorg. Chem.* **1980**, *19*, 1470.

(152) Chodosh, D. F.; Crabtree, R. H.; Felkin, H.; Morehouse, S.; Morris, G. E. *Inorg. Chem.* **1982**, *21*, 1307.

(153) Xu, Y.; Celik, M. A.; Thompson, A. L.; Cai, H.; Yurtsever, M.; Odell, B.; Green, J. C.; Mingos, D. M. P.; Brown, J. M. *Angew. Chem., Int. Ed.* **2009**, *48*, 582.

(154) Crabtree, R. H.; Felkin, H.; Morris, G. E. *J. Organomet. Chem.* **1977**, *141*, 205.

(155) Ohno, K.; Tsuji, J. *J. Am. Chem. Soc.* **1968**, *90*, 99.

(156) Doughty, D. H.; Pignolet, L. H. *J. Am. Chem. Soc.* **1978**, *100*, 7083.

(157) Saunders, M.; Kates, M. R. *J. Am. Chem. Soc.* **1978**, *100*, 7083.

(158) Anderson, M. P.; Casalnuovo, A. L.; Johnson, B. J.; Mattson, B. M.; Mueting, A. M.; Pignolet, L. H. *Inorg. Chem.* **1988**, *27*, 1649.

(159) Iwai, T.; Fujihara, T.; Tsuji, Y. *Chem. Commun.* **2008**, 6215.

(160) Roa, A. E.; Salazar, V.; Lopez-Serrano, J.; Onate, E.; Paneque, M. *Organometallics* **2012**, *31*, 716.

(161) Ho, H.-A.; Manna, K.; Sadow, A. D. *Angew. Chem., Int. Ed.* **2012**, *51*, 8607.

(162) Abu-Hasanayn, F.; Goldman, M. E.; Goldman, A. S. *J. Am. Chem. Soc.* **1992**, *114*, 2520.

(163) Kreis, M.; Palmelund, A.; Bunch, L.; Madsen, R. *Adv. Synth. Catal.* **2006**, *348*, 2148.

(164) Wambach, T. C.; Ahn, J. M.; Patrick, B. O.; Fryzuk, M. D. *Organometallics* **2013**, *32*, 4431.

(165) Addison, A. W.; Rao, T. N.; Reedijk, J.; van Rijn, J.; Verschoor, G. C. *J. Chem. Soc., Dalton Trans.* **1984**, 1349.

(166) Friedrich, A.; Drees, M.; Schmedt auf der Günne, J.; Schneider, S. *J. Am. Chem. Soc.* **2009**, *131*, 17552.

(167) Gusev, D. G.; Vymenits, A. B.; Bakhmutov, V. I. *Inorg. Chem.* **1992**, *31*, 1.

(168) Bolton, P. D.; Grellier, M.; Vautravers, N.; Vendier, L.; Sabo-Etienne, S. *Organometallics* **2008**, *27*, 5088.

(169) Jessop, P. G.; Morris, R. H. *Coord. Chem. Rev.* **1992**, *121*, 155.

(170) Hatakeyama, T.; Ito, S.; Nakamura, M.; Nakamura, E. *J. Am. Chem. Soc.* **2005**, *127*, 14192.

(171) Suzuki, T., Personal Communication.

(172) Smith, D. A.; Herbert, D. E.; Walensky, J. R.; Ozerov, O. V. *Organometallics* **2013**, *32*, 2050.

(173) Blackburn, L.; Taylor, R. J. K. *Org. Lett.* **2001**, *3*, 1637.

(174) Crochet, P.; Gimeno, J.; Borge, J.; Garcia-Granda, S. *New J. Chem.* **2003**, *27*, 414.

(175) Li, B.-Z.; Chen, J.-S.; Dong, Z.-R.; Li, Y.-Y.; Li, Q.-B.; Gao, J.-X. *Journal of Molecular Catalysis A: Chemical* **2006**, *258*, 113.

(176) Blackwell, J. M.; Sonmor, E. R.; Scoccitti, T.; Piers, W. E. *Org. Lett.* **2000**, *2*, 3921.

(177) Wang, Z.; Cheng, M.; Wu, P.; Wei, S.; Sun, J. *Org. Lett.* **2006**, *8*, 3045.

(178) Dahlenburg, L. *Coord. Chem. Rev.* **2005**, *249*, 2962.

(179) Rankin, M. a.; McDonald, R.; Ferguson, M. J.; Stradiotto, M. *Organometallics* **2005**, *24*, 4981.

(180) Bendeif, E.-E.; Matta, C. F.; Stradiotto, M.; Fertey, P.; Lecomte, C. *Inorg. Chem.* **2012**, *51*, 3754.

(181) Ozerov, O. V.; Guo, C.; Papkov, V. A.; Foxman, B. M. *J. Am. Chem. Soc.* **2004**, *126*, 4792.

Appendices

Appendix A

A.1 Experimental Procedures

All procedures and manipulations were performed under an atmosphere of dry, oxygen-free dinitrogen or argon by means of standard Schlenk or glove box techniques. Argon and dinitrogen were dried and deoxygenated by passing the gases through a column containing molecular sieves and a Cu catalyst. Dihydrogen and carbon monoxide were dried by passage through activated molecular sieves prior to use. D_2 and ^{13}CO gas were purchased from Cambridge Isotope Laboratories and used as received. Hexanes, toluene, THF, and diethyl ether were purchased from Aldrich, dried by passage through a tower of alumina, and degassed by passage through a tower of Q-5 catalyst under positive pressure of nitrogen. Pentane was dried using Na/K and benzophenone and collected from a solvent still. Dichloromethane was dried over CaH_2 and collected from a solvent still. Deuterated toluene, benzene, and THF were dried over NaK/ benzophenone, trap-to-trap distilled, and freeze-pump-thaw degassed three times. Deuterated dichloromethane was purchased in ampoules from Aldrich and used as received. Potassium hydride was purchased as a suspension in mineral oil, and collected by filtration using standard Schlenk techniques. The resulting solid potassium hydride was washed with dry hexanes. Potassium *tert*-butoxide was purchased and purified by sublimation. Isopropanol, cyclohexanol, and benzylalcohol were dried over sodium, then distilled into a Kontes sealed flask and freeze-pump-thaw degassed. Diisopropyl amine was distilled and freeze-pump-thaw degassed. Dichlorophenylphosphine, cyclooctene, cyclooctadiene, cyclopentanone, 2,6-dimethylaniline, 2,6-diisopropylaniline, n-butyl lithium, and diphenylchlorophosphine were purchased, and used as received. Triisopropylphosphine, di-*tert*-butyl chlorophosphine, and

diisopropyl chlorophosphine were synthesized from PCl_3 from an adaptation of a standard literature procedure and purified by distillation.[163,164] $RhCl_3$ hydrate was purchased from Johnson Matthey Materials Technology and used as received. $IrCl_3$ hydrate and $RuCl_3$ hydrate were purchased from Pressure Chemical Company and used as received. $[RhCl(COE)_2]_2$,[165] $[IrCl(COD)]_2$[166] and $RuHCl(PPr^i_3)_2(CO)$[167] were all synthesized by literature procedures. The syntheses of **2.1a,b** have been previously reported in a publication form this laboratory.[15] **3.6a,b** were synthesized according to literature procedures.[127] Synthesis and characterization data for **4.1c** has been previously reported,[128] and is reported again here for the sake of completeness. ATR (attenuated total reflectance) FTIR (Fourier transform infrared spectroscopy) spectra were recorded on a Perkin Elmer Frontier FTIR spectrometer. NMR (nuclear magnetic resonance) spectra were recorded on Bruker Avance II 300 MHz or Bruker Avance 400 MHz spectrometers unless otherwise noted. Chemical shifts for ^{31}P nuclei were referenced to 85% H_3PO_4 in H_2O (0 ppm). ^1H nuclei were referenced to resonances of the residual protonated solvents relative to tetramethylsilane (0 ppm), and ^{13}C spectra were referenced to the solvent carbon resonance(s). Elemental analysis was performed at the facilities of the Chemistry Department of the University of British Columbia. Quantification of conversion of benzyl alcohol to benzyl benzoate at was performed using a Bruker 450-GC equipped with a Varian CP8907 column (15m length. 0.25 mm diameter, 0.25 μm thick dimethylpolysiloxane film) and a flame ionization detector. Gas chromatography/ mass spectrometry (GC-MS) analysis were preformed on an Agilent 6890N instrument using an Agilent HP-5MS column (30 m length, 0.25 mm diameter, 0.25 μm film). Quantitative ^1H NMR spectra recorded using 1,3,5-trimethoxybenzene as an internal standard were recorded using a relaxation delay time (d1) of 57s. ***Caution!*** *All reactions that resulted in a pressure of 1.5 atm or greater within a sealed vessel upon warming to room temperature were*

performed with great care, and always manipulated behind a blast shield. Pressurized NMR tubes were allowed to warm to room temperature in a safe location and used with caution, protective eye wear was warn at all times.

Synthesis of **RhCl{(NPN)^{DMP}H$_2$}(COE) (2.3 a)**. **2.1a** (0.143 g, 0.298 mmol) and [RhCl(COE)$_2$]$_2$ (0.107 g, 0.149 mmol) were combined in hexanes (12 ml) and stirred for 30 minutes. The reaction turns from orange to yellow, a yellow precipitate forms. The yellow precipitate corresponding to the product was collected on a sinter glass filter (0.161 g, 74.1 %). ^{31}P{^{1}H} NMR (CD_2Cl_2, 161.9 MHz, 298 K): δ 49.3 (d, $^1J_{Rh\text{-}P}$ = 189.5 Hz, 1P) ^{1}H NMR (CD_2Cl_2, 400.0 MHz, 298K): δ 1.2 (m. 4H, CH_2), 1.3 (m, 2H, CH_2), 1.5 (m, 4H, CH_2), 1.6 (m, 2H, CH_2), 1.8 (m, 1H, CH_2), 2.0 (m, 4H, CH_2), 2.0 (s, 3H, *N*-CH_3), 2.0(7) (s, 3H, *N*-CH_3), 2.1(1) (m, 2H, CH_2), 2.2(8) (m, 3H, CH_2), 2.3 (s, 3H, *N*-CH_3), 2.6 (m, 2H, CH_2), 2.8 (s, 3H, *N*-CH_3), 3.6 (m, 1H, α-CH), 3.7 (m, 1H, *COE*-CH), 4.0 (br.s, 1H, *COE*-CH), 5.6 (ddd, $^2J_{PH}$ = 12.4 Hz, $^3J_{HH}$ = 8.5 Hz, $^3J_{HH}$ = 2.9 Hz, 1H, α-CH), 7.0 (m, 4H, ArCH), 7.0(6) (d, $^3J_{HH}$ = 7.1 Hz, 1H, ArCH), 7.2 (d, $^3J_{HH}$ = 7.1 Hz, 1H, ArCH), 7.6 (m, 3H, ArCH), 8.5 (ddd, $^4J_{HH}$ = 1.6 Hz, $^3J_{HH}$ = 7.4 Hz, $^3J_{PH}$ = 9.3 Hz, 2H, *P*-*o*-ArCH). ^{13}C APT NMR (CD_2Cl_2, 100.6 MHz, 298 K): δ 18.5 (s, *N*-CH_3), 19.0 (s, *N*-CH_3), 19.9 (s, *N*-CH_3), 20.1 (s, *N*-CH_3), 24.2 (d, *J* = 7.6 Hz, CH_2), 25.0 (d, *J* = 6.9 Hz, CH_2), 27.2 (d, *J* = 26.7 Hz, CH_2), 27.7 (s, CH_2), 27.9 (s, CH_2), 28.2 (s, CH_2), 29.4 (s, CH_2), 30.7 (d, *J* = 7.5 Hz, CH_2), 31.2 (br.s, 2x CH_2), 31.7 (s, CH_2), 34.3 (d, *J* = 3.3 Hz, CH_2), 40.1 (d, $^1J_{PC}$ = 21.6 Hz, α-CH), 57.0 (d, $^1J_{PC}$ = 23.5 Hz, α-CH), 65.8 (d, $^2J_{PC}$ = 13.0 Hz, *COE*-CH), 68.6 (d, *J* = 12.4 Hz, *COE*-CH), 123.7 (s, ArCH), 125.6 (s, ArCH), 127.3 (s, CAr), 128.4 (s, 3x ArCH), 128.7 (s, ArCH), 129.0 (d, J_{PC} = 9.6 Hz, *P*-ArCH), 130.1 (s, CAr), 130.5 (s, CAr), 131.7 (s, ArCH), 136.2 (d, $^2J_{PC}$ = 11.9 Hz, *P*-*o*-ArCH), 148.7 (s, CAr), 150.0 (s, CAr), 180.3 (s, *N*-C_{imine}), 199.5 (d, $^2J_{PC}$

= 36.4 Hz, *N*-C_{imine}), *P*-CAr not identified, CAr not identified. Anal. Calcd for $C_{40}H_{51}ClN_2PRh$: C, 65.89; H, 7.05; N, 3.84. Found: C, 65.72; H, 7.18; N, 4.96.

Synthesis of **RhCl{(NPN)^{DIPP}H$_2$}(COE) (2.3b)**. **2.1b** (0.201 g, 0.339 mmol) and $[RhCl(COE)_2]_2$ (0.122 g, 0.170 mmol) were combined in hexanes (12 ml) and stirred for 30 minutes. The reaction turns from orange to yellow, a yellow precipitate forms. The yellow precipitate corresponding to the product was collected on a sinter glass filter (0.156 g - 0.170 g, 54.7 - 59.7 %). $^{31}P\{^1H\}$ NMR (C_6D_6, 161.9 MHz, 298 K): δ 46.6 (d, $^1J_{Rh-P}$ = 183.5 Hz, 1P). ^1H NMR (C_6D_6, 400.0 MHz, 298 K): δ 0.86 (d, $^3J_{HH}$ = 6.9 Hz, 3H, *N*-Pr^{i}CH$_3$), 1.00 (d, $^3J_{HH}$ = 6.9 Hz, 3H, *N*-Pr^{i}CH$_3$), 1.22 (d, $^3J_{HH}$ = 7.1 Hz, 3H, *N*-Pr^{i}CH$_3$), 1.2(3) (d, $^3J_{HH}$ = 6.8 Hz, 3H, *N*-Pr^{i}CH$_3$), 1.3 - 1.6 (m, 12H, CH$_2$), 1.59 (d, $^3J_{HH}$ = 6.7 Hz, 3H, *N*-Pr^{i}CH$_3$), 1.61 (d, 3H, $^3J_{HH}$=6.9 Hz, 3H, *N*-Pr^{i}CH$_3$), 1.77 (m, 4H, CH$_2$), 1.87 (d, $^3J_{HH}$ = 6.7 Hz, 3H, *N*-Pr^{i}CH$_3$), 1.92 (d, $^3J_{HH}$ = 6.7 Hz, 3H, *N*-Pr^{i}CH$_3$), 2.10 (m, 2H, CH$_2$), 2.63 (m, 2H, CH$_2$), 2.6 (m, 2H, CH$_2$), 2.92 (sept, $^3J_{HH}$ = 6.9 Hz, 1H, *N*-Pr^{i}CH), 3.14 (sep, $^3J_{HH}$ = 6.8 Hz, 1H, *N*-Pr^{i}CH), 3.23 (m, 1H, α-CH), 3.32 (m, 2H, CH$_2$), 3.57 (sep, $^3J_{HH}$ = 6.8 Hz, 1H, *N*-Pr^{i}CH), 3.68 (sept, $^3J_{HH}$ = 6.8 Hz, 1H, *N*-Pr^{i}CH), 3.94 (dq, 1H, J_{HH} = 3.8 Hz, J_{HH} = 7.0 Hz, 1H, *COE*-CH), 4.12 (m, 1H, *COE*-CH), 5.53 (td, $^3J_{HH}$ = 8.2 Hz, $^3J_{HH}$ = 12.5 Hz, 1H, α-CH), 7.1 (dd, J_{HH} = 3.8 Hz, $^3J_{HH}$ = 5.5 Hz, 1H, ArCH), 7.12 (m, 3H, ArCH), 7.20 (dd, $^3J_{HH}$=7.3, J_{HH} = 5.7 Hz, 1H, ArCH), 7.28 (dd, $^3J_{HH}$ = 6.85 Hz, $^3J_{HH}$=7.3 Hz, 3H, ArCH), 7.34 (dd, $^3J_{HH}$=6.6 Hz, J_{HH} = 2.5 Hz, 1H, ArCH), 8.34 (vt, $^3J_{HH}$ = 8.81 Hz, $^3J_{HH}$=8.3, 2H, *P*-*o*-ArCH). ^{13}C APT NMR (C_6D_6, 100.6 MHz, 298 K): δ 22.4 (s, *N*-Pr^{i}CH$_3$), 22.8 (s, *N*-Pr^{i}CH$_3$), 23.0 (s, *N*-Pr^{i}CH$_3$), 23.8 (s, *N*-Pr^{i}CH$_3$), 23.9 (d, J_{PC} = 8.9 Hz, CH$_2$), 24.3 (s, *N*-Pr^{i}CH$_3$), 24.6 (s, *N*-Pr^{i}CH$_3$), 24.7(9) (s, *N*-Pr^{i}CH$_3$), 25.8(1) (s, CH$_2$), 26.0 (s *N*-Pr^{i}CH$_3$), 26.5 (s, CH$_2$), 27.1 (d, J_{PC} = 15.0 Hz, CH$_2$), 27.6 (d, J_{PC} = 7.1 Hz, CH$_2$), 27.9 (d, J_{PC} = 1.7 Hz, CH$_2$), 28.3 (s, *N*-Pr^{i}CH), 28.7(0) (s, *N*-Pr^{i}CH), 28.7(3) (s, *N*-Pr^{i}CH), 29.3 (s, *N*-Pr^{i}CH), 29.5 (s, CH$_2$), 29.8 (s,

CH_2), 31.1 (s, CH_2), 31.5 (s, CH_2), 31.9 (d, J_{PC} = 8.9 Hz, CH_2), 34.3 (d, J_{PC} = 4.5, CH_2), 40.4 (d, J_{PC} = 18.9 Hz, α-CH), 56.8 (d, $^1J_{PC}$ = 21.8 Hz, α-CH), 65.6 (d, J_{PC} = 12.9 Hz, *COE*-CH), 67.9 (dd, J_{PC} = 13.2, J_{RhH} = 2.1 Hz, *COE*-CH), 123.2 (s, *N*-ArCH), 123.4 (s, *N*-ArCH), 123.9 (s, *N*-ArCH), 124.1 (s, *N*-ArCH), 124.7 (s, *N*-ArCH), 126.6 (s, *N*-ArCH), 130.4 (s, *N*-ArCH), 131.0 (d, $^1J_{PC}$ = 31.0 Hz, *P*-CAr), 131.1 (d, $^3J_{PC}$=2.1 Hz, *P*-ArCH), 135.7 (s, CAr), 136.2 (d, $^2J_{PC}$=12.2 Hz, *P*-*o*-ArCH), 137.0 (s, CAr), 138.0 (s, CAr), 140.5 (s, CAr), 145.6 (s, CAr), 147.5 (d, *J* = 1.0 Hz, CAr), 179.5 (d, $^2J_{PC}$=1.8 Hz, *N*-C_{imine}), 198.2 (d, $^1J_{PC}$ =11.4 Hz, *N*-C_{imine}). Anal. Calcd for $C_{48}H_{67}ClN_2PRh$: C, 68.52; H, 8.03; N, 3.33. Found: C, 68.82; H, 8.39; N, 3.23.

Synthesis of **RhCl{(NPN)^{DMP}H$_2$}(CO) (2.4a)**. **2.3a** (0.146 g, 0.200 mmol) was dissolved in dichloromethane (5 ml) and transferred into a Kontes sealed reaction vessel equipped with a stir bar. The mixture was freeze-pump-thaw degassed using high vacuum three times and backfilled with CO at -196 ºC. The reaction vessel was quickly sealed and allowed to warm to room temperature behind a blast shield. After stirring for 2 hours, the reaction was treated with hexanes. Yellow crystals formed, which were collected by filtration (0.075 g, 57.9%). Treating the mother liquor formed after the first crop of crystals were collected with hexanes resulted in formation of X-ray quality crystals. $^{31}P\{^1H\}$ NMR (CD_2Cl_2, 161.9 MHz, 298 K): δ 66.1 (d, $^1J_{RhP}$ = 171.8 Hz, 1P). ^1H NMR (CD_2Cl_2, 400.0 MHz, 298K): δ 1.5 (m, 1H, CH_2), 1.6 (m, 1H, CH_2), 1.7 (m, 1H, CH_2), 1.8(7) (m, 2H, CH_2), 1.9(3) (m, 1H, CH_2), 2.0 (s, 3H, *N*-CH_3), 2.0(5)(m, 2H, CH_2), 2.1 (s, 3H, *N*-CH_3), 2.1(4) (s, 3H, *N*-CH_3), 2.2 (m, 2H, CH_2), 2.3 (m, 2H, CH_2), 2.6 (s, 3H, *N*-CH_3), 3.8 (m, 1H, α-CH), 5.6 (v.td, *J* = 8.2 Hz, *J* = 12.1 Hz, 1H, α-CH), 6.9 (t, 1H, ArCH), 7.0 (m, 3H, ArCH), 7.0(6) (d, $^3J_{HH}$ = 7.5 Hz, 1H, ArCH), 7.0(7) (d, $^2J_{HH}$ = 7.3 Hz, 1H, ArCH), 7.6 (m, 3H, ArCH), 8.3 (dd, $^3J_{HH}$ = 7.8 Hz, $^3J_{PH}$ = 10.5 Hz, 2H, *P*-*o*-

ArCH). ^{13}C APT NMR (CD_2Cl_2, 100.6 MHz, 298 K): δ 18.4 (s, *N*-CH_3), 18.8 (s, *N*-CH_3), 19.3 (s, *N*-CH_3), 21.2 (s, *N*-CH_3), 24.0 (d, J_{PC} = 9.3 Hz, CH_2), 25.8 (d, J_{PC} = 7.1 Hz, CH_2), 27.9 (d, J_{PC} = 8.2 Hz, CH_2), 28.4 (d, J_{PC} = 3.8 Hz, CH_2), 31.0 (d, J_{PC} = 7.9 Hz, CH_2), 33.7 (d, J_{PC} = 2.7 Hz, CH_2), 41.5 (dd, $^1J_{PC}$ = 31.0 Hz, $^3J_{Rh}$ = 2.8 Hz, α-CH), 56.1 (d, $^2J_{PC}$ = 22.4 Hz, α-CH), 123.9 (s, ArCH), 125.9 (s, J_{PC} = 1.6 Hz, CAr), 126.4 (s, ArCH), 127.1 (d, J_{PC} = 1.7 Hz, CAr), 128.2 (s, ArCH), 128.4 (s, CAr), 128.4 (s, ArCH), 128.6 (s, ArCH), 128.7 (s, ArCH), 129.1 (d, J_{PC} = 10.6 Hz, ArCH), 129.7 (dd, $^2J_{RhC}$ = 1.2 Hz, $^1J_{PC}$ = 41.1 Hz, *P*-CAr), 130.2 (s, CAr), 132.5 (d, J_{PC} = 2.3 Hz, ArCH), 136.2 (d, $^2J_{PC}$ = 13.0 Hz, *P*-*o*-ArCH), 146.3 (s, CAr), 149.9 (s, CAr), 180.3 (d, $^2J_{PC}$ = 2.0 Hz, *N*-C_{imine}), 190.7 (dd, $^2J_{PC}$ = 17.9 Hz, $^1J_{RhC}$ = 69.0 Hz, *Rh*-CO), 201.2 (d, $^2J_{PC}$ = 13.0 Hz, *N*-C_{imine}). ATR-FTIR νCO (cm^{-1}): 1968. Anal. Calcd for $C_{33}H_{37}N_2OPRh$: C, 61.26; H, 5.76; N, 4.33. Found: C, 59.64; H, 6.01; N, 3.86.

Synthesis of **RhCl{(NPN)^{DIPP}H$_2$}(CO) (2.4b)**. **2.3b** (0.123 g, 0.146 mmol) was dissolved in dichloromethane (5 ml) and transferred into a Kontes sealed reaction vessel equipped with a stir bar. The mixture was freeze-pump-thaw degassed three times using high vacuum and backfilled with CO at -196 ºC. The reaction vessel was quickly sealed and allowed to warm to room temperature behind a blast shield. After stirring for 2 hours, the reaction was treated with hexanes. Yellow crystals formed which were collected by filtration (0.067 g, 70.9%). $^{31}P\{^1H\}$ NMR (CD_2Cl_2, 161.9 MHz, 298 K): δ: 64.3 (d, $^1J_{RhP}$ = 170.5 Hz, 1P). ^{1}H NMR (CD_2Cl_2, 400.0 MHz, 298K): δ 0.8 (d, $^3J_{HH}$ = 6.9 Hz, 3H, *N*-Pr^iCH_3), 0.9 (t, $^3J_{HH}$ = 6.9 Hz, 3H, *N*-Pr^iCH_3), 1.2 (t, $^3J_{HH}$ = 6.9 Hz, 3H, *N*-Pr^iCH_3), 1.2(3) (d, $^3J_{HH}$ = 6.7, 3H, *N*-Pr^iCH_3), 1.2(6) (d, $^3J_{HH}$ = 6.9 Hz, 3H, *hexanes*), 1.3(2) (d, $^3J_{HH}$ = 7.0 Hz, 3H, *N*-Pr^iCH_3), 1.3(4) (d, $^3J_{HH}$ = 6.9 Hz, 3H, *N*-Pr^iCH_3), 1.4(3) (d, $^3J_{HH}$ = 6.7 Hz, 3H, *N*-Pr^iCH_3), 1.4(4) (d, $^3J_{HH}$ = 6.7 Hz, 3H, *N*-Pr^iCH_3), 1.5-2.0 (m, 9H, CH_2), 2.2(m, 2H, CH_2), 2.4 (m, 1H, CH_2), 2.7 (sept., $^3J_{HH}$ = 6.8 Hz, 1H,

N-Pr^{i}CH), 2.9 (sept., $^{3}J_{HH}$ = 6.8 Hz, 2H, 2x *N*-Pr^{i}CH), 3.8 (m, 1H, α-CH), 3.9 (sept., $^{3}J_{HH}$ = 6.8 Hz, 1H, *N*-Pr^{i}CH), 5.5 (ddd, *J* = 8.5, *J* = 12.0 Hz, *J* = 12.5 Hz, 1H, α-CH), 7.1 (m, 2H, ArCH), 7.1(2) (m, 2H, ArCH), 7.2 (m, 1H, ArCH), 7.2(3) (m, 1H, ArCH), 7.6 (m, 3H, ArCH), 8.3 (ddd, $^{4}J_{HH}$ = 1.2 Hz, $^{3}J_{HH}$ = 7.5 Hz, $^{3}J_{PH}$ = 9.4 Hz, 2H, *P*-*o*-ArCH). ^{13}C APT NMR (CD_2Cl_2, 100.6 MHz, 298 K): δ 20.4 (s, *N*-Pr^{i}CH_3), 23.0(7) (s, *n-hexanes*), 23.1 (s, *N*-Pr^{i}CH_3), 23.4(7) (s, *N*-Pr^{i}CH_3), 23.4(8) (s, *N*-Pr^{i}CH_3), 24.1 (d, J_{PC} = 10.8 Hz, CH_2), 24.6 (s, *N*-Pr^{i}CH_3), 24.8 (s, *N*-Pr^{i}CH_3), 25.0 (s, *N*-Pr^{i}CH_3), 25.6 (d, J_{PC} = 7.7 Hz, CH_2), 25.9 (s, *N*-Pr^{i}CH_3), 28.2 (d, J_{PC} = 7.5 Hz, CH_2), 28.4 (s, 2x *N*-Pr^{i}CH), 28.6 (s, *N*-Pr^{i}CH), 29.2 (d, J_{PC} = 3.9 Hz, CH_2), 29.3 (s, *N*-Pr^{i}CH), 32.8 (d, J_{PC} = 7.5 Hz, CH_2), 34.5 (d, J_{PC} = 4.0 Hz, CH_2), 42.0 (dd, $^{1}J_{PC}$ = 31.6 Hz, $^{2}J_{RhC}$ = 3.3 Hz, α-CH), 49.6 (s, *unknown impurity*), 56.6 (d, *J* = 21.1 Hz, α-CH), 123.2 (s, ArCH), 123.9 (s, ArCH), 124.2 (s, ArCH), 124.3 (s, ArCH), 124.6 (s, ArCH), 127.3 (s, ArCH), 128.9 (d, J_{PC} = 10.4 Hz, ArCH), 130.3 (d, $^{1}J_{PC}$ = 40.1 Hz, *P*-CAr), 132.5 (d, J_{PC} = 2.3 Hz, ArCH), 136.5 (d, $^{2}J_{PC}$ = 12.6 Hz, *P*-*o*-ArCH), 136.7 (d, J_{PC} = 1.4 Hz, CAr), 137.8 (d, J_{PC} = 1.3 Hz, CAr), 138.9 (s, CAr), 140.9 (s, CAr), 143.4 (s, CAr), 147.4(3) (d, J_{PC} = 1.9 Hz, CAr), 180.0 (s, *N*-C_{imine}), 190.7 (dd, $^{1}J_{RhC}$ = 71.3 Hz, $^{2}J_{PC}$ = 17.8 Hz, *Rh*-CO), 200.79 (dd, $^{2}J_{PC}$ = 12.1 Hz, $^{3}J_{RhC}$ = 0.9 Hz, *N*-C_{imine}). ATR-FTIR νCO (cm^{-1}): 1971. Anal. Calcd for $C_{41}H_{53}ClN_2OPRh$: C, 64.86; H, 7.04; N, 3.69. Found: C, 63.69; H, 7.12; N, 3.91.

Synthesis of **$RhCl_2H${(NPN)^{DMP}H_2} (2.5a)**. **2.3a** (0.127 g, 0.174 mmol) was dissolved in dichloromethane (5 ml) and transferred into a Kontes sealed reaction vessel equipped with a stir bar. The mixture was freeze-pump-thaw degassed three times using high vacuum and backfilled with H_2 at -196 ºC. After stirring overnight, the solution is a red-orange color. The H_2 pressure was released and the reaction mixture was concentrated and treated with hexanes. Off white solid was collected by filtration through a sinter glass frit (0.070 g, 61.4 %, ~90 % pure by ^{1}H

NMR, EA not preformed). $^{31}P\{^{1}H\}$ NMR (CD_2Cl_2, 161.9 MHz, 298 K): δ 110.2 (d, $^{1}J_{RhP}$ = 130.3 Hz, 1P). ^{1}H NMR (CD_2Cl_2, 400.0 MHz, 298K): δ -15.7 (d, $^{2}J_{PH}$ = 2.1 Hz, $^{1}J_{RhH}$ = 19.5 Hz, 1H, *Rh*-H), 1.4 (m, 2H, CH_2), 1.6 (m, 2H, CH_2), 1.9 (m, 4H, CH_2), 2.0 (s, 6H, *N*-CH_3), 2.3(5) (m, 4H, CH_2), 2.3(9) (s, 6H, *N*-CH_3), 6.0 (td, $^{3}J_{HH}$ = 8.4 Hz, $^{3}J_{PH}$ = 12.7 Hz, 2H, α-CH), 6.9 (dd, *J* = 2.7 Hz, *J* = 5.9 Hz, 1H, ArCH), 7.0 (m, 4H, ArCH), 7.7 (s, 4H, ArCH), 8.0 (ddd, $^{4}J_{HH}$ = 1.7 Hz, $^{3}J_{HH}$ = 7.2 Hz, $^{3}J_{PH}$ = 10.7 Hz, 2H, *P*-*o*-ArCH). ^{13}C APT NMR (CD_2Cl_2, 100.6 MHz, 298 K): δ 19.3 (s, *N*-CH_3), 20.1 (s, *N*-CH_3), 27.4 (d, J_{PC} = 10.8 Hz, CH_2), 27.5 (d, J_{PC} = 7.2 Hz, CH_2), 32.4 (d, J_{PC} = 9.7 Hz, CH_2), 54.5 (d, $^{1}J_{PC}$ = 26.5 Hz, α-CH), 120.2 (d, $^{2}J_{RhC}$ = 2.2 Hz, $^{1}J_{PC}$ = 48.2 Hz, *P*-CAr), 126.9 (s, ArCH), 127.2 (s, CAr), 128.5 (s, ArCH), 129.1 (s, ArCH), 129.8 (d, $^{3}J_{PC}$ = 10.9 Hz, *P*-*m*-ArCH), 132.4 (s, CAr), 133.5 (d, J_{PC} = 2.3 Hz, ArCH), 135.4 (d, $^{2}J_{PC}$ = 11.2 Hz, *P*-*o*-ArCH), 147.0 (s, CAr), 201.2 (d, $^{2}J_{PC}$ = 10.7 Hz, *N*-C_{imine}).

Synthesis of **$RhCl_2H\{(NPN)^{DIPP}H_2\}$ (2.5b)**. **2.3b** (0.120 g, 0.143 mmol) was dissolved in dichloromethane (15 ml) and transferred into a Kontes sealed reaction vessel equipped with a stir bar. The mixture was freeze-pump-thaw degassed using high vacuum three times and backfilled with H_2 at -196 ºC. After two days, the solution is a red-orange color, after eight days the H_2 pressure was released. The reaction mixture was concentrated and treated with hexanes, an off white solid was collected by filtration through a sinter glass frit (0.058 g, 52.8 % ~60 % pure by ^{1}H NMR, EA not preformed). $^{31}P\{^{1}H\}$ NMR (CD_2Cl_2, 161.9 MHz, 298 K): δ 108.0 (d, $^{1}J_{RhP}$ = 131.4 Hz, 1P). ^{1}H NMR (CD_2Cl_2, 400.0 MHz, 298K): δ -15.5 (d, $^{1}J_{RhH}$ = 17.9 Hz, 1H, *Rh*-H), 0.9 (d, $^{3}J_{HH}$ = 6.9 Hz, 6H, *N*-$Pr^{i}CH_3$), 1.0 (d, $^{3}J_{HH}$ = 6.9 Hz, 6H, *N*-$Pr^{i}CH_3$), 1.3 (d, $^{3}J_{HH}$ = 6.6 Hz, 6H, *N*-$Pr^{i}CH_3$), 1.4(7) (d, $^{3}J_{HH}$ = 6.7 Hz, 6H, *N*-$Pr^{i}CH_3$), 1.5 (m, 2H, CH_2), 1.6 (m. 2H, CH_2), 2.0 (br.m, 6H, CH_2), 2.3 (m, 2H, CH_2), 2.8 (sept. $^{3}J_{HH}$ = 6.8 Hz, 2H, *N*-$Pr^{i}CH$), 3.8 (sept.

$^{3}J_{HH}$ = 6.7 Hz, 2H, *N*-Pr^{i}CH), 6.0 (td, $^{3}J_{HH}$ = 8.4 Hz, $^{3}J_{PH}$ = 12.9 Hz, 2H, α-CH), 7.0 (dd, $^{4}J_{HH}$ = 1.0 Hz, $^{3}J_{HH}$ = 7.6 Hz, 2H, ArCH), 7.1 (dd, $^{4}J_{HH}$ = 1.1 Hz, $^{3}J_{HH}$ = 7.7 Hz, 2H, ArCH), 7.2 (t, $^{3}J_{HH}$ = 7.7 Hz, 2H, ArCH), 7.7 (m, 3H, ArCH), 8.0 (ddd, $^{1}J_{HH}$ = 2.8 Hz, $^{3}J_{HH}$ = 6.5 Hz, $^{3}J_{PH}$ = 10.6 Hz, 2H, *P*-*o*-ArCH). ^{13}C APT NMR (CD_2Cl_2, 100.6 MHz, 298 K): δ 23.7 (s, *N*-Pr^{i}CH$_3$), 24.6 (s, *N*-Pr^{i}CH$_3$), 24.8 (s, *N*-Pr^{i}CH$_3$), 25.0 (s, *N*-Pr^{i}CH$_3$), 27.2 (d, J_{PC} = 7.0 Hz, CH_2), 27.4 (d, J_{PC} = 10.1 Hz, CH_2), 27.8 (s, *N*-Pr^{i}CH), 28.0 (s, *N*-Pr^{i}CH), 33.6 (d, J_{PC} = 9.6 Hz, CH_2), 54.0 (d, J_{PC} = 26.9 Hz, α-CH, *overlapping with CD_2Cl_2 signal*), 120. (d, $^{1}J_{PC}$ = 47.8 Hz, *P*-CAr), 124.0 (s, ArCH), 125.1 (s, ArCH), 127.6 (s, ArCH), 129.5 (d, J_{PC} = 10. 9 Hz, ArCH), 133.6 (s, ArCH), 135.2 (d, J_{PC}= 11.2 Hz, *P*-*o*-ArCH), 138.0 (CAr), 142.6 (CAr), 144.6 (CAr), *N*-C_{imine} resonance not observed due to poor signal to noise ratio.

Synthesis of **[(NP)^{DIPP}K(THF)]$_2$ (3.7a)**. In a Schlenk flask **3.6a** (8.83 g, 20.7 mmol) was added to excess potassium hydride (1.86 g, 46.4 mmol). THF (100 ml) was added and the suspension was stirred overnight. During this time, the solution became a bright yellow color and small bubbles were observed. After the reaction is complete, the mixture was filtered through Celite. The solvent was removed by vacuum, a yellow oil results. Triturating the yellow oil with pentane or hexanes gave a slurry containing yellow solids. Collecting these solids by filtration produces a yellow powder corresponding to the final product (8.73 g, 79%). ^{31}P{^{1}H} NMR (C_6D_6, 161.9 MHz, 298 K): δ -19.1 (s). ^{1}H NMR (C_6D_6, 400.0 MHz, 298 K): δ 1.1 (d, 6H, $^{3}J_{HH}$ = 6.9 Hz, *N*-Pr^{i}CH$_3$), 1.4 (m, 4H, *THF*-CH_2), 1.4 (d, 6H, $^{3}J_{HH}$ = 6.8 Hz, *N*-Pr^{i}CH$_3$), 1.9 (m, 2H, γ-CH_2), 2.3 (t, 2H, $^{3}J_{HH}$ = 7.3 Hz, β-CH_2), 2.7 (t, 2H, $^{3}J_{HH}$ = 6.6 Hz, δ-CH_2), 3.4 (m, 4H, *THF*-CH_2), 3.5 (m, 2H, *N*-Pr^{i}CH) 7.0 (t, 1H, $^{3}J_{HH}$ = 7.5 Hz, *N*-*p*-ArCH), 7.1 (m, 4H, *N*-*m*/*P*-*p*-ArCH), 7.2 (v.t, 4H, *J* = 7.3 Hz, *P*-*m*-ArCH), 7.7 (v.t, 4H, *J* = 7.2 Hz, *P*-*o*-ArCH). ^{13}C APT NMR (C_6D_6, 100.6 MHz, 298 K): δ 24.3 (s, *N*-Pr^{i}CH$_3$), 24.6 (s, γ-CH_2), 24.7 (s, *N*-Pr^{i}CH),

25.7 (s, *THF*-CH_2), 27.8 (s, *N*- Pr^iCH_3), 32.2 (d, $^2J_{PC}$ = 4.6, β-CH_2), 35.8 (d, $^3J_{PC}$ = 9.0 Hz, δ-CH_2), 67.8 (s, *THF*-CH_2), 69.2 (d, $^1J_{PC}$ = 14.8 Hz, α-C), 120.1 (s, *N*-*p*-ArCH), 123.2 (s, *N*-*m*-ArCH), 127.1 (s, *P*-*p*-ArCH), 128.4 (d, $^3J_{PC}$ = 6.1 Hz, *P*-*m*-ArCH), 133.2 (d, $^2J_{PC}$ = 16.4 Hz, *P*-*o*-ArCH) 142.2 (s, *N*-ArCPr^i), 142.4 (d, $^2J_{PC}$ = 3.1 Hz, *N*-$C_{enamide}$), 154.4 (s, *N*-CAr), 175.8 (d, $^1J_{PC}$ = 32.7 Hz, *P*-CAr). Anal. Calcd. for $C_{33}H_{41}KNOP$: C, 73.70; H, 7.68; N, 2.60. Found: C, 73.64; H, 7.92; N, 2.99.

Synthesis of **$[(NP)^{DMP}K(THF)]_2$ (3.7b)**. An adaptation of the procedure described above was used. Upon collecting the yellow product by filtration, the mother liquor was concentrated and treated with hexanes. X-ray quality crystals grew (performed on a variety of scales, yield: 68%). $^{31}P\{^1H\}$ NMR (C_6D_6, 161.9 MHz, 298 K): δ -22.1 (s). ^1H NMR (C_6D_6, 400.0 MHz, 298 K): δ 1.4 (m, 4H, *THF*-CH_2), 1.9 (m, 2H, γ-CH_2), 2.0 (s, 6H, *N*-CH_3), 2.2 (t, 2H, $^3J_{HH}$ = 7.5 Hz, δ-CH_2), 2.6 (t, 2H, $^3J_{HH}$ = 6.7 Hz, β-CH_2), 3.5 (m, 4H, *THF*-CH_2), 6.9 (t, 1H, $^3J_{HH}$ = 7.4 Hz, *N*-*p*-ArCH), 7.1 (d, 2H, $^3J_{HH}$ = 7.4 Hz, *N*-*m*-ArCH), 7.2 (t, 2H, $^3J_{HH}$ = 7.3 Hz, *P*-*p*-ArCH), 7.3 (v.t, 4H, *J* = 7.2 Hz, *P*-*m*-ArCH), 7.5 (v.t, 4H, *J* = 7.3 Hz, *P*-*o*-ArCH). ^{13}C APT NMR (C_6D_6, 100.6 MHz, 298 K): δ 20.0 (s, *N*-CH_3), 24.2 (d, $^2J_{PC}$ = 4.4 Hz, γ-CH_2), 25.7 (s, *THF*-CH_2), 32.5 (d, $^3J_{PC}$ = 4.8 Hz, δ-CH_2), 36.1 (d, $^3J_{PC}$ = 7.9 Hz, γ-CH_2), 67.8 (s, *THF*-CH_2), 69.9 (d, $^1J_{PC}$ = 9.8 Hz, α-C), 120.0 (s, *N*-*p*-ArCH), 127.3 (s, *P*-*p*-ArCH), 128.4 (d, $^3J_{PC}$ = 6.4 Hz, *P*-*m*-ArCH), 128.7 (s, *N*-*m*-ArCH), 131.6 (s, *N*-ArCMe), 133.4 (d, $^2J_{PC}$ = 16.9 Hz *P*-*o*-ArCH), 141.6 (d, $^2J_{PC}$ = 3.3 Hz, *N*-$C_{enamide}$), 156.9 (s, *N*-CAr), 175.9 (d, $^1J_{PC}$ = 32.4 Hz, *P*-CAr). Anal. Calcd. for $C_{29}H_{33}KNOP$: C, 72.23; H, 6.91; N, 2.91. Found: C, 71.43; H, 6.53; N, 3.76.

Synthesis of **Ir{$(NP)^{DIPP}$}(COD) (3.8a)**. **3.7a** (1.41 g, 1.31 mmol) was combined with $[IrCl(COD)]_2$ (0.881 g, 1.31 mmol) in toluene (50 ml), and the mixture was stirred for approximately 20 minutes. The solution became an intense red and a white precipitate

(potassium chloride) formed, which was removed by Celite filtration. The solvent was removed, and the product was dried under vacuum to give a bright red solid (1.29 g, 68%). Recrystallization by slow evaporation of hexanes or cooling a concentrated hexanes solution to -35 °C results in formation of X-ray quality crystals. This reaction was performed on various scales. Conversion is quantitative by $^{31}P\{^{1}H\}$ and ^{1}H NMR spectroscopy. $^{31}P\{^{1}H\}$ NMR (C_6D_6, 161.9 MHz, 298 K): δ 12.1 (s). ^{1}H NMR (C_6D_6, 400 MHz, 298 K): δ 1.3 (d, 6H, $^{3}J_{HH}$ = 6.8 Hz, *N*-Pr^{i}CH$_3$), 1.5 (d, 6H, $^{3}J_{HH}$ = 6.9 Hz, *N*-Pr^{i}CH$_3$), 1.5 (m, 2H, *COD*-CH$_2$), 1.7 (m, 2H, *COD*-CH$_2$), 2.1 (m, 8H, γ-CH$_2$, 2x *COD*-CH$_2$, β-CH$_2$), 2.4 (t, 2H, $^{3}J_{HH}$ = 6.5 Hz, δ-CH$_2$), 3.3 (br. d, 2H, J_{HH} = 2.7 Hz, *trans*-*N*-*COD*-CH), 4.0 (m, 2H, *N*-Pr^{i}CH), 4.1 (m, 2H, *trans*-*P*-*COD*-CH), 7.0-7.1 (m, 2H, *P*-*p*-ArCH), 7.1-7.2 (m, 5H, *N*-*p*/*P*-*m*-ArCH), 7.2 (m, 2H, *N*-*m*-ArCH), 7.8 (m, 4H, *P*-*o*-ArCH). ^{13}C APT NMR (C_6D_6, 100.6 MHz, 298 K): δ 24.5 (s, *N*-Pr^{i}CH$_3$), 25.6 (s, δ-CH$_2$), 25.6 (s, *N*-Pr^{i}CH$_3$), 27.8 (s, *N*-Pr^{i}CH), 28.7 (d, $^{2}J_{PC}$ = 8.7 Hz, β-CH$_2$), 30.1 (d, $^{3}J_{PC}$ = 1.2 Hz, *COD*-CH$_2$), 32.1 (d, $^{3}J_{PC}$ = 16.8 Hz, γ-CH$_2$), 33.0 (d, J_{PC} = 3.2 Hz, *COD*-CH$_2$), 53.9 (s, *trans*-*N*-*COD*-CH), 87.7 (d, $^{1}J_{PC}$ = 61.0 Hz, α-C), 90.2 (d, J_{PC} = 12.8 Hz, *trans*-*P*-*COD*-CH), 123.6 (s, *N*-*m*-ArCH), 125.7 (s, *N*-*p*-ArCH), 128.7 (d, $^{3}J_{PC}$ = 10.0 Hz, *P*-*m*-ArCH), 129.9 (d, $^{3}J_{PC}$ = 1.8 Hz, *P*-*p*-ArCH), 133.0 (d, $^{2}J_{PC}$ = 11.0 Hz, *P*-*o*-ArCH), 134.5 (d, $^{2}J_{PC}$ = 52.5 Hz, *N*-C$_{enamide}$), 145.2 (s, *N*-ArCPr^{i}), 147.9 (s, *N*-CAr), 189.9 (d, $^{1}J_{PC}$ = 32.3 Hz, *P*-CAr). Anal. Calcd. for $C_{37}H_{46}IrNP$: C, 61.05; H, 6.34; N, 1.92. Found: C, 61.24; H, 6.15; N, 1.91.

Synthesis of **Ir{(NP)^{DMP}}(COD) (3.8b)**. A similar procedure to that used for the synthesis of **3.8a** was employed (performed on a variety of scales, 57% EA not preformed). $^{31}P\{^{1}H\}$ NMR (C_6D_6, 161.9 MHz, 298 K): δ 11.5 (s). ^{1}H NMR (C_6D_6, 400 MHz, 298 K): δ 1.6 (m, 2H, *COD*-CH$_2$), 1.8 (m, 2H *COD*-CH$_2$), 2.0 (m, 2H, β-CH$_2$), 2.1 (m, 2H, *COD*-CH$_2$), 2.2 (m, 2H, *COD*-CH$_2$), 2.3 (m, 2H, γ-CH$_2$), 2.5 (t, 2H, $^{3}J_{HH}$ = 6.7 Hz, δ-CH$_2$), 2.7 (s, 6H, *N*-CH$_3$), 3.4

(dd, 2H, *J* = 2.7 Hz, *J* = 5.6 Hz, *trans-N-COD*-CH), 4.1 (dd, 2H, *J* = 2.6 Hz, *J* = 6.2 Hz, *trans-P-COD*-CH), 7.1 (t, 1H, $^{3}J_{HH}$ = 7.5 Hz, *N-p*-ArCH), 7.2 (m, 2H, *P-p*-ArCH), 7.2-7.3 (m, 6H, *N-m-/P-m*-ArCH), 7.9 (ddd, 4H, *J* = 1.1 Hz, *J* = 8.0 Hz, *J* = 9.6 Hz, *P-o*-ArCH). ^{13}C APT NMR (C_6D_6, 100.6 MHz, 298 K): δ 19.1 (s, *N*-CH_3), 25.4 (s, δ-CH_2), 28.2 (d, $^{3}J_{PC}$ = 9.1 Hz, γ-CH_2), 30.5 (d, J_{PC} = 2.0 Hz, *COD*-CH_2), 30.9 (d, $^{2}J_{PC}$ = 17.2 Hz, β-CH_2), 33.1 (d, J_{PC} = 3.4 Hz, *COD*-CH_2), 54.0 (s, *trans-N-COD*-CH), 87.5 (d, $^{1}J_{PC}$ = 60.8 Hz, α-C), 90.0 (d, J_{PC} = 12.8 Hz, *trans-P-COD*-CH), 124.7 (s, *N-p*-ArCH), 128.1 (s, *N-m*-ArCH), 128.8 (d, $^{3}J_{PC}$ = 10.0 Hz, *P-m*-ArCH), 129.0 (d, $^{4}J_{PC}$ = 2.2 Hz, *P-p*-ArCH), 133.0 (d, $^{2}J_{PC}$ = 11.1 Hz, *P-o*-ArCH), 134.4 (d, $^{2}J_{PC}$ = 52.0 Hz, *N*-$C_{enamide}$), 135.2 (s, *N*-ArMe), 150.6 (s, *N*-CAr), 188.6 (d, $^{1}J_{PC}$ = 32.6 Hz, *P*-CAr).

Synthesis of **[(NP)^{DIPP}Ir(H)$_3$]$_2$ (3.9a)**. **3.8a** (0.405 g, 0.557 mmol) was dissolved in toluene (30 ml) in a Kontes sealed reaction vessel (80 ml). Isopropanol (30 ml) was added; the flask was sealed and heated to 100 °C overnight. A yellow precipitate formed. The precipitate was allowed to settle and the reaction mixture was decanted. The solid was washed with hexanes and taken to dryness to give a yellow powder (0.192 g, 55%).

Alternatively, a J. Young tube is charged with **3.8a** (0.033 g, 0.045 mmol), 0.5 ml (C_6H_6) and isopropanol (0.5 ml). Clear, yellow, X-ray quality crystals form upon heating to 90 °C overnight.

Alternatively, **3.8a** (0.135 g, 0.186 mmol) was dissolved in pentane (30 ml) in a Kontes sealed reaction vessel. This mixture was freeze-pump-thaw degassed three times using high vacuum. The headspace of the reaction vessel was back filled with H_2 at -196 °C. The flask was sealed and allowed to warm to room temperature under 4 atm of H_2. After stirring the mixture overnight, a yellow precipitate forms. The H_2 pressure was released and the mixture was taken to dryness. Addition of pentane or hexanes to the reaction vessel forms a slurry. Filtration of

this suspension allowed for the isolation of the desired product as a yellow powder (0.060 g, 51%). $^{31}P\{^{1}H\}$ NMR (CD_2Cl_2, 161 MHz, 298 K): δ 32.7 (s). ^{1}H NMR (CD_2Cl_2, 400 MHz, 298 K): δ -23.2 (v.dd, $^{2}J_{PH}$ = 8.6 Hz, $^{2}J_{HH}$ = 3.7 Hz, 2H, *trans-H-Ir*-H), -20.0 (t, $^{2}J_{PH}$ = 28.6 Hz, 2H, *bridging-Ir*-H), -8.6 (d, $^{2}J_{PH}$ = 82.9 Hz, 2H, *trans-N-Ir*-H), 0.81 (d, 6H, $^{3}J_{HH}$ = 6.7 Hz, *N*-$Pr^{i}CH_3$), 0.9 (d, 6H, $^{3}J_{HH}$ = 8.5 Hz, *N*-$Pr^{i}CH_3$), 0.9(2) (d, 6H, $^{3}J_{HH}$ = 7.1 Hz, *N*-$Pr^{i}CH_3$), 1.3 (m, 2H, δ-CH_2), 1.5 (d, 6H, $^{3}J_{HH}$ = 6.5 Hz, *N*-$Pr^{i}CH_3$), 1.7 (m, 2H, γ-CH_2), 1.8 (m, 2H, γ-CH_2), 1.9 (m, 2H, β-CH_2), 2.0 (m, 2H, β-CH_2), 2.3 (m, 2H, δ-CH_2), 2.8 (m, 2H, $^{3}J_{HH}$ = 6.5 Hz, *N*-$Pr^{i}CH$), 3.4 (m, 2H, $^{3}J_{HH}$ = 6.7 Hz, *N*-$Pr^{i}CH$), 3.7 (v.dt, 2H $^{3}J_{PH}$ = 9.5 Hz, $^{3}J_{HH}$ = 11.3 Hz, α-CH), 6.9 (d, 2H, $^{3}J_{HH}$ = 7.2 Hz, *N-m*-ArCH), 7.1 (t, 2H, $^{3}J_{HH}$ = 7.5 Hz, *N-p*-ArCH), 7.2 (d, 2H, $^{3}J_{HH}$ = 6.1 Hz, *N-m*-ArCH), 7.3 (m, 6H, *P-m/p*-ArCH), 7.4 (br.s, 6H, *P-m/p*-ArCH), 7.5 (br.m, 4H, *P-o*-ArCH), 7.8 (m, 4H, *P-o*-ArCH). ^{13}C APT NMR (CD_2Cl_2, 241.7 MHz, 298 K): δ 23.2 (s, *N*-$Pr^{i}CH_3$), 24.6 (s, *N*-$Pr^{i}CH_3$), 24.7 (s, *N*-$Pr^{i}CH_3$), 25.2 (s, *N*-$Pr^{i}CH_3$), 27.6 (d, $^{2}J_{PC}$ = 7.4 Hz, β-CH_2), 27.9 (s, *N*-$Pr^{i}CH$), 28.1 (s, *N*-$Pr^{i}CH$), 28.2 (d, $^{3}J_{PC}$ = 5.6 Hz, δ-CH_2), 31.2 (d, $^{3}J_{PC}$ = 6.3 Hz, γ-CH_2), 62.8 (d, $^{1}J_{PC}$ = 33.1 Hz, α-CH), 123.6 (s, *N-m*-ArCH), 123.7 (s, *N-m*-ArCH), 125.2 (s, *N-p*-ArCH), 127.8 (d, $^{3}J_{PC}$ = 9.7 Hz, *P-m*-ArCH), 128.1 (d, $^{3}J_{PC}$ = 10.4 Hz, *P-m*-ArCH), 129.6(7) (d, $^{4}J_{PC}$ = 1.3 Hz, *P-p*-ArCH), 129.7(2) (d, $^{4}J_{PC}$ = 1.2 Hz, *P-p*-ArCH), 131.0 (d, $^{1}J_{PC}$ = 34.0 Hz, *P*-CAr), 133.7 (d, $^{2}J_{PC}$ = 11.4 Hz, *P-o*-ArCH), 134.5 (d, $^{2}J_{PC}$ = 13.1 Hz, *P-o*-ArCH), 138.6 (d, $^{1}J_{PC}$ = 61.3 Hz, *P*-ArC), 139.1 (s, *N*-ArCPr^{i}), 140.0, (s, *N*-ArCPr^{i}), 149.6 (s, *N*-Ar). A peak corresponding to C_{imine} could not be identified from -20 to 200 ppm in the ^{13}C APT NMR spectrum. Anal. Calcd. for $C_{29}H_{37}IrNP$: C, 55.93; H, 5.99; N, 2.25. Found: C, 56.05; H, 5.93; N, 2.63.

Synthesis of **Ir{(NP)^{DIPP}}(CO)$_2$ (3.10a)**. **3.8a** (0.250 g, 0.344 mmol) was dissolved in hexanes (30 ml) in a Kontes sealed vessel. The mixture was degassed with three freeze-pump-thaw cycles using high vacuum. After the final cycle, the solvent was allowed to thaw to room

temperature in the sealed reaction vessel under vacuum. CO was backfilled to the evacuated vessel. The solution instantly lightened in color. After stirring for approximately 30 minutes, the reaction was taken to dryness. The mixture was then dissolved in a minimal amount of hexanes and left to crystallize at -35 °C. X-ray quality crystals formed and the mother liquor was removed by pipette. The crystals were dried under vacuum (0.145 g, 63%). $^{31}P\{^{1}H\}$ NMR (C_6D_6, 161.9 MHz, 298 K): δ 21.3 (s). ^{1}H NMR (C_6D_6, 400.0 MHz, 298 K): δ 1.2 (d, 6H, $^{3}J_{HH}$ = 6.9 Hz, *N*-Pr^{i}CH$_3$), 1.4 (d, 6H, $^{3}J_{HH}$ = 6.8 Hz, *N*-Pr^{i}CH$_3$), 2.0 (t, 2H, $^{3}J_{HH}$ = 7.3 Hz, γ-CH$_2$), 2.2 **(**m, 2H, δ-CH$_2$**),** 2.4 (t, 2H, $^{3}J_{HH}$ = 6.6 Hz, β-CH$_2$), 3.9 (hept, 2H, $^{3}J_{HH}$ = 6.8 Hz, *N*-Pr^{i}CH), 7.0-7.1(m, 9H, ArCH), 7.8 (ddd, $^{3}J_{PC}$ = 12.2 Hz, $^{3}J_{HH}$ = 7.7 Hz, $^{4}J_{HH}$ = 1.7 Hz, *P*-*o*-ArCH). ^{13}C APT NMR (C_6D_6, 100.6 MHz, 298 K): δ 24.2 (s, Pr^{i}CH$_3$), 24.3(s, Pr^{i}CH$_3$), 26.4 (s, β-CH$_2$), 28.2 (s, Pr^{i}CH), 29.6 (d, $^{3}J_{PC}$ = 9.2 Hz, δ-CH$_2$), 31.3 (d, $^{3}J_{PC}$ = 17.7 Hz, γ-CH$_2$), 83.5 (d, $^{1}J_{PC}$ = 64.4 Hz, α-C), 123.4 (s, *N*-*m*-ArCH), 126.4 (s, *N*-*p*-ArCH), 129.2 (d, $^{3}J_{PC}$ = 11.0 Hz, *P*-*m*-Ar-CH), 130.9 (s, *P*-*p*-ArCH), 132.5 (s, *N*-C$_{enamide}$), 133.0 (d, $^{2}J_{PC}$ = 11.6 Hz, *P*-*o*-ArCH), 144.0 (s, *N*-CArPr^{i}), 152.5 (s, *N*-CAr), 180.1(d, $^{2}J_{PC}$ = 11.1 Hz, *trans*-*N*-CO), 181.5 (d, $^{2}J_{PC}$ = 103.5 Hz, *trans*-*P*-CO), 189.3 (d, $^{1}J_{PC}$ = 32.5 Hz, *P*-CAr). Anal. Calcd. for $C_{31}H_{34}IrNO_2P$: C, 55.10; H, 5.07; N, 2.07. Found: C, 54.35; H, 4.89; N, 2.33. ATR-FTIR νCO (cm^{-1}): 1966, 2041.

Synthesis of **Ir{(NP)^{DIPP}}(^{13}CO)$_2$ (3.10a*)**. **3.8a** (0.100 g, 0.138 mmol) was dissolved in hexanes (10 ml) in a Kontes sealed reaction vessel. The mixture was freeze-pump-thaw degassed 3x, after the final cycle, the solvent was allowed to warm to room temperature in the sealed reaction vessel. ^{13}CO was backfilled to the evacuated vessel from a 1L ^{13}CO glass bulb. The solution instantly lightened in color. After stirring for approximately 30 minutes, the reaction was taken to dryness. The mixture was then dissolved in a minimal amount of hexanes and left to crystallize at -35 °C. Red crystals formed, and the mother liquor was removed by

pipette. The crystals were dried under vacuum (yield: 0.060 g, 65%). $^{31}P\{^{1}H\}$ NMR (C_6D_6, 161.9 MHz, 298 K): δ 21.3 (dd, $^{2}J_{PC}$ = 11.2 Hz, $^{2}J_{PC}$ = 103. 4 Hz). ^{1}H NMR (C_6D_6, 400.0 MHz, 298 K): δ unchanged from 12-carbon monoxide analogue. ^{13}C APT NMR (C_6D_6, 100.6 MHz, 298 K): δ unchanged from 12-carbon monoxide analogue with the exception of the two resonances which correspond to the 13-carbon labeled peaks: 180.1(dd, $^{2}J_{PC}$ = 11.1 Hz, $^{2}J_{CC}$ = 4.2 Hz, *trans*-*N*-CO), 181.5 (dd, $^{2}J_{PC}$ = 103.5 Hz, $^{2}J_{CC}$ = 4.2 Hz, *trans*-*P*-CO).

Monitoring conversion of **$[Ir(H)_3\{(NP)^{DIPP}H\}]_2$ (3.9a)** to **$Ir\{(NP)^{DIPP}\}(CO)_2$ (3.10a)** under CO.

1 atm of CO: A suspension of **3.9a** (0.020 g, 0.016 mmol) in d_8-THF (0.5 ml) was formed. This mixture was transferred to a J. Young tube and freeze-pump-thaw degassed three times. After the final degassing cycle, the mixture was warmed to room temperature and left under vacuum. The headspace was backfilled with CO and the reaction was monitored by multinuclear NMR spectroscopy. To deliver ^{13}CO, analogous conditions were used; however, the 13-carbon labeled material was delivered from a 1L glass bulb filled with 1 atm of gas.

4 atm of CO: A suspension of **3.9a** (0.020 g, 0.016 mmol) in d_8-THF (0.5 ml) was formed. This mixture was transferred to a NMR tube attached to a ground glass fitting sealed with a ground glass tap. The mixture was degassed by three freeze-pump-thaw cycles using high vacuum. The headspace of the NMR tube was backfilled with CO to a pressure of approximately 150 mmHg (slight vacuum) at -196 °C. The NMR tube is flame sealed at this temperature. To deliver ^{13}CO analogous conditions were used; however, the carbon-13 labeled CO was delivered from a 1L glass bulb filled with 1 atm of gas. The apparatus was allowed to stand at -196 °C for 30 min before it was flame sealed when ^{13}CO was used. A complex mixture

results after 3 days under 1 atm of CO, only the identified peaks are reported based on experiments with 1 atm of CO. Similar resonances are identified under 4 atm of CO.

1 atm ^{12}CO after 3 days:

^{31}P{^{1}H} NMR (d_8-THF, 161.9 MHz, 298 K): δ 7.3 (s, **3.12**), 1.6 (s, **3.14**), -30.6 (s, **3.16**). ^{1}H NMR (d_8-THF, 400.0 MHz 298 K): δ -12.1 (d, $^{2}J_{PC}$ = 80.3 Hz, *trans-P-Ir*-H**$_{3.16}$**), -11.6 (d, $^{2}J_{PH}$ = 52.2 Hz, *cis-P-Ir*-H**$_{3.14}$**), -11.2 (dt, $^{2}J_{PH}$ = 121.7 Hz, *trans-P-Ir*-H**$_{3.12}$**), -10.9 (d, $^{2}J_{PH}$ = 18.0 Hz *cis-P-Ir*-H**$_{3.12}$**, -10.8 (d, $^{2}J_{PH}$ = 16.4 Hz, *cis-P-Ir*-H**$_{3.12}$**), 4.2 (v.td, $^{2}J_{HH}$ = 7.7 Hz, $^{2}J_{PH}$ = 13.5 Hz, α-CH**$_{3.12/3.14}$**), 6.0 (s, *N*-H**$_{3.16}$**).

Slightly less than 1 atm ^{13}CO after 3 days:

^{31}P{^{1}H} NMR (d_8-THF, 161.9 MHz, 298 K): δ 7.3 (s, **3.12**), 1.6 (s, **3.14**), -30.6 (s, **3.16**). ^{1}H NMR (d_8-THF, 400.0 MHz, 298 K): δ -12.1 (dq, $^{2}J_{PH}$ = 80.3 Hz, $^{2}J_{CH}$ = 5.3 Hz, *trans-P-Ir*-H**$_{3.16}$**), -11.6 (d, $^{2}J_{PH}$ = 52.2 Hz, *cis-P-Ir*-H**$_{3.14}$**), -11.2 (dt, $^{2}J_{PH}$ = 121.7 Hz, $^{2}J_{CH}$ = 4.5 Hz, *trans-P-Ir*-H**$_{3.12}$**), -10.9 (m, *cis-P-Ir*-H**$_{3.12}$**) -10.8 (m, *cis-P-Ir*-H**$_{3.12}$**), 4.2 (v.td, $^{2}J_{HH}$ = 7.7 Hz, $^{2}J_{PH}$ = 13.5 Hz, α-CH**$_{3.12/3.14}$**), 6.0 (s, *N*-H**$_{3.16}$**). ^{13}C APT NMR (d_8-THF, 100.6 MHz, 298 K): δ 47.7 (d, $^{2}J_{PH}$ = 29.9 Hz, α-CH**$_{3.14}$**), 172.2 (d, $^{2}J_{PC}$ = 3.8 Hz, *cis-P*-CO**$_{3.12}$**), 172.7 (d, $^{2}J_{PC}$ = 4.8 Hz, *cis-P*-CO**$_{3.12}$**), 176.6 (d, $^{2}J_{PC}$ = 8.5 Hz, *cis-P*-CO**$_{3.16}$**), 176.9 (s, *cis-P*-CO**$_{3.14}$**).

Monitoring the reaction of **Ir{(NP)^{DIPP}}(CO)$_2$ (3.10a)** with H_2. A solution of **3.10a** (0.035 g, 0.081 mmol) in d_8-THF (0.5 ml) was formed. This mixture was transferred to a NMR tube attached to a ground glass fitting sealed with a ground glass tap. The mixture was degassed with three freeze-pump-thaw cycles using high vacuum, and then left under vacuum. The headspace of the NMR tube was backfilled with H_2 to a pressure of approximately 150 mmHg (slight vacuum) at -196 °C. The NMR tube is flame sealed at this temperature. After allowing the mixture to react overnight two species (**3.12** and **3.17**) can be identified, the resonances used

to identify them are reported below. $^{31}P\{^{1}H\}$ NMR (d_8-THF, 161.9 MHz, 298 K): δ 7.3 (s, **3.12**), 3.0 (s, **3.17**). ^{1}H NMR (d_8-THF, 400.0 MHz, 298 K): δ -11.2 (d, $^{2}J_{PH}$ = 121.7 Hz, *trans-P-Ir*-$H_{\mathbf{3.12}}$), -10.9 (d, $^{2}J_{PH}$ = 18.0 Hz, *cis-P-Ir*-$H_{\mathbf{3.12}}$), -10.8 (d, $^{2}J_{PH}$ = 16.4 Hz, *cis-P-Ir*-$H_{\mathbf{3.12}}$), -8.4 (d, $^{2}J_{PH}$ =123.0 Hz, *trans-P-Ir*-$H_{\mathbf{3.17}}$), -7.7 (d, $^{2}J_{PH}$ = 12.8 Hz, *cis-P-Ir*-$H_{\mathbf{3.17}}$) Under these conditions very little **3.12** is present in solution. The α-CH proton of **3.12** could not be observed.

Monitoring the reaction of **Ir{(NP)^{DIPP}}(^{13}CO)$_2$ (3.10a*)** with H_2. Identical conditions to what is describe above were used, however **3.10a*** was used in place of **3.10a**. After allowing the reaction to proceed overnight **3.12*** and **3.17*** can be identified, the signals used to identify them are reported below. $^{31}P\{^{1}H\}$ NMR (d_8-THF, 161.9 MHz, 298 K): δ 7.3 (m, **3.12***), 3.0 (m, **3.17***). ^{1}H NMR (d_8-THF, 400.0 MHz, 298 K): δ -11.2 (dt, $^{2}J_{PH}$ = 121.7 Hz, $^{2}J_{CH}$ = 4.5 Hz *trans-P-Ir*-$H_{\mathbf{3.12*}}$), -10.9 (m, *cis-P-Ir*-$H_{\mathbf{3.12*}}$), -10.8 (m, *cis-P-Ir*-$H_{\mathbf{3.12*}}$), -8.4 (v.dt, $^{2}J_{PH}$ =123.0 Hz, $^{2}J_{CH}$ = 4.4 Hz *trans-P-Ir*-$H_{\mathbf{3.17*}}$), -7.7 (ddd, $^{2}J_{CH}$ = 20.0 Hz, $^{2}J_{CH}$ = 7.3 Hz, $^{2}J_{PH}$ = 12.8 Hz, *cis-P-Ir*-$H_{\mathbf{3.17*}}$) Under these conditions very little **3.12*** is present in solution. The α-CH proton of **3.12*** could not be observed.

General procedures for the synthesis of **^{Pri}(NP)^{Pri}H (4.1a)**, **^{Me}(NP)^{Pri}H (4.1b)**, **^{Pri}(NP)^{But}H (4.1c)**, **^{Pri}(NP)^{But}H (4.1d)**.

For synthesis of ^{Pri}(NP)^{Pri}H (**4.1a**) and ^{Me}(NP)^{Pri}H (**4.1b**) the imine precursors *N*-(2,6-diisopropylphenyl)cyclopentylideneimine or *N*-(2,6-dimethylphenyl)cyclopentylideneimine (20.5 mmol) were dissolved in diethyl ether (30 ml). In a separate Schlenk flask, LDA was prepared by dissolving diisopropylamine (3.16 ml, 22.5 mmol) in diethyl ether (10 ml) and cooling the solution to -78 °C. Dropwise addition of 1.6 M n-butyl lithium (12.8 ml, 20.5 mmol, ether or hexanes solutions used interchangeably) to the chilled solution of diisopropyl amine generates LDA. After dropwise addition concludes, the reaction was allowed to warm to room

temperature to stir for 30 minutes. The LDA mixture was cooled to -78 °C and the imine solution was added dropwise by cannula. After the addition concludes, the mixture was warmed to room temperature and stirred for 30 minutes. The reaction was cooled to -78 °C for a final time, and a solution of chlorodiisopropylphosphine (3.27 ml, 20.5 mmol) in diethyl ether (200 ml) was added dropwise. After the addition was complete, the reaction was stirred overnight. The consumption of chlorodiisopropylphosphine from the reaction was monitored by $^{31}P\{^{1}H\}$ NMR spectroscopy to establish full conversion to product. Upon completion, the solvent was removed under vacuum and the oil that results was dissolved in a minimal amount of toluene. This slurry was filtered through Celite, and the Celite cake was rinsed with a few small portions of toluene until the filtrate was no longer colored. Removal of toluene under vacuum gave crude yellow oil that could be purified by high vacuum distillation.

There are some minor modification to the above procedure for synthesis of **^{Pri}(NP)^{But}H (4.1c)** and **^{Me}(NP)^{But}H (4.1d)**. THF was used as the solvent instead of diethyl ether. Instead of stirring the reaction mixture overnight at room temperature the reaction was heated to 65 °C in a flask fitted with a reflux condenser that was attached to a nitrogen manifold vented through a mercury bubbler.

^{Pri}(NP)^{Pri}H (4.1a). Crude yellow oil was obtained which was distilled using a short path distillation apparatus under high vacuum ($1.0x10^{-1}$ torr, oil bath: 200 °C). The final product is a clear, colorless oil (crude yield: 7.186 g, 98 %, after distillation, 4.028 g, 50 %). $^{31}P\{^{1}H\}$ NMR (C_6D_6, 161.9 MHz, 298 K): δ -19.3 (s, 1P, $P_{enamine}$), 15.1 (s, 1P, P_{imine}) ratio imine to enamine is 1.0:3.0. ^{1}H NMR (C_6D_6, 400.0 MHz, 298 K, *only enamine resonances identified*): 1.1 (m, 34H (*overlapping with imine peaks, expect 24H*), *N/P*-Pr^{i}CH$_3$), 1.6 (m, 2H, γ-CH$_2$), 2.0 (d. sept., $^{3}J_{PH}$ = 2.7 Hz, $^{3}J_{HH}$ = 7.0 Hz, 2H, *P*-Pr^{i}CH), 2.1 (t, $^{3}J_{HH}$ = 7.4 Hz, 2H, β-CH$_2$), 2.4 (t, $^{3}J_{HH}$ = 6.8 Hz,

2H, δ-CH_2), 3.5 (sept. $^3J_{HH}$ = 6.9 Hz, 2H, *N*-Pr^{i}CH), 6.3 (d, J_{PH} = 7.2Hz, 1H, *N*-H), 7.1(d, $^3J_{HH}$ = 7.8 Hz, 2H, *N*-*m*-ArCH), 7.1(4) (m 1H, *N*-*p*-ArCH). ^{13}C APT NMR (C_6D_6, 100.6 MHz, 298 K): δ 20.3 (d, $^2J_{PC}$ = 9.0 Hz, *P*-Pr^iCH_3), 20.9 (d, $^2J_{PC}$ = 18.6 Hz, *P*-Pr^iCH_3), 23.0 (br.s, *N*-Pr^iCH_3), 23.1 (d, $^1J_{PC}$ = 6.8 Hz, *P*-Pr^{i}CH), 23.3 (d, $^3J_{PC}$ = 2.0 Hz, γ-CH_2), 24.8 (br.s, *N*-Pr^iCH_3), 28.5 (s, *N*-Pr^{i}CH), 33.2 (d, $^2J_{PC}$ = 5.2 Hz, β-CH_2), 33.3 (d, $^2J_{PC}$ = 5.8 Hz, δ-CH_2), 96.2 (d, $^1J_{PC}$ = 10.3 Hz, α-C), 123.5 (s, *N*-*m*-ArCH), 127.6 (s, *N*-*p*-ArCH), 137.5 (s, *N*-CAr), 148.0 (s, *N*-ArCPr^i), 161.1 (d, $^2J_{PC}$ = 25.3 Hz, *N*-$C_{enamine}$). Anal. Calcd for: $C_{23}H_{38}NP$: C 76.84; H 10.65; N 3.90. Found: C 76.50; H 10.55; N 4.98; (this is the highest purity achieved to date.) HRMS-EI (m/z) calculated for $C_{23}H_{38}NP$: 359.27419, Found: 359.27406.

^{Me}(NP)^{Pri}H (4.1b). Crude yellow oil was obtained which was distilled using a short path distillation apparatus under high vacuum ($1.5x10^{-1}$ torr, oil bath:190 ºC). The final product is a clear, colorless oil (crude yield: 4.409 g, 71 %, after distillation, 3.074 g, 50 %). ^{31}P{^{1}H} NMR (C_6D_6, 161.9 MHz, 298 K): δ 14.7 (s, 1P, P_{imine}), -19.5 (s, 1P, $P_{enamine}$) ratio imine to enamine is 1:2.9. ^{1}H NMR (C_6D_6, 400.0 MHz, 298 K, *only enamine resonances identified*): 1.1 (dd, $^3J_{HH}$ = 7.0 Hz, $^3J_{PH}$ = 11.5 Hz, 6H, *P*-Pr^iCH_3), 1.2 (dd, $^3J_{HH}$ = 7.1 Hz, $^3J_{PH}$ = 15.4 Hz, 6H, *P*-Pr^iCH_3), 1.6 (m, 2H, γ-CH_2), 2.0 (m, overlapping with other signals, identified by ^{1}H-^{13}C HSQC and ^{1}H-^{1}H COSY, 4H, β-CH_2, *P*-Pr^{i}CH), 2.2 (s, 6H, *N*-CH_3), 2.4 (t, $^3J_{HH}$ = 6.4 Hz, 2H, δ-CH_2), 6.1 (d, J_{PH} = 5.1 Hz, 1H, *N*-H), 6.9 (br. s, 2H, *N*-*p*-ArCH), 7.0 (t, $^3J_{HH}$ = 6.6 Hz, 1H, *N*-*m*-ArCH). ^{13}C APT NMR (C_6D_6, 100.6 MHz, 298 K, *only enamine resonances identified*): 18.6 (s, *N*-CH_3), 20.3 (d, $^2J_{PC}$= 9.1 Hz, *P*-Pr^iCH_3), 21.0 (d, $^2J_{PC}$ = 19.0 Hz, *P*-Pr^iCH_3), 23.2 (d, $^4J_{PC}$ = 1.4 Hz, γ-CH_2), 23.3 (d, $^1J_{PC}$ = 7.0 Hz, *P*-Pr^{i}CH), 33.1 (d, $^3J_{PH}$ = 5.3 Hz, δ-CH_2), 33.2 (d, $^3J_{PH}$ = 5.8 Hz, β-CH_2), 96.5 (d, $^1J_{PC}$ = 10.7 Hz, α-C), 126.3 (s, *N*-*p*-ArCH), 128.3 (s, *N*-*m*-ArCH), 137.3 (s, *N*-

ArCCH$_3$), 140.4 (s, *N*-CAr), 160.1 (d, $^2J_{PC}$ = 25.0 Hz, *N*-C$_{enamine}$). Anal. Calcd for: $C_{17}H_{30}NP$: C 75.21; H 9.97; N 4.62. Found: C 75.51, H 9.89; N 5.83 (this is the highest purity achieved to date). HRMS-EI (m/z) calculated for $C_{17}H_{30}NP$: 303.21159, Found: 303.2115.

^{Pri}(NP)^{But}H (4.1c). Crude yellow oil was obtained which was distilled using a short path distillation apparatus under high vacuum (5.3x10^{-2} torr, oil bath: 200 °C.). The final product is clear, colourless oil (crude yield: 6.830 g, 80 %, after distillation, 2.108 g, 27 %). $^{31}P\{^1H\}$ NMR (C_6D_6, 161.9 MHz, 298 K): δ 5.5 (s, 1P, P$_{enamine}$), ^{1}H NMR (C_6D_6, 400.0 MHz, 298 K): δ 1.2(8) (d, $^3J_{HH}$ = 6.8 Hz, 6H, *N*-Pr^{i}CH$_3$), 1.3 (d, $^3J_{HH}$ = 6.9 Hz, 6H, *N*-Pr^{i}CH$_3$), 1.4 (d, $^3J_{PH}$ = 11.8 Hz, 18H, *P*-Bu^{t}CH$_3$), 1.8 (p, $^3J_{HH}$ = 7.2 Hz, 2H, γ-CH$_2$), 2.2 (t, $^3J_{HH}$ = 7.4 Hz, 2H, β-CH$_2$), 2.8 (t, $^3J_{HH}$ = 6.8 Hz, 2H, δ-CH$_2$), 3.6 (sept. $^3J_{HH}$ = 6.8 Hz, 2H, *N*-Pr^{i}CH), 6.8 (d, J_{PH} = 8.4 Hz, 1H, *N*-H), 7.2 (d, $^3J_{HH}$ = 8.0 Hz, 2H, *N*-*m*-ArCH), 7.3 (t, $^3J_{HH}$ = 7.3 Hz, 1H, *N*-*p*-ArCH). ^{13}C APT NMR (C_6D_6, 100.6 MHz, 298 K): δ 22.8 (s, *N*-Pr^{i}CH$_3$), 23.4 (d, $^3J_{PC}$ = 1.8 Hz, γ-CH$_2$), 24.8 (s, *N*-Pr^{i}CH$_3$), 28.6 (s, *N*-Pr^{i}CH), 31.1 (d, $^2J_{PH}$ = 13.9 Hz, *P*-Bu^{t}CH$_3$), 32.6 (d, $^2J_{PC}$ = 5.7 Hz, β-CH$_2$), 33.1 (d, $^1J_{PC}$ = 15.5 Hz, *P*-CBu^t), 35.5 (d, $^3J_{PC}$ = 5.9 Hz, δ-CH$_2$), 96.2 (d, $^1J_{PC}$ = 14.6 Hz, α-C), 123.5 (s, *N*-*m*-ArCH), 127.5 (s, *N*-*p*-ArCH), 137.8 (d, $^4J_{PC}$ = 1.9 Hz, *N*-CAr), 147.9 (s, *N*-ArCPr^i), 161.3, (d, $^2J_{PC}$ = 26.9 Hz, *P*-C$_{enamine}$). Anal. Calcd for: $C_{25}H_{42}NP$: C 77.47; H 10.92; N 3.61. Found: C 77.07, H 10.82, N 3.76. HRMS-EI (m/z) calculated for $C_{25}H_{42}NP$: 387.20649, Found; 387.30580.

^{Me}(NP)^{But}H (4.1d). Crude yellow oil was obtained which was distilled using a short path distillation apparatus under high vacuum (2.6x10^{-1} torr, oil bath: 200 °C). The final product is a clear colourless oil (crude yield: 6.367 g, 94 %, after distillation, 1.735 g, 26 %). $^{31}P\{^1H\}$ NMR (C_6D_6, 161.9 MHz, 298 K): δ 5.4 (s, 1P, P$_{enamine}$) ^{1}H NMR (C_6D_6, 400.0 MHz, 298 K): δ 1.3 (d,

$^3J_{PH}$ = 11.7 Hz, 18H, *P*-Bu^{t}CH$_3$), 1.6 (m, 2H, γ-CH$_2$), 2.0 (t, $^3J_{HH}$ = 7.3 Hz, 2H, β-CH$_2$), 2.2 (s, 6H, *N*-CH$_3$), 2.7 (t, $^3J_{HH}$ = 6.7 Hz, 2H, δ-CH$_2$), 6.4 (d, J_{PH} = 7.4 Hz, 1H, *N*-H), 6.9 (m, 3H, *N*-ArCH). ^{13}C APT NMR (C_6D_6, 100.6 MHz, 298 K): δ 18.7 (s, *N*-CH$_3$), 23.4 (s, γ-CH$_2$), 31.2 (d, $^3J_{PH}$ = 14.0 Hz, *P*-Bu^{t}CH$_3$), 32.5 (d, $^2J_{PC}$ = 5.6 Hz, β-CH$_2$), 33.2 (d, $^1J_{PC}$ = 15.9 Hz, *P*-CBu^t), 35.5 (d, $^3J_{PH}$ = 6.0 Hz, δ-CH$_2$), 96.5 (d, $^1J_{PC}$ = 15.1 Hz α-C), 126.3 (s, *N*-*p*-ArCH), 128.2 (s, *N*-*m*-ArCH), 137.3 (s, *N*-ArCCH$_3$), 140.6 (d, $^4J_{PC}$ = 1.9 Hz, *N*-CAr), 160.4 (d, $^2J_{PC}$ = 27.3 Hz, *N*-C$_{enamine}$). Anal. Calcd for: $C_{12}H_{34}NP$: C 76.09, H 10.34, N 4.23. Found: C 80.17, H 10.67, N 5.53 (this is the highest purity achieved to date). HRMS-EI (m/z) calculated for $C_{19}H_{30}NP$: 303.21159, Found: 303.21153.

General procedure for the synthesis of **RuH{^{Pri}(NP)^{Pri}}(PPr$^i_3$)(CO) (4.2a)**, **RuH{^{Me}(NP)^{Pri}}(PPr$^i_3$)(CO) (4.2b)**, **RuH{^{Pri}(NP)^{But}}(PPr$^i_3$)(CO) (4.2c)**, and **RuH{^{Me}(NP)^{But}}(PPr$^i_3$)(CO) (4.2d)**. The appropriate imine-phosphine ligand (0.411 mmol) was combined with RuHCl(PPr$^i_3$)$_2$(CO) (0.200 g, 0.411 mmol) and potassium *tert*-butoxide (0.046 g, 0.411 mmol) in a vial in the glove box fitted with a stir bar. THF (5 mL) was added, which immediately produced a dark red color indicative of formation of the desired product. The reaction mixture was stirred for approximately 4 hours and monitored by ^{31}P{^{1}H} NMR spectroscopy until complete. After the reaction is complete, the mixture was taken to dryness and the residue was dissolved in a minimal amount of pentane (~ 5 mL). The pentane solution was filtered through celite into a small round bottom flask and the pentane and free PPr$^i_3$ were removed under vacuum. The crude product was dissolved in a minimal amount of pentane, upon cooling to -35 °C overnight analytically pure crystalline samples of each complex were obtained.

RuH{^{Pri}(NP)^{Pri}}(PPr$^{i}_{3}$)(CO) (4.2a) (yield after recrystallization: 0.097 g, 36 %). ^{31}P{^{1}H} NMR (C_6D_6, 161.9 MHz, 298 K): δ 39.5 (d, $^{2}J_{PP}$ = 245.2 Hz, 1P, *Ru*-PPr$^{i}_{3}$), 59.8 (d, $^{2}J_{PP}$ = 245.2 Hz, 1P, *Ru*-P$_{ligand}$). ^{1}H NMR (C_6D_6, 400 MHz, 298 K): δ -23.3 (dd, $^{2}J_{PH}$ = 18.6 Hz, $^{2}J_{PH}$ = 22.1 Hz, 1H, *Ru*-H), 0.83 (dd, $^{3}J_{HH}$ = 7.2 Hz, $^{3}J_{PH}$ = 11.9 Hz, 9H, *P*-Pr^{i}CH$_3$), 1.1-1.3(4) (m, 34H (*30H expected, trace PPr$^{i}_{3}$ may explain slight over integration*), *N/P*-Pr^{i}CH$_3$), 1.5 (dd, $^{3}J_{HH}$ = 7.0 Hz, $^{3}J_{PC}$ = 16.9 Hz, 3H, *P*-Pr^{i}CH$_3$), 1.7 (m, 1H, β-CH$_2$), 2.0 (m, 1H, β-CH$_2$), 2.1 (m, 4H, 3x *P*-Pr^{i}CH / γ-CH$_2$), 2.2 (m, 2H, *P*-Pr^{i}CH, γ-CH$_2$), 2.3 (m, 1H, δ-CH$_2$), 2.5 (m, 1H, δ-CH$_2$), 2.7 (d. sept, $^{2}J_{PH}$ = 4.4 Hz, $^{3}J_{HH}$ = 6.6 Hz, 1H, *P*-Pr^{i}CH), 3.4 (sept, $^{3}J_{HH}$ = 6.9 Hz, 1H, *N*-Pr^{i}CH), 3.5 (sept, $^{3}J_{HH}$ = 6.7 Hz, 1H, *N*-Pr^{i}CH), 7.1 (m, 3H, *N*-ArCH). ^{13}C APT NMR (C_6D_6, 100.6 MHz, 298 K): δ 18.1 (d, $^{3}J_{PC}$ = 3.5 Hz *P*-Pr^{i}CH$_3$), 18.5(5) (d, $^{3}J_{PC}$ = 2.4 Hz, *P*-Pr^{i}CH$_3$), 18.6 (d, $^{2}J_{PC}$ = 2.4 Hz, *P*-Pr^{i}CH$_3$), 18.7 (s, *P*-Pr^{i}CH$_3$), 19.6 (d, $^{3}J_{PC}$ = 4.0 Hz, *P*-Pr^{i}CH$_3$), 20.1 (s, *P*-Pr^{i}CH$_3$), 23.0, (s, *N*-Pr^{i}CH$_3$), 23.3 (s, *N*-Pr^{i}CH$_3$), 23.5 (d, $^{3}J_{PC}$ = 28.9 Hz, *P*-Pr^{i}CH), 24.0 (s, *N*-Pr^{i}CH$_3$), 25.1 (d, $^{1}J_{PC}$ = 27.1 Hz, *P*-Pr^{i}CH), 25.2 (s, *N*-Pr^{i}CH$_3$), 26.0 (dd, $^{3}J_{PC}$ = 1.9 Hz, $^{1}J_{PC}$ = 14.8 Hz, *P*-Pr^{i}CH), 28.2 (s, *N*-Pr^{i}CH), 28.7 (s, *N*-Pr^{i}CH), 28.8 (d, $^{3}J_{PC}$ = 6.2 Hz, γ-CH$_2$), 29.5 (m, δ-CH$_2$), 33.1 (d, $^{3}J_{PC}$ = 16.6 Hz, β-CH$_2$), 84.4 (d, $^{1}J_{PC}$ = 41.6 Hz, α-C), 122.6 (s, *N*-*p*-ArCH), 123.4 (s, *N*-*m*-ArCH), 124.3 (s, *N*-*m*-ArCH), 142.8 (s, *N*-ArCPr^{i}), 143.3 (s, *N*-ArCPr^{i}), 156.4 (s, *N*-CAr), 187.5 (dd, $^{3}J_{PC}$ = 4.3Hz, $^{2}J_{PC}$ = 33.3 Hz *N*-C$_{enamide}$), 207.3 (v.t, $^{2}J_{PC}$ = 14.9 Hz, *Ru*-CO). ATR-FTIR νCO (cm^{-1}): 1899. Anal. Calcd for $C_{33}H_{59}NOP_2Ru$: C, 61.09; H, 9.17; N, 2.16. Found: C, 61.19, H, 9.45, N, 2.11.

RuH{^{Me}(NP)^{Pri}}(PPr$^{i}_{3}$)(CO) (4.2b). (yield after recrystallization: 0.063 g, 26 %). ^{31}P{^{1}H} NMR (C_6D_6, 161.9 MHz, 298 K): δ 47.4 (d, $^{2}J_{PP}$ = 243.9 Hz, 1P, *Ru*-PPr$^{i}_{3}$), 59.1 (d, $^{2}J_{PP}$ = 243.9 Hz, 1P, *Ru*-P$_{ligand}$). ^{1}H NMR (C_6D_6, 400 MHz, 298 K): δ -24.1 (dd, $^{2}J_{PH}$ = 18.0 Hz, $^{2}J_{PH}$

= 20.5 Hz, 1H, *Ru*-H), 0.97 (dd, $^{3}J_{HH}$ = 7.2 Hz, $^{3}J_{PH}$ = 12.4 Hz, 9H, *P*-Pr^{i}CH$_3$), 1.1 (dd, $^{2}J_{HH}$ = 7.1 Hz, $^{2}J_{PH}$ = 12.7 Hz, 9H, *P*-Pr^{i}CH$_3$), 1.1(6) (dd, $^{3}J_{HH}$ = 6.0 Hz, $^{3}J_{PC}$ = 10.8 Hz, 3H, *P*-Pr^{i}CH$_3$), 1.2(2) (dd, $^{2}J_{HH}$ = 6.9 Hz, $^{3}J_{PH}$ = 15.9 Hz, 3H, *P*-Pr^{i}CH$_3$), 1.3 (dd, $^{3}J_{HH}$ = 6.9 Hz, $^{3}J_{PH}$ = 15.7 Hz, 3H, *P*-Pr^{i}CH$_3$), 1.4 (dd, $^{3}J_{HH}$ = 7.0 Hz, $^{3}J_{PH}$ = 16.6 Hz, 3H, *P*-Pr^{i}CH$_3$), 1.7 (dq, $^{3}J_{HH}$ = 6.8 Hz, $^{3}J_{PH}$ = 13.4 Hz, 3H, *P*-Pr^{i}CH), 1.9 (m, 2H, β-CH$_2$), 2.1 (m, 3H, γ-CH$_2$ / *P*-Pr^{i}CH), 2.2 (s, 3H, *N*-CH$_3$), 2.3 (s, 3H, *N*-CH$_3$), 2.3(5) (m, 1H, δ-CH$_2$), 2.4 (m, 1H, δ-CH$_2$), 2.7 (m, 1H, *P*-Pr^{i}CH$_3$), 6.7 (v.dd, $^{3}J_{HH}$ = 7.2 Hz, $^{3}J_{HH}$ = 7.6 Hz, 1H, *N*-*p*-ArCH), 7.0 (v.d, *J* = 7.4 Hz, 2H, N-*m*-ArCH). ^{13}C APT NMR (C$_6$D$_6$, 100.6 MHz, 298 K): δ 18.3 (d, $^{3}J_{PC}$ = 3.2 Hz *P*-Pr^{i}CH$_3$), 18.8 (d, $^{3}J_{PC}$ = 5.3 Hz, 2x *P*-Pr^{i}CH$_3$), 19.4 (d, $^{2}J_{PC}$ = 4.0 Hz, *P*-Pr^{i}CH$_3$), 19.9 (s, *P*-Pr^{i}CH$_3$), 20.0 (s, *N*-CH$_3$), 20.1 (s, *N*-CH$_3$), 20.6 (s, *P*-Pr^{i}CH$_3$), 23.2 (d, $^{1}J_{PC}$ = 31.9 Hz, *P*-Pr^{i}CH), 25.5 (s, *P*-Pr^{i}CH), 25.6 (dd, $^{3}J_{PC}$ = 2.1, $^{1}J_{PC}$ = 15.2 Hz, *P*-Pr^{i}CH), 28.7 (d, $^{3}J_{PC}$ = 6.4 Hz, δ-CH$_2$), 29.7 (br.s, γ-CH$_2$), 31.4 (d, $^{2}J_{PC}$ = 16.7 Hz, β-CH$_2$), 84.7 (d, $^{1}J_{PC}$ = 41.2 Hz, α-C), 123.2 (s, *N*-*p*-ArCH), 127.5 (s, *N*-*m*-ArCH), 127.7 (s, *N*-*m*-ArCH), 134.1 (s, *N*-ArCMe), 135.0 (s, *N*-ArCMe), 157.9 (s, *N*-CAr), 185.7 (dd, $^{3}J_{PC}$ = 4.1 Hz, $^{2}J_{PC}$ = 33.3 Hz, *N*-C$_{enamide}$), 207.0 (dd, $^{3}J_{PC}$ = 15.4 Hz, $^{2}J_{PC}$ = 25.1 Hz, *Ru*-CO). ATR-FTIR νCO (cm^{-1}): 1894. Anal. Calcd for $C_{29}H_{51}NOP_2Ru$: C, 58.76; H, 8.67; N, 2.36. Found: C, 58.73, H, 8.64, N, 2.37.

RuH{^{Pri}(NP)^{But}}(PPr$^{i}_3$)(CO) (4.2c) (yield after recrystallization: 0.153 g, 55 %). ^{31}P{^{1}H} NMR (C$_6$D$_6$, 161.9 MHz, 298 K): δ 39.5 (d, $^{2}J_{PP}$ = 245.7 Hz, 1P, *Ru*-PPr$^{i}_3$), 73.2 (d, $^{2}J_{PP}$ = 245.7 Hz, 1P, *Ru*-P$_{ligand}$). ^{1}H NMR (C$_6$D$_6$, 400 MHz, 298 K): δ -24.0 (dd, $^{2}J_{PH}$ = 18.8 Hz, $^{2}J_{PH}$ = 20.2 Hz, 1H, *Ru*-H), 0.9 (dd, $^{3}J_{HH}$ = 7.2 Hz, $^{3}J_{PC}$ = 12.1 Hz, 9H, *P*-Pr^{i}CH$_3$), 1.1 (m, 12H, N/*P*-Pr^{i}CH$_3$), 1.2 (d, $^{3}J_{HH}$ = 6.7 Hz, 3H, *N*-Pr^{i}CH$_3$), 1.2(8) (d, $^{3}J_{HH}$ = 6.7 Hz, 3H, *N*-Pr^{i}CH$_3$), 1.2(9) (d, $^{3}J_{HH}$ = 6.9 Hz, 3H, *N*-Pr^{i}CH$_3$), 1.5 (d, $^{3}J_{PH}$ = 13.1 Hz, 9H, *P*-Bu^{t}CH$_3$), 1.6 (d, $^{3}J_{PH}$ = 12.9 Hz, 9H,

P-Bu^{t}CH$_3$), 1.7 (m, 1H, β-CH$_2$), 1.8(9) (m, 1H, β-CH$_2$), 2.0 (m, 2H, γ-CH$_2$), 2.1 (m, 3H, *P*-Pr^{i}CH), 2.5 (m, 1H, δ-CH$_2$), 2.7 (m, 1H, δ-CH$_2$), 3.4 (sept. $^3J_{HH}$ = 6.9 Hz, 1H, *N*-Pr^{i}CH), 3.6 (sept. $^3J_{HH}$ = 6.7 Hz, 1H, *N*-Pr^{i}CH), 7.1 (br. s, 3H, *N*-ArCH). ^{13}C APT NMR (C_6D_6, 100.6 MHz, 298 K): δ 18.9 (s, *P*-Pr^{i}CH$_3$), 20.0 (s, *P*-Pr^{i}CH$_3$), 23.4 (s, *N*-Pr^{i}CH$_3$), 23.9 (s, *N*-Pr^{i}CH$_3$), 24.1 (s, *N*-Pr^{i}CH$_3$), 25.0 (s, *N*-Pr^{i}CH$_3$), 25.7 (d, $^3J_{PC}$ = 1.8 Hz, $^1J_{PC}$ = 15.2 Hz, *P*-Pr^{i}CH), 28.3 (s, *N*-Pr^{i}CH), 28.4(7) (s, *N*-Pr^{i}CH), 28.5 (m, γ-CH$_2$), 30.3(5) (d, $^2J_{PC}$ = 3.8 Hz, *P*-Bu^{t}CH$_3$), 30.4 (d, $^2J_{PC}$ = 4.4 Hz, *P*-Bu^{t}CH$_3$), 32.3 (m, δ-CH$_2$), 33.5 (d, $^2J_{PC}$ = 16.4 Hz, β-CH$_2$), 36.0 (d, $^1J_{PC}$ = 23.7 Hz, *P*-Bu^{t}C), 40.9 (d, $^1J_{PC}$ = 20.6 Hz, *P*-Bu^{t}C), 86.7 (d, $^1J_{PC}$ = 38.4 Hz, α-C), 122.9 (s, *N*-*m*-ArCH), 123.3 (s, *N*-*m*-ArCH), 124.3 (s, *N*-*p*-ArCH), 143.1 (s, *N*-ArCPr^i), 143.6 (*N*-ArCPr^i), 156.6 (*N*-CAr), 186.7 (dd, $^2J_{PC}$ = 4.5 Hz, $^2J_{PC}$ = 33.0 Hz, *N*-C$_{enamide}$), *Ru*-CO not observed. ATR-FTIR νCO (cm^{-1}): 1893. Anal. Calcd for $C_{35}H_{63}NOP_2Ru$: C, 62.10; H, 9.38; N, 2.07. Found: C, 61.93, H, 9.61, N, 2.04.

RuH{^{Me}(NP)^{But}}(PPr$^i_3$)(CO) (4.2d). (yield after recrystallization: 0.215g, 55 %). ^{31}P{^{1}H} NMR (C_6D_6, 161.9 MHz, 298 K): δ 46.5 (d, $^2J_{PP}$ = 242.6 Hz, 1P, *Ru*-PPr$^i_3$), 72.4 (d, $^2J_{PP}$ = 242.6 Hz, 1P, *Ru*-P$_{ligand}$). ^{1}H NMR (C_6D_6, 400 MHz, 298 K): δ -24.8 (dd, $^2J_{PP}$ = 18.0 Hz, $^2J_{PP}$ = 18.8 Hz, 1H, *Ru*-H), 1.0 (dd, $^3J_{HH}$ = 7.2 Hz, $^3J_{PH}$ = 12.7 Hz, 9H, *P*-Pr^{i}CH$_3$), 1.1 (dd, $^3J_{HH}$ = 7.2 Hz, $^3J_{PH}$ = 12.5 Hz, 9H, *P*-Pr^{i}CH$_3$), 1.5 (d, $^3J_{PH}$ = 13.2 Hz, 9H, *P*-Bu^{t}CH$_3$), 1.5(1) (d, $^3J_{PH}$ = 12.8 Hz, 9H, *P*-Bu^{t}CH$_3$), 1.7 (m, 3H, *P*-Pr^{i}CH), 1.8 (v.t, *J* = 2.2 Hz, 2H, β-CH$_2$), 2.1 (m, 2H, γ-CH$_2$), 2.2 (s, 3H, *N*-CH$_3$), 2.4 (s, 3H, *N*-CH$_3$), 2.5 (m, 1H, δ-CH$_2$), 2.6 (m, 1H, δ-CH$_2$), 6.9 (t, $^3J_{HH}$ = 6.9 Hz, 1H, *N*-*p*-ArCH), 7.0 (v.d, $^3J_{HH}$ = 7.4 Hz, 2H, *N*-*m*-ArCH). ^{13}C APT NMR (C_6D_6, 100.6 MHz, 298 K): δ 20.0 (s, *P*-Pr^{i}CH$_3$), 20.2 (s, *P*-Pr^{i}CH$_3$), 20.3 (s, 2x *N*-CH$_3$), 25.0 (dd, $^4J_{PC}$ = 1.8 Hz, $^1J_{PC}$ = 15.5 Hz, *P*-Pr^{i}CH), 28.8 (d, $^3J_{PC}$= 6.0 Hz, γ-CH$_2$), 30.1 (v.t, $^2J_{PC}$ = 3.8 Hz, 2x *P*-

Bu^tCH_3), 31.8 (d, $^2J_{PC}$ = 16.4 Hz, β-CH_2), 32.4 (v.t, J_{PC} = 1.9 Hz, δ-CH_2), 35.2 (dd, $^3J_{PC}$= 1.3 Hz, $^1J_{PC}$ = 22.9 Hz, *P*-CBu^t), 42.2 (d, $^1J_{PC}$ = 21.0 Hz, *P*-CBu^t), 86.5 (d, $^1J_{PC}$ = 39.4 Hz, α-C), 123.1 (s, *N*-*p*-ArCH), 127.7 (s, 2x *N*-*m*-ArCH), 134.2 (s, *N*-ArCMe), 135.4 (s, *N*-ArCMe), 158.0 (s, *N*-CAr),184.5 (dd, $^3J_{PC}$ = 4.0 Hz, $^2J_{PC}$ = 32.4 Hz, *N*-$C_{enamide}$), 207.2 (dd, $^2J_{PC}$ = 13.7 Hz, $^2J_{PC}$ = 15.2 Hz, *Ru*-CO). ATR-FTIR νCO (cm^{-1}): 1895. Anal. Calcd for $C_{31}H_{55}NOP_2Ru$: C, 59.98; H, 8.93; N, 2.26. Found: C, 59.99, H, 9.06, N, 2.51.

Synthesis of **$RuH_2\{^{Pri}(NP)^{Pri}H\}(PPr^i_3)(CO)$ (4.3a)**. **4.2a** (0.100 g, 0.204 mmol) was taken into hexanes (5 ml) in a thick walled glass vessel fitted with a Kontes valve. The mixture was freeze-pump-thaw degassed three times using high vacuum. The headspace of the reaction vessel, frozen in liquid nitrogen, was back filled with dihydrogen. The Kontes valve was sealed and the reaction was allowed to warm to room temperature behind a blast shield. Upon warming to room temperature, the reaction gradually lightened in color. After 24 hours, a pale red-yellow solution is observed. At this time, the reaction was refrozen in liquid nitrogen and the hydrogen pressure was released by carefully opening the Kontes valve to a Schlenk line connected to a mercury bubbler. Hexanes were removed under vacuum and a minimal amount of pentane was added to dissolve all of the solids. This mixture was stored at -35 °C overnight. Small clusters of colorless crystals resulted (yield, 0.046 g, 46 %). $^{31}P\{^1H\}$ NMR (C_6D_6, 161.9 MHz, 298 K): δ 74.5 (d, $^2J_{PP}$ = 252.3 Hz, 1P, *Ru*-PPr^i_3), 92.9 (d, $^2J_{PP}$ = 252.3 Hz, 1P, *Ru*-P_{ligand}). ^1H NMR (C_6D_6, 400 MHz, 298 K): δ -18.4 (ddd, $^2J_{HH}$ = 6.7 Hz, $^2J_{PH}$ = 18.4 Hz, $^2J_{PH}$ = 28.8 Hz, 1H, *trans*-*N*-*Ru*-H), -5.5 (ddd, $^2J_{HH}$ = 6.7 Hz, $^2J_{PH}$ = 22.1Hz, $^2J_{PH}$ = 32.2 Hz, 1H, *trans*-*CO*-*Ru*-H), 1.2 (m, 33H, *N*/*P*-Pr^iCH_3), 1.3 (d, $^3J_{HH}$ = 7.2 Hz, 3H, *N*-Pr^iCH_3), 1.4 (d, $^3J_{HH}$ = 7.2 Hz, 4H, *N*-Pr^iCH_3/ γ-CH_2), 1.4(6) (m, 1H, δ-CH_2), 1.6 (m, 4H, 2x β-CH_2/ δ-CH_2/ γ-CH_2), 1.7 (d, $^3J_{HH}$ = 6.6 Hz, 3H, *N*-

Pr^iCH_3), 1.9 (m, 2H, *P*-Pr^iCH_3), 2.0 (m, 3H, *P*-Pr^iCH_3), 3.0 (sept. $^3J_{HH}$ = 6.72 Hz, 1H, *N*-Pr^iCH), 3.2 (v.dd, *J* = 10.3 Hz, *J* = 20.1 Hz, 1H, α-CH), 3.7 (sept. $^2J_{HH}$ = 6.76 Hz, 1H, *N*-Pr^iCH), 7.0 (dd, $^4J_{HH}$ = 1.0 Hz, $^3J_{HH}$ = 7.5 Hz, 1H, *N*-*m*-ArCH), 7.1 (v.t, $^3J_{HH}$ = 7.6 Hz, 1H, *N*-*p*-ArCH), 7.1 (dd, $^4J_{HH}$ = 1.0 Hz, $^3J_{HH}$ = 7.7 Hz, 1H, *N*-*m*-ArCH). ^{13}C APT NMR (C_6D_6, 100.6 MHz, 298 K): δ 18.3 (d, $^2J_{PC}$ = 7.4 Hz, *P*-Pr^iCH_3), 19.1 (d, $^2J_{PC}$ = 5.7 Hz, *P*-Pr^iCH_3), 19.2 (s, *P*-Pr^iCH_3), 21.0 (m, *P*-Pr^iCH_3), 21.1 (d, $^2J_{PC}$ = 3.7 Hz, *P*-Pr^iCH_3), 21.5 (d, $^2J_{PC}$ = 3.5 Hz, *P*-Pr^iCH_3), 23.8 (dd, $^3J_{PC}$ = 2.4 Hz, $^1J_{PC}$ = 11.5 Hz, *P*-Pr^iCH), 24.2 (s, *N*-Pr^iCH_3), 24.7 (s, *N*-Pr^iCH_3), 25.2 (s, *N*-Pr^iCH_3), 25.5 (dd, $^4J_{PC}$ = 1.4 Hz, $^3J_{PC}$ = 4.5 Hz, δ-CH_2), 25.7 (s, *N*-Pr^iCH_3), 26.5 (dd, $^3J_{PC}$ = 2.7 Hz, $^1J_{PC}$ = 16.7 Hz, *P*-Pr^iCH), 26.9 (s, *N*-Pr^iCH), 27.4 (s, *N*-Pr^iCH), 27.6 (d, $^3J_{PC}$ = 4.2 Hz, γ-CH_2), 31.2 (dd, $^3J_{PC}$ = 2.3 Hz, $^1J_{PC}$ = 30.6 Hz, *P*-Pr^iCH), 33.0 (d, $^2J_{PC}$ = 5.5 Hz, β-CH_2), 55.7 (d, $^1J_{PC}$ = 11.0 Hz, α-CH), 123.6 (s, *N*-*m*-ArCH), 125.1 (s, *N*-*p*-ArCH), 125.5 (s, *N*-*m*-ArCH), 137.8 (s, *N*-$ArCPr^i$), 139.2 (s, *N*-$ArCPr^i$), 150.7 (s, *N*-CAr), 193.5 (dd, $^3J_{PC}$ = 2.6 Hz, $^2J_{PC}$ = 9.8 Hz, *N*-C_{imine}), 208.9 (v.t, $^3J_{PC}$ = 9.7 Hz, *Ru*-CO). ATR-FTIR νCO (cm^{-1}): 1881. Anal. Calcd for $C_{33}H_{61}NOP_2Ru$: C, 60.90; H, 9.45; N, 2.15. Found: C, 61.26; H, 9.52; N, 2.25.

General procedure for monitoring formation of **$RuH_2\{^{Pri}(NP)^{Pri}H\}(PPr^i_3)(CO)$ (4.3a)**, **$RuH_2\{^{Me}(NP)^{Pri}H\}(PPr^i_3)(CO)$ (4.3b)**, **$RuH_2\{^{Me}(NP)^{Pri}H\}(PPr^i_3)(CO)$ (4.3c)**, and **$RuH_2\{^{Me}(NP)^{Pri}H\}(PPr^i_3)(CO)$ (4.3d)** under H_2.

4.2a, 4.2b, **4.2c**, or **4.2d** (0.031 mmol) was dissolved in d_8-toluene (0.50 ml) in a flame sealable NMR tube attached to a Kontes valve by a ground glass joint. The d_8-toluene contained 1,3,5-trimethoxybenzene as an internal standard. The mixture was freeze-pump-thaw degassed three times using high vacuum. After this process, the tube is left submerged in liquid N_2. The headspace of the NMR tube was backfilled such that a meter stick attached to a column of

mercury read 38.0 mmHg. The Kontes valve was sealed. The NMR tube was flame sealed such that 210 mm of headspace existed above the frozen toluene solution. The NMR tube was removed from liquid N_2 and allowed to warm to room temperature in a safe location. When the toluene solution melted, the time was recorded as the start of the reaction. After 30 min, a quantitative ^{1}H NMR spectrum was recorded. The tube was allowed to sit for two days; then characterization by multinuclear NMR spectroscopy was performed.

$RuH_2\{^{Pri}(NP)^{Pri}H\}(PPr^i_3)(CO)$ (4.3a). The reaction is complete after 12 hours using the above conditions. Multinuclear NMR data is reported above in the synthesis of **4.3a**. .

$RuH_2\{^{Me}(NP)^{Pri}H\}(PPr^i_3)(CO)$ (4.3b). After 2 days, two products are observed in a 2.4: 1.0 ratio by $^{31}P\{^1H\}$ NMR. The compound with $^2J_{PP}$ = 251.9 Hz is present in higher concentration than the compound with $^2J_{PP}$ = 248.7 Hz. $^{31}P\{^1H\}$ NMR (d_8-toluene, 161.9 MHz, 298 K): δ 72.4 (d, $^2J_{PP}$ = 248.7 Hz), 73.3 (d, $^2J_{PP}$ = 251.9 Hz), 89.7 (d, $^2J_{PP}$ = 248.7 Hz), 95.4 (d, $^2J_{PP}$ = 251.9 Hz). ^{1}H NMR (d_8-toluene, 400 MHz, 298 K): Only resonances assigned to the major isomer are listed, all the resonances except for the hydrides were identified with the aid of a ^{1}H-^{13}C HSQC NMR spectrum. There are many overlapping signals present. δ -17.5 (ddd, $^2J_{HH}$ = 6.6 Hz, $^2J_{PH}$ = 18.3 Hz, $^2J_{PH}$ = 28.2 Hz, 1H, *trans-N-Ru*-H), -5.6 (ddd, $^2J_{HH}$ = 6.8 Hz, $^2J_{PH}$ = 21.5 Hz, $^2J_{PH}$ = 31.9 Hz, 1H, *trans-CO-Ru*-H), 1.3-1.5 (m, 21H, *P*-Pr^{i}CH$_3$), 1.5-1.6 (m, 11H, *P*-Pr^{i}CH$_3$, 2x β-CH$_2$), 1.6(3) (m, 2H, γ-CH$_2$/ δ-CH$_2$), 1.8 (m, 2H, γ-CH$_2$/ δ-CH$_2$), 2.0 (s, 3H, *N*-CH$_3$), 2.0(1)-2.2 (m, 5H, *P*-Pr^{i}CH), 2.6 (s, 3H, *N*-CH$_3$), 3.4 (dd, *J* = 9.0 Hz, *J* = 20.3 Hz, 1H, α-CH), 6.9-7.0 (m, 2H, *N*-ArCH), 7.1 (m, 1H, *N*-ArCH). ^{13}C APT NMR (d_8-toluene, 100.6 MHz, 298 K): δ 18.1 (d, $^2J_{PC}$ = 7.5 Hz, *P*-Pr^{i}CH$_3$),18.3 (s, *N*-CH$_3$), 18.9 (s, *N*-CH$_3$), 19.4 (d, $^2J_{PC}$ = 4.3 Hz, *P*-Pr^{i}CH$_3$), 20.7 (m, *P*-Pr^{i}CH$_3$, signal obscured by d_8-toluene CD$_3$ signal, identified by ^{1}H-

^{13}C HSQC), 20.9 (d, $^{2}J_{PC}$ = 2.8 Hz, *P*-Pr^{i}CH$_3$), 21.1 (s, *P*-Pr^{i}CH$_3$), 21. 4 (s, *P*-Pr^{i}CH$_3$), 23.7 (dd, $^{3}J_{PC}$ = 2.4 Hz, $^{1}J_{PC}$ = 12.0 Hz, *P*-Pr^{i}CH), 25.3 (v.t, $^{2}J_{PC}$ = 6.8 Hz, β-CH$_2$), 26.2 (d, $^{1}J_{PC}$ = 16.9 Hz, *P*-Pr^{i}CH), 27.5 (d, $^{3}J_{PC}$ = 4.1 Hz, γ-CH$_2$), 31.1 (dd, $^{3}J_{PC}$ = 2.1 Hz, $^{1}J_{PC}$ = 24.3 Hz, *P*-Pr^{i}CH), 35.3 (s, *P*-Pr^{i}CH), 55.2 (d, $^{1}J_{PC}$ = 11.9 Hz, α-CH$_2$), 124.5 (s, *N*-ArCH), 127.9 (s, *N*-ArCH), 129.1 (s, *N*-ArCH), 152.1 (s, *N*-ArCCH$_3$), 191.3 (m, *N*-C$_{imine}$), 209.63 (m, *Ru*-CO), resonances for *N*-CAr, and *N*-ArCMe not observed, potentially due to poor (S/N).

RuH$_2$\{^{Pri}(NP)^{But}H\}(PPr$^{i}_3$)(CO) (4.3c). After 2 days, only signals assigned to the expected product could be detected by ^{1}H NMR spectroscopy. Allowing the reaction to proceed for 8 days gave approximately 40 % conversion to **4.3c**. ^{31}P\{^{1}H\} NMR (*d*$_8$-toluene, 161.9 MHz, 298 K): δ 76.0 (d, $^{2}J_{PP}$ = 251.5 Hz, 1P, *Ru*-PPr$^{i}_3$), 116.0 (d, $^{2}J_{PP}$ = 251.5 Hz, 1P, *Ru*-P$_{ligand}$). ^{1}H NMR (*d*$_8$-toluene, 400 MHz, 298 K): δ -18.2 (ddd, $^{2}J_{HH}$ = 6.7 Hz, $^{2}J_{PH}$ = 18.7 Hz, $^{2}J_{PH}$ = 26.7 Hz, 1H, *trans*-*N*-*Ru*-H), -5.7 (v.dt, $^{1}J_{HH}$ = 6.7 Hz, $^{2}J_{PH}$ = 25.4 Hz, 1H, *trans*-*CO*-*Ru*-H).

RuH$_2$\{^{Me}(NP)^{But}H\}(PPr$^{i}_3$)(CO) (4.3d). After 2 days approximately 10% conversion is observed. Only one product is detected by ^{31}P\{^{1}H\} NMR. The ^{1}H NMR spectrum shows a major and minor set of resonances corresponding to new products. The ratio between the major to the minor isomers is ~ 1:4. ^{31}P\{^{1}H\} NMR (*d*$_8$-toluene, 161.9 MHz, 298 K): δ 74.0 (d, $^{2}J_{PP}$ = 250.8 Hz, 1P, *Ru*-PPr$^{i}_3$), 117.9 (d, $^{2}J_{PP}$ = 250.7 Hz, 1P, *Ru*-P$_{ligand}$). ^{1}H NMR (*d*$_8$-toluene, 400 MHz, 298 K): δ -17.5 (ddd, $^{2}J_{HH}$ = 7.7 Hz, $^{2}J_{PH}$ = 19.3 Hz, $^{2}J_{PH}$ = 27.6 Hz, 1H, *Ru*-H$_{minor}$), -17.3 (ddd, $^{2}J_{HH}$ = 7.0 Hz, $^{2}J_{PH}$ = 19.0 Hz, $^{2}J_{PH}$ = 27.0 Hz, 1H, *Ru*-H$_{major}$), -14.7 (dd, $^{2}J_{PH}$ = 15.7 Hz, $^{2}J_{PH}$ = 20.1 Hz, 1H, *Ru*-H), -7.4 (br.s, 4H, *Ru*-(H$_2$)(H)$_2$), -5.9 (m, 1H, *Ru*-H$_{minor}$), -5.8 (dd, $^{2}J_{HH}$ = 6.9 Hz, $^{2}J_{PH}$ = 25.7 Hz, 1H, *Ru*-H$_{major}$).

Formation of **$RuH_2(H_2)\{^{Pri}(NP)^{Pri}H\}(PPr^i_3)(CO)$ (4.4)** under H_2. **4.2a** (0.020 g, 0.031 mmol) was dissolved in C_6D_6 (0.5 ml). This solution was transferred to a flame sealable NMR tube attached to a Kontes valve with a ground glass joint. The mixture was freeze-pump-thaw degassed three times using high vacuum and left submerged in liquid nitrogen. The headspace of the NMR tube was backfilled such that a meter stick attached to a column of mercury read 38.0 mmHg. The Kontes valve was sealed. The NMR tube was flame sealed. The tube was removed from liquid nitrogen and allowed to warm to room temperature in a safe location. Within 20 min, the mixture mostly corresponds to **4.4**, such that meaningful multinuclear NMR spectra could be recorded. No attempts were made to isolate this intermediate as a pure solid. $^{31}P\{^1H\}$ NMR (C_6D_6, 161.9 MHz, 298 K): δ 80.1 (d, $^2J_{PP}$ = 195.8 Hz,) and 41.2 (d, $^2J_{PP}$ = 195.8 Hz). ^1H NMR (C_6D_6, 400 MHz, 298 K): δ -7.2 (br. s, 4H, *Ru*-$(H_2)H_2$), 1.0 (dd, $^3J_{HH}$ = 7.3 Hz, $^3J_{PH}$ = 13.8 Hz, 3H, *P*-Pr^iCH_3), 1.1 (dd, $^3J_{HH}$ = 7.1 Hz, $^3J_{PH}$ = 13.4 Hz, 18H, *P*-Pr^iCH_3), 1.2 (m, 12H, *N*/ *P*-Pr^iCH_3), 1.3 (d, $^3J_{HH}$ = 6.8 Hz, 3H, *N*-Pr^iCH_3), 1.3(5) (d, $^3J_{HH}$ = 6.8 Hz, 3H, *N*-Pr^iCH_3), 1.4 (d, $^3J_{HH}$ = 6.8 Hz, 3H, *N*-Pr^iCH_3), 1.5 (m, 2H, γ-CH_2), 1.9 (td, $^3J_{HH}$ = 6.8 Hz, $^2J_{PH}$ = 13.8 Hz, 3H, *P*-Pr^iCH), 2.0 (m, 1H, *P*-Pr^iCH), 2.1 (t, $^3J_{HH}$ = 7.3 Hz, 2H, β-CH_2), 2.2 (td, $^3J_{HH}$ = 6.7 Hz, $^3J_{PH}$ = 13.4 Hz, 1H, *P*-Pr^iCH), 2.5 (t, $^3J_{HH}$ = 6.7 Hz, 2H, δ-CH_2), 3.6 (sept, $^3J_{HH}$ = 6.8 Hz, 2H, *N*-Pr^iCH), 7.0(9) (m, 2H, *N*-*m*-ArCH), 7.1 (m, 1H, *N*-*p*-ArCH), 8.9 (s, 1H, $N_{enamine}$-H).

Formation of **$RuD_2(D_2)\{^{Pri}(NP)^{Pri}D\}(PPr^i_3)(CO)$ (4.4)** under D_2. Similar conditions to those used to observe formation of **$RuH_2(H_2)\{^{Pri}(NP)^{Pri}H\}(PPr^i_3)(CO)$ (4.4)** were used. $^{31}P\{^1H\}$ NMR (C_6D_6, 161.9 MHz, 298 K): No notable changes from reactions using H_2 are observed. ^1H NMR (C_6D_6, 400 MHz, 298 K): The signals at δ -7.2 (br.s, 4H, *Ru*-$(H_2)H_2$) and 8.9 (s, 1H, $N_{enamine}$-H) are changed from the spectrum recorded using H_2 gas. Integration of these

resonances relative to a resonance at δ 2.5 (t, $^3J_{HH}$ = 6.7 Hz, 2H, δ-CH_2) that does not incorporate deuterium, gives the following ratio: 11: 1: 75; *Ru*-(H_2)H_2: $N_{enamine}$-H: δ-CH_2.

Determination of the T_{1min} for **$RuH_2(H_2)\{^{Pri}(NP)^{Pri}H\}(PPr^i_3)(CO)$ (4.4)**. **4.2a** (0.033 g, 0.068 mmol) was dissolved 5% CH_2Cl_2 in d_8-toluene (0.5 ml). This mixture was transferred to a J. Young NMR tube and degassed by three freeze-pump-thaw cycles using high vacuum. The J. Young tube was sealed under vacuum and warmed to room temperature; the headspace was backfilled with H_2. After sealing the J. Young tube, the mixture was shaken intermittently for approximately 30 minutes. The sample was then introduced into a Bruker Avance 400 MHz spectrometer. ^{1}H NMR T_1 relaxation measurements were performed at various temperatures using a standard inversion-recovery pulse sequence (180°-τ-90°).

Table A.1: T_1 and Temperature values for **$RuH_2(H_2)\{^{Pri}(NP)^{Pri}H\}(PPr^i_3)(CO)$** (**4.4**)

Temperature (K)	**T_1 (s) $RuH_2(H_2)$**
298	0.0450
253	0.0252
243	0.0230
238	0.0223
233	0.0223
228	0.0223
223	0.0252
218	0.0288
213	0.0324
203	0.0432

A general procedure for the catalytic dehydrogenation of isopropanol to acetone and cyclohexanol to cyclohexanone using **RuH{^{Pri}(NP)^{Pri}}(PPr$^{i}_{3}$)(CO) (4.2a)**.

A three neck flask (100 ml), fitted with a small stir bar and a reflux condenser connected to an Ar manifold vented to a mercury bubbler was used as the reaction vessel. In the glove box, the three neck flask was charged with **4.2a** (0.040 g, 0.062 mmol) dissolved in toluene (2.00 ml). Using Schlenk techniques, the appropriate alcohol (6.2 mmol) was added. The three neck flask was lowered into a 60 °C oil bath and heated for approximately 12 hours. After this period, the reaction mixture was sampled and analyzed by GC/MS. The trace showed complete consumption of isopropanol, and formation of acetone. By similar methods, it was determined approximately 50% of the cyclohexanol had been converted to cyclohexanone after 12 hours.

Monitoring dehydrogenation of isopropanol to acetone by **RuH{^{Pri}(NP)^{Pri}}(PPr$^{i}_{3}$)(CO) (4.2a)** by NMR. **4.2a** (0.020 g, 0.031 mmol) was dissolved in d_8-toluene (0.5 ml) in a J. Young NMR tube. Isopropanol (0.024 ml, 0.31 mmol) was added to this mixture. The NMR tube was heated to 60 °C in the sealed tube overnight. Some conversion of isopropanol to acetone was detected under these conditions (3 %). At room temperature, the headspace of the J. Young tube was evacuated. The J. Young tube was sealed under vacuum and lowered into a 60 °C oil bath for 2 hours. More acetone formation was observed (5 %). Monitoring the reaction while evacuating the headspace every hour showed an increase in percent conversion to acetone with time (8 %, 4 hours) and (9 %, 9 hours). The ratio between **4.2a**: **4.3a** varies but is approximately 1:1.2. The multinuclear NMR data reported below corresponds to the final reaction mixture. $^{31}P\{^{1}H\}$ NMR (d_8-toluene, 161.9 MHz, 298 K): δ -19.5 (s,1P), 19.9 (s, 1P, PPr$^{i}_{3}$), 39.5 (d, $^{2}J_{PP}$ = 245.4 Hz, 1P, *Ru*-PP$^{i}_{3\mathbf{4.2a}}$), 59.8 (d, $^{2}J_{PP}$ = 254.5 Hz, 1P, *Ru*-P$_{ligand\mathbf{4.2a}}$), 74.6 (d, $^{2}J_{PP}$ = 252.5 Hz,

1P, *P*-RuPr$^{i}_{3}$**4.3a**), 93.0 (d, $^{2}J_{PP}$ = 252.5 Hz, 1P, *Ru*-P$_{ligand}$**4.3a**), 95.4 (s, 1P). ^{1}H NMR (d_8-toluene, 400 MHz, 298 K): δ -23.4 (t, $^{2}J_{PH}$ =20.2 Hz, *Ru*-H**4.2a**), -18.6 (ddd, $^{2}J_{HH}$ = 6.6 Hz, $^{2}J_{PH}$ = 18.3 Hz, $^{2}J_{PH}$ = 25.5 Hz, *Ru*-H**4.3a**), -16.0 (d, $^{3}J_{PH}$ = 22.2 Hz, *Ru*-H), -5.6 (ddd, $^{2}J_{HH}$ = 6.6 Hz, $^{2}J_{PH}$ = 21.9 Hz, $^{2}J_{HH}$ = 29.0 Hz, *Ru*-H**4.3a**), 1.0 (d, $^{3}J_{HH}$ = 6.1 Hz, *Pr^{i}OH*-CH$_3$), 1.6 (s, acetone), 1.7 (s, *Pr^{i}OH*-OH), 3.7 (m, *Pr^{i}OH*-CH).

General procedure for attempted catalytic dehydrogenation of benzyl alcohol to benzyl benzoate using **RuH{^{Pri}(NP)^{Pri}}(PPr$^{i}_{3}$)(CO) (4.2a)**.

In the glove box in a Schlenk flask (50 ml) fitted with a small stir bar, **4.2a** (0.020 g, 0.041 mmol) was dissolved in a 1.0 M solution of mesitylene in d_8-toluene (2.0 ml). On the Schlenk line, benzyl alcohol (0.42 ml, 4.1 mmol) was added to the mixture. The Schlenk flask was connected to a reflux condenser under a flow of Ar. The reaction vessel was lowered into a 60 °C oil bath. The reaction was vented to the Ar manifold of the Schlenk line, which was attached to a mercury bubbler. Before heating, and after 16 hours, a small aliquot (0.5 ml) of the reaction mixture was sampled for analysis by NMR spectroscopy.

No additive:

Prior to heating ^{31}P{^{1}H} NMR (C_6D_6, 161.9 MHz, 298 K): δ 19.6 (s, *P*-Pr$^{i}_{3}$), 57.5 (s), 60.8 (s), 79.8 (s), 94.3 (s).

After heating to 60 °C : ^{31}P{^{1}H} NMR (C_6D_6, 161.9 MHz, 298 K): δ 19.6 (s, *P*-Pr$^{i}_{3}$), 57.5 (s), 61.5 (s), 78.5 (d, $^{2}J_{PP}$ = 196.6 Hz), 80.3 (d, $^{2}J_{PP}$ = 196.6 Hz), 94.2 (s). ^{1}H NMR (d_8-toluene, 400 MHz, 298 K): δ -8.6 (td, $^{3}J_{HH}$ = 5.4 Hz, $^{2}J_{PH}$ = 23.1 Hz, *Ru*-H), -8.4 (td, $^{2}J_{HH}$ = 5.4 Hz, $^{2}J_{PH}$ = 22.7 Hz, *Ru*-H) 2.1 (s, *mesitylene*-CH$_3$), 3.3 (s, *benzyl alcohol*-OH), 4.3 (s, *benzyl alcohol*-CH$_2$), 5.0 (s, *benzyl benzoate*-CH$_2$), 6.6 (*mesitylene*-ArCH), 7.0-7.1 (ArCH). Based on integration of

the CH_2 resonances of benzyl benzoate and benzyl alcohol ~ 1 % conversion occurred over 16 hours.

Addition of PMe_3: The conditions described above were repeated; however, PMe_3 (4.1 μl, 0.041 mmol) was added to the mixture of **4.2a** (0.020g, 0.041 mmol) dissolved in a 1.0 M solution of mesitylene in d_8-toluene (2.0 ml).

Prior to heating to 60 °C: $^{31}P\{^1H\}$ NMR (d_8-toluene, 161.9 MHz, 298 K): δ 19.6 (s, *P*-Pr^i_3), 61.5 (s), 94.3 (s).

After heating to 60 °C: $^{31}P\{^1H\}$ NMR (d_8-toluene, 161.9 MHz, 298 K): δ 19.6 (s, *P*-Pr^i_3), 57.5 (s), 61.3 (s), 78.5 (d, $^2J_{PP}$ = 196.6 Hz), 80.3 (d, $^2J_{PP}$ = 196.6 Hz), 94.2 (s). ^1H NMR (d_8-toluene, 400 MHz, 298 K): δ -8.6 (td, $^2J_{HH}$ = 5.4 Hz, $^2J_{PH}$ = 23.1 Hz, *Ru*-H), -8.4 (td, $^2J_{HH}$ = 5.4 Hz, $^2J_{PH}$ = 22.7 Hz, *Ru*-H). Similar chemical shifts to those reported above for benzyl alcohol, benzyl benzoate and mesitylene are observed here. Based on integration of the CH_2 resonances of benzyl benzoate and benzyl alcohol ~ 3 % conversion has occurred over 16 hours.

Addition of pyridine: The conditions described above were repeated; however, pyridine (3.3 μl, 0.041 mmol) was added to the mixture of **4.2a** (0.020g, 0.041 mmol) dissolved in 1.0 M mesitylene in d_8-toluene (2.0 ml).

Prior to heating to 60 °C: $^{31}P\{^1H\}$ NMR (d_8-toluene, 161.9 MHz, 298 K): δ 5.6 (s), 19.6 (s, *P*-Pr^i_3), 21.5 (s), 22.4 (s), 23.1 (s).

After heating to 60 °C: $^{31}P\{^1H\}$ NMR (d_8-toluene, 161.9 MHz, 298 K): δ 19.6 (s), 57.5 (s), 61.7 (s), 75.2 (s), 94.2 (s). ^1H NMR (d_8-toluene, 400 MHz, 298 K): Similar chemical shifts to those reported above for benzyl alcohol, benzyl benzoate and mesitylene are observed here. Based on

the integration of the CH_2 resonances of benzyl benzoate and benzyl alcohol ~2 % conversion has occurred over 16 hours.

Synthesis of **2-(cyclopentylideneamino)-*N*,*N*-diethylethan-1-amine (5.1)**. 4 Å molecular sieves (12.0 g) contained in a Kontes sealed glass vessel were activated using high vacuum and a heat gun. The procedure used to activate the sieves consisted of heating the flask three times until a drastic decrease in vacuum occurred (monitored using a vacuum gauge), at this point the vessel is allowed to cool to room temperature; this procedure was repeated three times. After the sieves were activated, *N*-*N*-diethylethylenediamine (11.62 g, 100 mmol) was added to the reaction vessel under a positive flow of N_2 by syringe. Cyclopentanone (8.41 g, 100 mmol) was added in a similar fashion immediately afterword. The reaction vessel was placed in an 80 °C oil bath, sealed using the Kontes valve and was left to react for 18 hours. After this time, the reaction was cooled to room temperature and a ^{1}H NMR spectrum of a small sample of the reaction mixture is recorded to ensure complete consumption of cyclopentanone and *N*,*N*-diethylethylenediamine. Generally, a complex mixture of products is observed at this point. For work up, in the open air, diethyl ether (20 ml) was added to the reaction vessel and the resulting mixture was quantitatively transferred into a sinter glass frit (to separate the reaction mixture from molecular sieves). The molecular sieves were washed five times with diethyl ether (20 ml). The solvent was removed under vacuum and the product was distilled at 95 °C using a short path distillation column (~ 2 inches) fitted with a water cooling jacket under vacuum (1.6-4.0 x 10^{-1} torr). The product was obtained as colorless oil (yield 16.7 g, 46 %). ^{1}H NMR ($CDCl_3$, 400.0 MHz, 298 K): δ 1.0 (t, $^3J_{HH}$ = 7.1 Hz, 6H, *N*-EtCH_3), 1.7 (dt, $^3J_{HH}$ = 6.6 Hz, $^2J_{HH}$ = 13.5 Hz, 2H, CH_2), 1.8 (dd, $^3J_{HH}$ = 6.9 Hz, $^3J_{HH}$ = 13.0 Hz, 2H, CH_2), 2.1 (t, $^2J_{HH}$ = 7.2 Hz, 2H, CH_2), 2.3 (t, $^3J_{HH}$ = 6.9 Hz, 2H, CH_2), 2.4 (q, $^3J_{HH}$ = 7.1 Hz, 4H, *N*-EtCH_2), 2.7 (m, 2H, CH_2), 3.2 (m, 2H,

CH_2). ^{13}C APT NMR ($CDCl_3$ 100.6 MHz, 298 K): δ 11.6 (s, *N*-EtCH_3), 24.0 (s, CH_2), 24.7 (s, CH_2), 28.8 (s, CH_2), 36.2 (s, CH_2), 47.3 (s, *N*-EtCH_2), 52.0 (s, CH_2), 53.4 (s, CH_2), 180.5 (s, *N*-C_{imine}). Anal. Calcd for: $C_{11}H_{22}N_2$, C, 72.47, H, 12.16, N, 15.37 Found: C, 70.60, H, 12.38, N, 15.97 (this is highest purity obtained to date). HRMS-EI (m/z) calculated for $C_{11}H_{22}N_2$: 182.17830, Found: 182.17845.

Synthesis of **$(PNN)^{But}$ (5.2a)**. 2-(cyclopentylideneamino)-*N*,*N*-diethylethan-1-amine (**5.1**) (4.94 g, 27.1 mmol) was dissolved in THF (30 ml). In a different reaction vessel, LDA was prepared by combining a small excess of diisopropyl amine (4.56 ml, 32.5 mmol) dissolved in THF (30 ml) with 1.6 M n-butyl lithium (diethyl ether or hexanes solutions of n-butyl lithium were used, 16.9 ml, 27.1 mmol) at - 78 ºC. After addition of n-butyl lithium, the mixture was warmed to room temperature and allowed to stir for 30 min. The flask containing LDA was then re-cooled to -78 °C. The previously prepared THF solution of imine **5.1** was added dropwise to the chilled LDA solution. After the addition was complete, the reaction was brought to room temperature and allowed to stir for 30 min. The mixture was cooled to -78 ºC again and a solution of di-*tert*-butylchlorophosphine (5.15 ml, 27.1 mmol) in THF (100 ml) was added to the reaction dropwise. The mixture was warmed to room temperature and subsequently heated to reflux for 26 hours. Monitoring the reaction by $^{31}P\{^1H\}$ NMR spectroscopy shows the disappearance of the resonance for di-*tert*-butylchlorophosphine and formation of the desired product. After 26 hours, the solvent is removed under vacuum. The remaining crude product is dissolved in toluene (20 ml); a slurry forms, which is filtered through Celite. From the filtrate, toluene was removed under vacuum to give a crude yellow-brown oil. This oil was distilled using a short path (~ 2 inches) distillation apparatus at $8.3x10^{-2}$ torr, at an oil bath temperature of 160 °C. The glass of the distillation apparatus was actively heated using a heat gun (6.314 g, 78

%). $^{31}P\{^{1}H\}$ NMR (C_6D_6, 161.9 MHz, 298 K): δ 5.8 (s, 1P). ^{1}H NMR (C_6D_6, 298 K): δ 0.9 (t, $^{3}J_{HH}$ = 7.1 Hz, 6H, *N*-EtCH_3), 1.3 (d, $^{3}J_{PH}$ = 11.6 Hz, 18H, *P*-Bu$^{t}CH_3$), 1.8 (m, 2H, CH_2), 2.3 (m, 8H, 2x CH_2, 2x *N*-EtCH_2), 2.7 (t, $^{3}J_{HH}$ = 6.8 Hz, 2H, CH_2), 2.9 (q, $^{3}J_{HH}$ = 6.2 Hz, 2H, CH_2), 5.5 (dd, *J*= 5.7 Hz, *J* = 11.5 Hz, 1H, *N*-H). ^{13}C APT NMR (C_6D_6, 100.6 MHz, 298 K): δ 12.6 (s, *N*-EtCH_3), 23.4 (s, CH_2), 24.9 (d, $^{1}J_{PC}$ = 54.6 Hz, *P*-Bu^{t}C), 31.3 (d, $^{2}J_{PC}$ = 14.3 Hz, *P*-Bu$^{t}CH_3$), 32.5 (d, J_{PC} = 10.9 Hz, CH_2), 35.7 (d, $^{3}J_{PC}$ = 5.8 Hz, CH_2), 43.7 (s, CH_2), 47.5 (s, *N*-EtCH_2), 54.1 (s, CH_2), 96.4 (d, $^{1}J_{PC}$ = 15.1 Hz, α-C), 161.3 (d, $^{2}J_{PC}$ = 27.6 Hz, *N*-$C_{enamine}$). Unidentified impurities were observed at δ 33.1 (d) and 36.5 (s). Anal. Calcd for: $C_{19}H_{39}N_2P$, C, 69.89, H, 12.04, N, 8.58 Found: C, 69.37, H, 12.12, N, 9.36 (highest purity obtained to date.) HRMS-EI (m/z) calculated for $C_{23}H_{36}NP$ (M+): 326.28509, Found: 326.28489.

Synthesis of **(PNN)^{Pri} (5.2b)**. 2-(cyclopentylideneamino)-*N*,*N*-diethylethan-1-amine (**5.1**) (6.11g, 33.5 mmol) was dissolved in diethyl ether (50 ml). In a different reaction vessel LDA was prepared by combining diisopropyl amine (4.70 ml, 33.5 mmol) dissolved in diethyl ether (20 ml) with 1.6 M n-butyl lithium (21.0 ml, 33.5 mmol, diethyl ether or hexanes solutions of n-butyl lithium were used interchangeably) at -78 °C. After addition of n-butyl lithium, the mixture was warmed to room temperature and allowed to stir for 30 min. The flask containing LDA was then re-cooled to -78 °C. The previously prepared diethyl ether solution of imine **5.1** was added dropwise to the chilled LDA solution. After the addition was complete, the reaction was brought to room temperature and allowed to stir for 30 min. The mixture was cooled to - 78 °C again and a solution of chlorodiisopropylphosphine (5.34 ml, 33.5 mmol) in diethyl ether (100 ml) was added to the reaction dropwise. The mixture was warmed to room temperature and allowed stir overnight. After this time the reaction is complete, the solvent is removed under vacuum and the resulting paste is suspended in hexanes. Several drops of 1,4-dioxane are added

to this slurry to insure precipitation of LiCl. The slurry is filtered through celite and taken to dryness. The resulting yellow-brown oil was distilled using a short path distillation apparatus at $8.6x10^{-2}$ torr, the oil bath temperature was 140-147 °C and the final product is a cloudy, colorless oil (5.587 g, 56 %). $^{31}P\{^{1}H\}$ NMR (C_6D_6, 161.9 MHz, 298 K): δ -18.6 (s, 1P). ^{1}H NMR (C_6D_6, 298 K): δ 0.9 (t, $^{3}J_{HH}$ = 7.1 Hz, 6H, *N*-EtCH$_3$), 1.1 (dd, $^{3}J_{HH}$ = 7.0 Hz, $^{3}J_{PH}$ = 11.7 Hz, 6H, *P*-Pr^{i}CH$_3$), 1.2 (dd, $^{3}J_{HH}$ = 7.1 Hz, 15.2 Hz, 6H, *P*-Pr^{i}CH$_3$), 1.8 (dt, $^{3}J_{HH}$ = 7.3 Hz, $^{1}J_{HH}$ = 14.4 Hz, 2H, CH$_2$), 1.9 (d. sept. $^{3}J_{HH}$ = 7.0 Hz, $^{2}J_{PH}$ = 3.6 Hz, 2H, *P*-Pr^{i}CH), 2.3 (m, 6H, *N*-EtCH$_2$, CH$_2$), 2.4 (m, 2H, CH$_2$), 2.5 (m, 2H, CH$_2$), 2.9 (dd, $^{3}J_{HH}$ = 6.2 Hz, $^{3}J_{HH}$ = 12.3 Hz, 2H, CH$_2$), 5.3 (dd, J_{PH} = 4.6 Hz, *J* = 10.3 Hz, *N*-H). ^{13}C APT NMR (C_6D_6, 100.6 MHz, 298 K): δ 12.6 (s, *N*-EtCH$_3$), 20.5 (s, *P*-Pr^{i}CH$_3$), 21.0 (s, *P*-Pr^{i}CH$_3$) 23.1 (s, CH$_2$), 23.5 (d, $^{1}J_{PC}$ = 7.9 Hz, *P*-Pr^{i}CH), 33.3 (d, J_{PC} = 5.6 Hz, CH$_2$), 33.4 (d, J_{PC} = 5.4 Hz, CH$_2$), 43.5 (d, J_{PC} = 1.6 Hz, CH$_2$), 47.4 (s, *N*-EtCH$_2$), 53.8 (s, CH$_2$), 95.8 (d, $^{1}J_{PC}$ = 10.9 Hz, α-C), 160.9 (d, $^{2}J_{PC}$ = 25.6 Hz, *N*-C$_{enamine}$). Anal. Calcd for: $C_{17}H_{35}N_2P$, C, 68.41, H, 11.82, N, 9.39 Found: C, 68.56, H, 12.07, N, 10.35 (highest purity obtained to date.) HRMS-EI (m/z) calculated for $C_{17}H_{35}NP$ (M+): 298.25379, Found: 298.25370.

Synthesis of **RuHCl{(PNN)^{But}}(CO) (5.3a)**. RuHCl(PPr$^{i}_3$)$_2$(CO) (0.500, 1.1 mmol) was combined with **5.2a** (0.460 g, 1.41 mmol) in a Kontes sealed reaction vessel fitted with a stir bar. THF was added (5 ml) and the reaction was heated to 65 ºC for 19 hours. During this time, the reaction lightened in color and an off white precipitate forms, which corresponds to the product. The reaction was taken to dryness and the remaining solids were suspended in pentane and collected on a glass frit. The precipitate was washed with pentane until it no longer lightened in color (yield: 0.444g, 84%). $^{31}P\{^{1}H\}$ NMR (CD_2Cl_2, 161.9 MHz, 298 K): δ 109.6 (s, 1P).

^{1}H NMR (CD_2Cl_2, 400 MHz, 298 K): δ -16.3 (d, $^{2}J_{PC}$ = 23.5 Hz, 1H, *Ru*-H), 1.0 (t, $^{3}J_{HH}$ = 7.2 Hz, 3H, *N*-EtCH_3), 1.3 (t, $^{3}J_{HH}$ = 7.1 Hz, 3H, *N*-EtCH_3), 1.3(1) (br.d, $^{3}J_{PH}$ = 10.5 Hz, 9H, *P*-Bu$^{t}CH_3$), 1.4 (d, $^{3}J_{PH}$ = 13.3 Hz, 9H, *P*-Bu$^{t}CH_3$), 2.1 (m, 2H, CH_2), 2.2 (m, 2H, CH_2), 2.3 (m, 1H, CH_2), 2.5(5) (m, 1H, CH_2), 2.6(3) (m, 1H, CH_2), 2.9 (dqd, *J* = 2.5 Hz, *J* = 6.7 Hz, *J* = 13.6 Hz, 1H, *N*-EtCH_2), 3.3 (br. dq, *J* = 7.2 Hz, *J* = 14.3 Hz, 1H, *N*-EtCH_2), 3.4 (m, 2H, CH_2/ *N*-EtCH_2), 3.5 (m, 2H, CH_2/ *N*-EtCH_2), 3.6 (m, 1H, CH_2), 4.0 (m, 1H, α-CH). ^{13}C APT NMR (CD_2Cl_2 100.6 MHz, 298 K): δ 8.7 (s, *N*-EtCH_3), 10.8 (s, *N*-EtCH_3), 27.0 (d, J_{PC} =6.8 Hz, CH_2), 27.3 (d, J_{PC} = 7.2 Hz, CH_2), 28.0 (d, J_{PC} = 5.9 Hz, CH_2), 29.9 (identified by HSQC, *P*-Bu$^{t}CH_3$), 31.7 (d, $^{2}J_{PC}$ = 3.7 Hz, *P*-Bu$^{t}CH_3$), 37.7 (d, $^{1}J_{PC}$ = 19.5 Hz, *P*-Bu^{t}C), 38.0 (d, $^{1}J_{PC}$ = 14.7 Hz, *P*-Bu^{t}C), 49.7 (s, *N*-EtCH_2), 51.6 (s, CH_2), 53.3 (s, *N*-EtCH_2), 56.9 (d, $^{1}J_{PC}$ = 9.8 Hz, α-CH), 57.8 (s, CH_2), 187.0 (d, $^{2}J_{PC}$ = 7.8 Hz, *N*-C_{imine}), 209.4 (d, $^{2}J_{PC}$ = 15.7 Hz, *Rh*-CO). ATR-FTIR ν(CO) (cm^{-1}): 1890. Anal. Calcd for: $C_{20}H_{41}ClN_2ORu$, C, 48.32, H, 8.19, N, 5.68 Found: C, 48.32, H, 7.98, N, 5.59.

Synthesis of **RuHCl{(PNN)^{Pri}}(CO) (5.3b)**. $RuHCl(PPr^{i}_3)_2(CO)$ (0.324 g, 0.666 mmol) was combined with a slight excess of **5.2b** (0.239 g, 0.800 mmol) in a vial with a small stir bar. Ether (10 ml) was added to the mixture, and the resulting orange slurry was stirred for 2 days at room temperature. During this time, the slurry lightened from bright orange to light yellow. The solvent volume was reduced by ~ 50% and the reaction was cooled to -35 °C for 30 minutes prior to filtration through a sinter glass frit. The white solid collected by filtration was washed with a minimal amount of diethyl ether (yield: 0.181 g, 59 %). ^{31}P{^{1}H} NMR (C_6D_6, 161.9 MHz, 298 K): δ 95.5 (s, 1P). ^{1}H NMR (C_6D_6, 400 MHz, 298 K): δ -15.1 (d, $^{2}J_{PH}$ = 22.1 Hz, 1H, *Ru*-H), 0.8 (dd, $^{3}J_{HH}$ = 6.7 Hz, $^{3}J_{PH}$ = 14.9 Hz, 3H, *P*-Pr$^{i}CH_3$), 0.9 (t, $^{3}J_{HH}$ = 7.2 Hz, 3H, *N*-

EtCH$_3$), 1.0 (dd, $^3J_{HH}$ = 6.8 Hz, $^3J_{PH}$ =16.0 Hz, 3H, *P*-Pr^{i}CH$_3$), 1.01 (t, $^3J_{HH}$ = 7.2 Hz, 3H, *N*-EtCH$_3$), 1.2 (dd, ^3JHH = 7.3 Hz, $^3J_{PH}$ = 13.3 Hz, 3H, *P*-Pr^{i}CH$_3$), 1.3 (m, 2H, CH$_2$), 1.4 (m 2H, CH$_2$), 1.5 (dd, $^3J_{HH}$ = 7.4 Hz, $^3J_{PH}$ = 15.6 Hz, 3H, *P*-Pr^{i}CH$_3$), 1.6 (m, 3H, CH$_2$, *P*-Pr^{i}CH), 2.2 (m, 1H, *N*-EtCH$_2$), 2.6 (m, 2H, CH$_2$/ *P*-Pr^{i}CH), 2.7 (m, 1H, CH$_2$), 3.0 (m, 1H, CH$_2$), 3.1 (m, 1H, *N*-EtCH$_2$), 3.2 (dt, $^3J_{HH}$ = 4.3 Hz, $^3J_{HH}$ = 11.9 Hz, 1H, CH$_2$), 3.7 (sept, $^3J_{HH}$ = 7.1 Hz, 2H, *N*-EtCH$_2$), 3.9 (td, $^3J_{HH}$ = 4.1 Hz, $^3J_{PH}$ = 11.1 Hz, 1H, α-CH). ^{13}C APT NMR (C$_6$D$_6$, 100.6 MHz, 298 K): δ 8.9 (s, *N*-EtCH$_3$), 10.7 (s, *N*-EtCH$_3$), 18.1 (d, $^2J_{PC}$ = 4.8 Hz, *P*-Pr^{i}CH$_3$), 19.3 (d, $^2J_{PC}$ = 2.4 Hz, 2x *P*-Pr^{i}CH$_3$), 21.3 (d, $^2J_{PC}$ = 2.0 Hz, *P*-Pr^{i}CH$_3$), 22.7 (d, $^1J_{PC}$ = 26.2 Hz, *P*-Pr^{i}CH), 24.6 (d, J_{PC} = 6.8 Hz, CH$_2$), 26.5 (d, J_{PC} = 7.5 Hz, CH$_2$), 27.8 (d, J_{PC} = 6.1 Hz, CH$_2$), 28.7 (d, $^1J_{PC}$ = 23.6 Hz, *P*-Pr^{i}CH), 49.9 (d, J_{PC} = 0.7 Hz, *N*-EtCH$_2$), 51.3 (s, CH$_2$), 53.1 (d, J_{PC} = 1.6 Hz, *N*-EtCH$_2$), 57.9 (d, $^1J_{PC}$ = 8.0 Hz, α-CH), 58.7 (d, J_{PC} = 1.3 Hz, CH$_2$), 187.0 (d, $^2J_{PC}$ = 7.9 HZ, *N*-C$_{imine}$), *Ru*-CO resonance not resolved from baseline. ATR-FTIR ν(CO) (cm^{-1}): 1888. Anal. Calcd for: C$_{20}$H$_{41}$ClN$_2$ORu, C, 46.60, H, 7.82, N, 6.04; Found: C, 46.62, H, 7.78, N, 6.18.

Synthesis of **RuH{(PNN)^{But}}(CO) (5.4a)**. RuHCl{(NNP)^{PtBu}}(CO) (**5.3a**) (0.200 g, 0.41 mmol) was combined with potassium *tert*-butoxide (0.046 g, 0.41 mmol) in a vial the glove box. THF (5 ml) was added and upon stirring the reaction became a dark red color. The reaction was allowed to stir for three hours, at which point ^{31}P{^{1}H} NMR spectroscopy indicated the reaction was complete. The volatiles were removed under vacuum and the resulting red solid was extracted with pentane (3 x 10 ml) until no red colored material remained in the reaction vial. The red pentane solution was filtered through Celite and taken to dryness (yield: 0.160 g, 93 %). The red powder, which results can be recrystallized by dissolving it in a minimal amount of pentane and storing at - 35 ºC overnight, suitable crystals for elemental analysis and X-ray

diffraction studies were grown in this manner. $^{31}P\{^{1}H\}$ NMR (C_6D_6, 161.9 MHz, 298 K): δ 92.3 (s, 1P). ^{1}H NMR (C_6D_6, 400 MHz, 298 K): δ -25.2 (d, $^{2}J_{PH}$ = 25.5 Hz, 1H, *Ru*-H), 0.94 (t, $^{3}J_{HH}$ = 7.2 Hz, 3H, *N*-EtCH$_3$), 1.0 (t, $^{3}J_{HH}$ = 7.1 Hz, 3H, *N*-EtCH$_3$), 1.4 (d, $^{3}J_{PH}$ = 13.2 Hz, 9H, *P*-Bu^{t}CH$_3$), 1.5 (d, $^{3}J_{PH}$ = 12.6 Hz, 9H, *P*-Bu^{t}CH$_3$), 2.1 (m, 1H, CH$_2$), 2.3 (m, 3H, CH$_2$, *N*-EtCH$_2$), 2.4 (m, 4H, CH$_2$, *N*-EtCH$_2$), 2.6 (m, 3H, CH$_2$, *N*-EtCH$_2$), 2.7 (td, 1H, *N*-EtCH$_2$), 3.1 (m, 1H, CH$_2$), 3.2 (m, 1H, CH$_2$). ^{13}C APT NMR (C_6D_6, 100.6 MHz, 298 K): δ 11.0 (s, *N*-EtCH$_3$), 11.3 (s, *N*-EtCH$_3$), 28.7 (d, J_{PC} = 6.8 Hz, CH$_2$), 28.9 (d, J_{PC} = 2.4 Hz, CH$_2$), 29.9 (d, J_{PC} = 4.2 Hz, *P*-Bu^{t}CH$_3$), 30.4 (d, J_{PC} = 4.3 Hz, *P*-Bu^{t}CH$_3$), 31.4 (s, *N*-EtCH$_2$), 34.9 (d, $^{1}J_{PC}$ =24.1 Hz, *P*-Bu^{t}C), 40.7 (d, $^{1}J_{PC}$ = 22.1 Hz, *P*-Bu^{t}C), 48.7 (s, *N*-EtCH$_2$), 49.1 (s, CH$_2$), 54.6 (s, CH$_2$), 60.0 (s, CH$_2$), 90.0 (s, $^{1}J_{PC}$ = 41.3 Hz, α-C), 180.2 (d, $^{2}J_{PC}$ = 26.0 Hz, *N*-C$_{enamide}$), 207.6 (d, $^{2}J_{PC}$ = 12.1 Hz, *Ru*-CO). ATR-FTIR ν(CO) (cm^{-1}): 1875. Anal. Calcd for: $C_{20}H_{39}N_2OPRu$, C, 52.73, H, 8.63, N, 6.15 Found: C, 52.93, H, 8.46, N, 6.02.

Synthesis of **RuH{(PNN)^{Pri}}(CO) (5.4b)**. (PNN)^{Pri}RuHCl(CO) (**5.3a**) (0.050 g, 0.11 mmol) was combined with potassium *tert*-butoxide (0.012 g, 0.11 mmol) in a vial in the glove box. THF (2 ml) was added and the reaction mixture turned dark red. The mixture was stirred for three hours, at which point $^{31}P\{^{1}H\}$ NMR spectroscopy indicated the reaction was complete. The volatiles were removed under vacuum and the resulting red solid was extracted with hexanes (3x ~ 2 ml) until no red colored material remained in the reaction vial. The red hexanes solution was filtered through Celite and taken to dryness (yield 0.030 g, 65 %). $^{31}P\{^{1}H\}$ NMR (C_6D_6, 161.9 MHz, 298 K): δ 76.4 (s, 1P) ^{1}H NMR (C_6D_6, 400 MHz, 298 K): δ -24.3 (d, $^{2}J_{PH}$ = 29.0 Hz, 1H, *Ru*-H), 0.9 (t, $^{3}J_{HH}$ = 7.2 Hz, 3H, *N*-EtCH$_3$), 1.0 (t, $^{3}J_{HH}$ = 7.1 Hz, 3H, *N*-EtCH$_3$), 1.1(6) (m, 6H, *P*-Pr^{i}CH$_3$), 1.2 (dd, $^{3}J_{HH}$ = 6.0 Hz, $^{3}J_{PH}$ = 15.1 Hz, 3H, *P*-Pr^{i}CH$_3$), 1.4 (dd, $^{3}J_{HH}$ = 7.0 Hz,

$^{3}J_{PH}$ = 1.8 Hz, 3H, P-Pr^{i}CH$_3$), 1.9 (m, 1H, *P*-Pr^{i}CH), 2.0 (m, 1H, CH$_2$), 2.4 (m, 10H, *P*-Pr^{i}CH, CH$_2$, 2x *N*-EtCH$_2$), 2.5 (m, 1H, *N*-EtCH$_2$), 2.7 (m, 1H, *N*-EtCH$_2$), 3.1 (m, 2H, CH$_2$). ^{13}C APT NMR (C_6D_6, 100.6 MHz, 298 K): δ 10.7 (s, *N*-EtCH$_3$), 11.6 (s, *N*-EtCH$_3$), 18.6 (s, *P*-Pr^{i}CH$_3$), 18.9 (s, $^{3}J_{PC}$ = 1.5 Hz, 2x *P*-Pr^{i}CH$_3$), 19.7 (d, $^{3}J_{PC}$ = 4.2 Hz, *P*-Pr^{i}CH$_3$), 24.1 (d, $^{1}J_{PC}$ = 33.0 Hz, *P*-Pr^{i}CH), 26.2 (d, $^{1}J_{PC}$ = 29.4 Hz, *P*-Pr^{i}CH), 28.6 (d, J_{PC} = 15.7 Hz, CH$_2$), 28.7 (d, J_{PC} = 6.8 Hz, CH$_2$), 28.9 (s, CH$_2$), 48.9 (s, *N*-EtCH$_2$), 49.1 (s, CH$_2$), 54.4 (s, *N*-EtCH$_2$), 59.9 (s, CH$_2$), 88.7 (d, $^{1}J_{PC}$ = 44.1 Hz, α-C), 180.6 (d, $^{2}J_{PC}$ = 18.4 Hz, *N*-C$_{enamide}$), 206.9 (d, $^{2}J_{PC}$ = 8.0 Hz, *Ru*-CO). Anal. Calcd for: $C_{18}H_{35}N_2OPRu$, C, 50.57, H, 8.25, N, 6.55 Found: C, 50.41, H, 8.36, N, 6.62. ATR-FTIR ν(CO) (cm^{-1}): 1874.

Reaction of **RuH{(PNN)^{But}}(CO) (5.4a)** with H_2. A solution of **5.4a** (0.013 g, 0.028 mmol) dissolved in C_6D_6 (0.5 ml) and placed as a solution in a flame-sealable NMR tube sealed with a Kontes valve. The solution was freeze-pump-thaw degassed three times under high vacuum and subsequently frozen in liquid nitrogen; the headspace was evacuated for a final time, and was then backfilled with H_2 to 0.97 atm of pressure at at -196 °C. The NMR tube, submerged in liquid nitrogen, was sealed with a torch and allowed to warm to room temperature in a safe location. Monitoring the reaction by ^{1}H and ^{31}P{^{1}H} NMR spectroscopy showed no reaction within 7 days, heating the mixture to 60 °C, and 80 °C resulted in no change, however heating to 100 °C for 24 hours resulted in approximate 13 % conversion to a new ^{31}P{^{1}H} resonance at δ 32.2 (s). At this point, the ^{1}H NMR spectrum showed no new hydride resonances.

Reaction of **RuH{(PNN)^{Pri}}(CO) (5.4b)** with H_2. A solution of **5.4b** (0.030 g, 0.070 mmol) dissolved in C_6D_6 (0.5 ml) was placed as a solution in a flame-sealable NMR tube sealed with a Kontes valve. The solution was freeze-pump-thaw degassed three times under high vacuum and subsequently frozen in liquid nitrogen; the headspace was evacuated for a final time

then backfilled with H_2 to 0.95 atm at -200 °C. The NMR tube, submerged in liquid nitrogen was sealed with a torch and allowed to warm to room temperature in a safe location. Monitoring the reaction by ^1H and $^{31}P\{^1H\}$ NMR after 1 hour shows a signal at δ 104.7, corresponding to an intermediate in the reaction and a smaller set of resonances at δ 90.5 (d, $^2J_{PP}$ = 6.9 Hz) and 79.0 (d, $^2J_{PP}$ = 6.9 Hz) corresponding to the final product. The largest signal observed is **5.4b** at this point; in addition to these resonances, other small signals are observed. Allowing the reaction to proceed for 13 hours gives a ratio of peaks of 1.8:1:1:6.6 corresponding to the resonances at δ 104.7:90.6:79.0:**5.4b**. After 10 days the mixture mostly corresponds to the resonances at δ 90.5 and 79.0, multinuclear NMR spectra were recorded at this time and diagnostic features are reported below. $^{31}P\{^1H\}$ NMR (C_6D_6, 161.9 MHz, 298 K): δ 79.0 (d, $^2J_{PP}$ = 6.9 Hz), 90.5 (d, $^2J_{PP}$ = 6.9 Hz). ^1H NMR (C_6D_6, 400 MHz, 298 K): δ -10.6 (br.d, J = 18.5 Hz), -10.5 (ddd, J_{HH} = 6.6 Hz, J_{PH} = 14.3 Hz, J_{PH} = 23.0 Hz), - 8.5 (dt, J = 5.4 Hz, J = 11.8 Hz).

Reaction of **RuH{(PNN)^{But}}(CO) (5.4a)** with $KHBEt_3$. In a vial equipped with a small stir bar **5.4a** (0.050 g, 0.102 mmol) was combined with $KHBEt_3$ (0.014 g, 0.102 mmol). THF (5 ml) was added to the solids. Stirring the reaction mixture for 10 minutes produced a clear, orange solution. Allowing the mixture to stir for longer periods of timed resulted in a gradual color change from orange to deep red. $^{31}P\{^1H\}$ NMR of the reaction during the initial period shows resonances 122.4 (s), 119.4 (s) and a resonance at 92.3 (s) consistent with **5.4a**. The relative ratio of these peaks is 1:1.3:0.4 after one hour. After allowing the reaction to stir for 2 hours the same peaks were observed in a ratio of 1:1:1.3, suggesting conversion of the resonances at δ 122.4 and 119.4 to **5.4a** is occurring. The reaction mixture was taken to dryness, producing a red oil, which was extracted with pentane (5 ml), a peach colored solid remained

which was dried in vacuum and analyzed by multinuclear NMR spectroscopy. As the ^{1}H NMR spectrum is of a mixture of products only diagnostic feature of the ^{1}H NMR spectrum are reported. $^{31}P\{^{1}H\}$ NMR (C_6D_6, 161.9 MHz, 298 K): δ 122.4 (s, ~ 8%), 119.4 (s, ~ 47 %), 110.6 (s, ~7 %), 108.8 (s, ~ 5%), 92.3 (s, ~ 33 %). ^{1}H NMR (C_6D_6, 400 MHz, 298 K): δ - 12.8 (td, $^{2}J_{HH}$ = 5.0 Hz, $^{2}J_{PH}$ = 18.0 Hz). -18.7 (br. d, 67.8 Hz) (these resonances show cross correlation to the signal at δ 119.4 by ^{1}H-^{31}P HMBC). A similar minor set of resonances that integrate 0.2:1 relative to the major resonances are identified at δ -13.0 (m) and δ - 8.6 (dt, $^{2}J_{HH}$ = 4.2 Hz, $^{2}J_{PH}$ = 9.7 Hz).

Catalytic AD of Benzyl Alcohol to Benzyl Benzoate using **RuH{(PNN)^{But}}(CO) (5.4a)** and **RuH{(PNN)^{Pri}}(CO) (5.4b)**.

a) **5.4a** (0.019 g, 0.041 mmol) was dissolved in a 1.0 M solution of mesitylene in d_8-toluene (0.50 ml) in the glove box in a J. Young tube. Using Schlenk techniques, benzyl alcohol (0.43 ml, 4.1 mmol) was added. The mixture was shaken, then the J. Young tube was opened to the Ar manifold of the Schlenk line and heated to 110 °C. The reaction was monitored intermittently by ^{1}H NMR spectroscopy to demine the percent conversion.

b) In the glove box **5.4a** or **5.4b** (0.0100 mmol) was added to a two neck flask (100 ml) equipped with a medium stir bar and a Schlenk arm gas inlet. Mesitylene (0.070 ml, 5.0 mmol) was added as an internal standard along with toluene (2.00 ml). The Schlenk flask was sealed and removed from the glove box. Using standard Schlenk techniques benzyl alcohol (1.04 ml, 10.0 mmol) was added. The Schlenk flask was fitted with a reflux condenser, connected to the Ar manifold and vented to a mercury bubbler, and the reaction was heated to 115 °C, under a stream of Ar from the reflux condenser. The reaction was sampled twice at two hour intervals for analysis by GC-FID by allowing the mixture to cool to room temperature for at least 30 min

and taking samples of at least 320 μl of the reaction mixture. After sampling, the reaction was allowed to proceed as previously described. In open air, a sample (320 μl) was diluted in toluene (10.00 ml) and subsequently analyzed by GC-FID.

Appendix B

B.1 Crystal Structure Refinement Details

Table B.1: Crystal structure refinement details for **2.1a** and **2.1b**

Compound	**2.1a**	**2.1b**
Empirical formula	$C_{32}H_{27}N_2O_{0.13}P$	$C_{40}H_{53}N_2P$
Formula weight [g/mol]	484.61	592.81
Color / Morphology	colorless / plate	colorless / plate
Crystal size [mm]	0.120, 0.200, 0.200	0.140, 0.240, 0.260
Temperature [K]	100	100
Wavelength [Å]	0.71069 (Mo-Kα)	0.71069 (Mo-Kα)
Crystal system	Monoclinic	Monoclinic
Space group	$P2_1/c$	$P2_1/c$
a [Å]	17.223(2)	15.28(3)
b [Å]	10.478(6)	10.699(2)
c [Å]	15.969(2)	21.645(6)
α, *β*, *γ* [°]	90, 112.681(3), 90	90, 91.872(7), 90
V (Å^3)	2658.9(2)	3531.5(2)
$\rho_{calc.}$ [g cm^{-1}]	1.211	1.115
Z	4	4
F(000)	1040	1288.0
μ [mm^{-1}]	0.128	0.107
T_{max}/T_{min}	0.975/ 0.985	0.973/ 0.985
hkl range	$-20 \leq h \leq 19$, $-12 \leq k \leq 12$, $-19 \leq l \leq 19$	$-17 \leq h \leq 16$, $-11 \leq k \leq 12$, $-25 \leq l \leq 25$
θ range [°]	2.33-25.07	1.34-24.838
Independent reflections, R_{int}	4664, 0.0295	6079, 0.0523
Completeness to θ_{max} (%)	98.8	97.3
Absorption correction	Multi-scan (SADABS)	Multi-scan (SADABS)
Refinement Method	Full-matrix least-squares on F^2	Full-matrix least-squares on F^2
Measured reflections	16818	24625
Data / restraints / parameters	4664/6/334	6079/6/404
Goodness-of-fit	1.033	1.024
R1, wR2 (I>2σ(I))	0.0528/ 0.1298	0.0462/ 0.1056
R1, *wR2* (all data)	0.0815/ 0.1486	0.0654/ 0.1171
Residual electron dens. [e Å^{-3}]	-0.40/ 0.75	-0.65/ 0.88

Table B.2: Crystal structure refinement details for **2.4a** and **2.5a**

Compound	**2.4a**	**2.5a** + 3(CH_2Cl_2)
Empirical formula	$C_{33}H_{37}ClN_2OPRh$	$C_{35.5}H_{40}Cl_9N_2PRh$
Formula weight [g mol^{-1}]	646.97	947.62
Color / Morphology	yello / prism	colourless / tablet
Crystal size [mm]	0.200, 0.240, 0.260	0.160, 0.220, 0.240
Temperature [K]	100	100
Wavelength [Å]	0.71069 (Mo-Kα)	0.71069 (Mo-Kα)
Crystal system	Monoclinic	triclinic
Space group	P21/c	P-1
a [Å]	14.7226(7)	12.214(9)
b [Å]	17.7439(2)	13.0176(9)
c [Å]	23.9853(2)	15.556(2)
α, *β, γ* [˚]	90, 101.712(2), 90	91.937(3), 113.497(3), 113.497(3)
V ($Å^3$)	6135.4(5)	2064.(2)
$\rho_{calc.}$ [g cm^{-1}]	1.401	1.531
Z	8	2
F(000)	2672.0	968.0
μ [mm^{-1}]	0.724	1.063
T_{max}/T_{min}	0.828/ 0.865	0.775/ 0.844
hkl range	$-17 \leq h \leq 17$, $-21 \leq k \leq 21$, $-28 \leq l \leq 28$	$-14 \leq h \leq 14$, $-13 \leq k \leq 15$, $-18 \leq l < 15$
θ range [˚]	1.438-25.332	1.438-24.994
Independent reflections, R_{int}	11224, 0.0359	7219, 0.0232
Completeness to θ_{max} (%)	82.8	99.4
Absorption correction	Multi-scan (SADABS)	Multi-scan (SADABS)
Refinement Method	Full-matrix least-squares on F^2	Full-matrix least-squares on F^2
Measured reflections	44967	26399
Data / restraints / parameters	11224/789/756	7219/0/478
Goodness-of-fit	1.025	1.060
R1, wR2 (I>2σ(I))	0.0320/ 0.0764	0.0292/ 0.0696
R1, wR2 (all data)	0.0439/ 0.0829	0.0343/ 0.0724
Residual electron dens. [e $Å^{-3}$]	-0.63/ 1.18	-1.42/ 1.17

Table B.3: Crystal structure refinement details for **2.5b** and **3.7b**

Compound	**2.5b** + CH_2Cl_2	**3.7b**
Empirical formula	$C_{41}H_{56}N_2PRhCl_4$	$C_{58}H_{66}K_2N_2O_2P_2$
Formula weight [g/mol]	852.55	963.27
Color / Morphology	colorless / prism	yellow / tablet
Crystal size [mm]	0.220, 0.220, 0.240	0.200, 0.220, 0.280
Temperature [K]	100	100
Wavelength [Å]	0.71069 (Mo-Kα)	0.71069 (Mo-Kα)
Crystal system	triclinic	Orthorhombic
Space group	P-1	Pbca
a [Å]	11.096(2)	17.479(5)
b [Å]	11.826(2)	15.373(5)
c [Å]	17.312(2)	19.062(5)
α, *β*, *γ* [°]	96.624(3)	90
V (Å^3)	2064.4(2)	5122(3)
$\rho_{calc.}$ [g cm^{-1}]	1.372	1.249
Z	2	4
F(000)	888.0	2048
μ [mm^{-1}]	0.742	0.291
T_{max}/T_{min}	0.849/ 0.837	0.943 / 0.926
hkl range	$-13 \leq h \leq 13$, $-14 \leq k \leq 14$, $-15 \leq l \leq 20$	$-18 \leq h \leq 20$, $-18 \leq k \leq 15$, $-22 \leq l \leq 22$
θ range [°]	1.19-25.031	2.1-25.0
Independent reflections, R_{int}	7189, 0.0291	5025, 0.0470
Completeness to θ_{max} (%)	98.7	99.8
Absorption correction	Multi-scan (SADABS)	Multi-scan (SADABS)
Refinement Method	Full-matrix least-squares on F^2	Full-matrix least-squares on F^2
Measured reflections	26363	28505
Data / restraints / parameters	7189 / 0 / 462	3882 / 0 / 359
Goodness-of-fit	1.072	1.015
R1, wR2 (I>2σ(I))	0.0244/ 0.0635	0.0410 / 0.1005
R1, wR2 (all data)	0.0265/ 0.0694	0.0490 / 0.1072
Residual electron dens. [e Å^{-3}]	-0.69/ 1.19	-0.669 / 0.632

Table B.4: Crystal structure refinement details for **3.8a** and **3.9a**

Compound	**3.8a**	**3.9a**
Empirical formula	$C_{37}H_{45}IrNP$	$C_{58}H_{71}Ir_2N_2P_2$
Formula weight [g mol^{-1}]	726.93	1242.5
Color / Morphology	red / prism	yellow / prism
Crystal size [mm]	0.150, 0.180, 0.240	0.040, 0.080, 0.100
Temperature [K]	100	100
Wavelength [Å]	0.71069 (Mo-Kα)	0.71069 (Mo-Kα)
Crystal system	Monoclinic	Orthorhombic
Space group	$P2_1/c$	$Pca2_1$
a [Å]	10.0087(3)	12.3140(4)
b [Å]	15.3810(5)	18.0350(6)
c [Å]	20.2598(5)	23.5100(9)
α, *β, γ* [˚]	90, 90.4970(10), 90	90
V (Å^3)	3118.75(16)	5221.2(3)
$\rho_{calc.}$ [g cm^{-1}]	1.548	1.581
Z	4	4
F(000)	1552	2468
μ [mm^{-1}]	4.366	5.192
T_{max}/T_{min}	0.519 / 0.405	0.812 / 0.614
hkl range	$-13 \leq h \leq 12$, $-13 \leq k \leq 19$, $-26 \leq l \leq 26$	$-14 \leq h \leq 12$, $-20 \leq k \leq 21$, $-27 \leq l \leq 28$
θ range [˚]	1.66 - 27.52	1.732 - 25.105
Independent reflections, R_{int}	7424, 0.0293	7910, 0.0285
Completeness to θ_{max} (%)	99.7	98.4
Absorption correction	Multi-scan (SADABS)	Multi-scan (SADABS)
Refinement Method	Full-matrix least-squares on F^2	Full-matrix least-squares on F^2
Measured reflections	27332	35451
Data / restraints / parameters	6178 / 0 / 365	9296 / 1909 / 594
Goodness-of-fit	1.015	1.03
R1, wR2 (I>2σ(I))	0.0293 / 0.0496	0.0285 / 0.0584
R1, wR2 (all data)	0.0221 / 0.0471	0.0408 / 0.0634
Residual electron dens. [e Å^{-3}]	-0.456 / 0.914	-0.575 / 1.683'

Table B.5: Crystal structure refinement details for **3.10a** and **4.2a**

Compound	**3.10a**	**4.2a**
Empirical formula	$C_{31}H_{33}IrNO_2P$	$C_{33}H_{59}NOP_2Ru$
Formula weight [g/mol]	674.75	648.82
Color / Morphology	red / plate	red / prism
Crystal size [mm]	0.100, 0.180, 0.220	0.110, 0.140, 0.300
Temperature [K]	100	100
Wavelength [Å]	0.71069 (Mo-Kα)	0.71069 (Mo-Kα)
Crystal system	Triclinic	Monoclinic
Space group	P-1	$P2_1/c$
a [Å]	8.700(5)	12.507(4)
b [Å]	9.338(5)	16.903(5)
c [Å]	18.565(5)	15.260(3)
α, *β, γ* [˚]	81.112(5), 78.791(5), 68.378(5)	90, 101.445(3)
V (Å)	1369.7(11)	3369(2)
$\rho_{calc.}$ [g cm^{-1}]	1.636	1.279
Z	2	4
F(000)	668	1384.0
μ [mm^{-1}]	4.961	0.585
T_{max}/T_{min}	0.609 / 0.356	0.938/ 0.906
hkl range	$-10 \leq h \leq 10$, $-10 \leq k \leq 11$, $-21 \leq l \leq 22$	$-17 \leq h \leq 17$, $-23 \leq k \leq 23$, $-22 \leq l \leq 22$
θ range [˚]	2.25 - 25.05	1.661-29.639
Independent reflections, R_{int}	4804, 0.0181	9463, 0.0281
Completeness to θ_{max} (%)	99.1	99.4
Absorption correction	Multi-scan (SADABS)	Multi-scan (SADABS)
Refinement Method	Full-matrix least-squares on F^2	Full-matrix least-squares on F^2
Measured reflections	17076	37019
Data / restraints / parameters	4664 / 0 / 329	9463/ 0 / 361
Goodness-of-fit	1.036	1.034
R1, wR2 (I>2σ(I))	0.0173 / 0.0445	0.0224/ 0.0508
R1, wR2 (all data)	0.0181 / 0.0449	0.0307/ 0.0542
Residual electron dens. [e $Å^{-3}$]	-0.777 / 0.079	-0.32/ 0.42

Table B.6: Crystal structure refinement details for **4.2c** and **4.3a**

Compound	**4.2c**	**4.3a**
Empirical formula	$C_{33}H_{59}NOP_2Ru$	$C_{33}H_{61}NOP_2Ru$
Formula weight [g/mol]	648.82	650.83
Color / Morphology	red / prism	yellow / irregular
Crystal size [mm]	0.130, 0.140, 0.230	0.040, 0.110, 0.130
Temperature [K]	100	90.15
Wavelength [Å]	0.71069 (Mo-Kα)	0.71069 (Mo-Kα)
Crystal system	triclinic	Monoclinic
Space group	P-1	$P2_1/c$
a [Å]	11.4257(2)	21.551(8)
b [Å]	11.6638(2)	9.7070(4)
c [Å]	15.9264(2)	33.0071(2)
α, *β*, *γ* [°]	83.077(2), 72.810(2), 63.467(2)	90, 90.028(2), 90
V (Å)	1813.9(3)	6907.2(5)
$\rho_{calc.}$ [g cm^{-1}]	1.256	1.252
Z	2	8
F(000)	733	2784.0
μ [mm^{-1}]	0.549	0.571
T_{max}/T_{min}	0.931 / 0.912	0.977/ 0.928
hkl range	$-16 \leq h \leq 16$, $-16 \leq k \leq 16$, $-22 \leq l \leq 22$	$28 \leq h \leq 28$, $0 \leq k \leq 12$, $0 \leq l \leq 43$
θ range [°]	1.952-30.106	1.554-27.887
Independent reflections, R_σ	10650, 0.0260	16128, 0.0647
Completeness to θ_{max} (%)	99.5	97.8
Absorption correction	Multi-scan (SADABS)	Multi-scan (SADABS)
Refinement Method	Full-matrix least-squares on F^2	Full-matrix least-squares on F^2
Measured reflections	40408	1151426
Data / restraints / parameters	10650 / 0 / 381	16128 / 0 / 701
Goodness-of-fit	1.039	1.124
R1, wR2 (I>2σ(I))	0.0279, 0.0664	0.0566, 0.1253
R1, *wR2* (all data)	0.0322, 0.0686	0.0846, 0.1359
Residual electron dens. [e $Å^{-3}$]	-0.59 /1.44	-0.79 / 0.88

Table B.7: Crystal structure refinement details for **5.4a**

Compound	**5.4a**
Empirical formula	$C_{20}H_{38}N_2OPRu$
Formula weight [g/mol]	454.56
Color / Morphology	red / rectangular prism
Crystal size [mm]	0.120, 0.150, 0.300
Temperature [K]	100
Wavelength [Å]	0.71069 (Mo-Kα)
Crystal system	monoclinic
Space group	$P2_1/m$
a [Å]	9.6117(8)
b [Å]	11.6787(2)
c [Å]	10.5243(2)
α, *β, γ* [°]	90, 111.025(2), 90
V (Å)	11.02.72(2)
$\rho_{calc.}$ [g cm^{-1}]	1.369
Z	2
F(000)	478.0
μ [mm^{-1}]	0.794
T_{max}/T_{min}	0.909, 0.867
hkl range	$-12 \leq h \leq 12$, $-15 \leq k \leq 15$, $-13 \leq l \leq 13$
θ range [°]	2.073-27.924
Independent reflections, R_{int}	2769, 0.0293
Completeness to θ_{max} (%)	99.9
Absorption correction	Multi-scan (SADABS)
Refinement Method	Full-matrix least-squares on F^2
Measured reflections	11859
Data / restraints / parameters	2769 / 212 / 185
Goodness-of-fit	1.048
R1, wR2 (I>2σ(I))	0.0244, 0.0560
R1, *wR2* (all data)	0.0298, 0.0586
Residual electron dens. [e $Å^{-3}$]	-0.41 / 0.40

Appendix C

C.1 N-M-P bite angles for a selection of cyclopentyl, aliphatic, ortho-phenylene and indene linked ligands.

Table C.1: N-M-P bite angles for a selection of cyclopentyl, aliphatic, ortho-phenylene and indene linked ligands

Complex	Linker	Ligand Formal Charge	N-M-P	Angle (°)	Reference
2.4a	cyclopentyl	0-imine phosphine	N1-Rh1-P1	83.21(7)	this work
2.5a	cyclopentyl	0-imine phosphine	N1-Rh1-P1	83.76(7)	this work
2.5a	cyclopentyl	0-imine phosphine	N2-Rh1-P1	83.53(7)	this work
2.5b	cyclopentyl	0-imine phosphine	N1-Rh1-P1	82.91(5)	this work
2.5b	cyclopentyl	0-imine phosphine	N2-Rh1-P1	83.80(5)	this work
3.8a	cyclopentyl	-1-enamide phosphine	N1-Rh1-P1	81.98(9)	this work
3.9a	cyclopentyl	0-imine phosphine	N1-Ir1-P1	81.3(2)	this work
3.9a	cyclopentyl	0-imine phosphine	N2-Ir2-P2	81.2(2)	this work
3.10a	cyclopentyl	-1-enamide phosphine	N1-Ir1-P1	82.26(7)	this work
4.2a	cyclopentyl	-1-enamide phosphine	N1-Ru1-P1	81.47(4)	this work
4.2c	cyclopentyl	-1-enamide phosphine	N1-Ru1-P1	81.05(4)	this work
4.3a	cyclopentyl	0-imine phosphine	N1-Ru1-P1	80.8(1)	this work
5.4a	cyclopentyl	-1-enamide phosphine	N1-Ru1-P1	82.58(8)	this work
-	(1*S*, 2*S*)-$Ph_2PCH(Ph)CH(Me)NHCH_2Ph$	0-amine phosphine	N1-Ir1-P1	83.06(6)	[16]
-	*trans*-1,2-$C_5H_8(PPh_2)_2$	0-bis(phosphine)	P1-Ru1-P2	85.1(2)	[178]
-	*trans*-1,2-$C_5H_8(PPh_2)_2$	0-bis(phosphine)	P1-Rh1-P2	84.67(4)	[178]
-	κ^2-*P*,*N*-1-PPr^i_2-2-NMe_2-indene	0-amine phosphine	N1-Ru1-P1	82.6(7)	[179]
-	κ^2-*P*,*N*-3-PPr^i_2-2-NMe_2-indene	0-amine phosphine	N1-Ru1-P1	81.67(4)	[179]
-	κ^2-*P*,*N*-3-PPr^i_2-2-NMe_2-indene	0-amine phosphine	N1-Ru1-P1	84.09(1)	[180]
-	κ^2-*P*,*N*-3-PPr^i_2-2-NMe_2-indenide	-1-enamide phosphine	N1-Ru1-P1	83.93(9)	[180]
-	ortho-phenylene	0-amine phosphine	N1-Rh1-P1	85.6(3)	[181]
-	ortho-phenylene	0-enamide phosphine	N1-Rh1-P1	82.8(4)	[181]
-	aliphatic	0-amido phosphine	N1-Ru1-P1	81.92(3)	[65]
-	aliphatic	0-amine phosphine	N1-Ir1-P1	83.76(1)	[72]